Principles of Applied Reservoir Simulation

THIRD EDITION

JOHN R. FANCHI, PH.D.

GPP

Principles of Applied Reservoir Simulation

Principles of Applied Reservoir Simulation

Third Edition

John R. Fanchi

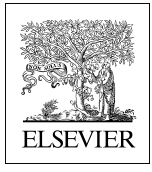

AMSTERDAM • BOSTON • HEIDELBERG • LONDON
NEW YORK • OXFORD • PARIS • SAN DIEGO
SAN FRANCISCO • SINGAPORE • SYDNEY • TOKYO
GULF PROFESSIONAL PUBLISHING IS AN IMPRINT OF ELSEVIER

Gulf Professional Publishing is an imprint of Elsevier
30 Corporate Drive, Suite 400, Burlington, MA 01803, USA
Linacre House, Jordan Hill, Oxford OX2 8DP, UK

Library of Congress Cataloging-in-Publication Data
Application submitted.

British Library Cataloguing-in-Publication Data
A catalogue record for this book is available from the British Library.

ISBN 13: 978-0-7506-7933-6

ISBN 10: 0-7506-7933-6

For information on all Gulf Professional Publishing publications visit our Web site at www.books.elsevier.com

05 06 07 08 09 10 10 9 8 7 6 5 4 3 2 1

Printed in the United States of America

In memory of my parents,

John A. and Shirley M. Fanchi

Chapter 1

Introduction to Reservoir Management

Modern reservoir simulators are computer programs that are designed to model fluid flow in porous media. Applied reservoir simulation is the use of these programs to solve reservoir flow problems. Reservoir flow modeling exists within the context of the reservoir management function.

Modern reservoir management is generally defined as a continuous process that optimizes the interaction between data and decision making during the life cycle of a field [Saleri, 2002, 2005]. This definition covers the management of hydrocarbon reservoirs as well as other reservoir systems, such as geothermal reservoirs and reservoirs that store carbon dioxide as part of a geological sequestration system. More specifically, reservoir management of hydrocarbon reservoirs is defined as the allocation of resources to optimize hydrocarbon recovery from a reservoir while minimizing capital investments and operating expenses [Wiggins and Startzman, 1990; Satter and Thakur, 1994; Al-Hussainy and Humphreys, 1996; Thakur, 1996]. The two outcomes of reservoir management in this definition – optimizing recovery and minimizing cost – often conflict with each other. Hydrocarbon recovery could be maximized if cost was not an issue, while costs could be minimized if the field operator had no desire or obligation to prudently manage a finite

resource. *The primary objective in a reservoir management study of hydrocarbon reservoirs is to determine the optimum conditions needed to maximize the economic recovery of hydrocarbons from a prudently operated field.*

Reservoir flow modeling is the most sophisticated methodology available for achieving the primary reservoir management objective for hydrocarbon reservoirs. Table 1-1 lists many reasons for performing a flow model study. Perhaps the most important, from a commercial perspective, is the ability to generate cash flow predictions. Reservoir flow modeling provides a production profile for preparing economic forecasts. The combination of production profile and price forecast gives an estimate of future cash flow. Several of the items are discussed in greater detail in later chapters.

Table 1-1
Why Simulate?

Corporate Impact
➢ Cash Flow Prediction
• Need Economic Forecast of Hydrocarbon Price
Reservoir Management
➢ Coordinate Reservoir Management Activities
➢ Evaluate Project Performance
• Interpret/Understand Reservoir Behavior
➢ Model Sensitivity to Estimated Data
• Determine Need for Additional Data
➢ Estimate Project Life
➢ Predict Recovery versus Time
➢ Compare Different Recovery Processes
➢ Plan Development or Operational Changes
➢ Select and Optimize Project Design
➢ Maximize Economic Recovery

1.1 Consensus Modeling

Reservoir flow modeling is the application of a computer simulation system to the description of fluid flow in a reservoir [for example, see Peaceman, 1977; Aziz and Settari, 1979; Mattax and Dalton, 1990; Munka and Pápay, 2001; Ertekin, et al., 2001; Carlson, 2003]. The computer simulation system is usually just one or more computer programs. To minimize confusion in this text, the computer simulation system is called the reservoir simulator, and the input data set is called the reservoir flow model. In the modern literature, the term "reservoir model" often refers to the geologic model of a reservoir.

The flow simulator has been the point of contact between disciplines for decades [e.g. see Craig, et al., 1977; and Harris and Hewitt, 1977]. It serves as a filter that selects from among all of the proposed descriptions of the reservoir. The simulator is not influenced by hand-waving arguments or presentation style. It provides an objective appraisal of each hypothesis, and constrains the power of personal influence described by Millheim [1997]. As a filter of hypotheses, the reservoir flow modeling team is often the first to know when a proposed hypothesis about the reservoir is inadequate.

Many different disciplines contribute to the preparation of the input data set of a flow model. The information is integrated during the reservoir flow modeling process, and the concept of the reservoir is quantified in the reservoir simulator. Figure 1-1 illustrates the contributions different disciplines make to reservoir flow modeling. One of the goals of recent technology development is to improve the software used to integrate data from different disciplines and to prepare shared earth models [Cope, 2001; Tearpock and Brenneke, 2001]. Many of the features of the simulator provided with this text are designed to enhance the integration of data from different disciplines. Fanchi [2002a] presents additional discussion of shared earth models and associated references.

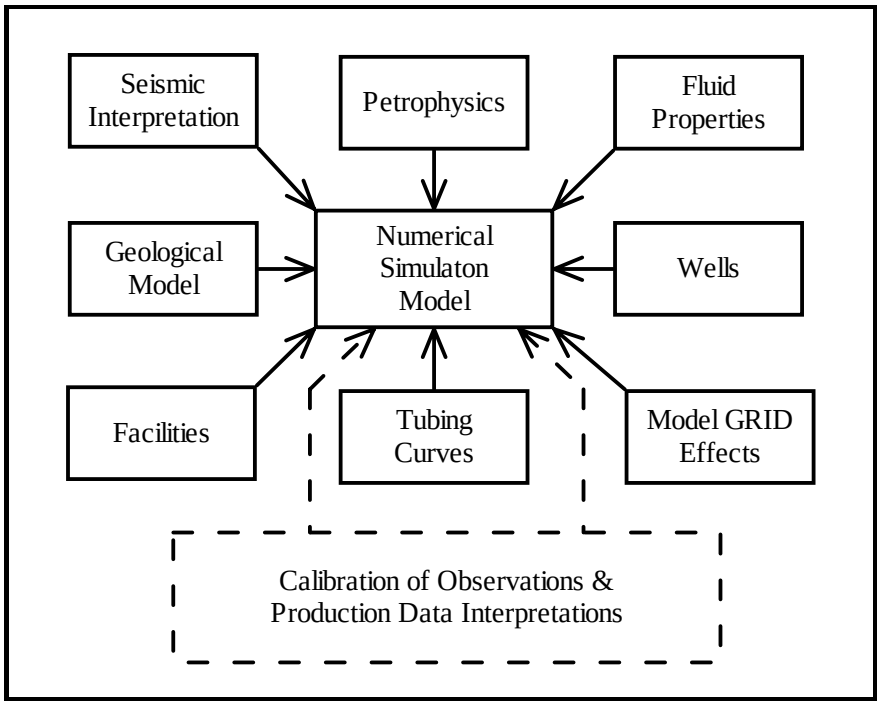

Figure 1-1. Disciplinary contributions to reservoir flow modeling (after H.H. Haldorsen and E. Damsleth, [1993]; reprinted by permission of the American Association of Petroleum Geologists)

One of the most important tasks of the flow modeling team is to achieve consensus in support of a reservoir representation. This task is made more complex when available field performance data can be matched by more than one reservoir flow model. The nonuniqueness of the model is discussed in greater detail throughout the text. It means that there is more than one way to perceive and represent available data. The modeling team must sort through the various reservoir representations and seek consensus among all stakeholders. This is often done by rejecting one or more proposed representations. As a consequence, the human

element is a factor in the process, particularly when the data do not clearly support the selection of a single reservoir representation from a set of competing representations. The dual criteria of reasonableness and Ockham's Razor [Jefferys and Berger, 1992] are essential to this process, as is an understanding of how individuals can most effectively contribute to the modeling effort.

1.2 Management of Simulation Studies

Modern simulation studies of major fields are performed by teams of specialists from different disciplines. The teams of specialists function as project teams in a matrix management organization. Matrix management is synonymous here with Project Management and has two distinct characteristics:

- "Cross-functional organization with members from different work areas who take on a project." [Staff-JPT, 1994]
- "One employee is accountable to two or more superiors, which can cause difficulties for managers and employees." [Staff-JPT, 1994]

According to Maddox [1988], teams and groups differ in the way they behave. Group behavior exhibits the following characteristics:

- "Members think they are grouped together for administrative purposes only. Individuals work independently, sometimes at cross purposes."
- "Members tend to focus on themselves because they are not sufficiently involved in planning the unit's objectives. They approach their job simply as hired hands."

By contrast, the characteristics of team behavior are the following:

- "Members recognize their interdependence and understand both personal and team goals are best accomplished with mutual sup-

port. Time is not wasted struggling over territory or seeking personal gain at the expense of others."

- "Members feel a sense of ownership for their jobs and unit because they are committed to goals they helped to establish."

Haldorsen and Damsleth [1993] have made similar observations:

- "Members of a team should necessarily understand each other, respect each other, act as a devil's advocate to each other, and keep each other informed."

Haldorsen and Damsleth [1993] argue that each team member should focus on innovation and creation of value through the team approach, and on customer orientation that conveys the attitude that "my output is your input."

Teams need time to develop. Team development proceeds in well known stages [Sears, 1994]:

- Introductions: Team members get to know each other.
- "Storming": Team members disagree over how to proceed.
  - Members can lose sight of goals.
- "Norming": Members set standards for team productivity.
- "Performing": Team members understand what each member can contribute and how the team works best.

Proper management recognizes these stages and allows time for the team building process to mature.

To alleviate potential problems, the project team should be constituted such that each member of the team is assigned a different task, and all members work toward the same goal. Team members should have unique roles to avoid redundant functions. If the responsibilities of two or more members of the team overlap considerably, confusion may ensue with regard to areas of responsibility and, by implication, of accountability. Each team member must be the key decision maker in a particular discipline, otherwise disputes may not get resolved in the time

available for completing a study. Teams should not be allowed to flounder in an egalitarian utopia that does not work.

McIntosh, et al. [1991] support the notion that each team member should fulfill a functional role, for example, geoscientist or engineer. A corollary is that team members should be able to understand their roles because the roles have been clearly defined. Wade and Fryer [1997] observe that "getting people to work together as a team rather than a group of individuals can be quite a bit more difficult than it would seem." They suggest that team members should only include people who spend 100% of their time on areas of responsibility assigned to their team. Bashore [2000] advises that team members should be located close to each other to facilitate communication and cooperation, but cautioned that multidisciplinary teams may become microcosms of functionally oriented organizations and never achieve true integration.

Effective teams may strive for consensus, but the pressure of meeting deadlines will require one team member to serve as team leader. Deadlines cannot be met if a team cannot agree, and there are many areas where decisions may have to be made without consensus. For this reason, teams should have a team leader with significant technical skills and broad experience. Shaw and Morris [2005] add that team leaders should have full management support. This can take the form of technical and monetary authority over the project. If team leaders are perceived as being without authority, they will be unable to fulfill their function. On the other hand, team leaders must avoid exercising authoritarian control or they will weaken the team and wind up with a group.

Proper management can improve the likelihood that a team will function as it should. A sense of ownership or "buy-in" can be fostered if team members participate in planning and decision making. Team member views should influence the work scope and schedule of activity. Many problems can be avoided if realistic expectations are built into project schedules at the beginning, and then adhered to throughout the

project. Expanding work scope without altering resource allocation or deadlines can be demoralizing and undermine the team concept.

Finally, an important caution should be borne in mind when performing studies using teams: “Fewer ideas are generated by groups than by individuals working alone – a conclusion supported by empirical evidence from psychology [Norton, 1994].” In describing changes in the work flow of exploration and development studies, Tobias [1998, pg. 38] observes that “asset teams have their drawbacks. The enhanced teamwork achieved through a team approach often comes at the expense of individual creativity, as group dynamics can and often does inhibit individual initiative [Kanter, 1988].” Tobias recommends that organizations allow “the coexistence of both asset teams and individual work environments.” His solution is a work flow that allows the “simultaneous coexistence of decoupled individual efforts and recoupled asset team coordination.”

1.3 “Hands-On” Simulation

The best way to learn how to apply reservoir flow simulators is to get some “hands-on” experience with a real reservoir flow simulator. Consequently, a reservoir flow simulator called IFLO is provided with this text. Many of the terms used in this section to describe IFLO are discussed in more detail in subsequent chapters.

The integrated flow model IFLO is a pseudomiscible, multicomponent, multidimensional fluid flow simulator [Fanchi, 2000]. IFLO is called an integrated flow model because it integrates a petrophysical model into a traditional flow simulator. This integration makes it possible to integrate data from such disciplines as geology, geophysics, petrophysics and petroleum engineering in a single software package.

IFLO can be used to model isothermal, Darcy flow in up to three dimensions. It assumes that reservoir fluids can be described by up to

three fluid phases (oil, gas, and water) with physical properties that depend on pressure and, to an extent, composition. Natural gas and injected solvent are allowed to dissolve in both the oil and water phases. IFLO includes a petrophysical algorithm that allows the calculation of reservoir geophysical attributes that make it possible to track changes in seismic variables as a function of time, and to perform geomechanical calculations. A coal gas desorption option is available for modeling coalbed methane production.

IFLO is a modified and significantly expanded version of MASTER, a black oil simulator with multicomponent, pseudomiscible options for modeling carbon dioxide or nitrogen flooding [Ammer, et al., 1991]. MASTER is an improved version of BOAST, a reservoir flow simulator that was published by the U.S. Department of Energy in 1982 [Fanchi, et al., 1982]. IFLO includes several enhancements to MASTER, including algorithms from BOAST, its successor BOAST II [Fanchi, et al., 1987], and several new features that are unique to IFLO.

A variety of useful geoscience, geomechanical, and reservoir engineering features are available in IFLO. Well modeling features include the representation of horizontal or deviated wells, a well productivity index calculation option, and a stress-dependent permeability model for improving the calculation of well and reservoir flow performance. Petrophysical features include improvements for modeling heterogeneous reservoir characteristics and a petrophysical model for calculating geophysical and geomechanical properties. The calculation of reservoir geophysical information can be used to model seismic data, including time-lapse seismic surveys. A coal gas production model is also available.

More technical information about the features in IFLO is provided throughout the text. Many of the exercises in the text will help you learn how to use the IFLO options. The exercises guide you through the application of IFLO to a wide range of important reservoir engineering problems.

1.4 Outline of the Text

The remainder of the text is organized as follows. Part I presents a primer on reservoir engineering. The primer is designed to provide background concepts and terminology in the reservoir engineering aspects of fluid flow in porous media. If you are already familiar with multiphase fluid flow concepts, you should review the exercises in Part I to learn more about IFLO features.

Material in Part II explains the concepts and terminology of reservoir flow simulation. Several exercises in Parts I and II use different sections of the user's manual presented in Part III. A typical exercise asks you to find and change data records in a specified example data file. These records of data must be modified based on an understanding of the reservoir problem and a familiarity with the accompanying computer program IFLO. If you work all the exercises, you will be familiar with the user's manual and IFLO by the time you have finished. Much of the experience gained by running IFLO is applicable to other flow simulators.

Exercises

Exercise 1.1 What is the primary objective of reservoir management?

Exercise 1.2 A three-dimensional, three-phase reservoir simulator (IFLO) is included with this book. Prepare a folder on your hard drive for running IFLO using the following procedure.

Copy all IFLO files to a folder on your hard drive before running the simulator. A good name for the folder is "path\IFLO". Path signifies the drive and directory path to the new folder. Copy all files for this book to the new directory. Some of the files may be labeled "Read Only" when you copy the files to your hard drive. To remove this restriction,

select the file(s) and change the properties of the file(s) by removing the check symbol adjacent to the "Read Only" attribute.

What is the size of the executable file IFLO.EXE in megabytes (MB)?

Exercise 1.3 Several example data files are provided with IFLO. Copy all files to the \IFLO folder on your hard drive using the procedure in Exercise 1.2. Make a list of the data files (files with the extension "dat"). Unless stated otherwise, all exercises assume IFLO and its data files reside in the \IFLO directory.

Exercise 1.4 The program IFLO runs the file called "itemp.dat". To run a new data file, such as newdata.dat, copy newdata.dat to itemp.dat. In this exercise, copy rim_2d.dat to itemp.dat and run IFLO by double clicking on the IFLO.EXE file on your hard drive. Select option "Y" to write the run output to files. When the program ends, it will print "STOP." Close the IFLO window. You do not need to save changes. Open run output file itemp.rof and find the line reading "MAX # OF AUTHORIZED GRID BLOCKS." How many gridblocks are you authorized to use with the simulator provided with this book?

Exercise 1.5 The program 3DVIEW may be used to view the reservoir structure associated win IFLO data files. 3DVIEW is a visualization program that reads IFLO output files with the extension "arr". To view a reservoir structure, proceed as follows:

Use your file manager to open your folder containing the IFLO files. Unless stated otherwise, all mouse clicks use the left mouse button.

a. Start 3DVIEW (Double click on the application entitled 3DVIEW.EXE)
b. Click on the button "File".

c. Click on “Open Array File”.
d. Click on “ITEMP.ARR” in the file list.
e. Click on “OK”.

At this point you should see a structure in the middle of the screen. The structure is an anticlinal reservoir with a gas cap and oil rim. To view different perspectives of the structure, hold the left mouse button down and move the mouse. With practice, you can learn to control the orientation of the structure on the screen.

The gridblock display may be smoothed by clicking on the “Project” button and selecting “Smooth Model Display”. The attribute shown on the screen is pressure “P”. To view other attributes, click on the “Model” button, set the cursor on “Select Active Attribute” and then click on oil saturation “SO”. The oil rim should be visible on the screen.

To exit 3DVIEW, click on the “File” button and then click “Exit”.

Chapter 2

Basic Reservoir Analysis

The tasks associated with basic reservoir analyses provide information that is needed to prepare input data for a simulation study. These tasks include volumetric analysis, material balance analysis, and decline curve analysis. In addition to providing estimates of fluids in place and forecasts of fieldwide production, they also provide an initial concept of the reservoir which can be used to design a model study. Each of these tasks is outlined below.

2.1 Volumetrics

Fluid volumes in a reservoir are values that can be obtained from a variety of sources, and therefore serve as a quality control point at the interface between disciplines. Volumetric analysis is used to determine volume from static information [see, for example, Tearpock, et al. 2002; Dake, 2001; Towler, 2002; Walsh and Lake, 2003; Craft, et al., 1991; Mian, 1992]. Static information is information that is relatively constant with respect to time, such as reservoir volume and original saturation and pressure distributions. By contrast, dynamic information such as pressure changes and fluid production is information that changes with respect to time. Material balance and reservoir flow modeling techniques use dynamic data to obtain original fluid volumes. An accurate characterization of the reservoir should yield consistent estimates of fluid volumes that

are originally in place in the reservoir regardless of the method chosen to determine the fluid volumes. In this section, we present the equations for volumetric estimates of original oil and gas in place. Material balance is considered in the next section.

Original oil in place (OOIP) in an oil reservoir is given by

$$N = \frac{7758\phi A h_o S_{oi}}{B_{oi}} \tag{2.1}$$

where

N original oil in place (STB)

ϕ reservoir porosity (fraction)

A reservoir area (acres)

h_o net thickness of oil zone (feet)

S_{oi} initial reservoir oil saturation (fraction)

B_{oi} initial oil formation volume factor (RB/STB)

Associated gas, or gas in solution, is the product of solution gas-oil ratio R_{so} and original oil in place N.

Original free gas in place for a gas reservoir is given by

$$G = \frac{7758\phi A h_g S_{gi}}{B_{gi}} \tag{2.2}$$

where

G original free gas in place (SCF)

h_g net thickness of gas zone (feet)

S_{gi} initial reservoir gas saturation (fraction)

B_{gi} initial gas formation volume factor (RB/SCF)

Equation (2.2) is often expressed in terms of initial water saturation S_{wi} by writing $S_{gi} = 1 - S_{wi}$. Initial water saturation is usually determined by well log or core analysis.

2.2 IFLO Volumetrics

The reservoir flow simulator IFLO accompanying this book calculates reservoir volume using the following procedure. The reservoir is modeled by subdividing the reservoir volume into an array, or grid, of smaller volume elements (Figure 2-1). Many names are used to denote the individual volume elements: for example, gridblock, cell, or node. The set of all volume elements is known by such names as grid or mesh.

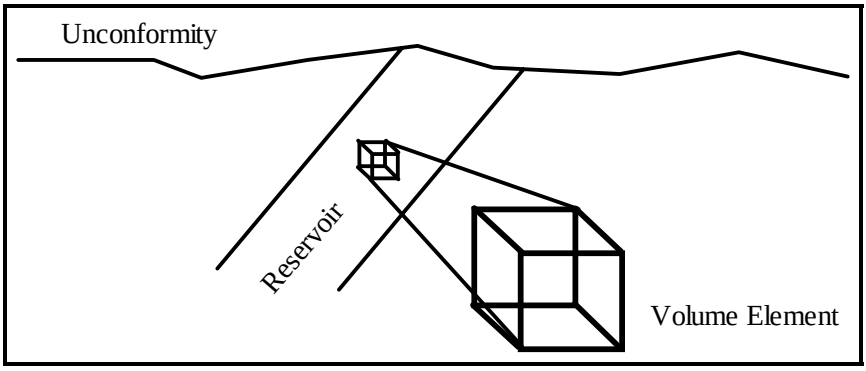

Figure 2-1. Subdivide reservoir into volume elements

Bulk volume V_B of each gridblock defined in a Cartesian coordinate system $\{x, y, z\}$ is calculated from the gross thickness $\Delta z = h$ of each gridblock and the gridblock lengths Δx, Δy along the x and y axes:

$$V_B = h \, \Delta x \, \Delta y \tag{2.3}$$

Porosity ϕ and net-to-gross ratio η are then used to calculate gridblock pore volume

$$V_P = \phi \eta V_B = \phi \eta h \Delta x \Delta y = \phi h_{net} \Delta x \Delta y \tag{2.4}$$

where net thickness is defined by $h_{net} = \eta h$. The volume of phase ℓ in the gridblock at reservoir conditions is the product of the gridblock pore volume and phase saturation, thus

$$V_\ell = S_\ell V_P = S_\ell \phi h_{net} \Delta x \Delta y \tag{2.5}$$

where S_ℓ is the saturation of phase ℓ. Total model volumes are calculated by summing over all gridblocks.

A comparison of reservoir simulator calculated volumetrics with volumetrics from another source, such as a material balance study or a computer mapping package, provides a means of validating volumetric estimates using independent sources.

2.3 Material Balance

The law of conservation of mass is the basis of material balance calculations. Material balance is an accounting of material entering or leaving a system. The calculation treats the reservoir as a large tank of material and uses quantities that can be measured to determine the amount of a material that cannot be directly measured. Measurable quantities include cumulative fluid production volumes for oil, water, and gas phases; accurate reservoir pressures; and fluid property data from samples of produced fluids.

Material balance calculations may be used for several purposes. They provide an independent method of estimating the volume of oil, water and gas in a reservoir for comparison with volumetric estimates. The magnitude of various factors in the material balance equation indicates the relative contribution of different drive mechanisms at work in the reservoir. Material balance can be used to predict future reservoir performance and aid in estimating cumulative recovery efficiency. More discussion of these topics can be found in references such as Dake [2001], Craft, et al. [1991], Ahmed [2000], Towler [2002], and Pletcher [2002].

The form of the material balance equation depends on whether the reservoir is predominately an oil reservoir or a gas reservoir. Each of these cases is considered separately.

2.3.1 Oil Reservoir Material Balance

The general material balance equation for an oil reservoir is the Schilthuis material balance equation [1961] expressed in a form given by Guerrero [1966]:

$$
\begin{aligned}
&N\left(B_t - B_{ti}\right) + NmB_{ti}\left(\frac{B_{gc} - B_{gi}}{B_{gi}}\right) \\
&+ N\frac{B_{ti}S_{wio}}{1 - S_{wio}}\left(\frac{B_{tw} - B_{twi}}{B_{twi}}\right) \\
&+ N\frac{mB_{ti}S_{wig}}{1 - S_{wig}}\left(\frac{B_{tw} - B_{twi}}{B_{twi}}\right) \\
&+ N\left(\frac{1}{1 - S_{wio}} + \frac{m}{1 - S_{wig}}\right)B_{ti}c_f\Delta P \\
&= N_p B_o - N_p R_{so} B_g \\
&+ \left[G_{ps}B_g + G_{pc}B_{gc} - G_i B_g{}'\right] \\
&- \left(W_e + W_i - W_p\right)B_w
\end{aligned}
\tag{2.6}
$$

This equation is derived by conserving volume and is referred to as the volumetric material balance by Dake [2001]. An illustration is shown in Section 18.5. All of the terms in Eq. (2.6) are defined in the Nomenclature table provided at the end of this chapter. The unit of each quantity is presented in square brackets in the Nomenclature table. The physical significance of the terms in Eq. (2.6) can be displayed by first defining the terms

$$
\begin{aligned}
D_o &= B_t - B_{ti}, \\
D_{go} &= mB_{ti}\left(\frac{B_{gc} - B_{gi}}{B_{gi}}\right), \\
D_w &= \frac{B_{ti}S_{wio}}{1 - S_{wio}}\left(\frac{B_{tw} - B_{twi}}{B_{twi}}\right), \\
D_{gw} &= \frac{mB_{ti}S_{wig}}{1 - S_{wig}}\left(\frac{B_{tw} - B_{twi}}{B_{twi}}\right), \\
D_r &= \left(\frac{1}{1 - S_{wio}} + \frac{m}{1 - S_{wig}}\right)B_{ti}c_f \Delta P
\end{aligned}
\tag{2.7}
$$

Substituting Eq. (2.7) in Eq. (2.6) gives the general material balance equation in the form

$$
\begin{aligned}
& N\left[D_o + D_{go} + D_w + D_{gw} + D_r\right] = N_p B_o \\
& - \quad N_p R_{so} B_g + \left[G_{ps} B_g + G_{pc} B_{gc} - G_i B_g{}'\right] \\
& - \quad \left(W_e + W_i - W_p\right)B_w
\end{aligned}
\tag{2.8}
$$

The terms in Eq. (2.8) have a physical significance. The terms on the right hand side of Eq. (2.8) represent fluid production and injection, while the terms on the left hand side represent volume changes. The physical significance of each term is summarized in Table 2-1.

Equation (2.6) is considered a general material balance equation because it can be applied to an oil reservoir with a gas cap and an aquifer. The derivation of the material balance equation is based on several assumptions: the system is in pressure equilibrium; the system is isothermal; available fluid property data are representative of reservoir fluids; production data is reliable; and gravity segregation of phases can be neglected. A discussion of the relative importance of drive mechanisms obtained from Eq. (2.6) is presented in Chapter 7.

Table 2-1
Physical Significance of Material Balance Terms

Term	Physical Significance
ND_o	Change in volume of initial oil and associated gas
ND_{go}	Change in volume of free gas
$N(D_w + D_{gw})$	Change in volume of initial connate water
ND_r	Change in formation pore volume
N_pB_o	Cumulative oil production
$N_pR_{so}B_g$	Cumulative gas produced in solution with oil
$G_{ps}B_g$	Cumulative solution gas produced as evolved gas
$G_{pc}B_{gc}$	Cumulative gas cap gas production
G_iB_g'	Cumulative gas injection
W_eB_w	Cumulative water influx
W_iB_w	Cumulative water injection
W_pB_w	Cumulative water production

2.3.2 Gas Reservoir Material Balance

The general material balance equation for a gas reservoir can be derived from Eq. (2.6) by first recognizing that the relationship

$$GB_{gi} = NmB_{ti} \tag{2.9}$$

defines original gas in place G. Substituting Eq. (2.9) into Eq. (2.6) gives the general material balance equation

$$
\begin{aligned}
&N\left(B_t - B_{ti}\right) + GB_{gi}\left(\frac{B_{gc} - B_{gi}}{B_{gi}}\right) \\
&+ N\frac{B_{ti}S_{wio}}{1 - S_{wio}}\left(\frac{B_{tw} - B_{twi}}{B_{twi}}\right) \\
&+ G\frac{B_{gi}S_{wig}}{1 - S_{wig}}\left(\frac{B_{tw} - B_{twi}}{B_{twi}}\right) \\
&+ \left(\frac{NB_{ti}}{1 - S_{wio}} + \frac{GB_{gi}}{1 - S_{wig}}\right)c_f \Delta P \\
&= N_p B_o + \left[G_{ps}B_g + G_{pc}B_{gc} - G_i B_g'\right] \\
&- N_p R_{so} B_g - \left(W_e + W_i - W_p\right)B_w
\end{aligned}
\tag{2.10}
$$

Equation (2.10) is further simplified by recognizing that the material balance for a gas reservoir does not include oil in place so that $N = 0$ and $N_p = 0$. The resulting material balance equation is

$$
\begin{aligned}
&GB_{gi}\left(\frac{B_{gc} - B_{gi}}{B_{gi}}\right) + G\frac{B_{gi}S_{wig}}{1 - S_{wig}}\left(\frac{B_{tw} - B_{twi}}{B_{twi}}\right) \\
&+ \left(\frac{GB_{gi}}{1 - S_{wig}}\right)c_f \Delta P = \left[G_{pc}B_{gc} - G_i B_g'\right] \\
&- \left(W_e + W_i - W_p\right)B_w
\end{aligned}
\tag{2.11}
$$

Water compressibility and formation compressibility are relatively small compared to gas compressibility. Consequently, Eq. (2.11) is often written in the simplified form

$$
\begin{aligned}
&GB_{gi}\left(\frac{B_{gc} - B_{gi}}{B_{gi}}\right) = \left[G_{pc}B_{gc} - G_i B_g'\right] \\
&- \left(W_e + W_i - W_p\right)B_w
\end{aligned}
\tag{2.12}
$$

2.4 Decline Curve Analysis

Arps [1945] studied the relationship between flow rate and time for producing wells. Assuming constant flowing pressure, he found the relationship:

$$\frac{dq}{dt} = -aq^{n+1} \tag{2.13}$$

where a and n are empirically determined constants. The empirical constant n ranges from 0 to 1.

Solutions to Eq. (2.13) show the expected decline in flow rate as the production time increases. Fitting an equation of the form of Eq. (2.13) to flow rate data is referred to as decline curve analysis. Three decline curves have been identified based on the value of n.

The *exponential decline* curve corresponds to $n = 0$. It has the solution

$$q = q_i e^{-at} \tag{2.14}$$

where q_i is initial rate and a is a factor that is determined by fitting Eq. (2.14) to well or field data.

The *hyperbolic decline* curve corresponds to a value of n in the range $0 < n < 1$. The rate solution has the form

$$q^{-n} = nat + q_i^{-n} \tag{2.15}$$

where q_i is initial rate and a is a factor that is determined by fitting Eq. (2.15) to well or field data.

The *harmonic decline* curve corresponds to $n = 1$. The rate solution is equivalent to Eq. (2.15) with $n = 1$, thus

$$q^{-1} = nat + q_i^{-1} \tag{2.16}$$

where q_i is initial rate and a is a factor that is determined by fitting Eq. (2.16) to well or field data.

Decline curves are fit to actual data by plotting the logarithm of observed rates versus time t. The semilog plot yields the following equation for exponential decline:

$$\ln q = \ln q_i - at \tag{2.17}$$

Equation (2.17) has the form $y = mx + b$ for a straight line with slope m and intercept b. In the case of exponential decline, time t corresponds to the independent variable x, $\ln q$ corresponds to the dependent variable y, $\ln q_i$ is the intercept b, and $-a$ is the slope m of the straight line. Cumulative production for decline curve analysis is the integral of the rate from the initial rate q_i at time $t = 0$ to the rate q at time t. For example, the cumulative production for the exponential decline case is

$$N_p = \int_0^t q\,dt = \frac{q_i - q}{a} \tag{2.18}$$

The decline factor a is for the exponential decline case and is found by rearranging Eq. (2.17), thus

$$a = -\frac{1}{t}\ln\frac{q}{q_i} \tag{2.19}$$

2.5 IFLO Application: Depletion of a Gas Reservoir

The material balance equation for a depletion drive gas reservoir can be derived from Eq. (2.12). The equation is

$$G_{pc} = \frac{\left[\left(P/Z\right)_i - \left(P/Z\right)_t\right] \times G}{\left(P/Z\right)_i} \tag{2.20}$$

where G is original free gas in place, G_{pc} is cumulative free gas produced, P is reservoir pressure and Z is the real gas compressibility factor. Subscript t indicates that the ratio P/Z should be calculated at the time t that corresponds to G_{pc} and subscript i indicates that the ratio P/Z should be calculated at the initial time. The units of G_{pc} and G must agree for the equation to be consistent.

Equation (2.20) can be used to validate the gas reservoir modeling features of a reservoir flow simulator such as IFLO if the flow

assumptions are consistent. In this case, Eq. (2.20) applies to the production of single phase gas from a gas reservoir. For example, suppose a gas reservoir has the production history shown in Table 2-2:

Table 2-2
Depletion of a Gas Reservoir

G_P (BSCF)	P (psia)	Z	P/Z (psia)
0.015	1946	0.813	2393
0.122	1934	0.813	2378
0.347	1909	0.814	2345
0.630	1874	0.815	2299
1.380	1792	0.819	2188
2.205	1698	0.823	2063
2.934	1620	0.828	1956
3.309	1578	0.830	1901
4.059	1492	0.835	1787
4.434	1453	0.838	1734
4.809	1411	0.841	1678
5.475	1333	0.847	1573

where G_P is cumulative gas production, P is pressure, and Z is the gas compressibility factor. Figure 2-2 is a plot of G_P versus P/Z. The original gas in place (OGIP) is the value of G_P at $P/Z = 0$. The OGIP for this case is about 15.9 BSCF. These results can be verified by running data file EXAM8_PVTG.DAT.

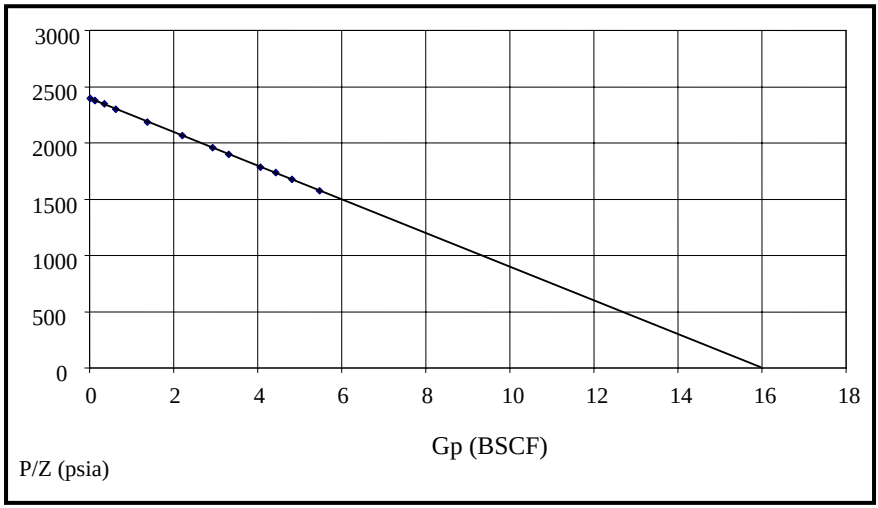

Figure 2-2. P/Z Plot for Depletion of a Gas Reservoir

Exercises

Exercise 2.1 Data file EXAM1.DAT is a material balance model of an undersaturated oil reservoir undergoing pressure depletion. Copy file EXAM1.DAT to file ITEMP.DAT and run IFLO. What are the volumes of initial fluids in place in the model? Hint: Open the run output file ITEMP.ROF to find initial fluids in place.

Exercise 2.2 Derive the material balance equation for a system with no gas cap beginning with Eqs. (2.6) and (2.7).

Exercise 2.3 Derive Eq. (2.18) for the exponential decline case by using Eq. (2.14) as the integrand and performing the integration.

Exercise 2.4A A formation consists of 20 feet of impermeable shale and 80 feet of permeable sandstone. What is the gross thickness of the formation?

Exercise 2.4B What is the net-to-gross ratio of the formation?

Exercise 2.5A Show that $q = q_i e^{-at}$ is a solution of the decline curve equation $dq/dt = -aq^{n+1}$ for the exponential decline case.

Exercise 2.5B Plot oil flow rate as a function of time for a well that produces 10,000 barrels per day with a decline factor a = 0.06 per year. Time should be expressed in years, and should range from 0 to 50 years.

Exercise 2.5C When does the flow rate drop below 1000 barrels per day?

Exercise 2.6A Show that $q^{-1} = at + q_i^{-1}$ is a solution of $\frac{dq}{dt} = -aq^2$ where a, q_i are constants?

Exercise 2.6B What is the value of q at $t = 0$?

Exercise 2.7 A barrier island is a large sand body. Consider a barrier island that averages 3 miles wide, 10 miles long, and is 30 feet thick. The porosity of the sand averages almost 25%. What is the pore volume of the barrier island? Express your answer in barrels and cubic meters.

Exercise 2.8 Use Eq. (2.12) to derive Eq. (2.20).

Exercise 2.9A The results shown in Table 2-2 were obtained from data file EXAM8_PVTG.DAT. Verify that the OGIP for the model is about 15.9 BSCF by running EXAM8_PVTG.DAT and finding the OGIP in WTEMP.ROF. How much oil and water were originally in place?

Exercise 2.9B Assume that the reservoir with the production history given in Table 2-2 is abandoned at pressure P_a = 1657 psia with Z_a = 0.826. Estimate cumulative gas production at abandonment from a graph of P/Z versus G_p (Figure 2-2).

Exercise 2.9C Run EXAM8_PVTG.DAT and determine the cumulative gas production at a pressure of 1657 psia from the timestep summary file ITEMP.TSS. How does this result compare to the value of cumulative gas production found in Part B?

Nomenclature for Equation (2.6)

B_g	gas formation volume factor (FVF) (RB/SCF)
B_{gc}	gas cap FVF (RB/SCF)
B_g'	injected gas FVF (RB/SCF)
B_o	oil FVF (RB/STB)
B_t	$B_o + (R_{si} - R_{so})B_g$ = composite oil FVF (RB/STB)
B_{tw}	$B_w + (R_{swi} - R_{sw})B_g$ = composite water FVF (RB/STB)
c_f	formation (rock) compressibility (1/psia)
G	initial gas in place (SCF)
G_i	cumulative gas injected (SCF)
G_{pc}	cumulative gas cap gas produced (SCF)
G_{ps}	cumulative solution gas produced as evolved gas (SCF)
m	ratio of gas reservoir volume to oil reservoir volume
N	initial oil in place (STB)
N_p	cumulative oil produced (STB)
R_{so}	solution gas-oil ratio (SCF/STB)
R_{si}	initial solution gas-oil ratio (SCF/STB)
R_{sw}	solution gas-water ratio (SCF/STB)
R_{swi}	initial solution gas-water ratio (SCF/STB)
S_g	gas saturation (fraction)
S_o	oil saturation (fraction)
S_w	water saturation (fraction)
S_{wi}	initial water saturation (fraction)
S_{wig}	initial water saturation in gas cap (fraction)
S_{wio}	initial water saturation in oil zone (fraction)
W_e	cumulative water influx (STB)
W_i	cumulative water injected (STB)
W_p	cumulative water produced (STB)
ΔP	$P_i - P$ = reservoir pressure change (psia)
P_i	initial reservoir pressure (psia)
P	reservoir pressure corresponding to cumulative fluid times (psia)

Chapter 3

Multiphase Flow Concepts

Several basic concepts are needed to understand multiphase flow. They include interfacial tension, wettability, and contact angle. These concepts lead naturally to a discussion of capillary pressure, mobility, and fractional flow.

3.1 Basic Concepts

The concepts of interfacial tension, wettability, and contact angle describe the behavior of two or more phases in relation to one another. They are defined here and then applied in later sections.

3.1.1 Interfacial Tension

On all interfaces between solids and fluids, and between immiscible fluids, there is a surface free energy resulting from electrical forces. These forces cause the surface of a liquid to occupy the smallest possible area and act like a membrane. Interfacial tension (IFT) refers to the tension between liquids at a liquid-liquid interface. Surface tension refers to the tension between fluids at a gas-liquid interface.

Interfacial tension is energy per unit of surface area, or force per unit length. The units of IFT are typically expressed in milli-Newtons per meter or the equivalent dynes per centimeter. The value of IFT depends

on the composition of the two fluids at the interface between phases. Table 3-1 lists a few examples:

Table 3-1
Examples of Interfacial Tension

Fluid Pair	IFT Range (mN/m or dyne/cm)
Air-Brine	72-100
Oil-Brine	15-40
Gas-Oil	35-65

Interfacial tension (IFT) can be estimated using the Macleod-Sugden correlation. The Weinaug-Katz variation of the Macleod-Sugden correlation is

$$\sigma^{1/4} = \sum_{i=1}^{N_c} P_{chi}\left(x_i \frac{\rho_L}{M_L} - y_i \frac{\rho_V}{M_V} \right) \tag{3.1}$$

where

σ interfacial tension (dyne/cm)

P_{chi} parachor of component i [(dynes/cm)$^{1/4}$/(g/cm^3)]

M_L molecular weight of liquid phase

M_V molecular weight of vapor phase

ρ_L liquid phase density (g/cm^3)

ρ_V vapor phase density (g/cm^3)

x_i mole fraction of component i in liquid phase

y_i mole fraction of component i in vapor phase

Parachors are empirical parameters. The parachor of component i can be estimated using the molecular weight M_i of component i and the empirical regression equation

$$P_{chi} = 10.0 + 2.92M_i \tag{3.2}$$

This procedure works reasonably well for molecular weights ranging from 100 to 500. A more accurate procedure for a wider range of molecular weights is given by Fanchi [1990].

3.1.2 Wettability

Wettability is the ability of a fluid phase to wet a solid surface preferentially in the presence of a second immiscible phase. The wetting, or wettability, condition in a rock/fluid system depends on IFT. Changing the type of rock or fluid can change IFT and, hence, the wettability of the system. Adding a chemical such as surfactant, polymer, corrosion inhibitor, or scale inhibitor can alter wettability.

3.1.3 Contact Angle

Wettability is measured by contact angle. Contact angle is always measured through the denser phase and is related to interfacial energies by

$$\sigma_{os} - \sigma_{ws} = \sigma_{ow} \cos\theta \tag{3.3}$$

where

σ_{os} interfacial energy between oil and solid (dyne/cm)

σ_{ws} interfacial energy between water and solid (dyne/cm)

σ_{ow} interfacial energy, or IFT, between oil and water (dyne/cm)

θ contact angle at oil-water-solid interface measured through the water phase (degrees)

Table 3-2 presents examples of contact angle for different wetting conditions.

Table 3-2
Examples of Contact Angle

Wetting Condition	Contact Angle (Degrees)
Strongly water-wet	0-30
Moderately water-wet	30-75
Neutrally wet	75-105
Moderately oil-wet	105-150
Strongly oil-wet	150-180

Wettability is usually measured in the laboratory. Several factors can affect laboratory measurements of wettability. Wettability can be changed by contact of the core during coring with drilling fluids or fluids on the rig floor, and by contact of the core during core handling with oxygen or water from the atmosphere. Laboratory fluids should also be at reservoir conditions to obtain the most reliable measurements of wettability. For example, a wettability measurement for an oil-water system should, in principle, use oil with dissolved gas at reservoir temperature and pressure. Based on laboratory tests, most known reservoirs have intermediate wettability and are preferentially water wet.

3.2 Capillary Pressure

Capillary pressure is the pressure difference across the curved interface formed by two immiscible fluids in a small capillary tube. The pressure difference is

$$P_c = P_{nw} - P_w \tag{3.4}$$

where

P_c capillary pressure (psi)

P_{nw} pressure in nonwetting phase (psi)

P_w pressure in wetting phase (psi)

3.2.1 Capillary Pressure Theory

Equilibrium between fluid phases in a capillary tube is satisfied by the relationship *force up = force down*. These forces are expressed in terms of the radius r of the capillary tube, the contact angle θ, and the interfacial tension σ. The forces are given by

$$\text{force up} = \text{IFT acting around perimeter of capillary tube}$$

$$= \sigma \cos\theta \times 2\pi r$$

and

$$\text{force down} = \begin{array}{l}\text{density gradient difference} \times \text{cross-sectional} \\ \text{area} \times \text{height } h \text{ of capillary rise in tube}\end{array}$$

The density gradient Γ is the weight of the fluid per unit length per unit cross-sectional area. For example, the density gradient of water Γ_w is approximately 0.433 psia/ft at standard conditions. If we assume an air-water system, the force down is

$$\text{force down} = (\Gamma_w - \Gamma_{air})\pi r^2 h$$

where the cross-sectional area of the capillary tube is πr^2. Capillary pressure P_c is defined as the force per unit area, thus

$$P_c = \text{force up} / \pi r^2 = \text{force down} / \pi r^2.$$

3.2.2 Capillary Pressure and Pore Radius

Expressing capillary pressure in terms of force up per unit area gives:

$$P_c = \frac{2\pi r \sigma \cos\theta}{\pi r^2} = \frac{2\sigma\cos\theta}{r} \tag{3.5}$$

where

r pore radius (cm)

σ interfacial (or surface) tension (mN/m or dynes/cm)

θ contact angle (degrees)

Equation (3.5) shows that an increase in pore radius will cause a reduction in capillary pressure while a decrease in IFT will cause a decrease in capillary pressure.

3.2.3 Equivalent Height

Expressing P_c in terms of force down leads to the expression

$$P_c = \frac{\pi r^2 h\left(\Gamma_w - \Gamma_{air}\right)}{\pi r^2} = h\left(\Gamma_w - \Gamma_{air}\right) \tag{3.6}$$

where

h height of capillary rise (ft)

P_c capillary pressure (psia)

Γ_w water, or wetting phase, density gradient (psia/ft)

Γ_{air} air, or nonwetting phase, density gradient (psia/ft)

Solving for h yields the defining relationship between capillary pressure P_c and equivalent height h, namely

$$h = \frac{P_c}{\left(\Gamma_w - \Gamma_{air}\right)} \tag{3.7}$$

The equivalent height is the height above the free fluid level of the wetting phase, where the free fluid level is the elevation of the

wetting phase at $P_c = 0$. For example, Ahmed [2000, pages 206-208] defines free water level as the elevation where capillary pressure equals zero at 100% water saturation and the water-oil contact is the uppermost depth in the reservoir where water saturation is 100%. Figure 3-1 illustrates these definitions.

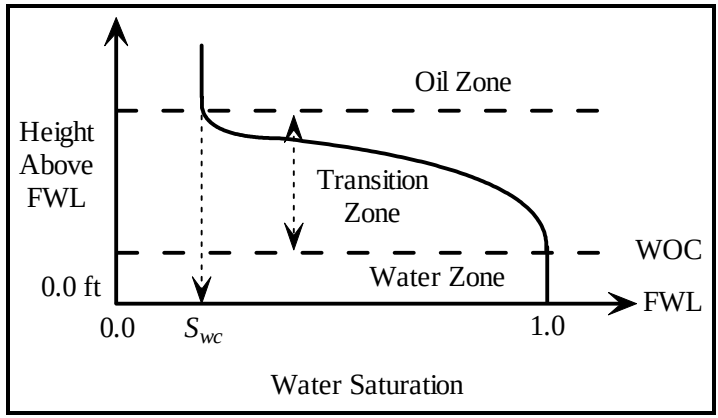

Figure 3-1. Sketch of an Oil-Water Transition Zone
Note that WOC is water-oil contact, FWL is free water level, and S_{wc} is irreducible or connate water saturation.

Equivalent height is inversely proportional to the difference in densities between two immiscible phases. The thickness of the transition zone between the wetting phase and the nonwetting phase is the difference in equivalent height between the wetting phase contact (the uppermost depth in the reservoir where wetting phase saturation is 100%) and the height where the wetting phase saturation is irreducible. For example, the thickness of the oil-water transition zone is the difference in equivalent height between the water-oil contact and the height where water saturation equals irreducible water saturation. The relatively large density difference between gas and liquid phases results in a smaller transition zone

thickness than the relatively small difference between two liquid phase densities.

The preceding definitions of free fluid level and fluid contact are based on capillary pressure. It is also possible to define free fluid level and fluid contact using measurements of formation pressure and pressure gradients in different fluid zones. The modeling team should know how free fluid levels and fluid contacts are defined to avoid confusion.

3.2.4 Oil-Water Capillary Pressure

Oil is the nonwetting phase in a water-wet oil-water reservoir. Capillary pressure for an oil-water system is

$$P_{cow} = P_o - P_w \tag{3.8}$$

where

P_o pressure in the oil phase (psia)

P_w pressure in the water phase (psia)

Capillary pressure increases with height above the oil-water contact (OWC) as water saturation decreases.

3.2.5 Gas-Oil Capillary Pressure

In gas-oil systems, gas usually behaves as the nonwetting phase and oil is the wetting phase. Capillary pressure between oil and gas in such a system is

$$P_{cgo} = P_g - P_o \tag{3.9}$$

where

P_g pressure in the gas phase (psia)

P_o pressure in the oil phase (psia)

Capillary pressure increases with height above the gas-oil contact (GOC) as gas saturation decreases.

3.2.6 Capillary Pressure Correction

The proper way to include capillary pressure in a flow model study is to correct laboratory measured values to reservoir conditions. This is done by applying the correction:

$$P_{c(res)} = P_{c(lab)}\eta_{corr}\,,\ \eta_{corr} \equiv \frac{\left(\sigma|\cos\theta|\right)_{res}}{\left(\sigma|\cos\theta|\right)_{lab}} \tag{3.10}$$

where σ is interfacial tension (IFT), and θ is wettability angle [Amyx, et al., 1960]. The subscripts *lab* and *res* refer to laboratory conditions and reservoir conditions respectively. If laboratory measurements of IFT are not available, IFT can be estimated from the Macleod-Sugden correlation for pure compounds or the Weinaug-Katz correlation for mixtures [Fanchi, 1990].

A problem with the capillary correction in Eq. (3.10) is that it requires data that are often poorly known, namely interfacial tension and wettability contact angle at reservoir conditions. Rao and Girard [1997] have described a laboratory technique for measuring wettability using live fluids at reservoir temperature and pressure. Alternative approaches include adjusting capillary pressure curves to be consistent with well log estimates of transition zone thickness, or assuming the contact angle factors out.

3.2.7 Leverett's *J*-Function

Rock samples with different pore-size distribution, permeability, and porosity will yield different capillary pressure curves.

Leverett's *J*-function is a technique for correlating capillary pressure to water saturation and rock properties. Leverett's *J*-function is

$$J(S_w) = \frac{P_{c(lab)}}{\sigma_{lab}\left|(\cos\theta)_{lab}\right|}\left(\sqrt{\frac{K}{\phi}}\right)_{lab} \tag{3.11}$$

where

$P_{c(lab)}$ Laboratory measured capillary pressure (psia)

$J(S_w)$ Leverett's *J*-function

K Core sample permeability (md)

ϕ Porosity (fraction)

σ_{lab} Laboratory value of IFT (dyne/cm)

θ_{lab} Laboratory value of contact angle

Given $J(S_w)$, we can estimate capillary pressure at reservoir conditions as

$$P_{c(res)} = \frac{\sigma_{res}\left|(\cos\theta)_{res}\right|}{\left(\sqrt{\frac{K}{\phi}}\right)_{res}} J(S_w) \tag{3.12}$$

where the value of $J(S_w)$ is obtained from the smooth curve constructed by the procedure in Table 3-3.

Table 3-3
Leverett's *J*-function Procedure

Step	Task
A	Calculate $J(S_w)$ for each capillary pressure point
B	Plot $J(S_w)$ versus water saturation for all points
C	Draw a smooth curve through the points

3.3 Relative Permeability

Relative permeability is used to describe multiphase fluid flow. The general definition of relative permeability is

$$k_r = \frac{k_{eff}}{k_{abs}} \tag{3.13}$$

where

k_r relative permeability between 0 and 1,

k_{eff} effective permeability (md)

k_{abs} absolute permeability (md)

Fluid phase relative permeabilities for oil, water and gas phases, respectively, are

$$k_{ro} = k_o / k, k_{rw} = k_w / k, k_{rg} = k_g / k \tag{3.14}$$

The variable k_ℓ is the effective permeability of phase ℓ for subscript ℓ denoting oil o, water w, or gas g. The relative permeability of phase ℓ is $k_{r\ell}$, and *k* is absolute permeability. Figure 3-2 shows a typical set of relative permeability curves.

Changes in the wettability conditions of the core can significantly affect relative permeability. Ideally, relative permeability should be measured in the laboratory under the same conditions of wettability that exist in the reservoir. One way to approximate this ideal is to use preserved, native state core samples. In practice, most relative permeability data are obtained using restored state cores in the laboratory.

Relative permeability data should be obtained by experiments that best model the type of displacement that is thought to dominate reservoir flow performance. For example, water-oil imbibition curves are representative of waterflooding, while water-oil

drainage curves describe the movement of oil into a water zone. The dependence of relative permeability on the history of saturation changes is called hysteresis. Relative permeability hysteresis effects can be included in some reservoir flow models (for example, see Killough [1976], Dake [2001], Carlson [2003]).

Relative permeability data are often measured and reported for laboratory analysis of several core samples from one or more wells in a field. The set of relative permeability curves should be sorted by lithology and averaged to determine a representative set of curves for each rock type. Several procedures exist for averaging relative permeability data [for example, see Schneider, 1987; Mattax and Dalton, 1990; Blunt, 1999; Fanchi, 2000].

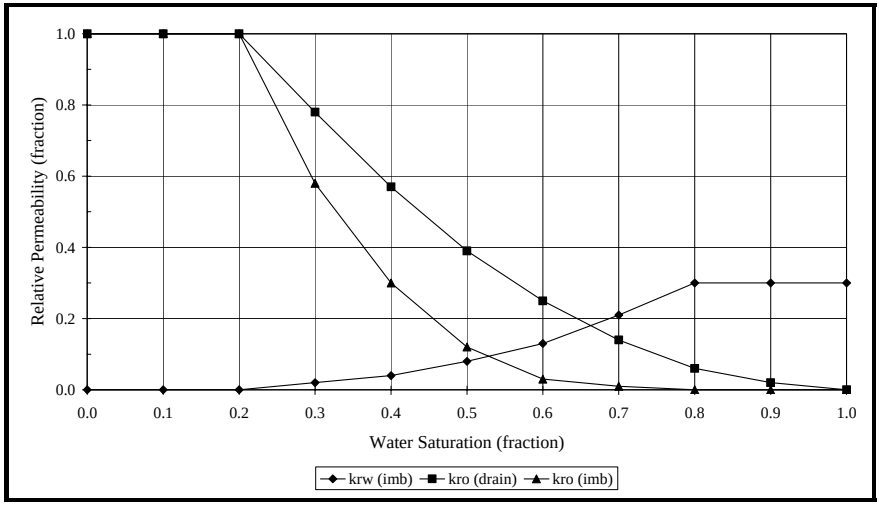

Figure 3-2. Typical Water-Oil Relative Permeability Curves

3.4 Mobility and Fractional Flow

Mobility is a measure of the ability of a fluid to move through interconnected pore space. Fractional flow is the ratio of the volume of

one phase flowing to the total volume flowing in a multiphase system. These concepts are defined here.

3.4.1 Mobility

Fluid phase mobility is defined as the ratio of effective phase permeability to phase viscosity. Mobility for oil, water and gas phases respectively are

$$\lambda_o = \frac{k_o}{\mu_o}, \lambda_w = \frac{k_w}{\mu_w}, \lambda_g = \frac{k_g}{\mu_g} \tag{3.15}$$

where μ_ℓ is the viscosity of phase ℓ. Relative mobility is defined as relative permeability divided by viscosity [Dake, 1978]. Absolute permeability is not a factor in the definition of relative mobility.

3.4.2 Mobility Ratio

Mobility ratio is defined as the mobility of the displacing fluid λ_D behind the front divided by the mobility of the displaced fluid λ_d ahead of the front, thus

$$M = \frac{\lambda_D}{\lambda_d} \tag{3.16}$$

An example of mobility ratio is the mobility ratio of water to oil for a waterflood:

$$M_{w,o} = \frac{(\lambda_w)_{S_{or}}}{(\lambda_o)_{S_{wc}}} = \frac{k_{rw}(S_{or})/\mu_w}{k_{ro}(S_{wc})/\mu_o} \tag{3.17}$$

In this case, relative permeability to water is evaluated at residual oil saturation S_{or}, and relative permeability to oil is evaluated at connate water saturation S_{wc}. Notice that absolute permeability factors out of the expression for mobility ratio. Consequently, mobility ratio can be calculated using either mobilities or relative mobilities.

3.4.3 Fractional Flow

The fractional flow of water is the ratio of water production rate to total production rate. In the case of an oil-water system, the fractional flow of water is given by

$$f_w = \frac{q_w}{q_t} = \frac{q_w}{q_w + q_o} \tag{3.18}$$

where

f_w fractional flow of water

q_w water volumetric flow rate (RB)

q_o oil volumetric flow rate (RB)

q_t total volumetric flow rate (RB)

Notice that the flow rates are expressed in terms of reservoir volumes. The fractional flow of oil f_o and the fractional flow of water are related by f_w= 1 - f_o for an oil-water system. Based on the definition of fractional flow, we see that fractional flow should have a value between 0 and 1.

3.4.4 Simplified Fractional Flow Equation

A simplified fractional flow equation is obtained by replacing flow rates with Darcy's Law in the definition of fractional flow. If we neglect gravity, Darcy's Law in one spatial dimension is

$$q_\ell = -\frac{kk_{r\ell}A}{\mu_\ell}\frac{\partial P_\ell}{\partial x} \tag{3.19}$$

where A is cross-sectional area and P_ℓ is the pressure of phase ℓ. Darcy's law says that flow rate is proportional to pressure gradient. The minus sign shows that the direction of flow is opposite to the direction of increasing pressure.

If we neglect capillary pressure, we have the equality of phase pressures $P_w = P_o$. Substituting Eq. (3.19) into Eq. (3.18) and neglecting capillary pressure gives

$$f_w = \frac{\dfrac{k_{rw}}{\mu_w}}{\dfrac{k_{rw}}{\mu_w} + \dfrac{k_{ro}}{\mu_o}} \tag{3.20}$$

Equation (3.20) can be expressed in terms of mobilities as

$$f_w = \frac{1}{1 + \dfrac{k_{ro}}{k_{rw}} \dfrac{\mu_w}{\mu_o}} = \frac{1}{1 + \dfrac{\lambda_o}{\lambda_w}} \tag{3.21}$$

The construction of Eq. (3.21) is based on the following simplifying assumptions: Darcy's Law adequately describes flow rate, and capillary pressure and gravity are negligible. Given these assumptions, we can calculate f_w at reservoir conditions.

3.4.5 Fractional Flow Equation with Gravity

Gravity can be included in the fractional flow equation as follows. First, let us consider the two-phase flow of oil and water in a tilted linear system. Darcy's Law, including capillary pressure and gravity effects for linear flow, is

$$\begin{aligned} q_w &= -\frac{kk_{rw}A}{\mu_w}\left(\frac{\partial P_w}{\partial x} + \rho_w g \sin\alpha\right) \\ q_o &= -\frac{kk_{ro}A}{\mu_o}\left(\frac{\partial P_o}{\partial x} + \rho_o g \sin\alpha\right) \end{aligned} \tag{3.22}$$

where

α dip angle of formation

g gravitational constant

If we differentiate capillary pressure for a water-wet system with respect to position x along the dipping bed, we find

$$\frac{\partial P_{cow}}{\partial x} = \frac{\partial P_o}{\partial x} - \frac{\partial P_w}{\partial x} \tag{3.23}$$

Combining Eqs. (3.22) and (3.23) gives

$$\frac{\partial P_{cow}}{\partial x} = -\frac{(q_t - q_w)\mu_o}{Akk_{ro}} - \rho_o g \sin\alpha + \frac{q_w \mu_w}{Akk_w} + \rho_w g \sin\alpha \tag{3.24}$$

where we have used $q_t = q_o + q_w$. If we write the density difference as

$$\Delta\rho = \rho_w - \rho_o \tag{3.25}$$

collect terms, and simplify we obtain

$$\frac{q_w}{Ak}\left(\frac{\mu_o}{k_{ro}} + \frac{\mu_w}{k_{rw}}\right) = \frac{q_t \mu_o}{Akk_{ro}} + \frac{\partial P_{cow}}{\partial x} - g\Delta\rho\sin\alpha \tag{3.26}$$

Rearranging and collecting terms gives the fractional flow to water f_w in conventional oilfield units:

$$f_w = \frac{q_w}{q_t} = \frac{1 + 0.001127\dfrac{Akk_{ro}}{\mu_o q_t}\left[\dfrac{\partial P_{cow}}{\partial x} - 0.433(\gamma_w - \gamma_o)\sin\alpha\right]}{1 + \dfrac{k_{ro}}{k_{rw}}\dfrac{\mu_w}{\mu_o}} \tag{3.27}$$

where

A cross-sectional area of flow system (ft^2)

k absolute permeability (md)

k_{ro} relative permeability to oil

k_{rw} relative permeability to water

μ_o oil viscosity (cp)

μ_w water viscosity (cp)

P_{cow} oil-water capillary pressure (psi) = P_o - P_w

x direction of linear flow (ft)

α dip angle of formation (degrees)

γ_o oil specific gravity (pure water = 1)

γ_w water specific gravity (pure water = 1)

The general expression for f_w includes all three terms governing immiscible displacement, namely the viscous term $(k_{ro}/k_{rw})(\mu_w/\mu_o)$, the capillary pressure term $\partial P_{cow}/\partial x$ and the gravity term $(\gamma_w - \gamma_o)\sin\alpha$.

It is interesting to note that the capillary pressure and gravity terms are multiplied by $1/q_t$ in Eq. (3.27). Most waterfloods have sufficiently high flow rates that capillary pressure and gravity effects can be neglected, leaving the simplified expression

$$f_w = \frac{1}{1+\dfrac{k_{ro}}{k_{rw}}\dfrac{\mu_w}{\mu_o}} \tag{3.28}$$

Equation (3.28) is in agreement with Eq. (3.21), as it should be.

3.4.6 Gas Fractional Flow

A similar analysis can be performed to determine the fractional flow of gas f_g. The result for a gas-oil system is

$$f_g = \frac{1+0.001127\dfrac{Akk_{ro}}{\mu_o q_t'}\left(\dfrac{\partial P_{cgo}}{\partial x} - 0.433(\gamma_g - \gamma_o)\sin\alpha\right)}{1+\dfrac{k_{ro}}{k_{rg}}\dfrac{\mu_g}{\mu_o}} \tag{3.29}$$

where oil phase properties are defined after Eq. (3.27) and the remaining variables are

k_{rg} relative permeability to gas

μ_g gas viscosity (cp)

P_{cgo} gas-oil capillary pressure = P_g - P_o (psi)

γ_g gas specific gravity (pure water = 1)

q_g gas volumetric flow rate (RB/day)

q_t' total volumetric flow rate = q_o + q_g (RB/day)

Immiscible displacement of oil by gas is analogous to water displacing oil with the water terms replaced by gas terms. In general, the gravity term in f_g should not be neglected unless q_t is very high because of the specific gravity difference between gas and oil.

3.5 Flow Concepts in Naturally Fractured Reservoirs

The most common types of reservoir rock are listed in Table 3-4. Siliciclastic rocks are composed of a variety of silica-based grains and may travel great differences from their source before being deposited. Carbonates form in shallow and deep marine environments and usually remain near their point of origin. In addition to sandstones and carbonates, shales are also often encountered in reservoir formations. Shales are laminated sediment and are predominantly composed of clay. They usually have negligible flow capacity and are primarily barriers to fluid flow. Uneven uplift and subsidence across a reservoir can cause natural fracturing of reservoir rock.

Table 3-4
Common Reservoir Rocks

Type	Comments
Siliciclastic	Composed of silica-based grains Formed by compacted sediment Examples: sandstone, conglomerate

Carbonates	Produced by chemical and biochemical sources Composed primarily of calcite and dolomite Examples: limestone, dolostone

Naturally fractured reservoirs are characterized by the juxtaposition of two rock types: reservoir matrix, and fractures. Reservoir matrix rock typically has a larger storage capacity than fractures, but the fractures have a larger flow capacity than the reservoir matrix. Bulk volume and porosity are typically larger in matrix rock than in fractures, while fracture permeability is typically much larger than matrix permeability. These characteristics result in two different flow regimes: the matrix flow regime and the fracture flow regime. Table 3-5 presents a classification of naturally fractured reservoirs based on fluid storage [Aguilera, 1999].

Table 3-5
Naturally Fractured Reservoir Types

Type	Storage of Fluid Volume
A	In matrix
B	In both matrix and fracture
C	In fracture

Production from a naturally fractured reservoir depends on both the matrix flow regime and the fracture flow regime. For example, most of the fluid volume in a Type A naturally fractured reservoir is stored in the matrix, and most of the fluid flow is in the fractures. Figure 3-3 is a sketch of a Type A naturally fractured reservoir with a horizontal fracture network. Horizontal fractures can also be created by hydraulic fracturing. The amount of fluid produced depends on how much fluid is in the fracture and the rate at which the fluid can enter the fracture network.

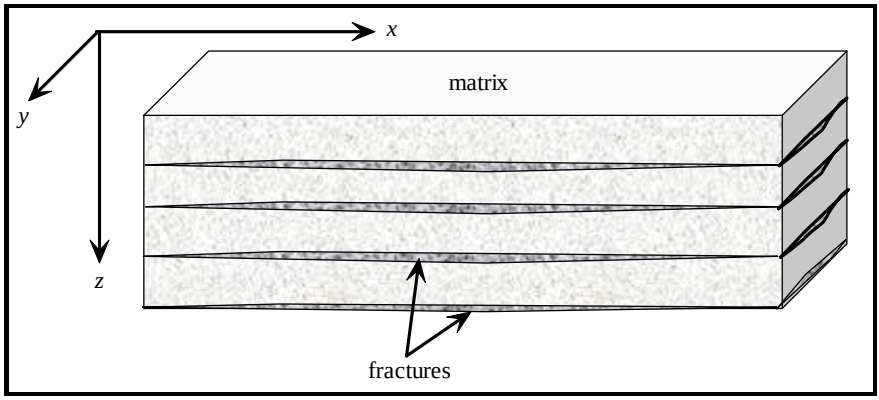

Figure 3-3. Sketch of a Naturally Fractured Reservoir with Horizontal Fractures

Production from naturally fractured reservoirs usually occurs from wells that intersect the network of interconnected fractures. Fluid flow in fractures depends on such factors as aperture size (width or diameter of the fracture), fracture orientation, net stress on the fracture, fracture permeability, and recovery mechanisms. Fluid in the matrix is usually recovered by flowing into fractures that are open to flow and in communication with a well. Fracture permeability can be diminished by mineralization. Open fractures have not undergone mineralization. Closed fractures are fractures with no permeability. Many fractures have been subjected to some mineralization and are partially open. Mechanisms for recovering fluid from the matrix-fracture system include water drive, capillary imbibition, solution gas drive, gravity drainage, gas cap expansion, and combination drive. Further discussion of recovery mechanisms in naturally fractured reservoirs is provided by Aguilera [1999], Firoozabadi [2000], Allan and Sun [2003], and references therein. These mechanisms depend on fracture capillary pressure and fracture relative permeability.

3.5.1 Fracture Capillary Pressure

Preuss and Tsang [1990] envisioned a fracture as a collection of narrow channels and assumed a log-normal distribution of aperture size.

The most probable aperture size for their log-normal distribution was 0.05 mm. The result of their study was a formula that related capillary pressure and wetting-phase saturation. Their curve for a water-oil system has the form of Leverett's *J*-function which is familiar from the study of unfractured porous media.

Firoozabadi and Hauge [1990] used a centrifuge to measure the capillary pressure across the interfaces between stacked matrix blocks. The typical aperture size was about 0.1 mm to 0.2 mm. They obtained a fracture capillary pressure curve for an oil-water system that was approximately represented by Leverett's *J*-function in accordance with the work by Preuss and Tsang [1990]. More recent discussions of fracture capillary pressure are presented by Akin [2001], and Deghmoum, et al. [2001].

3.5.2 Fracture Relative Permeability

Fracture apertures can range in size from very small to very large. When fracture apertures are very small, wall roughness and tortuosity can affect fluid flow. In this case, it is reasonable to assume that two or more flowing phases may interfere with one another as if they were confined to the pore space of an unfractured porous medium. The resulting fracture relative permeability curves will be nonlinear functions of wetting phase saturation [Preuss and Tsang, 1990]. Nonlinear relations between relative permeability and saturation have been observed by several authors, including Persoff, et al. [1991], McDonald, et al. [1991], Akin [2001], and Deghmoum, et al. [2001].

If fracture aperture size is large, two or more fluid phases can flow in the fracture without significantly interfering with each other. The resulting relative permeability curves are approximately straight lines. In the absence of experimental data to the contrary, fracture relative permeability and capillary pressure are usually assumed to be linear functions of wetting phase saturation. Fracture relative permeability curves are illustrated in Figure 3-4 for an oil-water system.

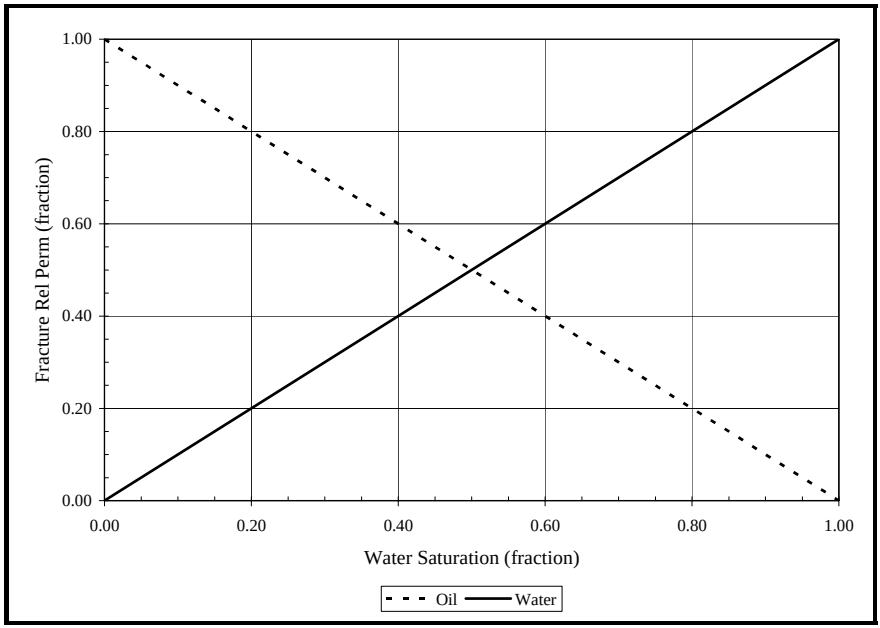

Figure 3-4. Illustration of Relative Permeability in a Fracture

Exercises

Exercise 3.1 Estimate the parachors for butane and decane.

Exercise 3.2A Derive the relationship between the equivalent height of a transition zone and pore radius by using Eq. (3.5) to eliminate capillary pressure from Eq. (3.7).

Exercise 3.2B Will the height of a transition zone be greater for a reservoir with small pore throats or large pore throats?

Exercise 3.3 Suppose $k_{rw}\,(S_{or}) \approx k_{ro}\,(S_{wc})$ in Eq. (3.17) and water viscosity is 1 cp. Plot $M_{w,o}$ versus oil viscosity for oil viscosity ranging from 0.1 cp to 100 cp.

Exercise 3.4 Derive Eq. (3.20) by neglecting gravity and substituting Eq. (3.19) into Eq. (3.18).

Exercise 3.5 Derive Eq. (3.24) from Eqs. (3.22) and (3.23).

Exercise 3.6 Suppose the density gradient for water is 0.43 psia/ft and the density gradient for oil is 0.35 psia/ft. What is the equivalent height of a water-oil transition zone if capillary pressure is 16 psia?

Exercise 3.7A Oil recovery by capillary imbibition of water into a matrix block from a fracture can be estimated from the relationship $R = R_\infty \left[1 - \exp\left(-\lambda t\right)\right]$ where R is oil recovery at time t, R_∞ is the limit toward which recovery converges, and λ is a constant specifying the rate of convergence towards the asymptotic limit. Plot oil recovery from a core versus time using data from the following table:

Time (hours)	0	5	10	15	20	30	40	60	80	100
Rec. (%)	0.0	3.8	8.1	10.9	13.1	16.0	17.8	18.7	19.2	19.4

Exercise 3.7B From the figure in Part A, determine R_∞.

Exercise 3.7C Find a value of λ by fitting $R = R_\infty \left[1 - \exp\left(-\lambda t\right)\right]$ to the data.

Exercise 3.7D Given R_∞ and your value of λ, calculate R at 10 hours, 20 hours, and 40 hours.

Exercise 3.8 Data file XS_FRACTURE.DAT is a cross-section model of a naturally fractured reservoir with a horizontal fracture network. Open the file and determine the porosity and lateral permeability of each layer in the model. What is the flow regime of each layer: matrix or fracture? Hint: fill in a table with the following form:

Layer	**Porosity**	**Lateral Permeability (md)**	**Flow Regime**
1			

Chapter 4

Fluid Displacement

Fluid displacement processes require contact between the displacing fluid and the displaced fluid. The movement of the interface between displacing and displaced fluids and the breakthrough time associated with the production of injected fluids at producing wells are indicators of sweep efficiency. This chapter shows how to calculate such indicators using two analytical techniques: the Buckley-Leverett theory with Welge's method for immiscible fluid displacement, and solution of the convection-dispersion equation for miscible fluid displacement.

4.1 Buckley-Leverett Theory

One of the simplest and most widely used methods of estimating the advance of a fluid displacement front in an immiscible displacement process is the Buckley-Leverett method. The Buckley-Leverett theory [1942] estimates the rate at which an injected water bank moves through a porous medium. The approach uses fractional flow theory and is based on the following assumptions:

- Flow is linear and horizontal
- Water is injected into an oil reservoir
- Oil and water are both incompressible
- Oil and water are immiscible
- Gravity and capillary pressure effects are negligible

The following analysis can be found in a variety of sources, such as Collins [1961], Dake [1978], Wilhite [1986], Craft, et al. [1991] and Towler [2002].

Frontal advance theory is an application of the law of conservation of mass. Flow through a small volume element (Figure 4-1) with length Δx and cross-sectional area A can be expressed in terms of total flow rate q_t as

$$q_t = q_o + q_w \tag{4.1}$$

where q denotes volumetric flow rate at reservoir conditions and the subscripts $\{o, w, t\}$ refer to oil, water, and total rate, respectively. The rate of water entering the element on the left hand side (LHS) is

$$q_t f_w = \text{entering LHS} \tag{4.2}$$

for a fractional flow to water f_w. The rate of water leaving the element on the right hand side (RHS) is

$$q_t\left(f_w + \Delta f_w\right) = \text{leaving RHS} \tag{4.3}$$

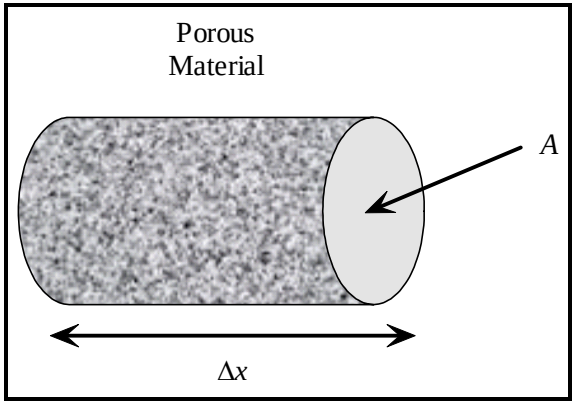

Figure 4-1. Flow Geometry

The change in water flow rate across the element is found by performing a mass balance. The movement of mass for an immiscible, incompressible system gives

$$\begin{aligned}\text{water rate} &= \text{water entering - water leaving} \\ &= q_t f_w - q_t\left(f_w + \Delta q_t f_w\right) \\ &= -q_t \Delta f_w\end{aligned} \tag{4.4}$$

The change in water saturation per unit time is the water rate in Eq. (4.4) divided by the pore volume of the element, thus

$$\frac{\Delta S_w}{\Delta t} = -\frac{q_t}{A\phi}\frac{\Delta f_w}{\Delta x} \tag{4.5}$$

In the limit as $\Delta t \to 0$ and $\Delta x \to 0$, we pass to the differential form of Eq. (4.5) for the water phase:

$$\frac{\partial S_w}{\partial t} = -\frac{q_t}{A\phi}\frac{\partial f_w}{\partial x} \tag{4.6}$$

A similar equation applies to the oil phase:

$$\frac{\partial S_o}{\partial t} = -\frac{q_t}{A\phi}\frac{\partial f_o}{\partial x} \tag{4.7}$$

Since f_w depends only on S_w, we can write the derivative of fractional flow as

$$\frac{\partial f_w}{\partial x} = \frac{df_w}{dS_w}\frac{\partial S_w}{\partial x} \tag{4.8}$$

Substituting $\partial f_w/\partial x$ into $\partial S_w/\partial x$ yields

$$\frac{\partial S_w}{\partial t} = -\frac{q_t}{A\phi}\frac{df_w}{dS_w}\frac{\partial S_w}{\partial x} \tag{4.9}$$

It is not possible to solve for the general distribution of water saturation $S_w(x, t)$ in most realistic cases because of the nonlinearity of the problem. For example, water fractional flow is usually a nonlinear function of water saturation. It is therefore necessary to consider a simplified approach to solving Eq. (4.9).

We begin by considering the total differential of $S_w(x, t)$:

$$\frac{dS_w}{dt} = \frac{\partial S_w}{\partial x}\frac{dx}{dt} + \frac{\partial S_w}{\partial t} \tag{4.10}$$

Equation (4.10) can be simplified by choosing x to coincide with a surface of fixed S_w so that $dS_w/dt = 0$ and

$$\left(\frac{dx}{dt}\right)_{S_w} = -\frac{\left(\frac{\partial S_w}{\partial t}\right)}{\left(\frac{\partial S_w}{\partial x}\right)} \tag{4.11}$$

Substituting Eqs. (4.8) and (4.9) into Eq. (4.11) gives the Buckley-Leverett frontal advance equation:

$$\left(\frac{dx}{dt}\right)_{S_w} = -\frac{q_t}{A\phi}\left(\frac{df_w}{dS_w}\right)_{S_w} \tag{4.12}$$

The derivative $(dx/dt)_{S_w}$ is the velocity of the moving plane with water saturation S_w, and the derivative $(df_w/dS_w)_{S_w}$ is the slope of the fractional flow curve. The integral of the frontal advance equation gives

$$x_{S_w} = \frac{W_i}{A\phi}\left(\frac{df_w}{dS_w}\right)_{S_w} \tag{4.13}$$

where

x_{S_w}	distance traveled by a particular S_w contour (ft)
W_i	cumulative water injected (cu ft)
$(df_w/dS_w)_{S_w}$	slope of fractional flow curve

4.1.1 Water Saturation Profile

A plot of S_w versus distance using Eq. (4.13) and typical fractional flow curves leads to the physically impossible situation of multiple values of S_w at a given location. A discontinuity in S_w at a cutoff location x_c is needed to make the water saturation distribution single valued and to provide a material balance for wetting fluids. The procedure is summarized below.

4.2 Welge's Method

In 1952, Welge published an approach that is widely used to perform the Buckley-Leverett frontal advance calculation. Welge's approach is best demonstrated using a plot of f_w versus S_w (Figure 4-2).

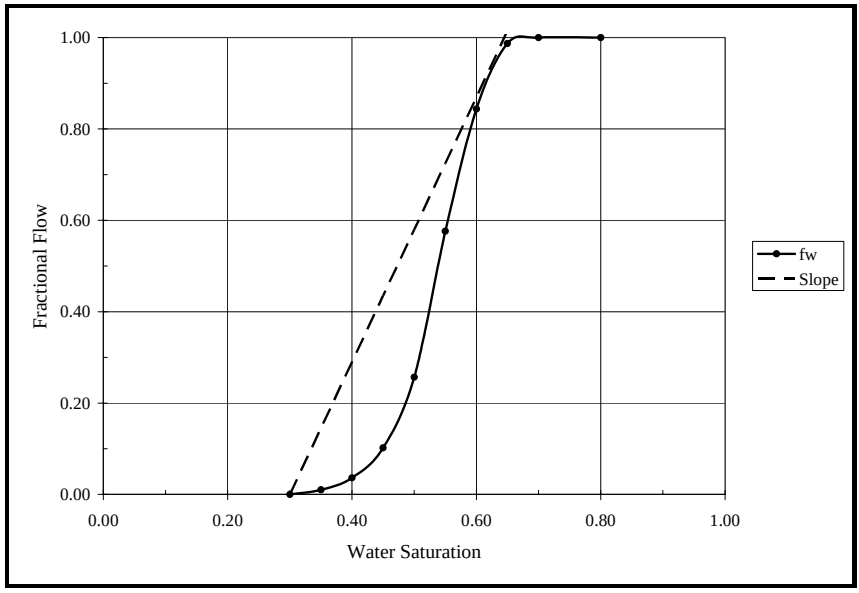

Figure 4-2. Welge's Method

A line is drawn with its intercept at the irreducible water saturation S_{wirr} – the water saturation S_w in front of the waterflood – and tangent to a point on the f_w curve. The resulting tangent line is called the breakthrough tangent, or slope. It is illustrated in Figure 4-2. Water saturation at the flood front S_{wf} is the point of tangency on the f_w curve. The water-oil flood front is sometimes called a shock front because of the abrupt change from irreducible water saturation in front of the waterflood and S_{wf}. Fractional flow of water at the flood front is f_{wf} and occurs at the point of tangency S_{wf} on the f_w curve. In Figure 4-2, S_{wf} is 62% and f_{wf} is 92. Average water saturation behind the flood front S_{wbt} is the intercept of the main tangent line with the upper limiting line where f_w = 1.0.

In Figure 4-2, average S_{wbt} is 65%. In summary, when injected water reaches the producer, Welge's approach gives the following results:

- Water saturation at the producing well is S_{wf}
- Average water saturation behind the front is S_{wbt}
- Producing water cut at reservoir conditions is f_{wf}

Welge's approach can be used to obtain other useful information about the waterflood. The time to water breakthrough at the producer is

$$t_{bt} = \frac{LA\phi}{q_i \left(df_w / dS_w\right)_{S_w}} \tag{4.14}$$

where

q_i	injection rate
$\left(df_w / dS_w\right)_{S_w}$	slope of main tangent line
L	linear distance from injection well to production well

Cumulative water injected is given by

$$Q_i = \frac{1}{\left(df_w / dS_w\right)_{S_{wf}}} \tag{4.15}$$

where Q_i is the cumulative pore volume of injected water. The slope of the water fractional flow curve with respect to water saturation df_w / dS_w evaluated at the water saturation at breakthrough S_{wbt} gives cumulative water injection Q_i at breakthrough.

4.2.1 Effects of Capillary Pressure and Gravity

In the absence of capillary pressure and gravity effects, the flood front propagates as a relatively "sharp" step function, or piston-like displacement. The example in Section 4.5 shows that the characterization of the front as sharp or piston-like is only approximate. In an ideal piston displacement, only one phase would flow on either side of the front.

The presence of capillary pressure leads to the imbibition of water ahead of the front. This causes a change in the behavior of produced fluid ratios. Rather than an abrupt increase in water-oil ratio (WOR) associated with piston-like displacement, the WOR will increase gradually as the leading edge of the mobile water reaches the well and is produced. In addition, the WOR will begin to increase sooner than it would have in the absence of capillary pressure. By contrast, gravity causes high S_w values to lag behind the front. The result is a smeared or "dispersed" flood front.

4.3 Miscible Displacement

Buckley-Leverett theory treats the displacement of one fluid by another under immiscible, piston-like conditions. An immiscible displacement occurs when the displaced fluid and the displacing fluid do not mix. The result is a readily discernible interface between the two fluids. In a miscible displacement, the displaced and displacing fluids mix and the interfacial tension between the fluids approaches zero at their interface. A miscible displacement system can be modeled by a convection-dispersion (C-D) equation. As an illustration, consider the one-dimensional *C-D* equation for the concentration *C* of the displacing fluid:

$$D\frac{\partial^2 C}{\partial x^2} - v\frac{\partial C}{\partial x} = \frac{\partial C}{\partial t} \tag{4.16}$$

We assume here that dispersion D and velocity v are real, scalar constants. The diffusion term has the Fickian form $D \cdot \partial^2 C/\partial x^2$ and the convection term is $v \cdot \partial C/\partial x$. When the diffusion term is much larger than the convection term, the *C-D* equation behaves like the heat conduction equation, which is a parabolic partial differential equation (PDE). If the diffusion term is much smaller than the convection term, the *C-D* equation behaves like a first-order hyperbolic PDE.

The *C-D* equation is especially valuable for studying numerical solutions of fluid flow equations because the *C-D* equation can be solved analytically and the *C-D* equation may be used to examine two important

classes of PDEs: parabolic PDEs and hyperbolic PDEs. To solve the *C-D* equation, we must specify two boundary conditions and an initial condition. The two boundary conditions are needed because the *C-D* equation is second-order in the space derivative. The initial condition satisfies the need for a boundary condition in time associated with the first-order derivative in time. The boundary conditions for the miscible displacement process are that the initial concentration of displacing fluid be equal to one at the inlet ($x = 0$), and zero for all other values of x. The mathematical expressions for these boundary conditions are concentration $C(0, t) \rightarrow 1$ at the inlet, concentration $C(\infty, t) \rightarrow 0$ at the edge of the linear system for all times t greater than the initial time $t = 0$, and the initial condition $C(x, 0) \rightarrow 0$ for all values of x greater than 0.

The propagation of the miscible displacement front is calculated by solving the *C-D* equation. The analytical solution of the one-dimensional *C-D* equation is [Peaceman, 1977]

$$C(x,t) = \frac{1}{2}\left\{ \operatorname{erfc}\left[\frac{x - vt}{2\sqrt{Dt}}\right] + e^{(vx/D)} \operatorname{erfc}\left[\frac{x + vt}{2\sqrt{Dt}}\right]\right\} \tag{4.17}$$

where the complementary error function erfc(y) is defined as

$$\operatorname{erfc}(y) = 1 - \frac{2}{\sqrt{\pi}} \int_0^y e^{-z^2}\, dz \tag{4.18}$$

Abramowitz and Stegun [1972] have presented an accurate numerical algorithm for calculating the complementary error function erfc(y).

We can compare the analytic solution of the *C-D* equation in Eq. (4.17) with a finite difference representation of the *C-D* equation as a means of validating a reservoir flow simulator. The partial derivatives in Eq. (4.16) are replaced with finite differences, which are in turn derived from Taylor's series. The finite difference representation of the *C-D* equation leads to a system of linear equations. The linear equations may be written as matrix equations and solved using computer based numerical techniques. A comparison of the analytical solution of the *C-D* equation with numerical solutions is given in Fanchi [2006].

4.4 Viscous Fingering

Viscous fingering is the unstable displacement of a more viscous fluid by a less viscous fluid. The fingering of an injection fluid into an *in situ* fluid can influence reservoir flow behavior and adversely impact recovery. It is important to note, however, that fingering occurs even in the absence of a porous medium. If a low viscosity fluid is injected into a cell containing a high viscosity fluid, the low viscosity fluid will begin to form fingers as it moves through the fluid. It will not uniformly displace the higher viscosity fluid. These fingers can have different shapes. Figure 4-3 shows an example of a “skeletal” finger [Daccord, et al., 1986] while Figure 4-4 illustrates “fleshy” fingers [for example, see Paterson, 1985; Fanchi and Christiansen, 1989]. If we watch fingers evolve in a homogeneous medium (Figure4-4), we see fingering display a symmetric pattern. The symmetry can be lost if there is some heterogeneity in the system.

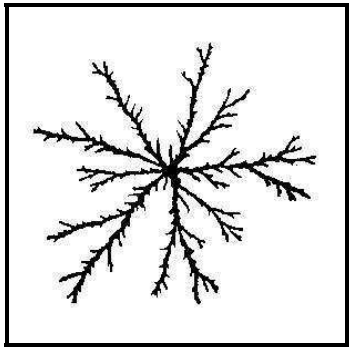

Figure 4-3. "Skeletal" Viscous Finger (after Daccord, et al. [1986]; reprinted by permission of the American Physical Society)

Fingering can be a reservoir heterogeneity problem or a fluid displacement problem. Most reservoir simulators do not accurately model fingering effects. It is possible to improve model accuracy by using a very fine grid to cover the area of interest, but the benefits

associated with such a fine grid are seldom sufficient to justify the additional cost.

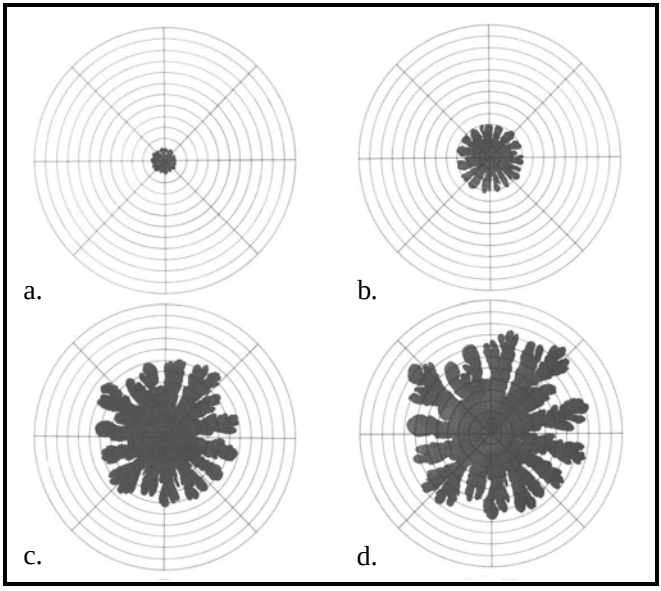

Figure 4-4. Fleshy Viscous Finger Growth (Fanchi and Christiansen [1989]; reprinted by permission of the Society of Petroleum Engineers)

4.5 IFLO Application: Buckley-Leverett Displacement

Flow models can be used to approximate Buckley-Leverett displacement. Figure 4-5 illustrates flow through a core and the corresponding flow model representation. A similar flow model can be used to approximate linear flow between an injection well and a production well in the field. Buckley-Leverett displacement is approximated in a flow model by making comparable assumptions. For example, fluid properties should be constant, the fluids should be treated as incompressible, and the displacement should be immiscible.

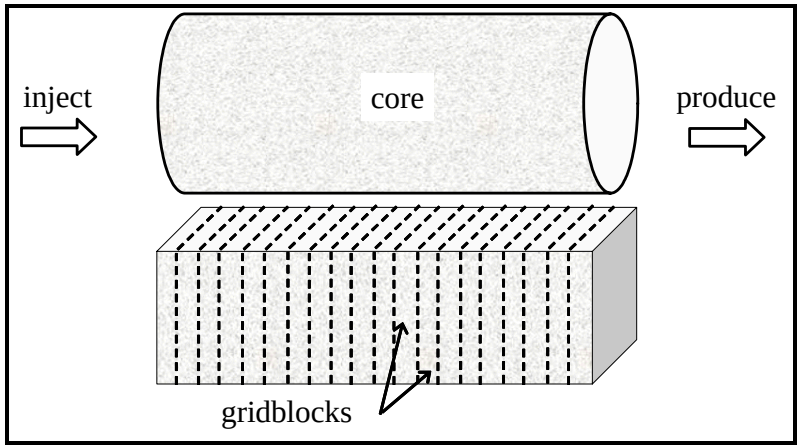

Figure 4-5. Modeling Linear Displacement

Figure 4-6 is a plot of water saturation versus gridblock number at 180 and 366 days for water displacing oil in a linear, horizontal displacement. Water is injected in gridblock 1 and oil is produced from gridblock 20. The water-oil front is moving from left to right. The front is represented by the increase in water saturation from irreducible water saturation ahead of the front. In this case, irreducible water saturation is 20%. Residual oil saturation in this example is also 20%.

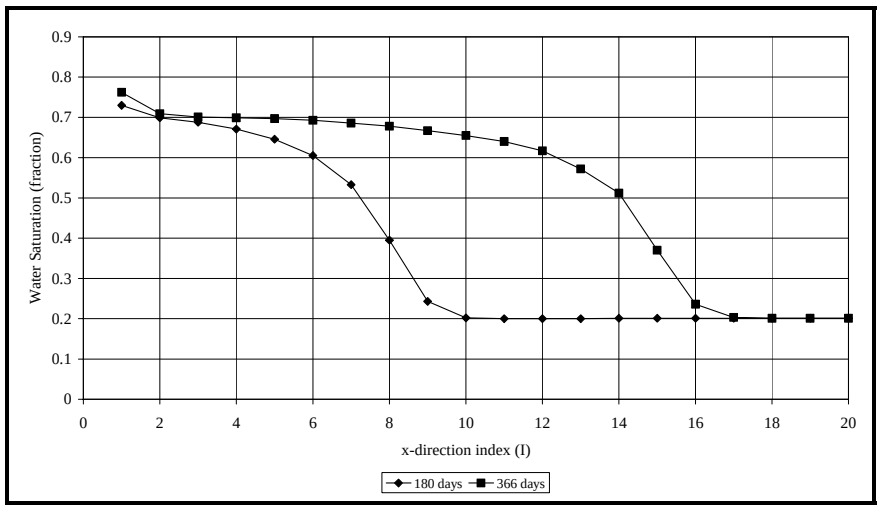

Figure 4-6. Frontal Advance in Linear Displacement

The front calculated by the flow model for Buckley-Leverett displacement does not exhibit the discontinuity, or "sharp" step function, associated with the Buckley-Leverett method. The degree of piston-like displacement is represented by the sharpness of the discontinuity in the water saturation profile between the irreducible water saturation ahead of the injected water and the water saturation behind the water-oil front. The flow model exhibits a smeared saturation front because it uses finite difference techniques to solve the flow equations. This introduces a dispersion effect that is discussed in more detail in Chapter 10.

Exercises

Exercise 4.1 Consider an oil-water system in which oil viscosity is 0.64 cp and water viscosity is 0.5 cp. Oil relative permeability (k_{row}) and water relative permeability (k_{rw}) are given in the following table as a function of water saturation (S_w). Complete the table by using the viscosity and relative permeability information to calculate oil mobility (λ_o), water mobility (λ_w), total mobility (λ_t), water fractional flow (f_w), and oil fractional flow (f_o). Total mobility is the sum of oil mobility and water mobility. Assume absolute permeability is 100 md.

S_w	k_{rw}	k_{row}	λ_o	λ_w	λ_t	f_w	f_o
0.30	0.000	1.000					
0.35	0.005	0.590					
0.40	0.010	0.320					
0.45	0.017	0.180					
0.50	0.023	0.080					
0.55	0.034	0.030					
0.60	0.045	0.010					
0.65	0.064	0.001					
0.70	0.083	0.000					
0.80	0.120	0.000					

Exercise 4.2 Plot λ_o, λ_w, and λ_t in Exercise 4.1 as a function of S_w. What is the mobility ratio of the oil-water system? Hint: see Eq. (3.14).

Exercise 4.3 Plot f_o and f_w in Exercise 4.1 as a function of S_w. Use the plot of f_w versus S_w and Welge's method to determine water saturation at the producing well, average water saturation behind the front, and producing water cut at reservoir conditions.

Exercise 4.4 Run EXAM3.DAT and plot water saturation as a function of distance between wells at 180 and 366 days. Hint: water saturation is reported in the run output file ITEMP.ROF.

Exercise 4.5A Buckley-Leverett displacement through a linear, horizontal fracture with a matrix rock undergoing water imbibition can be modeled by the equation

$$-u\frac{\partial f_{wf}}{\partial x} = \frac{\partial S_w}{\partial t} + \frac{\lambda R_\infty}{\phi_f}\int_0^t e^{-\lambda(t-\varepsilon)}\frac{\partial S_{wf}}{\partial \varepsilon}d\varepsilon$$

where:

u = $q_t/A\phi_f$ = interstitial velocity (ft/day)

f_{wf} = fractional flow of water in fracture

S_{wf} = water saturation in fracture (fraction)

ϕ_f = fracture porosity (fraction)

ε = dummy integration variable (days)

R_∞ = asymptotic limit of oil recovery from the matrix into the fracture

λ = rate of convergence toward the asymptotic limit (day^{-1})

The integral term in the equation represents the matrix-fracture interaction, i.e. fluid flow between the matrix and the fracture. Is there flow between the matrix and fracture if λ or R_∞ is zero?

Exercise 4.5B Does the water imbibition rate from the fracture increase or decrease when λ increases in the range 0 $day^{-1} \le \lambda \le 1$ day^{-1}?

Exercise 4.6 Plot the concentration $C(x, t)$ in Eq. (4.17) given the following physical parameters: $D = 0.1$ ft^2/day, $v = 1$ ft/day. The plot should present $C(x, t)$ in the range $0 \leq x \leq 1$ for the three times $t = 0.1$ day, 0.2 day, 0.3 day. This data represents fluid movement in porous media, such as water draining through sand on a beach.

Chapter 5

Frontal Stability

The stability of a flood front can influence the efficiency of fluid displacement. A front is stable if it retains the shape of the interface between displaced and displacing fluids as the front moves through the medium. An analysis of frontal stability is presented in this chapter in terms of a specific example – the advance of a water-oil displacement front. The stability of the front is considered both in the absence of gravity and in the presence of gravity. Front stability is then studied using linear stability analysis.

5.1 Frontal Advance Neglecting Gravity

The displacement of one phase by another may be analytically studied if we simplify the problem to displacement in a linear, homogenous porous medium. Let us first consider the displacement of oil by water in a horizontal porous medium of length L. We assume piston-like displacement of a front located at x_f. Application of Darcy's Law and the continuity equation leads to a pressure distribution described by Poisson's equation. The absence of sources or sinks in the medium reduces Poisson's equation to the Laplace equation for the water phase pressure:

$$\frac{\partial^2 P_w}{\partial x^2} = 0,\ 0 < x < x_f \tag{5.1}$$

The corresponding equation for oil phase pressure is

$$\frac{\partial^2 P_o}{\partial x^2} = 0, \; x_f < x < L \tag{5.2}$$

Equations (5.1) and (5.2) apply to those parts of the medium containing water and oil respectively. They assume that the fluids are incompressible, and that the oil-water interface is a piston-like displacement in the *x*-direction. The piston-like displacement assumption implies a discontinuous change from mobile oil to mobile water at the displacement front. This concept differs from the Buckley-Leverett analysis presented in Chapter 4.

Buckley-Leverett theory with Welge's method shows the existence of a transition zone as saturations grade from mobile oil to mobile water. The saturation profile at the interface between the immiscible phases depends on the fractional flow characteristics of the system. The present method of analysis has less structure in the saturation profile, but is more readily suited for analyzing the stability of the displacement front.

Boundary conditions at the displacement front are given by continuity of phase pressure

$$P_o = P_w \text{ at } x = x_f(t) \tag{5.3}$$

and continuity of phase velocity

$$v_w = v_o \text{ or } \lambda_w \frac{\partial P_w}{\partial x} = \lambda_o \frac{\partial P_o}{\partial x} \tag{5.4}$$

where λ_ℓ is the mobility of phase ℓ. Equation (5.3) is valid when we neglect capillary pressure, and the effect of gravity has been excluded from Eq. (5.4). The exclusion of gravity corresponds physically to flow in a horizontal medium. Boundary conditions at the edges of the porous medium are

$$P_w = P_1 \text{ at } x = 0 \tag{5.5}$$

and

$$P_o = P_2 \text{ at } x = L \tag{5.6}$$

Equations (5.1) through (5.6) may be solved analytically. We begin by integrating Eqs. (5.1) and (5.2) to find the general solutions

$$P_w = A_w\, x + B_w \tag{5.7}$$

and

$$P_o = A_o\, x + B_o \tag{5.8}$$

where the constant coefficients $\{A_\ell, B_\ell\}$ are determined by applying the boundary conditions. Substituting Eq. (5.5) into Eq. (5.7) gives

$$B_w = P_1 \tag{5.9}$$

The remaining coefficients are found by simultaneously solving Eqs. (5.4), (5.7), and (5.8) subject to Eqs. (5.3), (5.5), and (5.6). The resulting coefficients are

$$A_w = -\frac{\Delta P}{ML + (1-M)x_f} \tag{5.10}$$

$$A_o = M\, A_w \tag{5.11}$$

$$B_o = P_1 = (A_w - A_o)x_f = P_1 + (1-M)A_w x_f \tag{5.12}$$

where M is the mobility ratio

$$M = \frac{\lambda_w}{\lambda_o} \tag{5.13}$$

and the pressure difference is

$$\Delta P = P_1 - P_2 \tag{5.14}$$

The frontal velocity v_f is given by

$$v_f \equiv \frac{dx_f}{dt} = \frac{v_w}{\phi\left(1 - S_{or} - S_{wc}\right)} \tag{5.15}$$

where S_{or} is residual oil saturation, S_{wc} is connate water saturation, and v_w is the Darcy velocity given by Darcy's Law without gravity effects in one spatial dimension, namely:

$$v_w = -\lambda_w \frac{\partial P_w}{\partial x} = -\lambda_w A_w \tag{5.16}$$

Substituting Eq. (5.16) into (5.15) gives

$$\frac{d\,x_f}{d\,t} = \frac{\lambda_w \Delta P}{\phi(1 - S_{or} - S_{wc})} \frac{1}{\left[ML + (1-M)x_f\right]} \tag{5.17}$$

The integral of Eq. (5.17) with respect to time gives the frontal advance.

5.2 Frontal Advance Including Gravity

Gravity is included in the analysis of frontal advance in a dipping reservoir (Figure 5-1) by replacing phase pressure in Eqs. (5.1) through (5.6) with phase potential

$$\Phi_\ell = P_\ell - \rho_\ell g\, x \sin\Theta$$

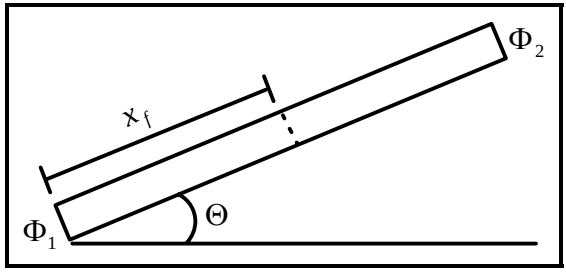

Figure 5-1. Geometry of Frontal Advance

The resulting equations for phase potentials are

$$\frac{\partial^2 \Phi_w}{\partial x^2} = 0,\ 0 < x < x_f \tag{5.18}$$

$$\frac{\partial^2 \Phi_o}{\partial x^2} = 0,\ x_f < x < L \tag{5.19}$$

The phase potentials at the flood front are related by

$$\Phi_o = \Phi_w + (\rho_o - \rho_w) g x_f \sin\Theta \tag{5.20}$$

with continuity of phase velocities

$$\lambda_w \frac{\partial \Phi_w}{\partial x} = \lambda_o \frac{\partial \Phi_o}{\partial x} \tag{5.21}$$

The boundary conditions for the phase potentials are

$$\Phi_w = \Phi_1 \text{ at } x = 0 \tag{5.22}$$

and

$$\Phi_o = \Phi_2 \text{ at } x = L \tag{5.23}$$

Capillary pressure is still neglected in this formulation. Equation (5.20) is the analog of Eq. (5.3).

The solutions of the second-order ordinary differential equations given by Eqs. (5.18) and (5.19) are the linear relationships

$$\Phi_w = A'_w x + B'_w \tag{5.24}$$

$$\Phi_o = A'_o x + B'_o \tag{5.25}$$

The coefficients are evaluated by substituting Eqs. (5.24) and (5.25) into Eqs. (5.18) and (5.19) and applying the boundary conditions. The coefficients are

$$A'_w = -\left[\frac{(\Phi_1 - \Phi_2) + x_f (\rho_o - \rho_w) g \sin\Theta}{ML + (1-M) x_f} \right] \tag{5.26}$$

$$A'_o = M A'_w \tag{5.27}$$

$$B'_w = \Phi_1 \tag{5.28}$$

$$B'_o = \Phi_2 - A'_o L = \Phi_2 - M A'_w L \tag{5.29}$$

The Darcy velocity of the water phase is

$$v_w = -\lambda_w \frac{\partial \Phi_w}{\partial x} = -\lambda_w A'_w \tag{5.30}$$

The velocity of frontal advance in a dipping reservoir is found by substituting Eq. (5.30) into Eq. (5.15) to yield the result

$$\frac{d\,x_f}{d\,t} = \frac{\lambda_w}{\phi(1-S_{or}-S_{wc})}\left\{\frac{(\Phi_1-\Phi_2)+[(\rho_o-\rho_w)\,g\sin\Theta]\,x_f}{ML+(1-M)\,x_f}\right\} \tag{5.31}$$

5.3 Linear Stability Analysis

The stability of frontal advance is determined by considering the rate of growth of a perturbation at the front. We first express the frontal advance velocity Eqs. (5.17) and (5.31) in the general form

$$\frac{d\,x_f}{d\,t} = \frac{\alpha+\beta\,x_f}{\gamma+\delta\,x_f} \tag{5.32}$$

where the coefficients $\{\alpha,\beta,\gamma,\delta\}$ are independent of time and frontal location. Equation (5.32) is a nonlinear, first-order differential equation. Imposing a slight perturbation ε on the front location gives

$$\frac{d(x_f+\varepsilon)}{dt} = \frac{\alpha+\beta(x_f+\varepsilon)}{\gamma+\delta(x_f+\varepsilon)} \tag{5.33}$$

The velocity of propagation of the perturbation is given by the difference between Eqs. (5.33) and (5.32):

$$\frac{d\varepsilon}{dt} = \frac{\alpha+\beta\,x_f+\beta\varepsilon}{\gamma+\delta\,x_f+\delta\varepsilon} - \frac{\alpha+\beta\,x_f}{\gamma+\delta\,x_f} \tag{5.34}$$

Combining fractions and simplifying yields

$$\frac{d\varepsilon}{dt} = \left\{\frac{\beta(\gamma+\delta\,x_f)-\delta(\alpha+\beta\,x_f)}{(\gamma+\delta\,x_f)^2\left[1+\dfrac{\delta\varepsilon}{\gamma+\delta x_f}\right]}\right\}\varepsilon \tag{5.35}$$

Further simplification is achieved by recognizing that the perturbation is slight so that we have the approximation

$$\frac{1}{1+\dfrac{\delta\varepsilon}{\gamma+\delta x_f}} \approx 1-\frac{\delta\varepsilon}{\gamma+\delta x_f} \text{ for } \delta\varepsilon << \gamma+\delta x_f \tag{5.36}$$

Substituting Eq. (5.36) into Eq. (5.35) gives

$$\frac{d\varepsilon}{dt}=\left\{\frac{\beta(\gamma+\delta x_f)-\delta(\alpha+\beta x_f)}{(\gamma+\delta x_f)^2}\right\}\left[1-\frac{\delta\varepsilon}{\gamma+\delta x_f}\right] \tag{5.37}$$

Keeping only terms to first order in ε and simplifying gives

$$\frac{d\varepsilon}{dt}=\frac{(\beta\gamma-\delta\alpha)\,\varepsilon}{(\gamma+\delta x_f)^2} \tag{5.38}$$

Equation (5.38) has the solution

$$\varepsilon=\varepsilon_0 e^{t\tau} \tag{5.39}$$

where ε_0 is an integration constant, and

$$\tau=\frac{\beta\gamma-\delta\alpha}{(\gamma+\delta x_f)^2} \tag{5.40}$$

If τ is negative, the perturbation decays exponentially. If τ is greater than zero, the perturbation grows exponentially. Finally, if τ equals zero, the perturbation does not propagate because $d\varepsilon/dt = 0$ in Eq. (5.38).

We can now examine the stability of a displacement front. Comparing Eq. (5.32) with (5.31) lets us make the identifications

$$\alpha=\frac{\lambda_w(\Phi_1-\Phi_2)}{\phi(1-S_{or}-S_{wc})} \tag{5.41}$$

$$\beta=\frac{\lambda_w(\rho_o-\rho_w)\,g\sin\Theta}{\phi(1-S_{or}-S_{wc})} \tag{5.42}$$

$$\gamma=ML \tag{5.43}$$

$$\delta=(1-M) \tag{5.44}$$

The resulting expression for the growth of a perturbation is

$$\frac{d\varepsilon}{dt} = -\frac{\lambda_w \varepsilon}{\phi(1-S_{or}-S_{wc})} \times \frac{(1-M)(\Phi_1-\Phi_2)+ML(\rho_o-\rho_w)g\sin\Theta}{\left[ML+(1-M)x_f\right]^2} \tag{5.45}$$

Equation (5.45) agrees with Eq. (7-104) in Collins [1961].

Zero growth rate of a perturbation is determined by setting the derivative $d\varepsilon/dt = 0$ in Eq. (5.45). The resulting condition for zero growth rate is

$$(1-M)(\Phi_1-\Phi_2)+ML(\rho_o-\rho_w)g\sin\Theta = 0 \tag{5.46}$$

If the medium is horizontal, the condition for a system without gravity is

$$(1-M)\Delta P = 0 \tag{5.47}$$

To see the effect of mobility ratio M on finger growth for the gravity-free case, we set $g = 0$ in Eq. (5.45) to get

$$\frac{d\varepsilon}{dt} = -\frac{\lambda_w \varepsilon}{\phi(1-S_{or}-S_{wc})}\frac{(1-M)\Delta P}{[ML+(1-M)x_f]^2} \tag{5.48}$$

The finger grows exponentially if $M > 1$, decays exponentially if $M < 1$, and does not propagate if $M = 1$.

5.4 IFLO Application: Frontal Advance in a Dipping Reservoir

The effect of mobility and gravity on frontal advance can be studied using a flow model of an oil reservoir waterflood. We consider a linear waterflood that has constant oil viscosity and constant water viscosity. Table 5-1 shows the four cases of interest. The cases differ by dip angle or oil viscosity. Each of these effects is considered separately.

Figure 5-2 shows the effect of gravity on water saturation profiles for Cases A and B. The figure is a plot of water saturation versus gridblock number. Water is injected in gridblock #1 and oil is produced from gridblock #20. Cases A and B are the same except for dip angle.

The effect of gravity is to make the frontal advance a bit more piston-like, but the effect is relatively minor for Cases A and B. The front in Figure 5-2 is represented by the increase in water saturation between blocks 14 and 16.

Table 5-1
Frontal Advance Cases

Case	Dip Angle (degrees)	Oil Viscosity (cp)	Mobility Ratio
A	0	2	1.56
B	25	2	1.56
C	25	5	3.89
D	25	1	0.78

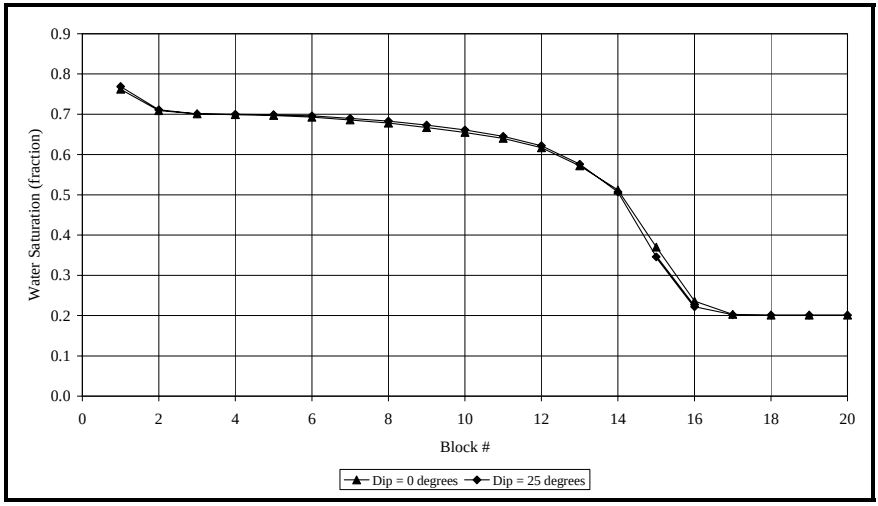

Figure 5-2. Effect of Dip Angle on Frontal Advance

Figure 5-3 shows the effect of mobility ratio on frontal advance. Cases B, C and D differ only by oil viscosity, which represents a difference in mobility ratio. The mobility ratio of Case D is less than one, which is considered favorable. The mobility ratios of Cases B and C are larger than one and are, therefore, considered unfavorable. Case D with a

favorable mobility ratio has a more piston-like displacement than either Case B or C. The front is less piston-like as mobility ratio increases. The water saturation profile for Case C shows that water breakthrough has occurred at the production well. This is verified by plotting water production rate as a function of time in Figure 5-4.

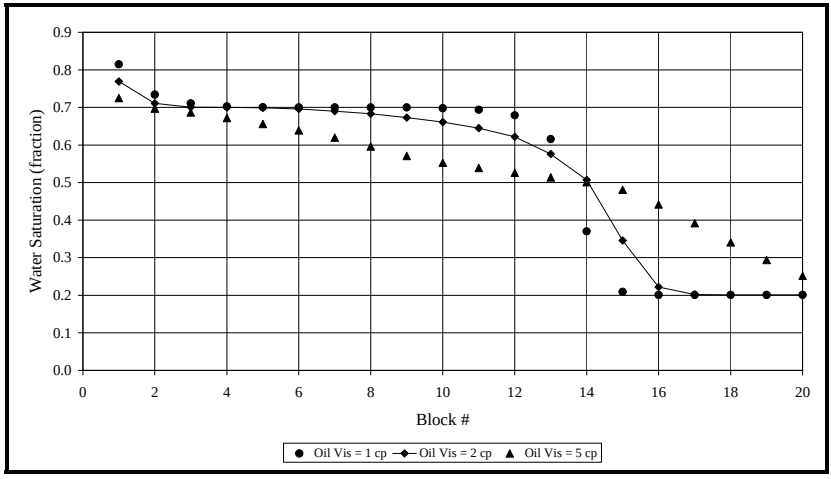

Figure 5-3. Effect of Mobility Ratio on Frontal Advance

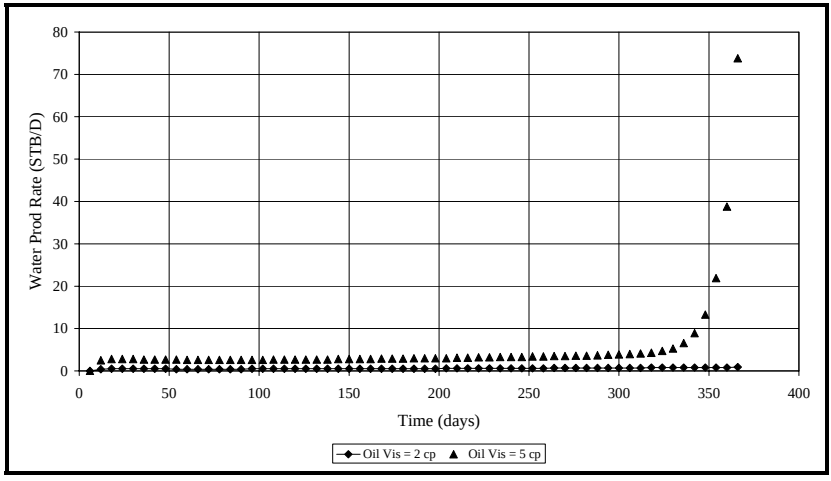

Figure 5-4. Water Production Rate for Cases B and C

Exercises

Exercise 5.1 Show that Eq. (5.7) is a solution of Eq. (5.1).

Exercise 5.2 Use Eq. (5.45) to determine the rate of finger growth of a unit mobility flood in a horizontal medium. Hint: set $M = 1$ in Eq. (5.45) and simplify.

Exercise 5.3 Use Eq. (5.48) to explain why the mobility ratio condition $M < 1$ is considered "favorable" for a displacement flood.

Exercise 5.4A Consider the following oil-water relative permeability table:

S_w	k_{rw}	k_{row}
0.30	0.000	1.000
0.35	0.005	0.590
0.40	0.010	0.320
0.45	0.017	0.180
0.50	0.023	0.080
0.55	0.034	0.030
0.60	0.045	0.010
0.65	0.064	0.001
0.70	0.083	0.000
0.80	0.120	0.000

What is the residual oil saturation?

Exercise 5.4B What is the connate water saturation?

Exercise 5.4C What is the relative permeability to oil at connate water saturation for the oil-water relative permeability curves?

Exercise 5.4D What is the relative permeability to water at residual oil saturation?

Exercise 5.4E Assume oil viscosity is 0.64 cp and water viscosity is 0.50 cp. Calculate the mobility ratio of a waterflood for water displacing oil using the oil-water relative permeability curves above.

Exercise 5.4F Is the mobility ratio favorable or unfavorable?

Exercise 5.5A Consider a linear flow system with area = 25 ft^2 and permeability = 100 md. End point *A* is 5 ft higher than end point *B*, and the distance between end points is 15 ft. Suppose the system contains oil with viscosity = 0.8 cp, gravity = 35° API (γ_o = 0.85), and FVF = 1.0 RB/STB. If the end point pressures are $P_A = P_B$ = 20 psia, is there flow? If so, how much and in what direction? Use Darcy's Law

$$q = -0.001127 \frac{k}{\mu} \frac{A}{\beta} \left[\frac{P_A - P_B}{L} + \rho g \sin \alpha \right]$$

with the gravity term and dip angle α.

Exercise 5.5B What should the pressure P_B be to prevent fluid flow?

Exercise 5.6A Files EXAM3A.DAT and EXAM3B.DAT model a linear waterflood in a formation with a dip angle of 25°. The oil viscosity is 2 cp in EXAM3A.DAT and 5 cp in EXAM3B.DAT. Run both data files and plot water production rate versus time using data from timestep summary file ITEMP.TSS.

Exercise 5.6B Run data files EXAM3A.DAT and EXAM3B.DAT. Plot water saturation at the end of the run versus gridblock number using data

from run output file ITEMP.ROF. There are twenty gridblocks in the *x*-direction.

Exercise 5.6C Explain the differences between the results in Parts A and B of this exercise.

Chapter 6

Pattern Floods

The effectiveness of a displacement process depends on many factors, including reservoir and fluid characteristics that are beyond our control, such as depth, structure, and fluid type. Other factors that influence displacement efficiency can be controlled, however. They include the number and type of wells, well rates, and well locations. The distribution of wells is known as the well pattern. The impact of well pattern on displacement effectiveness is discussed after definitions of recovery efficiency are presented. The selection of a development plan depends on a comparison of the economics of alternative development concepts. Reservoir flow models are especially useful tools for performing these studies.

6.1 Recovery Efficiency

Recovery efficiency is quantified by comparing initial and final volumes of fluid in place. It takes into account volumetric and displacement efficiencies. The different aspects of recovery efficiency are defined and then combined to form overall recovery efficiency.

Displacement efficiency accounts for the efficiency of recovering mobile hydrocarbon. To be specific, we define displacement efficiency for oil as the ratio of mobile oil to original oil in place at reservoir conditions:

$$E_D = \frac{V_p S_{oi} - V_p S_{or}}{V_p S_{oi}} = \frac{S_{oi} - S_{or}}{S_{oi}} \tag{6.1}$$

where

V_p initial pore volume

S_{oi} initial oil saturation

S_{or} residual oil saturation

Residual oil saturation is replaced by oil saturation at abandonment in floods that do not reduce initial oil saturation to residual oil saturation during the life of the flood. Displacement efficiency can approach 100% if residual oil saturation can be driven to zero. One of the goals of enhanced oil recovery processes such as micellar-polymer flooding or miscible flooding is to reduce residual oil saturation and increase displacement efficiency.

The definition of displacement efficiency can be modified to include the effects of swelling. Swelling is represented by using surface volume rather than reservoir volume in the definition of displacement efficiency. The volume conversion is achieved by dividing reservoir volume by formation volume factor (FVF). For example, the displacement efficiency of a waterflood is

$$E_D = \frac{\dfrac{V_p S_{oi}}{B_{oi}} - \dfrac{V_p S_{or}}{B_{oa}}}{\dfrac{V_p S_{oi}}{B_{oi}}} = \frac{\dfrac{S_{oi}}{B_{oi}} - \dfrac{S_{or}}{B_{oa}}}{\dfrac{S_{oi}}{B_{oi}}} \tag{6.2}$$

where

B_{oi} oil FVF at the beginning of waterflood

B_{oa} oil FVF at the waterflood pressure

Notice that oil formation volume factor is at its maximum value at the bubble point pressure of the oil. If the waterflood is conducted at or just above the bubble point pressure, the value of B_{oa} will be maximized and

the residual oil term will be minimized. The resulting displacement efficiency for a waterflood is then maximized.

Displacement efficiency is a measure of how effectively mobile hydrocarbons can be recovered. Although the above definitions of displacement efficiency have been given for oil, similar definitions can be provided for gas.

In addition to displacement efficiency, volumetric factors are needed to determine overall recovery efficiency. Areal and vertical sweep efficiencies are defined by

$$E_A = \frac{\text{swept area}}{\text{total area}} \tag{6.3}$$

and

$$E_V = \frac{\text{swept thickness}}{\text{total thickness}} \tag{6.4}$$

Reservoir flow models are useful tools for quantifying both swept area and swept thickness. Vertical sweep efficiency depends on the vertical distribution of the flow capacity of each formation intersected by the wellbore, where flow capacity is the product of permeability and net thickness. The flow capacity of a model layer should honor observed reservoir flow capacity, especially if high flow capacity thief zones are present. The product of areal and vertical sweep efficiency is the volumetric sweep efficiency E_{vol}:

$$E_{vol} = E_A \times E_V \tag{6.5}$$

where

E_A areal sweep efficiency

E_V vertical sweep efficiency

Overall recovery efficiency must account for both volumetric and displacement effects. It is therefore defined as the product of volumetric sweep efficiency and displacement efficiency:

$$RE = E_D \times E_{vol} = E_D \times E_A \times E_V \tag{6.6}$$

where

RE recovery efficiency

Notice that each of the efficiency factors in recovery efficiency can be relatively large, and yet recovery efficiency will be relatively small. For example, suppose both the areal and vertical efficiencies are 70% and displacement efficiency is 80%, the product of these efficiencies is approximately 39%. This means that even the reservoirs with the best recovery efficiency often have a substantial volume of unrecovered hydrocarbon remaining in the ground. The most important goal of improved recovery techniques is the recovery of this remaining resource.

6.2 Patterns and Spacing

The analytical techniques for describing displacement that were discussed previously study fluid displacement between one injection well and one production well. The alignment of the injector-producer pair represents a linear displacement process. It is the simplest pattern involving injection and production wells. A variety of other patterns may be defined. Several examples are shown in Figure 6-1. A representative pattern element for the five-spot pattern is identified using shaded wells.

The ratio of the number of producing wells to the number of injection wells is shown in Table 6-1. The patterns depicted in Table 6-1 and Figure 6-1 are symmetric patterns that are especially effective for reservoirs with relatively small dip and large areal extent. The injectors and producers are generally interspersed. Other patterns in which injectors and producers are grouped together may be needed for reservoirs with significant dip. For example, a peripheral or flank injection pattern may be needed to effectively flood an anticlinal or monoclinal reservoir.

Direct Line-Drive Pattern a = distance between neighboring wells d = distance between rows of wells • denotes production well ◊ denotes injection well	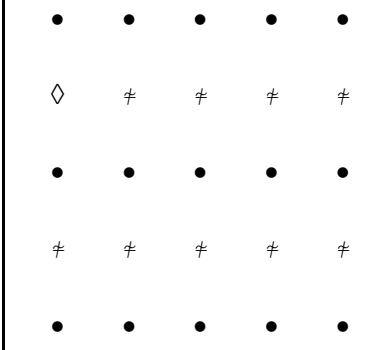
Staggered Line-Drive Pattern a = distance between neighboring wells d = distance between rows of wells • denotes production well ◊ denotes injection well	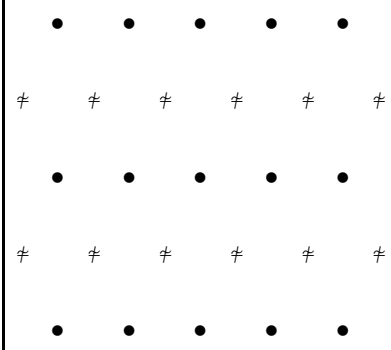
Five-Spot Pattern d = distance between neighboring producers = distance between neighboring injectors • denotes production well ◊ denotes injection well	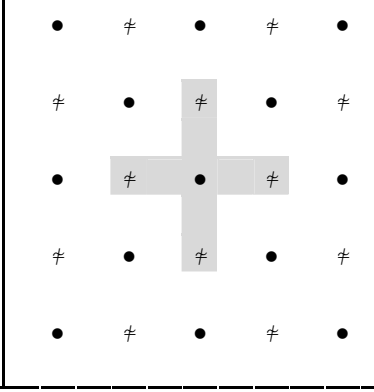

Figure 6-1. Well Locations in Selected Well Patterns

Table 6-1
Producer-to-Injector Ratios for Common Well Patterns

Well Pattern	Producer : Injector Ratio
Four-Spot	2
Five-Spot	1
Direct Line-drive	1
Staggered Line-drive	1
Seven-Spot	1 / 2
Nine-Spot	1 / 3

In addition to reservoir geometry and the displacement process, the well pattern depends on the distribution and orientation of existing production wells, and the desired spacing of wells. Wells may be oriented vertically, horizontally, or at some deviation angle between horizontal and vertical. The orientation of a well depends on such reservoir features as formation orientation and, if fractures are present, fracture orientation. For example, if a reservoir contains many fractures that are oriented in a particular direction, recovery is often optimized by drilling a horizontal well in a direction that intersects as many fractures as possible. Recovery is optimized because recovery from fractured reservoirs usually occurs by producing fluid that flows from the matrix into the fractures and then to the wellbore.

Well spacing depends on the area being drained by a production well. A reduction in well spacing requires an increase in the density of production wells. The density of production wells is the number of production wells in a specified area. Well density can be increased by drilling additional wells in the space between wells in a process called infill drilling, which is discussed further in the next section.

6.3 Advances in Drilling Technology

Improvements in drilling technology are having a dramatic impact on reservoir management. Longer wellbores that follow subsurface formations are providing access to more parts of the reservoir. The additional information is being integrated into reservoir characterization at the same time that more detailed reservoir models are helping guide the longer wellbore trajectories. Four areas of drilling technology are briefly discussed here: infill drilling, multilateral wells, geosteering, and intelligent wells.

6.3.1 Infill Drilling

Infill drilling is a means of improving sweep efficiency by increasing the number of wells in an area. Well spacing is reduced to provide access to unswept parts of a field. Modifications to well patterns and the increase in well density can change sweep patterns and increase sweep efficiency, particularly in heterogeneous reservoirs. Infill drilling can improve recovery efficiency, but can also be more expensive than a fluid displacement process.

6.3.2 Multilateral Wells and Extended Reach Drilling

Multilateral well technology is revolutionizing extraction technology and reservoir management. A multilateral well is a well that has more than one flow conduit. Although the use of multilateral wells is considered a relatively recent development, Golan [2000] reported that the Russians had drilled a type of multilateral well in the Bashkiria Field as long ago as 1955. It had ten branches and its well schematic was published in the Russian literature and reported in *Drilling Journal* in December 1955 [page 87].

Multilateral wells were introduced into the modern industry as sidetracked wells that were drilled for the purpose of bypassing wells with casing problems. Today, multilateral wells make it possible to connect multiple well paths to a common wellbore. Figure 6-2 illustrates a multilateral well trajectory.

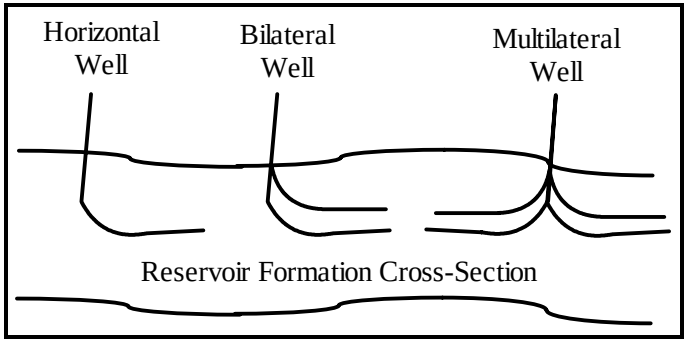

Figure 6-2. Example of a Multilateral Well

Multilateral wells have many applications. For example, they are useful in offshore environments where the number of well slots is substantially limited by the amount of space available on a platform. They can also be used to produce highly compartmentalized reservoirs and reservoirs with low permeability. Extended reach horizontal or multilateral wells are useful in environmentally or commercially sensitive areas where placing a drilling rig is undesirable or prohibited.

6.3.3 Geosteering

Geosteering is a technology for reaching drilling target locations and is a prerequisite for successful extended reach drilling. Extended reach drilling is used to drill a well with very long horizontal displacement away from the drilling rig. Extended reach drilling provides a means of reaching commercial subsurface deposits at great distances from a fixed drilling rig location. Three of the longest applications of extended reach drilling are at the Wytch Farm oil field offshore Britain, the Xijiang field in the South China Sea, and the Ara field offshore

Tierra del Fuego, Argentina. These projects have drilled extended reach wells with approximately 8 km of horizontal displacement from the drilling rig. Geosteering and extended reach drilling have many benefits, including reducing costs associated with the construction of new platforms. Extended reach drilling lets an operator minimize the environmental footprint of a field development project.

6.3.4 Intelligent Wells

It is often necessary in the management of a modern reservoir to alter the completion interval in a well. These adjustments are needed to modify producing well fluid ratios such as water-oil ratio or gas-oil ratio. One way to minimize the cost associated with completion interval adjustments is to design a well that can change the completion interval automatically. This is an example of an intelligent well, which is also known as a "smart well."

Intelligent wells are designed to give an operator remote control of subsurface well characteristics such as completion interval. In addition, intelligent wells are being designed to provide information to the operator using downhole measurements of physical properties such as pressure, temperature and seismic vibrations. One goal of intelligent well technology is to convey a stream of continuous and real-time information to the operator who can monitor this information and make adjustments as needed to achieve reservoir management objectives.

6.4 Pattern Recovery

Optimum performance may be achieved with the patterns defined in the previous section by controlling the rates of injectors and producers. These calculations can be performed analytically if we assume that the displacing and displaced fluids are incompressible, the mobility ratio is one, and the reservoir has uniform properties. Values of injection rates for the three patterns shown in Figure 6-1 are presented in Table 6-2 [Wilhite, 1986]. Units and nomenclature for the rate equations

in Table 6-2 are barrels per day for rate q; darcies for permeability k; feet for thickness h; well separations a and d, and wellbore radius r_w; pounds per square inch for pressure change ΔP; and centipoise for viscosity μ. The well separations are defined in Figure 6-1.

Table 6-2
Analytical Injection Rates for Selected Well Patterns

Pattern	Rate
Direct Line-Drive	$q_D = \dfrac{3.541\,kh\,\Delta P}{\mu\left[\ln\left(\dfrac{a}{r_w}\right)+1.571\dfrac{d}{a}-1.838\right]}, \dfrac{d}{a}\geq 1$
Staggered Line-Drive	$q_S = \dfrac{3.541\,kh\,\Delta P}{\mu\left[\ln\left(\dfrac{a}{r_w}\right)+1.571\dfrac{d}{a}-1.838\right]}$
Five-Spot	$q_F = \dfrac{3.541\,kh\,\Delta P}{\mu\left[\ln\left(\dfrac{a}{r_w}\right)-0.619\right]}$

The calculation of analytical injection rates, even under a set of restrictive assumptions, provides a methodology for designing well patterns without using a reservoir simulator. More accurate estimates of injection rates under a less restrictive set of assumptions are obtained using reservoir simulators. For example, simulators have been used to correlate volumetric sweep efficiency with mobility ratio and permeability variation in a reservoir that is being subjected to a pattern flood [Wilhite, 1986]. One measure of permeability variation is the Dykstra-Parsons coefficient of permeability variation.

The Dykstra-Parsons coefficient can be estimated for a log-normal permeability distribution as

$$V_{DP} = 1 - \exp\left[-\sqrt{\ln(k_A/k_H)}\right]$$

where k_A is the arithmetic average permeability for n samples

$$k_A = \frac{1}{n}\sum_{i=1}^{n} k_i$$

and k_H is the harmonic average permeability

$$\frac{1}{k_H} = \frac{1}{n}\sum_{i=1}^{n} \frac{1}{k_i}$$

The Dykstra-Parsons coefficient should be in the range $0 \le V_{DP} \le 1$. For a perfectly homogeneous reservoir, $V_{DP} = 0$ because $k_A = k_H$. An increase in reservoir heterogeneity increases V_{DP}. Typical values of the Dykstra-Parsons coefficient are in the range $0.4 \le V_{DP} \le 0.9$.

Correlations of volumetric sweep efficiency with mobility ratio and permeability variation show that volumetric sweep efficiency declines as reservoir heterogeneity increases or mobility ratio increases, particularly for mobility ratios greater than one. This makes sense physically if we recall that mobility ratio is the mobility of the displacing fluid behind the front divided by the mobility of the displaced fluid ahead of the front. If the mobility of the displacing fluid is greater than the mobility of the displaced fluid, then the mobility ratio is greater than one and is considered unfavorable. On the other hand, if the mobility of the displacing fluid is less than the mobility of the displaced fluid, then the mobility ratio is less than one and is considered favorable. Unfavorable mobility ratios often occur when gas displaces oil or when water displaces high viscosity oil. An example of a flood with a favorable mobility ratio is the displacement of low viscosity oil by water.

6.5 IFLO Application: Five-Spot Waterflood

One of the most widely used patterns for waterflooding and gasflooding is the five-spot pattern. We illustrate a pattern flood by considering the flood of the region shown in Figure 6-3. Well P-1 is an

oil production well that is surrounded by four injection wells. This model is similar to the example presented by Fanchi, et al. [1982].

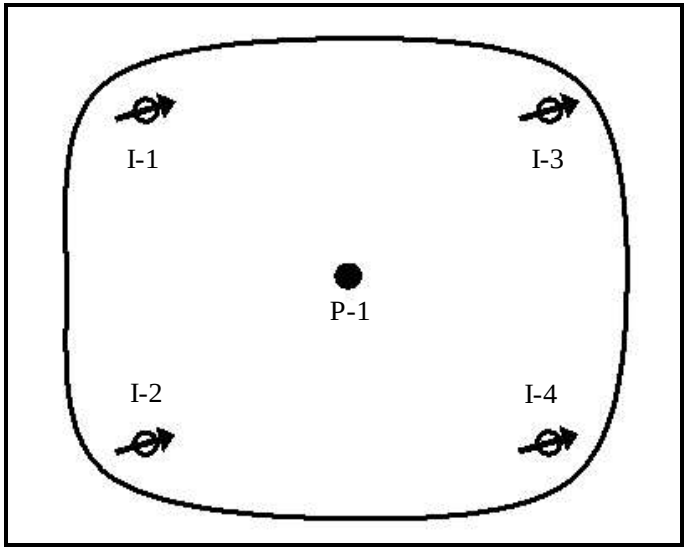

Figure 6-3. Five-Spot Waterflood

The reservoir consists of two communicating layers. The flow capacity in the upper layer is less than the flow capacity in the lower layer, and the volume of oil in the upper layer is less than the volume of oil in the lower layer. Well P-1 drained the initially undersaturated reservoir for one year prior to the onset of water injection. Bubble point pressure is 4014.7 psia. Primary depletion resulted in a substantial decline in reservoir pressure, the formation of a free gas phase, and a decline in oil production rate. Water injection was needed for pressure support and to sustain oil production rate.

Figure 6-4 and Figure 6-5 present reservoir pressure, oil production rate, and produced gas-oil ratio. Notice the change in the rate of reservoir pressure decline when reservoir pressure drops below bubble point pressure. The producing gas-oil ratio increases as a result of the formation of a free gas phase.

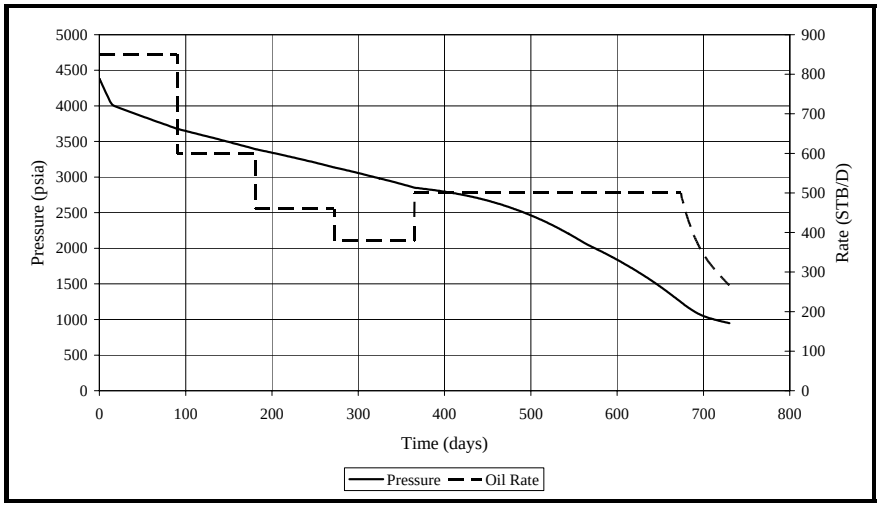

Figure 6-4. Pressure and Oil Rate

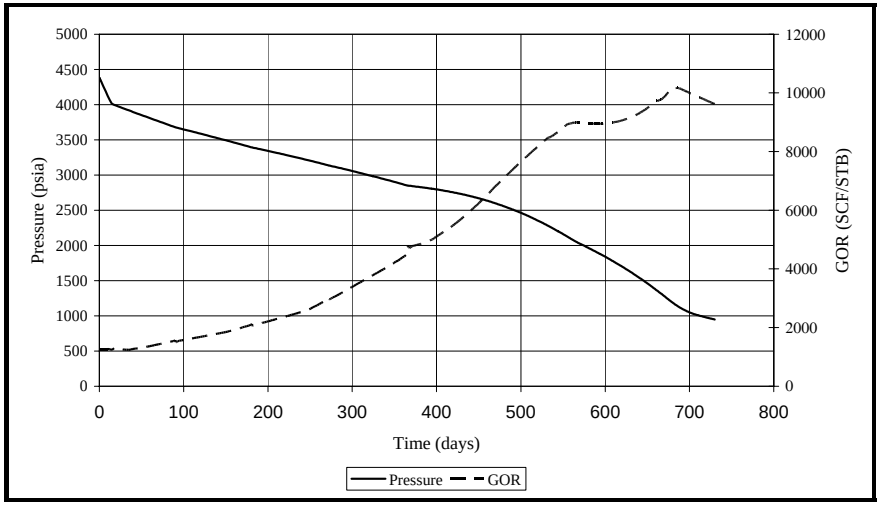

Figure 6-5. Pressure and Gas-Oil Ratio (GOR)

6.6 IFLO Application: Line-Drive Waterflood in a Naturally Fractured Reservoir

Injector-producer pairs can be used to help recover oil from a naturally fractured reservoir. In this example, we model a line-drive waterflood of the naturally fractured reservoir introduced in Section 3.5. Figure 6-6 shows the grid used in this model. It is a cross-section model with four rock matrix layers and four horizontal fracture layers. Most of the oil is in the rock matrix, and most of the flow capacity is in the fractures. In this example, the oil is initially undersaturated. Approximately 0.1% of the original oil in place is in the fractures and 99.9% is in the rock matrix.

Figure 6-6 is an example of a dual continuum model. Dual continuum models can model flow in two continua: the rock matrix, and fractures. To do so, they require data for both continua. It is necessary, for example, to provide porosity, permeability, and relative permeability curves for both the rock matrix and fractures. For this reason, models of naturally fractured reservoirs may be referred to as dual porosity, dual permeability models. Unfractured reservoirs would be referred to in this terminology as single porosity models even though their porosity and permeability distributions may be heterogeneous and anisotropic. For additional discussion of reservoir simulation of naturally fractured reservoirs, see Ganzer [2002], Carlson [2003], Ouenes, et al. [2004] and references therein.

An injection well injects water into the rock matrix and fractures in the first column on the left side of Figure 6-6. A production well in the first column on the right side of the figure produces fluids from the rock matrix and fractures. The system is flooded with water for 365 days. Figure 6-7 shows the water production rate. Water is being produced from well completions in the fractures. The water production rate shows large initial water production followed by rapid decline in water production from the fracture until the fractures have essentially been drained. Water

production rate increases again as injected water reaches the production well.

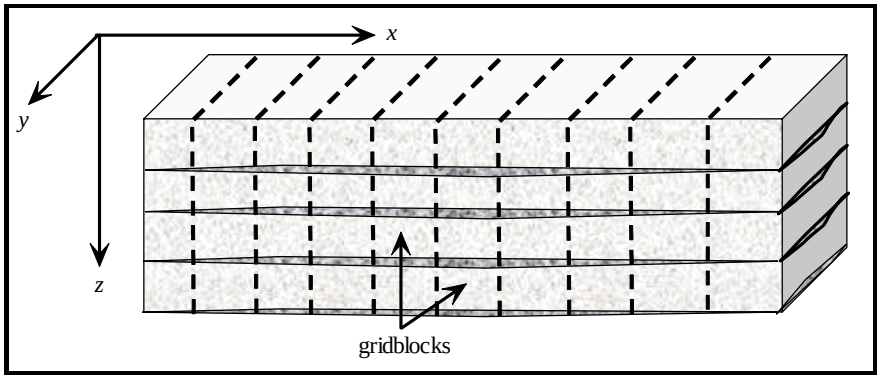

Figure 6-6. Cross-Section Model of a Reservoir with Horizontal Fractures

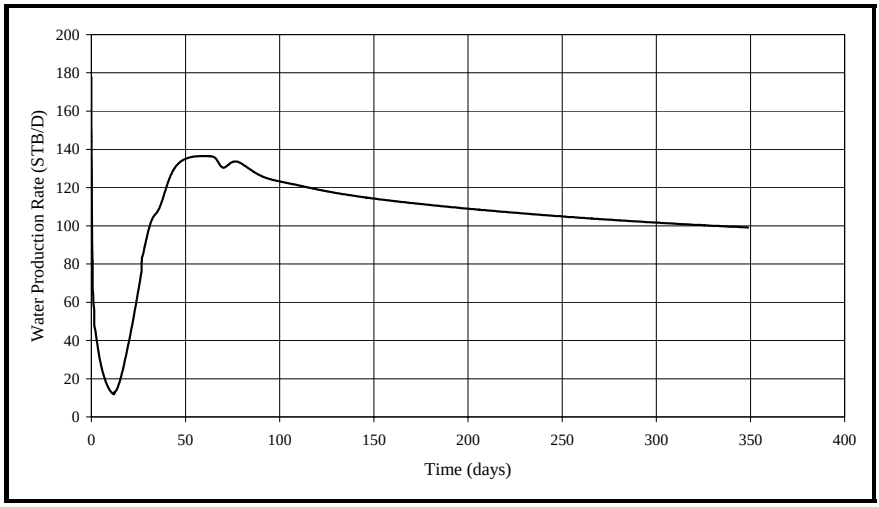

Figure 6-7. Water Production Rate

Water production is primarily from fractures, which we can see by looking at production from individual completions, and by looking at water saturation profiles. Figure 6-8 shows the water saturation profiles for the second matrix layer (model layer K = 3) and the second fracture (model layer K = 4). Irreducible water saturation is 30% in the matrix

and 0% in the fracture. The fracture relative permeability curves for this application are the linear functions shown in Section 3.5. Figure 6-8 shows that considerable water displacement has occurred in the fractures while relatively little water invasion has occurred in the rock matrix.

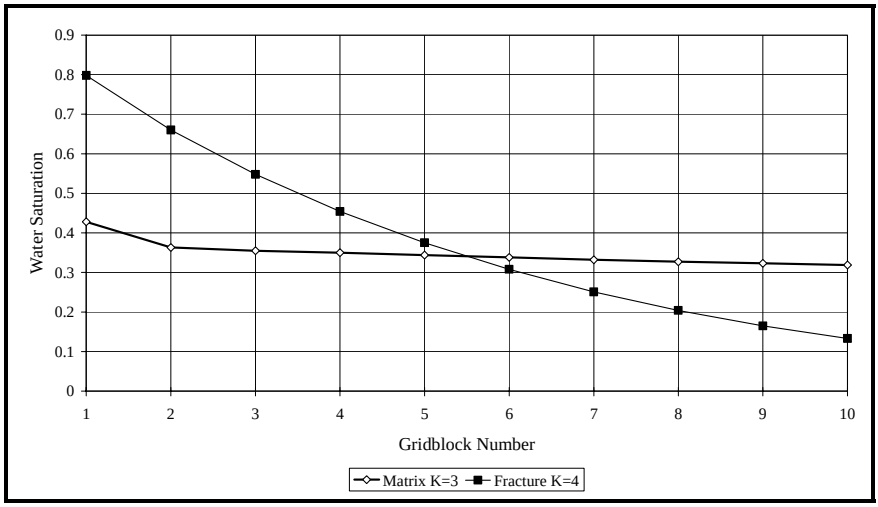

Figure 6-8. Water Saturation Profiles at 365 Days

Exercises

Exercise 6.1 Core floods show that the waterflood of a core with 80% initial oil saturation leaves a residual oil saturation of 30%. If the same core is resaturated with oil and then flooded with carbon dioxide, the residual oil saturation is 10%. What are the displacement efficiencies for the waterflood and the carbon dioxide flood if swelling effects are neglected?

Exercise 6.2 Assuming a log-normal distribution, estimate the Dykstra-Parsons coefficient for three sample permeabilities: k_1 = 35 md; k_2 = 48 md; k_3 = 126 md.

Exercise 6.3A File EXAM6.DAT is a model of a five-spot waterflood. The model volume is depleted by a single producer for one year. Four

water injectors are then added and the five-spot waterflood is implemented. Run EXAM6.DAT and record the time, pressure, oil rate, water rate, gas rate, producing GOR, initial oil in place, cumulative oil produced, and cumulative gas produced at the end of the run. Hint: initial oil in place is output in the run output file ITEMP.ROF. Verify the results shown in Figure 6-4 and Figure 6-5.

Exercise 6.3B What is the oil recovery efficiency at the end of the run?

Exercise 6.3C Use 3DView to view waterflood advance. Hint: open ITEMP.ARR, select water saturation (SW) as the active attribute, and select a display after 365 days.

Exercise 6.4 Calculate volumetric sweep efficiency E_{vol} and recovery efficiency *RE* from the following table:

Initial oil saturation Oil saturation at abandonment	0.75 0.30
Area Swept Total Area	750 hectares 1000 hectares
Thickness Swept Total Thickness	10 meters 15 meters
Neglect swelling effects, i.e. assume $B_{oi} \approx B_{oa}$	

Exercise 6.5 The Dykstra-Parsons coefficient for field A is 0.8 and for field B is 0.6. Which field is more heterogeneous?

Exercise 6.6A Suppose a reservoir is 3 mi. long by 5 mi. wide, has an average gross thickness of 50 ft., a net-to-gross ratio of 0.7, and a porosity of 0.18. Well logs show an average water saturation of 0.30. What is original oil in place if the oil formation volume factor is 1.4 RB/STB?

Express your answer in STB and note that 1 mi = 5280 ft and 1 bbl = 5.6146 cu ft.

Exercise 6.6B How much oil can be recovered if expected primary recovery is 15% and incremental oil recovery from waterflood is 20%?

Exercise 6.7 Calculate the Dykstra-Parsons coefficient for each of the following permeability distributions assuming permeability is log normally distributed.

Dykstra-Parsons Coefficient			
Assume log-normal distribution of permeability			
Layer	**kx_1**	**kx_2**	**kx_3**
	(md)	**(md)**	**(md)**
1	35	100	1
2	48	100	2
3	148	100	4
4	202	100	8
5	90	100	16
6	418	100	32
7	775	100	64
8	60	100	128
9	682	100	256
10	472	100	512
11	125	100	1024
12	300	100	2048
13	138	100	4096

14	191	100	8192
15	350	100	16384
Arithmetic Average			
Harmonic Average			
VDP			

Exercise 6.8A Run data file XS_FRACTURE.DAT and verify the results shown in Figure 6-7. Hint: gas production rates are listed in the timestep summary file ITEMP.TSS.

Exercise 6.8B Run data file XS_FRACTURE.DAT and verify the results shown in Figure 6-8. Hint: the water saturation values are found in the run output file ITEMP.ROF.

Chapter 7

Recovery of Subsurface Resources

Fluid recovery concepts during the life of a reservoir are summarized in this chapter. A review of the various production stages during the life of a conventional reservoir is followed by a discussion of recovery mechanisms for enhanced oil recovery (EOR) and unconventional fossil fuels.

7.1 Production Stages

The production life of a reservoir begins when reservoir fluid is withdrawn from the reservoir. Production can begin immediately after the discovery well is drilled, or several years later after several delineation wells have been drilled. Delineation wells are used to define the reservoir boundaries, while development wells are used to optimize resource recovery. Optimization criteria are defined by management and should take into account relevant governmental regulations. The optimization criteria may change during the life of the reservoir for a variety of reasons, including changes in technology, economic factors, and new information obtained during various stages of reservoir production. The stages of reservoir production are described below.

7.1.1 Primary Production

Primary production is ordinarily the first stage of production. It relies entirely on natural energy sources. To remove petroleum from the pore space it occupies, the petroleum must be replaced by another fluid, such as water, natural gas, or air. Oil displacement is caused by the expansion of *in situ* fluids as pressure declines during primary reservoir depletion. The natural forces involved in the displacement of oil during primary production are called reservoir drives. The most common reservoir drives for oil reservoirs are water drive, solution or dissolved gas drive, and gas cap drive.

The most efficient drive mechanism is water drive. In this case, water displaces oil as oil flows to production wells. An effective reservoir management strategy for a water drive reservoir is to balance oil withdrawal with the rate of water influx. Water drive recovery typically ranges from 35% to 75% of the original oil in place (OOIP).

In solution gas drive, gas dissolved in the oil phase at reservoir temperature and pressure is liberated as pressure declines. Some oil moves with the gas to the production wells as the gas expands and moves to the lower pressure zones in the reservoir. Recovery by solution gas drive ranges from 5% to 30% OOIP.

A gas cap is a large volume of gas at the top of a reservoir. When production wells are completed in the oil zone below the gas cap, the drop in pressure associated with pressure decline causes gas to move from the higher pressure gas cap down toward the producing wells. The gas movement drives oil to the wells, and eventually large volumes of gas will be produced with the oil. Gas cap drive recovery ranges from 20% to 40% OOIP, although recoveries as high as 60% can occur in steeply dipping reservoirs with enough permeability to allow oil to drain to downstructure production wells.

Gravity drainage is the least common of the primary production mechanisms. In this case, oil moves downstructure to a producing well. Downstructure movement of oil in an oil-water system is the result of a pressure gradient that favors downstructure oil flow over oil movement

upstructure due to gravity segregation. Gravity drainage can be effective when it works. It is most likely to occur in shallow, highly permeable, steeply dipping reservoirs.

A schematic comparison of primary production mechanisms on reservoir pressure and recovery efficiency is sketched in Figure 7-1. In many cases, two or more drive mechanisms are functioning simultaneously. The behavior of the field depends on which mechanism is most important at various times during the life of the field. The best way to predict the behavior of such fields is by using sophisticated reservoir flow models.

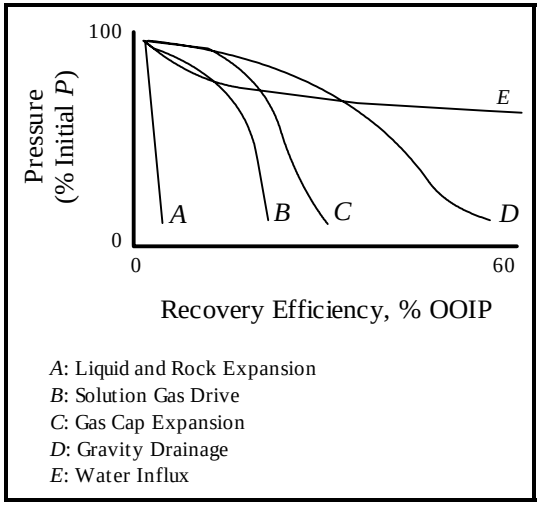

Figure 7-1. Comparison of primary production mechanisms

If we rearrange the terms in the general material balance equation for an oil reservoir, Eq. (2.6), we can estimate the relative importance of different drive mechanisms. Table 7-1 gives the indices representing different drives relative to the hydrocarbon production given by

$$D_{HC} = N_p B_o + G_{pc} B_{gc} + \left[G_{ps} - N_p R_{so}\right] B_g \tag{7.1}$$

Table 7-1
Drive Indices from the Schilthuis Material Balance Equation

Drive	Index
Solution Gas	$I_{sg} = ND_o / D_{HC}$
Gas Cap	$I_{gc} = ND_{go} / D_{HC}$
Water	$I_w = [(W_e - W_p)B_w] / D_{HC}$
Injected Fluids	$I_i = [W_iB_w + G_iB'_g] / D_{HC}$
Connate Water and Rock Expansion	$I_e = [N(D_w + D_{gw}) + ND_r] / D_{HC}$

The sum of the drive indices equals one, thus

$$I_{sg} + I_{gc} + I_w + I_i + I_e = 1 \qquad (7.2)$$

Equation (7.2) can be derived by rearranging Eq. (2.6). A comparison of the magnitudes of the drive indices indicates which drive is dominating the performance of the reservoir. If the sum of the drive indices in Eq. (7.2) does not equal one based on available data, Pletcher [2002, page 49] has cautioned that the drive indices should not be normalized to one because this may obscure the usefulness of the drive indices and "lead to a false sense of security."

Although the above discussion refers to oil reservoirs, similar comments apply to gas reservoirs. Water drive and gas expansion with reservoir pressure depletion are the most common drives for gas reservoirs. Gas reservoir recovery can be as high as 70% to 90% of original gas in place (OGIP) because of the high mobility of gas relative to oil mobility.

Gas storage reservoirs have a different life cycle than gas reservoirs that are being depleted. Gas storage reservoirs are used as a warehouse for gas. If the gas is used as a fuel for power plants, it will also need to be periodically produced and replenished. The performance attributes of a gas storage reservoir are [Tek, 1996, pg. 4]:

- Verification of inventory
- Assurance of deliverability
- Containment against migration

The gas inventory consists of working gas and cushion gas. Gas deliverability must be sufficient to account for swings in demand. Demand can vary daily and seasonally. Gas containment is needed to conserve the amount of stored gas. For more discussion of natural gas storage in reservoirs, see references such as Tek [1996], Smith [1990], and Katz and Lee [1990].

7.1.2 Secondary Production

Primary depletion is usually not sufficient to optimize recovery from an oil reservoir. Oil recovery can be both accelerated and increased by supplemental natural reservoir energy. The supplemental energy is provided using an external energy source, such as water injection or gas injection. The injection of water or natural gas may be referred to as pressure maintenance or secondary production. The latter term arose because injection usually follows a period of primary pressure depletion, and is therefore the second production method used in a field. Many modern reservoirs incorporate pressure maintenance early in the production life of the field, sometimes from the beginning of production. In this case the reservoir is not subjected to a conventional primary production phase. The term *pressure maintenance* more accurately describes the reservoir management strategy for these fields than the term *secondary production*.

7.1.3 Alternative Classifications

Both primary and secondary recovery processes are designed to produce oil using immiscible methods. Additional methods may be used to improve oil recovery efficiency by reducing residual oil saturation. The reduction of residual oil saturation requires a change in such factors

as interfacial tension (IFT) or wettability. Methods designed to reduce residual oil saturation have been referred to in the literature as:

- Tertiary Production
- Enhanced Oil Recovery
- Improved Oil Recovery

The term *tertiary production* was originally used to identify the third stage of the production life of the field. Typically the third stage occurred after waterflooding. The third stage of oil production would involve a process that was designed to mobilize waterflood residual oil. An example of a tertiary production process is a chemical flood process such as surfactant flooding.

Tertiary production processes were designed to improve displacement efficiency by injecting fluids or heat. They were referred to as enhanced recovery processes. It was soon learned, however, that some fields would perform better if the enhanced recovery process was implemented before the third stage in the life of the field. In addition, it was found that enhanced recovery processes were often more expensive than just drilling more wells in a denser pattern.

The drilling of wells to reduce well spacing and increase well density is called infill drilling. The birth of the term *infill drilling* was coincident with the birth of another term, *improved recovery*, which includes enhanced oil recovery and infill drilling. Some major improved recovery processes are waterflooding, gasflooding, chemical flooding, and thermal recovery [Dyke, 1997]. They are discussed in more detail below.

7.2 Enhanced Oil Recovery

Improved recovery technology includes traditional secondary recovery processes such as waterflooding and immiscible gas injection, as well as enhanced oil recovery (EOR) processes. EOR processes are usually classified as follows: chemical, miscible, thermal, and microbial.

A brief description of each of these processes is presented below. The success of an EOR project depends on good planning. Hite, et al. [2005] recommend the following steps for planning an EOR project [paraphrased from Hite, et al., 2005, page 28]:

1. Identify the appropriate EOR process
2. Characterize the reservoir
3. Determine engineering design parameters
4. Conduct pilot or field tests as needed
5. Finish with a plan to manage the project

Reservoir flow models are an important tool in the EOR project planning process.

The literature on EOR is extensive. For more detailed discussions of EOR, including screening criteria and analyses of displacement mechanisms, see such references as Taber and Martin [1983], Lake [1989], Martin [1992], Taber, et al. [1997a,b], and Green and Willhite [1998].

7.2.1 Chemical

Chemical flooding methods include polymer flooding, micellar-polymer flooding or surfactant-polymer flooding, and alkaline or caustic flooding. Polymer flooding is designed to improve the mobility ratio and fluid flow patterns of a displacement process by increasing the viscosity of the injected aqueous phase. In this case, high molecular weight polymer is added to injected water. Micellar-polymer flooding uses a detergent-like solution to lower residual oil saturation to waterflooding. The polymer slug injected after the micellar slug is designed to improve displacement efficiency. Alkaline flooding uses alkaline chemicals that can react with certain types of *in situ* crude. The resulting chemical product is miscible with the oil and can reduce residual oil saturation to waterflooding.

7.2.2 Miscible

Miscible flooding methods include carbon dioxide injection, natural gas injection, and nitrogen injection. Miscible gas injection must be performed at a high enough pressure to ensure miscibility between the injected gas and *in situ* oil. Miscibility is achieved when interfacial tension (IFT) between the aqueous and oleic phases is significantly reduced. The desired IFT reduction is typically from around 1 dyne/cm to 0.001 dyne/cm or less. Any reduction in IFT can improve displacement efficiency, and a near miscible process can yield much of the incremental oil that might be obtained from a miscible process. If reservoir pressure is not maintained above the minimum miscibility pressure (MMP) of the system, the gasflood will be an immiscible gas injection process.

Immiscible gas can be used as the principal injection fluid in a secondary displacement process, or it can be used as the injection fluid for a tertiary process. Two improved recovery processes based on immiscible gas injection are the double displacement process (DDP) and the second contact water displacement (SCWD) process [Novakovic, 1999]. Both processes require the injection of immiscible gas into reservoirs that have been previously waterflooded. The processes require favorable gas-oil and oil-water interfacial tensions. Oil remaining after waterflood can coalesce into a film when exposed to an immiscible gas. The oil film can be mobilized and produced by downdip gravity drainage (the DDP process) or by water influx from either an aquifer or water injection (SCWD) following the immiscible gas injection period.

7.2.3 Thermal

Thermal flooding methods include hot water injection, steam drive, steam soak, and *in situ* combustion. The injection or generation of heat in a reservoir is designed to reduce the viscosity of *in situ* oil and improve the mobility ratio of the displacement process. Electrical methods can also be used to heat fluids in relatively shallow reservoirs containing high viscosity oil, but electrical methods are not as common

as hot fluid injection methods. The *in situ* combustion method requires compressed air injection after *in situ* oil has been ignited. Steam injection methods require the injection of steam into a reservoir. Steam and hot water injection processes are the most common thermal methods because of the relative ease of generating hot water and steam. The *in situ* combustion process is more difficult to control than steam injection processes and it requires *in situ* oil that can be set on fire. Hot gases and heat advance through the formation and displace the heated oil to production wells.

7.2.4 Microbial

Microbial EOR uses the injection of microorganisms and nutrients in a carrier medium to increase oil recovery, reduce water production in petroleum reservoirs, or both. Dietrich, et al. [1996] summarized the results of five successful commercial microbial EOR projects. The projects reflected a diversity of locations, lithologies, depths, porosities, permeabilities, and temperatures. Two of the projects were in the United States, two were in China, and one was in Argentina. The projects included sandstone, fractured dolomite, siltstone-sandstone, and fractured sandstone reservoirs. Reservoir depths ranged from 4450 ft. to 6900 ft., temperatures from 110° F to 180° F, porosity from 0.079 to 0.232, and effective permeability from 1.7 md to 300 md. Evidence from laboratory research and field case studies shows that microbial EOR processes can result in the incremental recovery of oil and also reduce water production from high permeability zones. However, research is continuing to maximize the technical and economic potential for microbial EOR. For example, the U.S. Department of Energy has underwritten the development of microbial transport simulators.

7.3 Unconventional Fossil Fuels

Oil and gas fields are considered conventional sources of fossil fuels. In the following, we discuss several unconventional sources of

fossil fuels. The unconventional sources are becoming a more important part of the global energy mix as the price of oil increases.

7.3.1 Coalbed Methane

Coalbeds are an abundant source of methane [Selley, 1998; Rogers, 1994]. The presence of methane gas in coal has been well known to coal miners as a safety hazard, but is now being viewed as a source of natural gas. The gas is bound in the micropore structure of the coalbed. It is able to diffuse into the natural fracture network when a pressure gradient exists between the matrix and the fracture network. The fracture network in coalbeds consists of microfractures. Coalbed microfractures allow Darcy flow and are called "cleats."

Gas recovery from coalbeds depends on three processes [Kuuskraa and Brandenburg, 1989]. Coalbed methane exists as a monomolecular layer on the internal surface of the coal matrix. Its composition is predominately methane, but can also include other constituents, such as ethane, carbon dioxide, nitrogen and hydrogen [Mavor, et al., 1999]. For this reason, coalbed methane is also known as coal gas to highlight the observation that gas from coalbeds is usually a mixture. Gas content can range from approximately 20 standard cubic feet (SCF) gas per ton of coal in the Powder River Basin of Wyoming [Mavor, et al., 1999] to 600 SCF per ton in the Appalachian Basin [Gaddy, 1999].

Gas recovery begins with desorption of gas from the internal surface to the coal matrix and micropores. The gas then diffuses through the coal matrix and micropores into the cleats. Finally, gas flows through the cleats to the production well. The flow rate depends, in part, on the pressure gradient in the cleats and the density and distribution of cleats. The controlling mechanisms for gas production from coalbeds are the rate of desorption from the coal surface to the coal matrix, the rate of diffusion from the coal matrix to the cleats, and the rate of flow of gas through the cleats. The flow rate in the cleats obeys Darcy's Law in many systems, but may also depend on stress-dependent permeability or gas slippage (the Klinkenberg effect). Shi and Durucan [2005] discuss the dependence

of coalbed permeability on stress. Stress-dependent permeability in oil and gas fields is discussed in more detail in Chapter 14.

The production performance of a well producing gas from a coalbed will typically exhibit three stages. The reservoir dewaters and methane production increases during the first stage of pressure depletion. Methane production peaks during the second stage. The amount of water produced is relatively small compared to gas production during the second stage because of gas-water relative permeability effects, and desorption of natural gas provides a counterbalance to permeability loss as a result of formation compaction. The third stage of production is similar to conventional gas field production in which gas rate declines as reservoir pressure declines.

Coalbed methane recovery can be enhanced by injecting carbon dioxide into the coal seam. Carbon dioxide preferentially displaces methane in the coal matrix. The displaced methane can then be produced through the cleat system. The resulting adsorption of carbon dioxide by coal can be used to sequester, or store, carbon dioxide in the coal seam. Carbon dioxide sequestration has an environmental benefit that is discussed in more detail in Chapter 8.

7.3.2 Gas Hydrates

The entrapment of natural gas molecules in ice at very low temperatures forms an ice-like solid which is a metastable complex called a gas hydrate. Gas hydrates are clathrates. A clathrate is a chemical complex that is formed when one type of molecule completely encloses another type of molecule in a lattice. In the case of gas hydrates, hydrogen-bonded water molecules form a cage-like structure in which mobile molecules of gas are absorbed or bound.

The presence of gas hydrates can complicate field operations. For example, the existence of hydrates on the ocean floor can affect drilling operations in deep water. The simultaneous flow of natural gas and water in tubing and pipelines can result in the formation of gas hydrates that can impede or completely block the flow of fluids through pipeline

networks. Heating the gas or treating the gas-water system with chemical inhibitors can prevent the formation of hydrates, but increases operating costs.

Gas hydrates are generally considered a problem for oil and gas field operations, but their potential commercial value as a clean energy resource is changing industry perception. The potential as a gas resource is due to the relatively large volume of gas contained in the gas hydrate complex. In particular, Makogon, et al. [1997] have reported that one cubic meter of gas hydrate contains 164.6 m^3 of methane. This is equivalent to one barrel of gas hydrate containing 924 ft^3 of methane, and is approximately six times as much gas as the gas contained in an unimpeded gas-filled pore system [Selley, 1998, pg. 25]. The gas in gas hydrates occupies approximately 20% of the volume of the gas hydrate complex. Water occupies the remaining 80% of the gas hydrate complex volume.

Gas hydrates can be found throughout the world [Selley, 1998; Makogon, et al., 1997]. They exist on land in sub-Arctic sediments and on seabeds where the water is near freezing at depths of at least 600 to 1500 feet. For instance, favorable conditions for gas hydrate formation exist at sea floor temperatures as low as 39°F in the Gulf of Mexico and as low as 30°F in some sections of the North Sea. According to Makogon, et al. [1997], over 700 trillion m^3 in explored reserves of methane in the hydrate state exist. Difficulties in cost effective production have hampered development of the resource.

7.3.3 Tight Gas Sands and Shale Gas

Unconventional gas resources include coalbed methane, tight gas sands and fractured gas shales. Coalbed methane was discussed above. Both tight gas sands and gas shales are characterized by low permeabilities, that is, permeabilities that are a fraction of a millidarcy. The low permeability associated with unconventional gas resources makes it more difficult to produce the gas at economical rates.

Economic production of gas from a gas shale or tight gas sand often requires the creation of fractures by a process known as hydraulic fracturing [Wattenbarger, 2002; Kuuskraa and Bank, 2003]. In this process, a fluid is injected into the formation at a pressure that exceeds the fracture pressure of the formation. Once fractures have been created in the formation, a proppant such as manmade pellets or coarse grain sand is injected into the fracture to prevent it from closing, or healing, when the injection pressure is removed. The proppant provides a higher permeability flow path for gas to flow to the production well. Unconventional low permeability gas sands and shales often require more wells per unit area than conventional higher permeability gas reservoirs. The key to managing an unconventional gas resource is to develop the resource with enough wells to maximize gas recovery without drilling unnecessary wells.

7.3.4 Shale Oil and Tar Sands

Shale oil is high API gravity oil contained in porous, low permeability shale. Sand grains that are cemented together by tar or asphalt are called tar sands. Tar and asphalt are highly viscous, plastic or solid hydrocarbons. Extensive shale oil and tar sand deposits are found throughout the Rocky Mountain region of North America, as well as in other parts of the world. Although difficult to produce, the volume of hydrocarbon in tar sands has stimulated efforts to develop production techniques.

The hydrocarbon in shale oil and tar sands can be extracted by mining when they are close enough to the surface. Tar pits have been found around the world and have been the source of many fossilized dinosaur bones. In locations where oil shale and tar sands are too deep to mine, it is necessary to increase the mobility of the hydrocarbon.

An increase in permeability or a decrease in viscosity can increase mobility. Increasing the temperature of high API gravity oil, tar or asphalt can significantly reduce viscosity. If there is enough permeability to allow injection, steam or hot water can be used to increase formation

temperature and reduce hydrocarbon viscosity. In many cases, however, permeability is too low to allow significant injection of a heated fluid. An alternative to fluid injection is electromagnetic heating. Radio frequency heating has been used in Canada, and electromagnetic heating techniques are being developed for other parts of the world.

7.4 IFLO Coal Gas Model

The coal gas model in IFLO is designed to model production of gas from coalbeds. Gas desorption from the coal matrix into the cleat system during depletion of a coal seam is included in the reservoir simulator flow equations as a gas desorption rate q_{cg}. Coal gas desorption is modeled as a process that obeys Fick's law of diffusion, namely

$$D_c\left[\frac{1}{r^2}\frac{\partial}{\partial r}r^2\frac{\partial C}{\partial r}\right]=\frac{\partial C}{\partial t},0<r\le r_c \tag{7.3}$$

where D_c is the diffusion coefficient, r is radius in spherical coordinates, r_c is the radius of a spherical coal particle, and C is the gas content of coal in SCF of gas per ton of coal. The diffusion process obeys the initial and boundary conditions

$$\left.\frac{\partial C}{\partial r}\right|_{r=0}=0;C\left(r_c,t\right)=G_c\left(P\right) \tag{7.4}$$

where the coal gas content $G_c(P)$ is a function of pressure given by the Langmuir isotherm

$$G_c=V_L\frac{P}{P_L+P} \tag{7.5}$$

The parameters V_L and P_L are the Langmuir volume and Langmuir pressure respectively.

The diffusion equation, Eq. (7.3), is first solved for the gas content $C(r,t)$. The rate of gas desorption q_{cg} is calculated from $C(r,t)$ as

$$q_{cg}=\rho_c V_c\frac{3D_c}{r_c}\left.\frac{\partial C}{\partial r}\right|_{r_c} \tag{7.6}$$

where V_c is the volume of coal and ρ_c is coal density [Ancell, et al., 1980; King and Ertekin, 1995]. The ratio D_c/r_c in Eq. (7.6) is called the diffusivity of the coal seam. A finite difference representation of the derivative $\partial C(r,t)/\partial r$ is then used to calculate q_{cg}. The user directly enters the parameters D_c, r_c, ρ_c, V_L and P_L. The coal volume V_c is calculated from the reservoir description provided by the user.

7.4.1 Critical Desorption Pressure

Gas content G_c in saturated coal seams is given by the Langmuir isotherm, Eq. (7.5). A coal seam is undersaturated if the laboratory measured gas content corresponds to a pressure on the Langmuir isotherm that is less than the initial reservoir pressure measured by a well test. To handle this case, the user may enter a critical desorption pressure P_{CD}. If the undersaturated coal gas model is selected, the gas content will depend on P_{CD}. In particular, gas content G_c at P_{CD} will be used when coal seam pressure $P > P_{CD}$, otherwise gas content G_c will be calculated at P.

7.5 IFLO Application: Coal Gas Production from a Fruitland Coal

We illustrate the application of the coal gas model to a scenario published by Paul, et al. [1990]. They presented a model of two coal layers with Fruitland coal formation properties separated by a sandstone layer. Properties for each layer in the Fruitland coal model are presented in Table 7-2. The Fruitland coal is in the San Juan Basin in the Four Corners region of the United States. The Four Corners region is located where the states of Utah, Colorado, New Mexico, and Arizona have a common border. Both coal layers are water saturated while the sandstone layer has a free gas saturation of 15%. An impermeable layer separates

each of the three permeable layers so that there is no vertical communication.

Table 7-2
Layer Properties for Fruitland Coal Model

Layer	Depth to Top of Layer (ft)	Lithology	Porosity (fraction)	Lateral Permeability (md)	Gross Thickness (ft)
1	2500	Coal	0.02	20	15
No Flow	2515				10
2	2525	Sandstone	0.20	100	5
No Flow	2530				10
3	2540	Coal	0.02	5	15

The model uses a 10 × 10 grid with 3 layers (coal – sandstone – coal). Three wells produce from all three layers and drain an area of 1 sq. mi. Well locations are shown in Figure 7-2. Further details are given in Problem 1 of Paul, et al. [1990].

We used the same porosity and permeability distributions, relative permeability curves, water properties, and initial pressure and saturation conditions specified as Paul, et al. [1990]. The gas properties used here were based on gas correlations for a gas with specific gravity of 0.60 at a reservoir temperature of 95°F. Paul, et al. [1990] assumed the formation was incompressible. By contrast, rock compressibility in our model was set to 3×10^{-6} psi^{-1}. Rock compressibility is needed to calculate uniaxial compaction, which was one of the original goals for developing IFLO [Fanchi, 2002b, 2003b]. We limit maximum water production rate to help reduce fluid throughput problems when production wells first begin to produce. Finally, our coalbed methane algorithm uses diffusivity while Paul, et al. [1990] used sorption time. Consequently, the gas diffusion parameters for our model were adjusted to approximate the

performance of the gas production model used by Paul, et al. [1990].

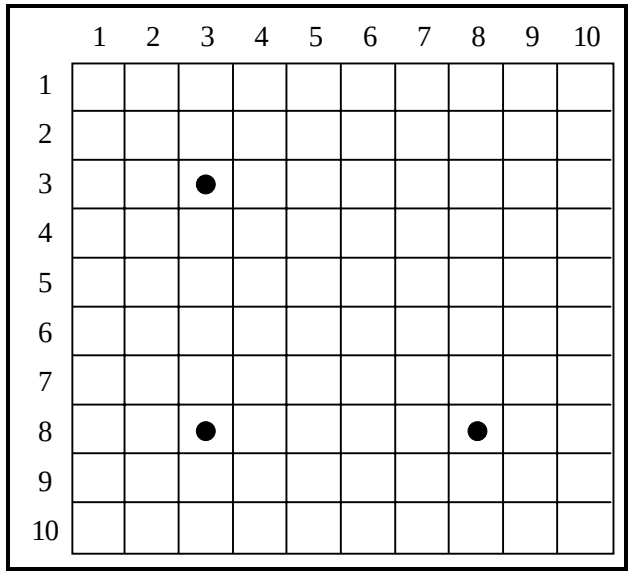

Figure 7-2. Well Locations for Fruitland Coal Model

Paul, et al. [1990] did not provide the static moduli needed for geomechanical property calculations. In the absence of measured data, static elastic properties were estimated from Young's modulus and Poisson's ratio for coal [Jones, et al., 1988]. The static to dynamic conversion of bulk modulus was made using a correlation between dynamic and static Young's modulus for soft rocks presented by Wang [2000]. The dynamic bulk modulus and shear modulus were estimated to be 8.2×10^5 psi and 3.2×10^5 psi respectively. The dynamic to static conversion was not made for the sandstone. The integrated flow model calculated the compressional velocity to shear velocity ratio V_P/V_S as 1.97 in the coal layers, and 1.61 in the sandstone layer. These results are reasonable. Schraufnagel [1991] has shown that V_P/V_S can vary over a wide range (1.7 to 2.7) for Black Warrior Basin coals. More accurate estimates of geomechanical information could be obtained by measuring moduli for the specific formations of interest. Sonic logs and vertical seismic profiles could be used to determine the desired petrophysical information.

Figure 7-3 shows gas and water production rates for this scenario. The sharp increases in water rate show when each water production well begins to produce. The water rate declines sharply as gas desorbs from the coal and flows through the cleat system to the wells.

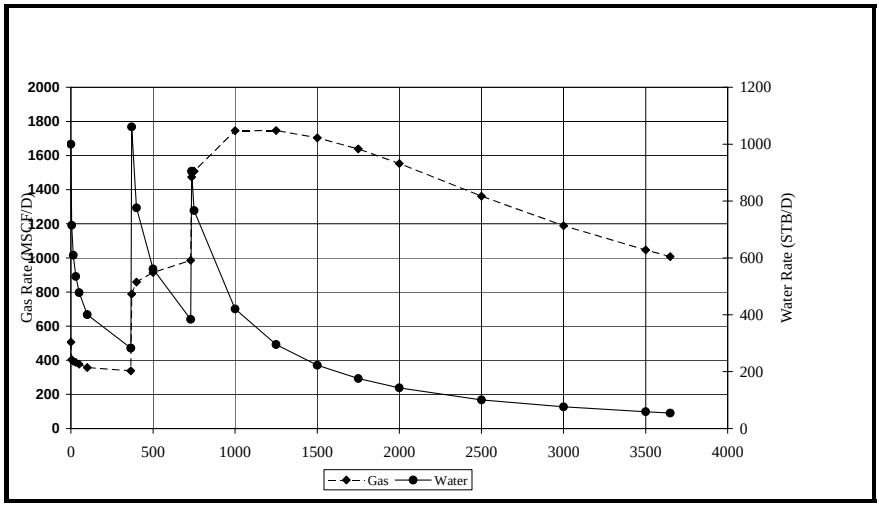

Figure 7-3. Gas and Water Rates for Production from Fruitland Coal

Exercises

Exercise 7.1 Use the definitions in Table 7-1 and Eq. (7-1) to derive Eq. (7-2) from Eq. (2.6).

Exercise 7.2A Which drive index in Table 7-1 will be largest in a field containing dead oil that is subjected to pressure depletion?

Exercise 7.2B Suppose a dead oil reservoir is subjected to a peripheral waterflood. Identify the two drive indices in Table 7-1 that will have the greatest influence on oil recovery.

Exercise 7.3A List the letters of the following recovery processes that are considered improved oil recovery methods.

a. steamflood	e. in situ combustion
b. solution gas drive	f. microbial EOR
c. waterflood	g. water drive by aquifer influx
d. miscible gas injection	h. polymer flooding

Exercise 7.3B List the letters of the recovery processes in Problem #3 that are considered enhanced oil recovery processes.

Exercise 7.4 What are the three stages of production performance for a coalbed methane well?

Exercise 7.5A A coal seam is 800 feet wide, 1 mile long, and 10 feet thick. The volume occupied by the fracture network is 1%. What is the volume of coal in the coal seam? Express your answer in ft^3 and m^3.

Exercise 7.5B If the density of coal is 1.7 lbm/ft^3, how many tonnes of coal are in the coal seam? Note that 1 ton = 2000 lbm = 907 kg = 0.907 tonne.

Exercise 7.6A Assume the Langmuir isotherm $G_c = V_L \frac{P}{P_L + P}$ for a coal seam has a Langmuir volume of 600 standard cubic feet per ton of coal (SCF/ton) and a Langmuir pressure of 450 psia. Calculate the volume of gas per ton of coal at a pressure of 1000 psia. Express your answer in SCF/ton where 1 ton = 2000 lbm.

Exercise 7.6B How much gas is contained in the coal? Assume the mass of coal is $mass_{coal} = 3.22 \times 10^4 \, tonne$. Express your answer in SCF and cubic meters. Note that 1 ton = 2000 lbm = 907 kg = 0.907 tonne.

Exercise 7.7 Some EOR simulators can be found on the internet. Access the internet and search for a website containing public domain EOR simulators. Hint: The United States Department of Energy is one governmental agency that has distributed EOR software using a website.

Exercise 7.8 Run file CBM_SPE20733-1_PVTG.dat and plot gas production rate and water production rate as functions of time.

Chapter 8

Economics and the Environment

Economic analyses are an essential aspect of a reservoir management study. The economic performance of a prospective project is often the deciding factor in determining whether to undertake a project. Consequently, it is important to be aware of basic economic concepts and factors that may affect the economic performance of a project. These topics are introduced here. Further details can be found in references such as Thompson and Wright [1985], Satter and Thakur [1994], Seba [1998], and Newendorp and Schuyler [2000].

8.1 Society of Petroleum Engineers and World Petroleum Congress Reserves

The analysis of a petroleum project depends on the amount of commercially valuable resource that is available. According to the Society of Petroleum Engineers (SPE) and the World Petroleum Congress (WPC) [Staff-JPT, 1997], reserves are those quantities of petroleum that are anticipated to be commercially recoverable from known accumulations from a given date forward. Table 8-1 summarizes the SPE/WPC definitions of reserves which include both qualitative and quantitative criteria. Although the SPE/WPC definitions have been adopted in many parts of the world, they are not universal. For example, a different, yet

analogous, set of definitions exists in the Russian Federation [Nemchenko, et al., 1995; Grace, et al., 1993].

Table 8-1
SPE/WPC Reserves Definitions

Category	Definitions
Proved reserves	➢ Those quantities of petroleum that, by analysis of geological and engineering data, can be estimated with reasonable certainty to be commercially recoverable, from a given date forward, from known reservoirs and under current economic conditions, operating methods, and government regulation. ➢ In general, reserves are considered proved if the commercial producibility of the reservoir is supported by actual production or formation tests. ➢ There should be at least a 90% probability (P_{90}) that the quantities actually recovered will equal or exceed the estimate.
Unproved reserves	Those quantities of petroleum which are based on geologic and/or engineering data similar to that used in estimates of proved reserves; but technical, contractual, economic, or regulatory uncertainties preclude such reserves from being classified as proved.
Probable reserves	➢ Those unproved reserves deemed more likely than not to be recoverable based on analysis of geological and engineering data. ➢ There should be at least a 50% probability (P_{50}) that the quantities actually recovered will equal or exceed the estimate.

Possible reserves	➢ Those unproved reserves deemed less likely to be recoverable than probable reserves based on analysis of geological and engineering data. ➢ There should be at least a 10% probability (P_{10}) that the quantities actually recovered will equal or exceed the estimate.

The probability distribution associated with the SPE/WPC reserves definitions can be estimated with relative ease if the modeling team has performed a sensitivity analysis that generates a set of cases that yield low, medium, and high reserve estimates. In the absence of data to the contrary, a reasonable first approximation is that each case is equally likely to occur. Given this assumption, an average μ and standard derivation σ may be calculated from the sensitivity analysis results to prepare a normal distribution of reserves. For a normal distribution with mean μ and standard deviation σ, the SPE/WPC reserves definitions are quantified as follows:

$$\text{Proved reserves} = P_{90} = \mu \sim 1.28\,\sigma$$

$$\text{Probable reserves} = P_{50} = \mu$$

$$\text{Possible reserves} = P_{10} = \mu + 1.28\,\sigma$$

The normal distribution can be used to associate an estimate of the likelihood of occurrence of any particular prediction case with its corresponding economic forecast. Keep in mind, however, that the actual distribution of reserves may not be normal, and that a detailed analysis of the distribution may be needed in many cases.

8.2 Basic Economic Concepts

The cash flow of a project is the net cash generated or expended on the project as a function of time. The time value of money is included in economic analyses by applying a discount rate to adjust the value of money to the value during a base year. Discount rate is the adjustment

factor, and the resulting cash flow is called the discounted cash flow. The net present value (NPV) of the cash flow is the value of the cash flow at a specified discount rate. The discount rate at which NPV is zero is called the discounted cash flow return on investment (DCFROI) or internal rate of return (IRR).

Figure 8-1 shows a typical plot of NPV as a function of time. The early time part of the figure shows a negative NPV and indicates that the project is operating at a loss. The loss is usually associated with initial capital investments and operating expenses that are incurred before the project begins to generate revenue. The reduction in loss and eventual growth in positive NPV is due to the generation of revenue in excess of expenses. The point in time on the graph where the NPV is zero after the project has begun is the discounted payout time. Discounted payout time on Figure 8-1 is approximately four years.

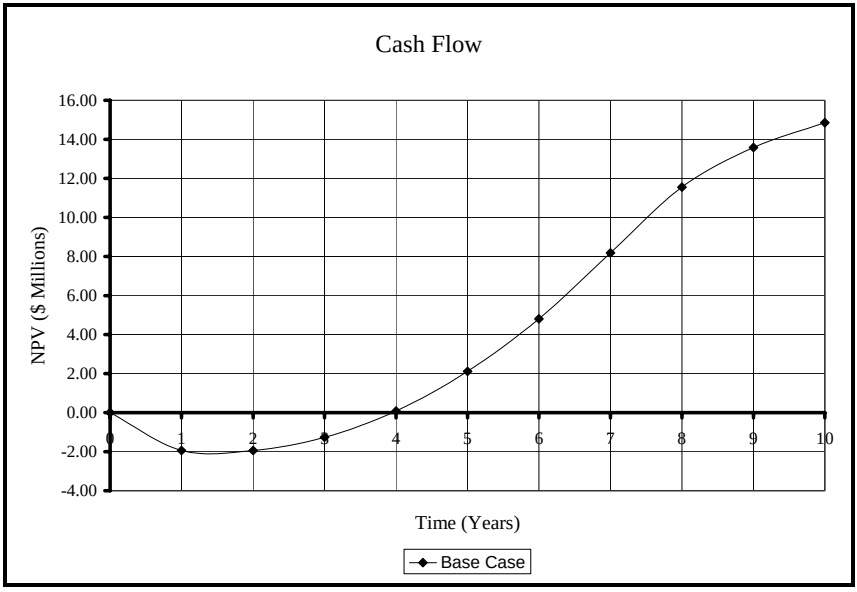

Figure 8-1. Typical cash flow

Discounted cash flow return on investment (DCFROI) and discounted payout time are measures of the economic viability of a project.

Another measure is the profit-to-investment (PI) ratio which is a measure of profitability. It is defined as the total undiscounted cash flow without capital investment divided by total investment. Unlike the DCFROI, the PI ratio does not take into account the time value of money. Table 8-2 presents the definitions of several commonly used economic measures. Useful plots include a plot of NPV versus time and a plot of NPV versus discount rate.

Table 8-2
Definitions of Selected Economic Measures

Economic Measure	Definition
Discount Rate	Factor to adjust the value of money to a base year.
Net Present Value (NPV)	Value of cash flow at a specified discount rate.
DCFROI or IRR	Discount rate at which NPV = 0.
Discounted Payout Time	Time when NPV = 0.
Profit-to-Investment (PI) Ratio	Undiscounted cash flow without capital investment divided by total investment.

The ideas discussed above are quantified as follows. *NPV* is the difference between the present value of revenue *R* and the present value of expenses *E*, thus

$$NPV = R - E \tag{8.1}$$

If we define $\Delta E(k)$ as the expenses incurred during a time period *k*, then *E* may be written as

$$E = \sum_{k=0}^{N \times Q} \frac{\Delta E(k)}{\left(1 + \frac{i'}{Q}\right)^k} \tag{8.2}$$

where i' is the annual inflation rate, N is the number of years of the expenditure schedule, and Q is the number of times interest is compounded each year. A similar expression is written for revenue R:

$$R = \sum_{k=0}^{N\times Q} \frac{\Delta R(k)}{\left(1+\frac{i}{Q}\right)^k} \tag{8.3}$$

where $\Delta R(k)$ is revenue obtained during time period k, and i is the annual interest or discount rate. Equations (8.2) and (8.3) include the assumptions that i and i' are constants over the life of the project, but i and i' are not necessarily equal. These assumptions let us compute the present value of money expended relative to a given inflation rate i' and compare the result to the present value of revenue associated with a specified interest or discount rate i.

8.2.1 Illustration: NPV and Breakeven Oil Price

The *NPV* and breakeven oil price for an oil production project can be obtained from the above analysis as an illustration of the concepts. We specify the base year for present value calculations as the year when the project begins. In this case, we have no initial revenue and the initial expense is just initial investment *II*, thus

$$\Delta R(0) = 0 \text{ and } \Delta E(0) = II \tag{8.4}$$

Substituting Eqs. (8.2) through (8.4) into Eq. (8.1) gives

$$NPV = \sum_{k=1}^{N\times Q} \frac{\Delta R(k)}{\left(1+\frac{i}{Q}\right)^k} - II - \sum_{k=1}^{N\times Q} \frac{\Delta E(k)}{\left(1+\frac{i'}{Q}\right)^k} \tag{8.5}$$

Revenue from the sale of oil during period k has the form

$$\Delta R(k) = P_o\left(1+\frac{i'}{Q}\right)^k \Delta N_p(k) \tag{8.6}$$

where P_o is the present price of oil, and $\Delta N_p^o(k)$ is the incremental oil production during period *k*. Notice that we are assuming the value of produced gas is negligible in this example. An inflation factor on the price of oil is included in Eq. (8.6). Combining Eqs. (8.4), (8.5), and (8.6) yields *NPV* for this project:

$$NPV = \sum_{k=1}^{N\times Q} \frac{P_o\left(1+\frac{i'}{Q}\right)^k \Delta N_P(k)}{\left(1+\frac{i}{Q}\right)^k} - II - \sum_{k=1}^{N\times Q} \frac{\Delta E(k)}{\left(1+\frac{i'}{Q}\right)^k} \tag{8.7}$$

$$\Delta R(k) = P_o\left(1+\frac{i'}{Q}\right)^k \Delta N_p(k)$$

The incremental oil production in Eq. (8.7) is typically obtained as a forecast using reservoir engineering methods. Some of the most frequently used methods include decline curve analysis, material balance analysis, or reservoir simulation. The oil production profile used in the economic analysis may represent both historical and predicted oil recovery. The predicted oil recovery is used to determine project reserves. Several different production profiles may be required to determine the probabilistic distribution of reserves and associated economic sensitivity.

A breakeven oil price P_{oe} for a specified rate of return $i = ROR$ and production profile is calculated by setting $NPV = 0$ as the breakeven condition in Eq. (8.7). Rearranging the resulting equation gives the following estimate of breakeven oil price:

$$P_{oe} = \frac{II + \sum_{k=1}^{N\times Q} \frac{\Delta E(k)}{\left(1+\frac{i'}{Q}\right)^k}}{\sum_{k=1}^{N\times Q} \frac{\left(1+\frac{i'}{Q}\right)^k}{\left(1+\frac{ROR}{Q}\right)^k} \Delta N_P(k)} \tag{8.8}$$

A plot of P_{oe} versus ROR shows the sensitivity of breakeven oil price to different rates of return.

8.2.2 Illustration: CAPEX, OPEX, and Discount Rate

We can account for the time value of money by introducing a discount rate r into the calculation. Revenue can be expressed as

$$R = \sum_{n=1}^{N} \frac{P_n Q_n}{(1+r)^n} \tag{8.9}$$

where N is the total number of years, P_n is price per unit quantity produced during year n, and Q_n is the quantity produced during year n. The quantity produced can be volume of oil or gas, kilowatt-hours of electricity, or any other appropriate measure of resource production. Expenses include capital expenditures $CAPEX_n$ during year n, operating expenditures $OPEX_n$ during year n, and taxes TAX_n during year n. Capital expenditures include the cost of facilities such as offshore platforms and pipelines. Operating expenses include on-going expenses such as salaries and maintenance costs. The resulting expression for expenses is

$$E = \sum_{n=1}^{N} \frac{CAPEX_n + OPEX_n + TAX_n}{(1+r)^n} \tag{8.10}$$

Substituting Eqs. (8.9) and (8.10) into Eq. (8.1) gives

$$NPV = \sum_{n=1}^{N} \frac{P_n Q_n - CAPEX_n - OPEX_n - TAX_n}{(1+r)^n} \qquad (8.11)$$

Equation (8.11) shows that *NPV* depends on the price of the resource, the quantity of the produced resource, discount rate, capital expenditures, operating expenditures, and taxes.

8.3 Investment Decision Analysis

Economic analyses are performed to provide information about the economic performance we can expect from a project relative to alternative investment options. The decision to invest in a project depends on many factors. Thompson and Wright [1985, pg. 3-2] list the following set of characteristics for measures of investment worth that can be used to compare and rank competing projects:

- Aligns with corporate goals.
- Is easy to understand and apply.
- Permits cost-effective decision making.
- Provides a quantitative measure for acceptance or rejection.
- Permits alternatives to be compared and ranked.
- Incorporates the time value of money.

Economic analyses using indicators of economic performance provide information about the relative performance of different investment options. Some commonly used economic measures are payout time, present worth, net present value, discount rate, profit-to-investment ratio, and internal rate of return. The economic measures that are used in investment decision analysis depend on the experience of the decision makers who will use them. The decision makers determine the relative importance of each economic measure.

Combinations of economic measures are often used as economic criteria for making decisions about projects. For example, a proposed project with an early payout but relatively low discount rate may be more

attractive to a company that needs to maintain a positive cash flow than another project with a higher discount rate but that does not payout as soon. The criteria for acceptance or rejection of a project may change, even within a company, as the economic environment changes. It should be remembered, however, that quantitative indicators provide useful information, but incomplete information. Economic viability is influenced by both tangible and intangible factors. Tangible factors such as drilling a well are relatively easy to quantify. Intangible factors such as environmental and socio-political concerns are relatively difficult to quantify, yet may be more important than tangible factors.

The future cost of some energy investment options may change significantly as a result of technological advances. The cost of a finite resource can be expected to increase as the availability of the resource declines, while the cost of an emerging technology will usually decline as the infrastructure for supporting the technology matures. Modern emerging technologies include advanced drilling techniques and time-lapse seismic analysis. Table 8-3 illustrates the sensitivity of oil producing techniques to the price of oil. The table shows that more sophisticated technologies can be justified as the price of oil increases. It also includes a price estimate for alternative energy sources, such as wind and solar power. In some cases, technologies overlap. For example, steam flooding is an enhanced oil recovery (EOR) process that can compete with oil recovery techniques, while chemical flooding is an EOR process that can be as expensive as many alternative energy sources.

Table 8-3
Sensitivity of Oil Recovery Technology to Oil Price

Oil Recovery Technology	Oil Price (US$ per barrel in year 2000 US$)
Conventional	10 – 30
Enhanced Oil Recovery (EOR)	20 – 40
Extra Heavy Oil (e.g. tar sands)	25 – 45
Alternative Energy Sources	40 +

Investment decision making depends on such factors as availability, accessibility, environmental acceptability, capital cost, and ongoing operating expenses. The analysis of the costs associated with a project should take into account the initial capital expenditures and annual operating expenses for the life of the system. This analysis is called life cycle analysis. The initial costs of one proposed project may be relatively low compared to those of competing projects. If we only consider initial cost in our analysis, we may select a project that is not optimum. For example, the annual operating expenses for one project we might choose based on initial cost may be significantly larger than those for an alternative option. In addition, projections of future cost may be substantially in error if the cost of one or more of the components contributing to a project changes significantly in relation to our original estimate. To avoid making suboptimum decisions, we should consider all of the life cycle costs of each investment option, and evaluate the sensitivity of cash flow predictions to plausible changes in cost as a function of time.

8.3.1 Risk Analysis and Real Options Analysis

A characteristic of natural resource management is the need to understand the role of uncertainty in decision making. The information we have about a natural resource is usually incomplete. What information we do have may contain errors. Despite the limitations of our knowledge, we must often make important decisions to advance a project. These decisions should be made with the recognition that risk, or uncertainty, is present and can influence investment decisions. Here, risk refers to the possibility that an unexpected event can adversely affect the value of an asset. Uncertainty is not the same as risk. Uncertainty is the concept that our limited knowledge and understanding of the future does not allow us to predict the consequences of our decisions with 100% accuracy. Risk analysis is an attempt to quantify the risks associated with investing under uncertainty.

One drawback of traditional risk analysis is the limited number of options that are considered. The focus of risk analysis is decision

making based on current expectations about future events. For example, the net present value analysis discussed above requires forecasts of revenue and expenses based on today's expectations. Technological advances or political instabilities are examples of events that may significantly alter our expectations. We might overlook or ignore options that would have benefited from the unforeseen events. An option in this context is a set of policies or strategies for making current and future decisions. Real Options Analysis attempts to incorporate some flexibility into the management of investment options that are subject to considerable future uncertainty.

The best way to incorporate options into the decision making process is to identify them during the early stages of analysis. Once a set of options has been identified for a particular project, we can begin to describe the uncertainties and decisions associated with the project. By identifying and considering an array of options, we obtain a more complete picture of what may happen as a consequence of the decisions we make. Real Options Analysis helps us understand how important components of a project, particularly components with an element of uncertainty, influence the value of the project [Chorn and Croft, 2000].

8.4 Environmental Impact

Environmental issues must always be considered in the development of a reservoir management strategy. For example, the Louisiana Offshore Oil Production (LOOP) facility is designed to keep the transfer of hydrocarbons between pipelines and tankers away from sensitive coastal areas. Periodic water sampling of surface and produced waters can assure that fresh water sources are not contaminated. In addition, periodic testing for the excavation or production of naturally occurring radioactive materials helps assure environmental compliance.

A well managed field should be compatible with both the surface and subsurface environment. The advantages of operating a field with prudent consideration of environmental issues can pay economic dividends. In addition to improved public relations, sensitivity to

environmental issues can minimize adverse environmental effects that may require costly remediation and financial penalties. Remediation often takes the form of cleanup, such as the cleanup required after the oil spill from the Exxon-Valdez oil tanker in Alaska. Technologies are being developed to improve our ability to cleanup environmental pollutants. For example, bioremediation uses living microorganisms or their enzymes to accelerate the rate of degradation of environmental pollutants [Westlake, 1999].

8.4.1 Sustainable Development

Failure to consider environmental issues adequately can lead to both tangible and intangible losses. Intangible losses are difficult to quantify, but can include loss of public support for an otherwise economically viable project. Tangible losses have more readily quantifiable economic consequences. For example, near- and long-term economic liabilities associated with potable water contamination can adversely affect project economics. It becomes a question of business ethics whether a practice that is legal but can lead to an adverse environmental consequence should nonetheless be pursued because a cost-benefit analysis showed that there were fewer economic liabilities than economic benefits.

Typically, arguments to pursue an environmentally undesirable practice based on cost-benefit analyses do not adequately account for intangible costs. For example, the decision by Shell to dispose of the Brent Spar platform by sinking it in the Atlantic Ocean led to public outrage in Europe in 1995. Reversing the decision and disassembling the platform for use as a quay in Norway resolved the resulting public relations problem, but the damage had been done. The failure to anticipate the public reaction reinforced a lack of public confidence in the oil and gas industry, and helped motivate government action to regulate the decommissioning of offshore platforms in northwestern Europe [Wilkinson, 1997; Offshore staff, 1998].

The problem facing the industry is to learn how to achieve sustainable development. The concept of sustainable development was introduced in 1987 in a report prepared by the United Nations' World Commission on Environment and Development [Brundtland, 1987]. The commission, known as the Brundtland Commission after chairwoman Gro Harlem Brundtland of Norway, said that societies should adopt a policy of sustainable development that allows them to meet their present needs while preserving the ability of future generations to meet their own needs.

Society desires, and industry is seeking to achieve, sustainable development. One industry response to environmental and social concerns in the context of sustainable development is the *triple bottom line* (TBL) [Whittaker, 1999]. According to this view, sustainable development must integrate social and environmental concerns into a development plan that optimizes economic profitability and value creation. The three components of sustainable development, and the three goals of the TBL, are economic prosperity, social equity, and environmental protection. The focus of TBL is the creation of long-term shareholder value by recognizing that corporations are dependent on licenses provided by society to do business. Whittaker [1999, pg. 25] reports that "After a period of serious introspection following the Brent Spar debacle, Royal Dutch/Shell is perhaps the most enthusiastic supporter of TBL." TBL policy includes the following key elements [Whittaker, 1999, pg. 25]:

- Performance measurements that include qualitative social indicators and ecoefficiency measures (such as energy consumption and recycling) in addition to compliance and pollutant emissions.
- Development and implementation of strategies that will enable the industry to meet both future global energy needs and environmental objectives.
- Investment in natural gas, low or zero emissions fuels, and renewable forms of energy.
- Improved communications with communities affected by operations.

Sustainable development takes into account the rights of future generations. It is possible to argue that future generations have no legal rights to current natural resources and are not entitled to any. From this perspective, each generation must do the best it can with available resources. On the other hand, many societies are choosing to adopt the value of preserving natural resources for future generations. National parks are examples of natural resources that are being preserved.

8.4.2 Global Climate Change

Measurements of ambient air temperature show a global warming effect that corresponds to an increase in the average temperature of the Earth's atmosphere. The increase in atmospheric temperature has been linked to the combustion of fossil fuels [Wigley, et al., 1996; Lide, 2002, page 14-32].

When a carbon-based fuel burns, carbon can react with oxygen and nitrogen in the atmosphere to produce carbon dioxide (CO_2), carbon monoxide, and nitrogen oxides (often abbreviated as NOx). The combustion byproducts, including water vapor, are emitted into the atmosphere in gaseous form. Some of the gaseous byproducts are called greenhouse gases because they contribute to the *greenhouse effect*, illustrated in Figure 8-2. Some of the incident solar radiation from the Sun is absorbed by the Earth, some is reflected into space, and some is captured by greenhouse gases in the atmosphere and reradiated as infrared radiation (heat). The reradiated energy would have escaped the Earth as reflected sunlight if greenhouse gases were not present in the atmosphere. Greenhouse gases include carbon dioxide, methane, and nitrous oxide, as well as other gases such as volatile organic compounds and hydrofluorocarbons.

Carbon dioxide (CO_2) is approximately 83% of the greenhouse gases emitted by the United States as a percent of the mass of carbon or carbon equivalent. Wigley, et al. [1996] projected ambient CO_2 concentration through the twenty-first century. Pre-industrial atmospheric CO_2 concentration was approximately 288 parts per million. Atmospheric CO_2 concentration is currently 340 parts per million. The concentration

of CO_2 that would establish an acceptable energy balance is considered to be 550 parts per million. To achieve the acceptable concentration of CO_2 through the next century, societies would have to reduce the volume of greenhouse gases entering the atmosphere.

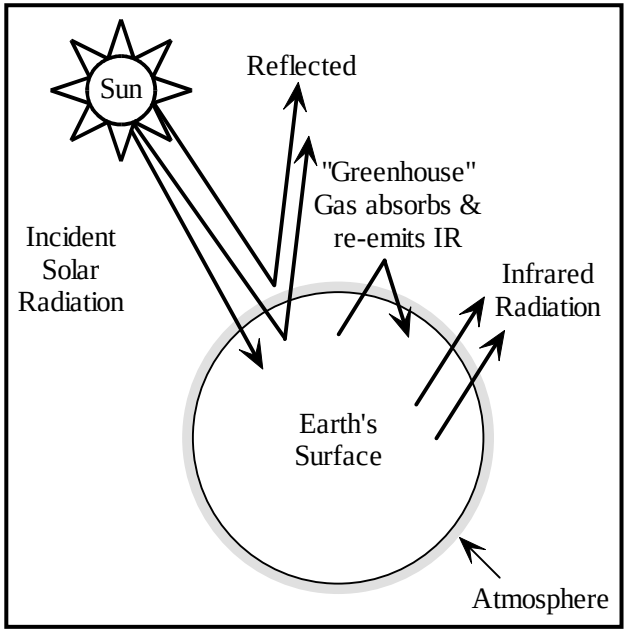

Figure 8-2. The Greenhouse Effect [after Fanchi, 2004]

The Kyoto Protocol is an international treaty that was negotiated in Kyoto, Japan in 1997 to establish limits on the amount of greenhouse gases a country can emit into the atmosphere. The Kyoto Protocol has not been accepted worldwide. Some countries believe the greenhouse gas emission limits are too low and would adversely impact national and world economies without solving the problem of global warming. Another criticism of the Kyoto Protocol is that it does not apply to all nations. For example, China is exempt from greenhouse gas emission limitations in the Kyoto Protocol even though it has one of the world's fastest growing economies and the world's largest population.

Government and industry are considering options for addressing the climate change issue. One of the leading options is to collect and

store CO_2 in reservoirs in a process known as geologic carbon sequestration. The goal of geologic carbon sequestration and similar programs is to provide economically competitive and environmentally safe options to offset all projected growth in baseline emissions of greenhouse gases.

8.4.3 Subsidence

Subsidence is a compressibility effect that depends on the geomechanics of the produced interval and its overburden. Subsidence, or the change in thickness Δh of the reservoir, can be estimated from the compressibility and pressure depletion of the system using the equation

$$\Delta h = c_B h \Delta P = \phi c_f h \Delta P$$

where

c_B bulk compressibility (psia^{-1})

c_f formation compressibility (psia^{-1})

h net thickness of reservoir (ft)

ϕ porosity (fraction)

ΔP pressure depletion (psia)

If properties like compressibility are measured hydrostatically, they should be corrected to uniaxial compressibilities [Teeuw, 1971] so that the subsidence estimate becomes

$$\Delta h_u = \frac{1}{3}\left(\frac{1+\nu}{1-\nu}\right)\phi c_f h \Delta P$$

where ν is Poisson's ratio and the subscript u denotes uniaxial compaction. The correction for uniaxial compaction recognizes that reservoirs with large lateral dimensions relative to their vertical thickness deform mainly in the vertical direction.

In many cases, subsidence has little or no adverse environmental effects. In some cases, however, subsidence can be a significant concern. For example, a pressure maintenance program in a field where surface

subsidence is a likely consequence of pressure depletion can improve resource recovery and help avoid economic liabilities resulting from damage caused by surface subsidence. Subsidence in the Long Beach, California, area due to production of the Wilmington field had to be mitigated with a pressure maintenance program. The pressure maintenance program can be as straightforward as water injection to replace the fluids that have been produced.

Subsidence has been responsible for production induced seismicity in areas such as the Rocky Mountain Arsenal near Denver, Colorado, where production induced seismicity was identified as the cause of earthquakes. Earthquakes due to natural causes have led to fatalities in tectonically active areas like the Sea of Okhotsk, off Sakhalin Island, in Russia. Development activities in tectonically active areas, such as offshore Sakhalin Island, need to anticipate the impact of subsidence and production induced seismicity as part of their reservoir management plans. Examples of compaction studies are presented by Teeuw [1971], Fredrich, et al. [1998], Settari and Walters [1999], Settari [2002], and Schutjens, et al. [2004].

8.5 IFLO Application: CO_2 Sequestration in a Mature Oil Field

Reservoir flow modeling can be used to help manage geologic carbon sequestration projects. Carbon dioxide may be sequestered in a variety of subsurface environments, such as CO_2 injection into an oil field as part of an improved recovery process; CO_2 injection into a mature oil field as a storage process; CO_2 injection into a coalbed to enhance coal gas recovery; and CO_2 injection into an aquifer as a storage process. We demonstrate the application of reservoir flow modeling to the management of geologic carbon sequestration by modeling CO_2 sequestration in a mature oil field [Fanchi, 2003b]. This application demonstrates enhanced oil recovery by miscible CO_2 injection and CO_2 sequestration.

8.5.1 East Vacuum Grayburg/San Andres Unit

The Vacuum field was discovered in 1929. It is located about fifteen miles west of Hobbs, New Mexico on the northwestern shelf of the Permian Basin and along the northern limit of the Delaware Basin [Brownlee and Sugg, 1987; Martin, et al., 1995]. Significant field development began in 1938 and was substantially completed in 1941. Waterflood development began in 1958. The East Vacuum Grayburg/San Andres Unit (EVGSAU) was formed in December 1978 and covers more than seven thousand acres on the eastern side of the Vacuum Field.

Oil with a gravity of 38°API has been produced from both the Grayburg and San Andres formations. The primary, productive interval at EVGSAU is the dolomitized carbonate sequence in the upper San Andres formation at a depth of approximately 4,400 ft. and a temperature of 101 °F. Infill drilling from forty-acre spacing to twenty-acre spacing in the EVGSAU began in 1979, and waterflooding began in 1980. The EVGSAU was converted to an eighty-acre inverted nine-spot pattern waterflood by 1982. A miscible CO_2 injection project began in September 1985, and a CO_2-foam pilot test began in September 1991.

Grigg and Schechter [1998] prepared a history match of the CO_2-foam pilot test area in the EVGSAU for the primary and waterflood periods (1959-1985). As part of their study, they published a model that included a characterization of the EVGSAU pilot area as well as saturation and pressure distributions at the end of waterflood. Their reservoir characterization was used to estimate the potential for sequestering CO_2 in a mature oil field.

8.5.2 Sequestration Potential

The EVGSAU model uses a 3-D grid with 16×16×7 gridblocks. Figure 8-3 shows well placement in the model. The sides of each square gridblock are 240.5 feet long. The reservoir at the start of the run is in a pressure-depleted state: initial pore volume weighted average reservoir

pressure is approximately 320 psia. For comparison, minimum miscibility pressure (MMP) is approximately 1190 psia. The model has approximately 46 million STB (MMSTB) oil in place and 10 MMSTB water in place at original conditions. Approximately 36 MMSTB oil and 22 MMSTB water are in place at the end of waterflood in 1985, which is the initial state of the EVGSAU model used in this study.

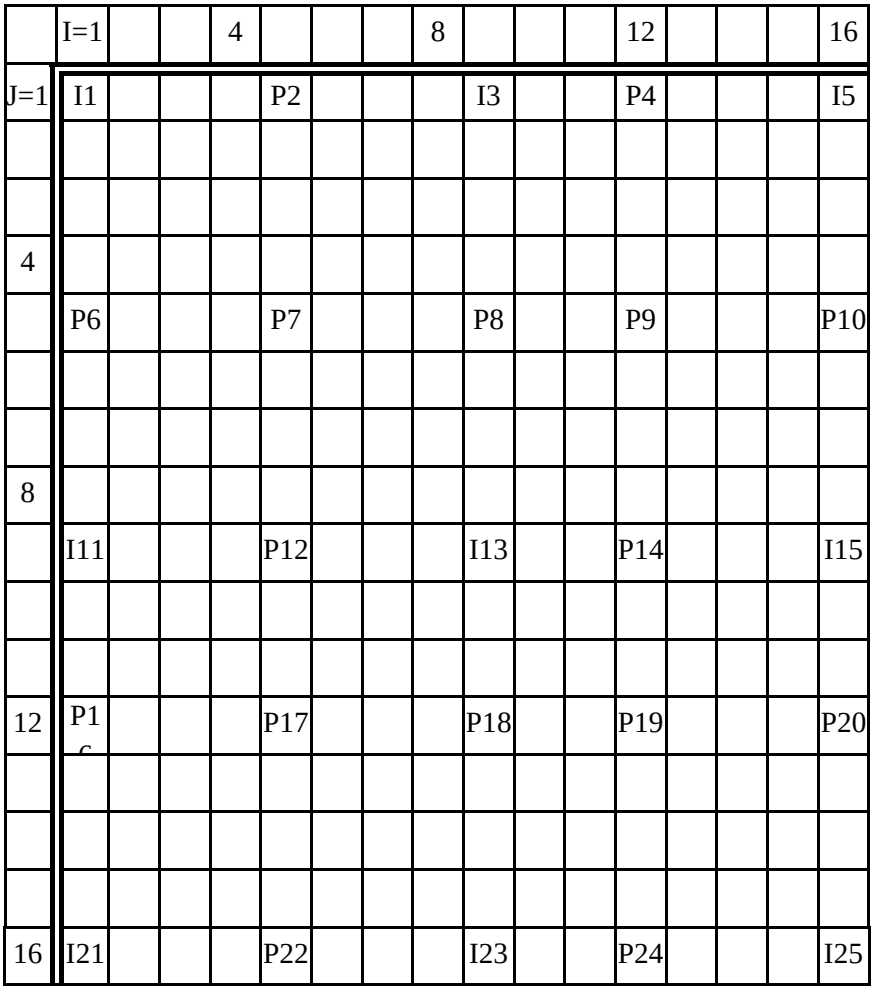

Figure 8-3. Well locations in 16×16 grid.
P# = Production well; I# = Injection well.

We consider three sequestration cases. Case A evaluates the potential of injecting CO_2 at immiscible conditions in the waterflooded zone. Immiscible CO_2 injection begins at the start of the run and continues for a period of ten years. In Case B, CO_2 is used to raise reservoir pressure above minimum miscibility pressure and then conduct a miscible flood. In Case C, water injection is conducted for one year to raise reservoir pressure above MMP. The waterflood is then replaced by CO_2 injection.

Table 8-4 shows the volume of CO_2 sequestered after ten years of project life for both cases. Much more CO_2 is sequestered if CO_2 is injected into the reservoir at miscible pressure conditions than at immiscible pressure conditions. More CO_2 is sequestered in Case B than in Case C because Case C includes one year of water injection prior to nine years of CO_2 injection. Although waterflooding delays CO_2 sequestration, waterflooding can improve time-lapse seismic monitoring. Time-lapse seismic monitoring is discussed in more detail in Part II.

Table 8-4
CO_2 Sequestration at Ten Years

Case	Injected Fluid	CO_2 Injected (BSCF)	CO_2 Produced (BSCF)	CO_2 Sequestered (BSCF)
A	Immiscible Gas	65.1	51.9	13.2
B	Miscible Gas	101.3	57.7	43.6
C	Water then Miscible Gas	92.1	51.4	40.7

Exercises

Exercise 8.1 Five independent studies determined the reserves for reservoir A in the table below. Assuming a normal distribution of reserves, estimate proved, probable, and possible reserves. Hint: Calculate the average and standard deviation for the oil recoveries reported above.

Study	1	2	3	4	5
Oil Recovery (MSTBO)	320	150	480	260	370

Note: MSTBO denotes thousand stock tank barrels of oil.

Exercise 8.2A What is life cycle analysis?

Exercise 8.2B What is the purpose of Real Options Analysis?

Exercise 8.3A Suppose the price of 1 liter of gasoline is US$1.10 in Europe. What is the price per gallon? Note: 1 L = 0.001 m^3 and 1 gal = 3.785×10^{-3} m^3.

Exercise 8.3B The price of gasoline is the sum of expenses plus taxes. If the expenses equal US$1.00 per gallon, what is the tax on a gallon of gasoline in Europe that has the price given in Part A?

Exercise 8.4A If US$100 billion is spent on the military in a year to protect the delivery of 20 million barrels of oil per day to the global market, how much does the military budget add to the cost of a barrel of oil?

Exercise 8.4B How much is this cost per gallon?

Exercise 8.5A What is geologic carbon sequestration?

Exercise 8.5B What is the Kyoto Protocol?

Exercise 8.6A How many barrels of oil would be needed to provide 100 quads of energy if the energy density of oil is 35,000 MJ/m^3? Note: 1 quad = 1.055×10^{12} MJ, 1 bbl = 0.1589 m^3,

Exercise 8.6B If the volume of oil in Part A is consumed annually, what is the daily consumption of oil (in bbl)?

Exercise 8.7A Suppose a reservoir has an average porosity of 20%, a formation compressibility of 20 x 10^{-6} $psia^{-1}$, a net thickness of 500 feet, and the reservoir is subjected to a pressure depletion of 3000 psia. Plot subsidence as a function of Poisson's ratio for a Poisson's ratio ranging from 0.10 to 0.35.

Exercise 8.7B If you are operating the field from a platform that is built with a deck that is 10 ft. above the maximum wave height, discuss the possible impact of subsidence on operations?

Exercise 8.7C Discuss the possible impact of subsidence on wellbore stability for deviated wells drilled from the platform.

Exercise 8.8A Typical reservoir values for formation, oil, water and gas compressibilities are

$$c_f = 3 \times 10^6/\text{psia}$$

$$c_o = 10 \times 10^6/\text{psia}$$

$$c_w = 3 \times 10^6/\text{psia}$$

$$c_g = 500 \times 10^6/\text{psia}$$

Use the relationship $c = -\frac{1}{V}\frac{\Delta V}{\Delta P}$ to estimate the fractional volume change $\Delta V/V$ of each substance for a pressure difference $\Delta P = P_{final} - P_{initial} = -100$ psia.

Exercise 8.8B Suppose oil saturation is 0.8 in an oil-water system. Calculate the bulk modulus of fluid assuming the compressibilities of oil and water are the values given above. Hint: first calculate water saturation and then calculate total fluid compressibility. Note that the bulk modulus of fluid is the inverse of fluid compressibility.

Exercise 8.8C Suppose a formation has the following properties: Poisson's ratio is 0.2, porosity is 15%, and net thickness is 100 ft. Estimate

subsidence for a pressure difference $\Delta P = P_{final} - P_{initial} = -1000$ psia and formation compressibility given in Part A.

Exercise 8.9 File EVGSAU_MISC_WG.DAT is Case C of the IFLO sequestration study using the EVGSAU flow model. Run the file and determine the amount of CO_2 sequestered at the end of the run. Hint: open the run output file ITEMP.ROF and find the cumulative injection and production of solvent 1. Solvent 1 is CO_2 in this model.

Exercise 8.10A File GOM_UNCONSOLIDATED.DAT is an example of production from unconsolidated sand in the Gulf of Mexico. Run the file and determine the maximum static uniaxial compaction at the end of the run. Hint: open the run output file ITEMP.ROF and find MAXIMUM STATIC UNIAXIAL COMPACTION at the end of the run.

Exercise 8.10B Assume that the northern part of the reservoir is upstructure and the southern part of the reservoir is downstructure. Is compaction greater on the west side of the reservoir or the east side of the reservoir at the end of the run?

Chapter 9

Multiphase Fluid Flow Equations

The literature contains many derivations of the equations describing fluid flow in porous media. Consequently, only a brief discussion will be presented here. We begin by introducing the continuity equation, and then present some important sets of fluid flow equations that are commonly used to model hydrocarbon reservoirs.

9.1 The Continuity Equation

The continuity equation can be derived by considering the flow of fluid into and out of a single reservoir gridblock (Figure 9-1). Let the symbol J denote fluid flux. Flux is defined as the rate of flow of mass per unit cross-sectional area normal to the direction of flow, which is the x direction in the present case. Assume fluid flows into the gridblock at x (J_x) and out of the gridblock at $x + \Delta x$ ($J_{x+\Delta x}$). By conservation of mass, we have the equality:

mass entering the gridblock − mass leaving the gridblock
= accumulation of mass in the gridblock.

If the gridblock has length Δx, width Δy, and depth Δz, we can write the mass entering the gridblock in a time interval Δt as

$$[(J_x)_x \Delta y \Delta z + (J_y)_y \Delta x \Delta z + (J_z)_z \Delta x \Delta y]\Delta t = \text{Mass in} \qquad (9.1)$$

where we have generalized the equation to allow flux in the *y* and *z* directions as well. The notation $(J_x)_x$ denotes the *x* direction flux at location *x*, with analogous meanings for the remaining terms.

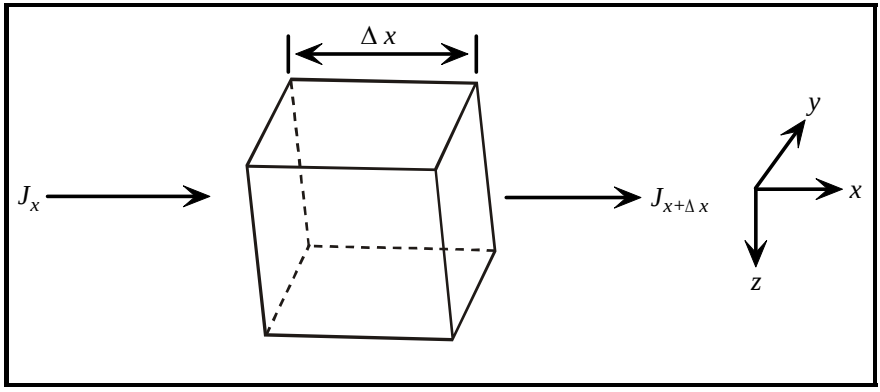

Figure 9-1. Reservoir Gridblock: Coordinate Convention follows Sawyer and Mercer [1978]

Corresponding to mass entering is a term for mass exiting which has the form

$$[(J_x)_{x+\Delta x}\Delta y\Delta z + (J_y)_{y+\Delta y}\Delta x\Delta z + (J_z)_{z+\Delta z}\Delta x\Delta y]\Delta t + q\Delta x\Delta y\Delta z\Delta t = \text{Mass out} \tag{9.2}$$

We have added a source/sink term *q* which represents mass flow into (source) or out of (sink) a well. A producer is represented by $q > 0$, and an injector by $q < 0$.

Accumulation of mass in the gridblock is the change in concentration C_ℓ of phase ℓ in the gridblock over the time interval Δt. If the concentration C_ℓ is defined as the total mass of phase ℓ (oil, water, or gas) in the entire reservoir gridblock divided by the gridblock volume, then the accumulation term becomes

$$\left[(C_\ell)_{t+\Delta t} - (C_\ell)_t\right]\Delta x\Delta y\Delta z = \text{Mass accumulation} \tag{9.3}$$

Using Eqs. (9.1) through (9.3) in the mass conservation equality

$$\text{Mass in} - \text{Mass out} = \text{Mass accumulation}$$

gives

$$\begin{aligned}&\left[\left(J_x\right)_x \Delta y\Delta z + \left(J_y\right)_y \Delta x\Delta z + \left(J_z\right)_z \Delta x\Delta y\right]\Delta t\\&-\left[\left(J_x\right)_{x+\Delta x} \Delta y\Delta z + \left(J_y\right)_{y+\Delta y} \Delta x\Delta z + \left(J_z\right)_{z+\Delta z} \Delta x\Delta y\right]\Delta t\\&- q\Delta x\Delta y\Delta z\Delta t = \left[\left(C_\ell\right)_{t+\Delta t} - \left(C_\ell\right)_t\right]\Delta x\Delta y\Delta z\end{aligned} \tag{9.4}$$

Dividing Eq. (9.4) by $\Delta x\Delta y\Delta z\Delta t$ and rearranging gives

$$\begin{aligned}&-\frac{\left(J_x\right)_{x+\Delta x} - \left(J_x\right)_x}{\Delta x} - \frac{\left(J_y\right)_{y+\Delta y} - \left(J_x\right)_y}{\Delta y} - \frac{\left(J_z\right)_{z+\Delta z} - \left(J_z\right)_z}{\Delta z}\\&\qquad - q = \frac{\left(C_\ell\right)_{t+\Delta t} - \left(C_\ell\right)_t}{\Delta t}\end{aligned} \tag{9.5}$$

In the limit as Δx, Δy, Δz, and Δt go to zero, Eq. (9.5) becomes the continuity equation

$$-\frac{\partial J_x}{\partial x} - \frac{\partial J_y}{\partial y} - \frac{\partial J_z}{\partial z} - q = \frac{\partial C_\ell}{\partial t} \tag{9.6}$$

The oil, water, and gas components each satisfy a mass conservation equation having the form of Eq. (9.6).

9.2 Conservation Laws

The basic conservation laws of reservoir simulation are the conservation of mass, energy, and momentum. Mass balance in a representative elementary volume (REV) or gridblock is achieved by equating the accumulation of mass in the gridblock with the difference between the mass leaving the gridblock and the mass entering the gridblock. A material balance is performed for each gridblock. The ability of the simulator to account for flow between gridblocks is what makes a simulator different from a reservoir engineering material balance program.

A material balance calculation is actually a subset of the simulator capability. This is an important point because it means a reservoir simulator can be used to perform material balance work. The advantage of using a simulator instead of a material balance program is that the

simulation model can be enlarged to include position-dependent effects by modifying the grid representing the reservoir architecture. Thus, a single gridblock material balance calculation in a reservoir simulation model can be expanded with relative ease to include flow in one, two, or three spatial dimensions. This procedure is used in the case study presented in Chapters 17 through 19. By contrast, one disadvantage of using a reservoir simulator for material balance calculations is that it takes longer to include information that would not be needed in a material balance program. Another disadvantage is that the fluid flow rates are treated differently in a reservoir simulator than they are in a material balance program.

Most reservoir simulators assume reservoirs are produced under isothermal conditions. They also assume complete and instantaneous phase equilibration in each cell. Thus, most simulators do not account for either temperature gradients or the time it takes a mixture to reach equilibrium. They assume, instead, that reservoir temperature remains constant throughout the life of the field and that equilibration is established instantaneously. These are often reasonable assumptions.

Momentum conservation is modeled using Darcy's Law. This assumption means that the model does not accurately represent turbulent flow in a reservoir or near the wellbore. Some well models allow the user to model turbulent flow, especially for high flow rate gas wells. Turbulent flow models relate pressure change to a linear flow term, as in Darcy's Law, plus a term that is quadratic in flow rate.

9.3 Flow Equations for Black Oil Simulation

Black oil simulators solve multiphase, multidimensional flow equations for fluids whose properties depend on pressure. The flow equations for an oil, water, and gas system are determined by specifying the fluxes and concentrations of the conservation equations for each of the three components in each of the three phases. A flux in a given direction can be written as the density of the fluid times its velocity in the

given direction. Letting the subscripts *o*, *w*, and *g* denote oil, water, and gas, respectively, the fluxes become:

$$\left(\vec{J}\right)_o = \frac{\rho_{osc}}{B_o}\vec{v}_o \tag{9.7}$$

$$\left(\vec{J}\right)_w = \frac{\rho_{wsc}}{B_w}\vec{v}_w \tag{9.8}$$

$$\left(\vec{J}\right)_g = \frac{\rho_{gsc}}{B_g}\vec{v}_g + \frac{R_{so}\rho_{gsc}}{B_o}\vec{v}_o + \frac{R_{sw}\rho_{gsc}}{B_w}\vec{v}_w \tag{9.9}$$

where R_{so} and R_{sw} are gas solubilities in oil and water respectively; B_o, B_w, and B_g are oil, water and gas formation volume factors; the subscript *sc* denotes standard conditions (usually 60°F and 14.7 psia in oilfield units); and ρ denotes fluid densities. The velocities $\vec{v}$ are assumed to be Darcy velocities and their *x* components are

$$v_{xo} = -K_x\lambda_o\frac{\partial}{\partial x}\left[P_o - \frac{\rho_o gz}{144g_c}\right] \tag{9.10}$$

$$v_{xw} = -K_x\lambda_w\frac{\partial}{\partial x}\left[P_w - \frac{\rho_w gz}{144g_c}\right] \tag{9.11}$$

$$v_{xg} = -K_x\lambda_g\frac{\partial}{\partial x}\left[P_g - \frac{\rho_g gz}{144g_c}\right] \tag{9.12}$$

where g is the acceleration of gravity in ft/s^2, and g_c is 32.174 ft/s^2 (IFLO assumes $g = g_c$). These equations should be valid for describing fluid flow in porous media even if g and g_c change, such as on the Moon, Mars, or the space shuttle. Similar expressions can be written for the *y* and *z* components.

The relative mobility λ_ℓ is the ratio of the relative permeability to flow of the phase divided by its viscosity, thus

$$\lambda_\ell = k_{r\ell}/\mu_\ell \tag{9.13}$$

Phase densities are related to formation volume factors and gas solubilities by

$$\rho_o = \frac{1}{B_o}\left[\rho_{osc} + R_{so}\rho_{gsc}\right] \tag{9.14}$$

$$\rho_w = \frac{1}{B_w}\left[\rho_{wsc} + R_{sw}\rho_{gsc}\right] \tag{9.15}$$

$$\rho_g = \frac{\rho_{gsc}}{B_g} \tag{9.16}$$

In addition to fluxes, we need concentrations for each component. These are given by

$$C_o = \phi\rho_{osc}\, S_o / B_o \tag{9.17}$$

$$C_w = \phi\rho_{wsc}\, S_w / B_w \tag{9.18}$$

$$C_g = \phi\rho_{gsc}\left[\frac{S_g}{B_g} + R_{so}\frac{S_o}{B_o} + R_{sw}\frac{S_w}{B_w}\right] \tag{9.19}$$

where ϕ is porosity and S_ℓ is the saturation of phase ℓ. The saturations satisfy the constraint

$$S_o + S_w + S_g = 1 \tag{9.20}$$

Combining Eqs. (9.6), (9.7) through (9.9), and (9.17) through (9.19) gives a mass conservation equation for each component:

Oil Component in Oil Phase:

$$-\left[\frac{\partial}{\partial x}\left(\frac{\rho_{osc}}{B_o}v_{xo}\right) + \frac{\partial}{\partial y}\left(\frac{\rho_{osc}}{B_o}v_{yo}\right) + \frac{\partial}{\partial z}\left(\frac{\rho_{osc}}{B_o}v_{zo}\right)\right] - q_o = \frac{\partial}{\partial t}\left(\phi\rho_{osc}\frac{S_o}{B_o}\right) \tag{9.21}$$

Water Component in Water Phase:

$$-\left[\frac{\partial}{\partial x}\left(\frac{\rho_{wsc}}{B_w}v_{xw}\right)+\frac{\partial}{\partial y}\left(\frac{\rho_{wsc}}{B_w}v_{yw}\right)+\frac{\partial}{\partial z}\left(\frac{\rho_{wsc}}{B_w}v_{zw}\right)\right] - q_w = \frac{\partial}{\partial t}\left(\phi\rho_{wsc}\frac{S_w}{B_w}\right) \tag{9.22}$$

Gas Component in Oil, Water, and Gas Phases:

$$\begin{aligned} &-\frac{\partial}{\partial x}\left(\frac{\rho_{gsc}}{B_g}v_{xg}+\frac{R_{so}\rho_{gsc}}{B_o}v_{xo}+\frac{R_{sw}\rho_{gsc}}{B_w}v_{xw}\right)\\ &-\frac{\partial}{\partial y}\left(\frac{\rho_{gsc}}{B_g}v_{yg}+\frac{R_{so}\rho_{gsc}}{B_o}v_{yo}+\frac{R_{sw}\rho_{gsc}}{B_w}v_{yw}\right)\\ &-\frac{\partial}{\partial z}\left(\frac{\rho_{gsc}}{B_g}v_{zg}+\frac{R_{so}\rho_{gsc}}{B_o}v_{zo}+\frac{R_{sw}\rho_{gsc}}{B_w}v_{zw}\right)\\ &-q_g=\frac{\partial}{\partial t}\left[\phi\rho_{gsc}\left(\frac{S_g}{B_g}+\frac{R_{so}S_o}{B_o}+\frac{R_{sw}S_w}{B_w}\right)\right] \end{aligned} \tag{9.23}$$

The densities at standard conditions are constants and can be divided out of the above equations. This reduces the equations to the following form:

Oil

$$-\left[\frac{\partial}{\partial x}\left(\frac{v_{xo}}{B_o}\right)+\frac{\partial}{\partial y}\left(\frac{v_{yo}}{B_o}\right)+\frac{\partial}{\partial z}\left(\frac{v_{zo}}{B_o}\right)\right]-\frac{q_o}{\rho_{osc}}=\frac{\partial}{\partial t}\left(\phi\frac{S_o}{B_o}\right) \tag{9.24}$$

Water

$$-\left[\frac{\partial}{\partial x}\left(\frac{v_{xw}}{B_w}\right)+\frac{\partial}{\partial y}\left(\frac{v_{yw}}{B_w}\right)+\frac{\partial}{\partial z}\left(\frac{v_{zw}}{B_w}\right)\right]-\frac{q_w}{\rho_{wsc}}=\frac{\partial}{\partial t}\left(\phi\frac{S_w}{B_w}\right) \tag{9.25}$$

Gas

$$
\begin{aligned}
&-\frac{\partial}{\partial x}\left(\frac{v_{xg}}{B_g}+\frac{R_{so}}{B_o}v_{xo}+\frac{R_{so}}{B_w}v_{xw}\right)\\
&-\frac{\partial}{\partial y}\left(\frac{v_{yg}}{B_g}+\frac{R_{so}}{B_o}v_{yo}+\frac{R_{sw}}{B_w}v_{yw}\right)\\
&-\frac{\partial}{\partial z}\left(\frac{v_{zg}}{B_g}+\frac{R_{so}}{B_o}v_{zo}+\frac{R_{sw}}{B_w}v_{zw}\right)\\
&-\frac{q_g}{\rho_{gsc}}=\frac{\partial}{\partial t}\left[\phi\left(\frac{S_g}{B_g}+R_{so}\frac{S_o}{B_o}+R_{sw}\frac{S_w}{B_w}\right)\right]
\end{aligned}
\tag{9.26}
$$

9.3.1 Flow Equations in Vector Notation

Equations (9.10) through (9.16), (9.20), and (9.24) through (9.26) are the basic fluid flow equations for a black oil simulator. Equations (9.24) through (9.26) illustrate the computational complexity of the basic three-dimensional, three-phase black oil simulator equations. Equivalent but much simpler looking forms of the flow equations are presented in terms of vector operators as

$$
-\nabla\bullet\frac{\vec{v}_o}{B_o}-\frac{q_o}{\rho_{osc}}=\frac{\partial}{\partial t}\left(\phi\frac{S_o}{B_o}\right) \tag{9.27}
$$

$$
-\nabla\bullet\frac{\vec{v}_w}{B_w}-\frac{q_w}{\rho_{wsc}}=\frac{\partial}{\partial t}\left(\phi\frac{S_w}{B_w}\right) \tag{9.28}
$$

and

$$
\begin{aligned}
&-\nabla\bullet\left(\frac{\vec{v}_g}{B_g}+\frac{R_{so}}{B_o}\vec{v}_o+\frac{R_{sw}}{B_w}\vec{v}_w\right)-\frac{q_g}{\rho_{gsc}}\\
&=\frac{\partial}{\partial t}\left[\phi\left(\frac{S_g}{B_g}+R_{so}\frac{S_o}{B_o}+R_{sw}\frac{S_w}{B_w}\right)\right]
\end{aligned}
\tag{9.29}
$$

where the symbol $\nabla \bullet \vec{v}$ denotes the divergence of the velocity vector and is mathematical shorthand for the expression

$$\nabla \bullet \vec{v} = \frac{\partial}{\partial x} v_x + \frac{\partial}{\partial y} v_y + \frac{\partial}{\partial z} v_z \tag{9.30}$$

A review of vector analysis can be found in many references, such as Kreyszig [1999] and Fanchi [2006].

9.4 Flow Equations for Compositional Simulation

Compositional simulators solve multiphase, multidimensional flow equations for fluids whose properties depend on pressure. Table 9-1 shows the general equations for describing fluid flow in a porous medium and Table 9-2 presents associated nomenclature.

Table 9-1
Molar Conservation Equation for Component *k*

Physical Source	Term
Dispersion	$\nabla \bullet \left[\sum_{\ell=1}^{n_p} \phi S_\ell \underline{\underline{D}}_{k\ell} \rho_\ell \cdot \nabla x_{k\ell} \right]$
Convection	$\nabla \bullet \left[\sum_{\ell=1}^{n_p} \rho_\ell x_{k\ell} v_\ell \right]$
Source/Sink	$+ Q_k$
Accumulation	$= \frac{\partial}{\partial t} \left[\phi \sum_{\ell=1}^{n_p} \rho_\ell x_{k\ell} S_\ell \right]$
Darcy's Law	$v_\ell = -\underline{\underline{K}} \frac{k_{r\ell}}{\mu_\ell} \bullet \left(\nabla P_\ell - \gamma_\ell \nabla z \right)$

The molar flow equations were derived using mass conservation. The molar conservation equation includes a dispersion term, a convection term, a source/sink term representing wells, and the time varying accumulation term. The dispersion term is usually neglected in most workhorse simulators such as black oil and compositional simulators. Neglecting dispersion simplifies program coding and is justified when dispersion is a second-order effect. In some situations, such as miscible gas injection, physical dispersion is an effect that should be considered. Dispersion is discussed further in Chapter 10.

Table 9-2
Terminology of Molar Conservation Equation

Variable	Meaning
$\underline{\underline{D}}_{k\ell}$	Dispersion tensor of component k in phase ℓ
$\underline{\underline{K}}$	Permeability tensor
$k_{r\ell}$	Relative permeability of phase ℓ
n_c	Number of components
n_p	Number of phases
P_ℓ	Pressure of phase ℓ
S_ℓ	Saturation of phase ℓ
v_ℓ	Darcy's velocity for phase ℓ
$x_{k\ell}$	Mole fraction of component k in phase ℓ
γ_ℓ	Pressure gradient of phase ℓ
μ_ℓ	Viscosity of phase ℓ
ρ_ℓ	Density of phase ℓ
ϕ	Porosity

An energy balance equation can be found in the thermal recovery literature [Prats, 1982; Green and Wilhite, 1998]. The energy balance equation contains additional nonlinear terms. Energy loss to adjacent nonreservoir rock must also be computed. The resulting complexity requires substantial computation to achieve an energy balance. In many realistic systems, reservoir temperature variation is slight and the energy balance equation can be neglected by imposing the isothermal approximation. The result is a substantial savings in computation expense with a reasonably small loss of accuracy for appropriate applications.

Several supplemental – or auxiliary – equations must be specified to complete the definition of the mathematical problem. There must be a flow equation for each modeled component. Commercial black oil and compositional simulators are formulated to model up to three phases: oil, water, and gas. Some simulators include gas in the water phase, though most neglect it. The ability to model gas solubility in water is useful for applications such as carbon dioxide (CO_2) flooding, coal gas production, or production from geopressured gas-water reservoirs. Some black oil simulator formulations include a condensate term which accounts for liquid yield associated with condensate reservoir performance.

In addition to modeling reservoir structure and fluid (PVT) data, simulators must include rate equations for modeling wells, phase potential calculations, and rock-fluid interaction data such as relative permeability curves and capillary pressure curves. Saturation-dependent rock-fluid interaction data are entered in either tabular or analytical form. More sophisticated simulators let the user represent different types of saturation change processes, such as imbibition, drainage, and hysteresis. Applying such options leads to additional computation and cost.

9.5 Flow Equations for IFLO

The fluid flow simulator IFLO accompanying this text is an integrated flow model. IFLO is a three-phase, three-dimensional, pseudocomponent simulator. A pseudocomponent is a mixture of pure components that is treated as a single component in the formulation of

the fluid flow equations. The use of pseudocomponents reduces the number of flow equations and reduces computation time, but may only approximate the physical behavior of the system. The oil and gas components in a black oil simulator are pseudocomponents, and most compositional models limit the number of components by defining pseudocomponent mixtures of pure components. The flow equations for the pseudocomponents in IFLO are presented below:

Stock Tank Oil:

$$\nabla \cdot \frac{K\, k_{ro}^{e}}{\mu_o^{e} B_o} \nabla \Phi_o - \frac{q_o}{\rho_{osc}} = \frac{\partial}{\partial t}\left(\phi \frac{S_o}{B_o} \right) \tag{9.31}$$

Water plus Surfactant:

$$\nabla \cdot \frac{K\, k_{rw}}{\mu_w B_w} \nabla \Phi_w - \frac{q_w}{\rho_{wsc}} = \frac{\partial}{\partial t}\left(\phi \frac{S_w}{B_w} \right) \tag{9.32}$$

Miscible Species (e.g. carbon dioxide):

$$\nabla \cdot x_s \frac{K\, k_{rw}}{\mu_w B_w} \nabla \Phi_w - x_s \frac{q_w}{\rho_{wsc}} = \frac{\partial}{\partial t}\left(\phi\, x_s \frac{S_w}{B_w} \right) \tag{9.33}$$

Soluble Species (e.g. natural gas):

$$\begin{aligned} &\nabla \cdot \left[v_i \frac{K\, k_{rg}^{e}}{\mu_i^{e} B_i} \nabla \Phi_i + v_i\, R_{io} \frac{K\, k_{ro}^{e}}{\mu_o^{e} B_o} \nabla \Phi_o + v_i\, R_{iw} \frac{K\, k_{rw}}{\mu_w B_w} \nabla \Phi_w \right] \\ &- \frac{q_i}{\rho_{isc}} = \frac{\partial}{\partial t} \left\{ \phi\, v_i \left[\frac{S_g}{B_i} + R_{io} \frac{S_o}{B_o} + R_{iw} \frac{S_w}{B_w} \right] \right\} \end{aligned} \tag{9.34}$$

for $I = \{g, 1, \ldots, N_s\}$. The miscible species has also been referred to as a surfactant, or surface active agent. The flow equations in IFLO are designed to model CO_2 as the surfactant. Table 9-3 presents the nomenclature for the symbols in Equations (9.31) through (9.34). The

superscript *e* indicates that an effective fluid property is being calculated, and the subscript *sc* refers to standard conditions.

Table 9-3
Nomenclature for IFLO Flow Equations

Symbol	Meaning
B_ℓ	Formation volume factor of phase ℓ
K	Absolute permeability
$k_{r\ell}$	Relative permeability of phase ℓ
N_s	Number of soluble species
q	Source/sink flow rate
$R_{i\ell}$	Solubility of soluble component i in phase ℓ
S_ℓ	Saturation of phase ℓ
v_i	Volume fraction of soluble component *i*
x_s	Surfactant volume fraction
μ_ℓ	Viscosity of phase ℓ
μ_i	Gas phase viscosity including effects of soluble component *i*
ρ	Density
Φ_ℓ	Potential of phase $\ell = P_\ell - \gamma_\ell z$ (or soluble component *i*)
P_ℓ	Pressure of phase ℓ (or soluble component *i*)
γ_ℓ	Pressure gradient of phase ℓ (or soluble component *i*)
ϕ	Porosity

9.6 Simulator Selection and Ockham's Razor

The selection of a reservoir simulator depends on such factors as the objectives of the study, fluid type, and dimensionality of the system. The wise modeler will recognize that you do not have to use a sledge hammer to open a peanut! If a material balance calculation can achieve the objectives of a study, then it should be used instead of a more sophisticated simulator. On the other hand, the best simulation technology available should be used when it is appropriate. For purposes of illustration, we focus our attention on a study that uses either a black oil simulator or a compositional simulator.

Standard black oil and compositional simulators assume isothermal flow and mass transfer within a gridblock is instantaneous. A compositional simulator represents the fluid as a mixture of hydrocarbon components. Black oil simulators may be viewed as compositional simulators with two components. They can have gas dissolved in the oil phase, as well as oil dissolved in the gas phase. Black oil simulators need both saturated and undersaturated fluid property data.

Simulator selection depends on the number of phases that are expected to appear during the life of the field. For example, if the pressure of an oil reservoir never declines below bubble point pressure, there is no need to include the modeling of a free gas phase. Similarly, if the pressure of a gas condensate reservoir stays above the dew point pressure, there is no need to include the modeling of a hydrocarbon liquid phase.

Systems that depend on temperature require thermal simulation. For example, dry gas injection in a nearly isothermal condensate reservoir is typically modeled with a compositional simulator, while steam flooding a heavy oil reservoir should be modeled with a thermal simulator.

Black oil and compositional simulators usually assume that fluids have a minimal effect on rock properties. Thus, standard versions of the simulators will not model changes in rock properties due to effects

like grain dissolution, tar mat formation, or gel formation resulting from a vertical conformance treatment. Special purpose simulators or special options within a standard simulator must be obtained to solve such problems.

Fluid type is needed to decide if the reservoir should be modeled using either a black oil simulator or a compositional simulator. Well logs can distinguish between oil and gas, but are less useful in further classifying fluid type. A pressure-temperature diagram is useful for determining reservoir fluid type, but its preparation requires laboratory work with a fluid sample. A simpler way that is often sufficient for classifying a fluid is to look at the solution gas-oil ratio. As a rule of thumb, compositional models should be used to model volatile oil and condensate fluids, while black oil and dry gas fluids are most effectively modeled with a black oil simulator. The applicability of this rule depends on the objectives of the study.

A few guidelines are worth noting with regard to simulator selection. Many novice modelers make the mistake of selecting models that are much more complex than they need to be to satisfy the objectives of the study. According to Coats [1969], the modeler should "select the least complicated model and grossest reservoir description that will allow the desired estimation of reservoir performance." This is a restatement of Ockham's Razor.

9.6.1 Ockham's Razor

William of Ockham, a fourteenth century English philosopher, said "plurality must not be posited without necessity" [Jefferys and Berger, 1992]. Today this is interpreted to mean that an explanation of the facts should be no more complicated than necessary. We should favor the simplest hypothesis that is consistent with the data.

Ockham's Razor should be applied with care, however, because one of the goals of a model study is to establish a consensus about how the reservoir behaves. This consensus is political, to an extent, because the model must satisfy the people who commissioned the study. Their

views may require using a model that has more complexity than required from a technical modeling perspective.

A wide variety of simulators are available for a price. The work horse simulators – black oil and compositional – can often be leased on an as-needed basis or are available through computer networks. More specialized simulators may be obtained from software vendors, or as publicly available research codes developed at university and government laboratories.

9.6.2 Simulator Options

Several requirements must be considered when selecting simulator options. These requirements can be classified into two general categories: reservoir and nonreservoir. From a reservoir perspective, we are interested in fluid type, reservoir architecture, and the types of recovery processes or drive mechanisms that are anticipated.

Reservoir architecture encompasses a variety of parameters that have a major impact on model design. Study objectives and the geologic model must be considered in establishing the dimensionality of the problem (1-D, 2-D, or 3-D) and the geometry of the grid. Do we need special grid options, such as radial coning or local grid refinement, or will Cartesian coordinates be satisfactory? If the study is designed to investigate near wellbore flow, it would be wise to select a grid that provides good spatial resolution near the wellbore, for example, radial coordinates. On the other hand, if the study is intended to provide an overview of field performance, a coarse Cartesian grid may be satisfactory.

The level of complexity of the geology will influence grid definition, and in the case of fractured reservoirs, the type of flow equations that must be used [for example, see Reiss, 1980; Aguilera, 1980; Golf-Racht, 1982; and Lough, et al., 1996]. A highly faulted reservoir or a naturally fractured reservoir is more difficult to describe numerically than homogeneous sand.

Nonreservoir requirements include personnel, simulator availability, and cost effectiveness. Personnel will be needed to gather and

evaluate data, prepare input data, perform the history match, and then make predictions. Data gathering may take a few days or several months depending on the quality and extent of the data base for a particular field. The same modeler does not necessarily have to perform the history matching and prediction stages. In some companies, history matching is done in a collaborative effort between a specialized technology center and a field office, while most of the prediction work is completed in the field office. This takes advantage of specialized expertise: technology centers, including outside consultants, routinely set up and run models, while day-to-day changes that impact production operations are handled in the field office. The division of labor between history matching and prediction makes sense in some circumstances.

As complexity increases, so also does cost. A good economic argument to support Ockham's Razor is to remember that the latest technology is not always the best technology for a project, and its use comes with a cost. Modeling teams are often tempted to apply the latest technology, even if it is not warranted. A wise modeling team will match the level of technology with the objectives of the study. The result will be the selection of the most cost effective method for achieving study objectives.

The cost of a simulation study can be estimated based on previous experience with similar studies. As an example of how to estimate the cost for a black oil simulation study, begin by calculating the product of the number of gridblocks and the number of timesteps denoted by GBTS. Once GBTS is known, it should be related to the computer processing (cpu) time needed to make a run. The amount of cpu time per GBTS is determined by dividing the cpu time needed to make previous model runs by the number of GBTS in those runs. The product of GBTS and cpu time per GBTS gives total cpu time needed for a run. The cost of the study then depends on the number of runs needed. A similar approach is applied to estimating the cost of making predictions. This does not include the cost of data collection and evaluation.

9.7 IFLO Application: Gas Injection into a Light Oil Reservoir

Simulator technology is generally considered proprietary technology, yet it has an economic impact that takes it out of the realm of the research laboratory and makes it a topic of importance in the corporate boardroom. Nevertheless, numerical representations of nature are subject to inaccuracies [for example, see Mattax and Dalton, 1990; Saleri, 1993; and Oreskes, et al., 1994]. This point has been illustrated in several simulator comparative solution projects sponsored by the Society of Petroleum Engineers (SPE) beginning with Odeh [1981]. Each comparative solution project was designed to allow comparisons of proprietary technology by asking participating organizations to solve the same predetermined problem. This IFLO application is based on the first SPE comparative solution project [Odeh, 1981].

The first project compared the performance of simulators modeling the injection of gas into a saturated black oil reservoir. A saturated, light (59^o API) oil is produced from a corner gridblock in the lowermost layer of a three-layer square grid. Lean gas is injected into the upper layer at the opposite corner. The injected gas is expected to propagate most rapidly through the upper layer. Figure 9-2 is taken from the first comparative solution project [Odeh, 1981]. It shows that differences in the formulations of several reservoir simulators lead to differences in predictions of economically important quantities such as oil production rate.

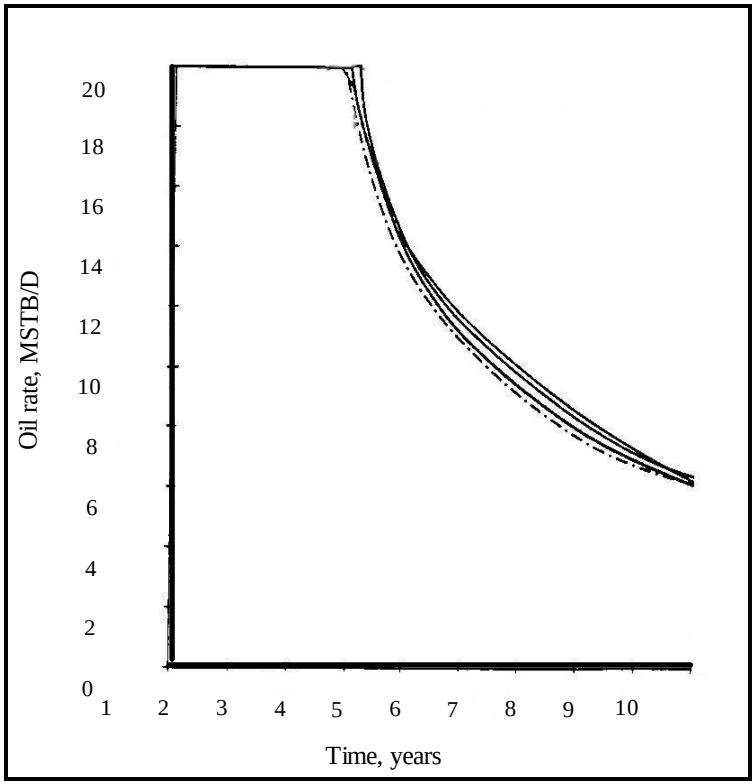

Figure 9-2. Oil Rate from the First SPE Comparative Solution Project, Case 2 (after Odeh [1981]; reprinted by permission of the Society of Petroleum Engineers)

Exercises

Exercise 9.1 Suppose the unit of density ρ_{osc} is mass per volume at standard conditions, and the unit of Darcy velocity is length per time. Use dimensional analysis to determine the unit of flux in Eq. (9.7).

Exercise 9.2 The densities in Eqs. (9.14) and (9.15) include gas dissolution. Rewrite Eqs. (9.19), (9.23), and (9.29) for a system with no gas dissolved in either the oil or water phases.

Exercise 9.3 Run EXAM3.DAT and record the time, pressure, oil rate, water rate, gas rate, and GOR at the end of the run. These values are obtained from the one line timestep summary file ITEMP.TSS. Is gas significant in this model? Note that the pressure reported for the reservoir is pore volume weighted average reservoir pressure P_{av}. Pore volume weighted average reservoir pressure is given by

$$P_{av} = \frac{\sum_{j=1}^{N} P_j V_{pj}}{\sum_{j=1}^{N} V_{pj}} \tag{9.35}$$

where N is the total number of gridblocks in the model grid, P_j is the oil phase pressure in gridblock j, and V_{pj} is the pore volume of gridblock j.

Exercise 9.4 Find the following properties in file EXAM8_PVTG.DAT:
a. What is gas gravity?
b. What is critical gas saturation?
c. In which layer is well GAS1 completed?
d. In which layer is well GAS2 completed?
e. What is the size of the gridblock in the x direction?
f. What is porosity in layer 1?
g. What is permeability in the x, y and z directions in layer 2?

Exercise 9.5 Find the following properties in file EXAM1.DAT:
a. What is the net-to-gross ratio?
b. What is residual oil saturation to a waterflood?
c. What is the bubble point pressure?
d. What is the depth to the midpoint of the gridblock?
e. What is rock compressibility at bubble point pressure?
f. Can any gas dissolve in water?

Exercise 9.6 A model has $10 \times 10 \times 4$ gridblocks and takes five minutes to run 100 timesteps. Calculate cpu time per gridblock-timestep (GBTS).

Estimate how long it would take to make 100 runs with 200 timesteps each.

Exercise 9.7 Data file EXAM7.DAT is one version of the Odeh [1981] SPE comparative solution problem. Run EXAM7.DAT and compare the oil rate to results reported by Odeh (see Figure 9-2). What is the IFLO material balance error? The material balance error associated with this data file provides a good test of the quality of IFLO relative to other programs based on the original version of BOAST [for example, Fanchi, et al., 1982; Fanchi, et al., 1987; Louisiana State University, 1997].

Exercise 9.8A A reservoir is 10 mi. long and 4 mi. wide. Define a grid with gridblock lengths $\Delta x = \Delta y = 1/8$ mi. What is the number of gridblocks needed to cover the areal extent of the reservoir? Note: 1 mi. = 5280 ft.

Exercise 9.8B If five model layers are used, what is the total number of gridblocks in the model?

Chapter 10

Fundamentals of Reservoir Simulation

Previous chapters describe much of the data that is needed by a reservoir simulator. Our goal here is to describe how the complex fluid flow equations presented in Chapter 9 are solved in practice. For a more detailed technical presentation, consult one of the many sources available in the literature [for example, see Aziz and Settari, 1979; Peaceman, 1977; Rosenberg, 1977; Thomas, 1982; Mattax and Dalton, 1990; Ertekin, et al., 2001; Munka and Pápay, 2001]. The technique used to solve the set of IFLO equations is presented as an illustration of a simulator solution procedure.

10.1 Simulator Solution Procedures

Fluid flow equations are a set of nonlinear partial differential equations that must be solved by computer. The partial derivatives are replaced with finite differences, which are in turn derived from Taylor's series. Table 10-1 outlines this procedure. The spatial finite difference interval Δx along the x-axis is called the gridblock length, and the temporal finite difference interval Δt is called the timestep. Indices i, j, and k are ordinarily used to label grid locations along the x, y, and z coordinate axes, respectively. Index n labels the present time level, so that n+1

represents a future time level. If the finite difference representations of the partial derivatives are substituted into the original flow equations, the result is a set of equations that can be algebraically rearranged to form a set of equations that can be solved numerically. The solution of these equations is the job of the simulator.

Table 10-1
Finite Difference Approximation

1. Formulate fluid flow equations, such as,

$$\frac{\partial}{\partial x}\left[\frac{Kk_r}{\mu B}\left(\frac{\partial P}{\partial x}\right)\right] + q_s\delta(x - x_0) = \frac{\partial}{\partial t}\left(\frac{\phi S}{B}\right)$$

2. Approximate derivatives with finite differences
   a. Discretize region into gridblocks Δx:

$$\frac{\partial P}{\partial x} \approx \frac{P_{i+1} - P_i}{x_{i+1} - x_i} \equiv \frac{\Delta P}{\Delta x}$$

   b. Discretize time into timesteps Δt:

$$\frac{\partial S}{\partial t} \approx \frac{S^{n+1} - S^n}{t^{n+1} - t^n} \equiv \frac{\Delta S}{\Delta t}$$

3. Numerically solve the resulting set of linear algebraic equations

The two most common solution procedures in use today are implicit pressure, explicit saturation (IMPES) and Newton-Raphson. The terms in the finite difference form of the flow equations are expanded in the Newton-Raphson procedure as the sum of each term at the current iteration level, plus a contribution due to a change of each term with respect to the primary unknown variables over the iteration. To calculate these changes, it is necessary to calculate derivatives, either numerically or analytically, of the flow equation terms. The derivatives are stored in a matrix called the acceleration matrix or the Jacobian. The Newton-Raphson technique leads to a matrix equation $\mathbf{J} \bullet \boldsymbol{\delta}\mathbf{X} = \mathbf{R}$ that equates the product of the acceleration matrix $\mathbf{J}$ and a column vector $\boldsymbol{\delta}\mathbf{X}$ of changes to the primary unknown variables to the column vector of residuals $\mathbf{R}$. The matrix equation is solved by matrix algebra to yield the

changes to the primary unknown variables $\boldsymbol{\delta X}$. These changes are added to the value of the primary unknown variables at the beginning of the iteration. If the changes are less than a specified tolerance, the iterative Newton-Raphson technique is considered complete and the simulator proceeds to the next timestep.

The three primary unknown variables for an oil-water-gas system are oil-phase pressure, water saturation, and either gas saturation or solution gas-oil ratio. The choice of the third variable depends on whether the gridblock contains free gas, which depends, in turn, on whether the gridblock pressure is above or below the bubble point pressure. Naturally, the choice of unknowns is different for a gas-water system or a water only system. The discussion presented here applies to the most general three-phase case.

The Newton-Raphson technique is known as a fully implicit technique because all primary variables are calculated at the same time; that is, primary variables at the new time level are determined simultaneously. A simpler procedure is the IMplicit Pressure-Explicit Saturation (IMPES) procedure. It is much like the Newton-Raphson technique except that flow coefficients are not updated in an iterative process. By contrast, the IMPES procedure solves for pressure at the new time level using saturations at the old time level, and then uses the pressures at the new time level to explicitly calculate saturations at the new time level. A variation of this technique is to iteratively substitute the new time level estimates of primary variables in the calculation of coefficients for the flow equations. The iterative IMPES technique takes longer to run than the noniterative technique, but generates less material balance error [Ammer and Brummert, 1991]. IFLO, the program provided with this book, is an implementation of an iterative IMPES formulation. The formulation is outlined below.

Figure 10-1 shows a flow chart for a typical simulator [see Crichlow, 1977]. The simulation program begins by reading input data and initializing the reservoir. This part of the model will not change as a function of time. Information for time-dependent data must then be read. This data includes well and field control data. The coefficients of the flow equations and the primary unknown variables are then calculated.

Once the primary variables are determined, the process can be repeated by updating the flow coefficients using the values of the primary variables at the new iteration level. This iterative process can improve material balance. When the solution of the fluid flow equations is complete, flow properties are updated and output files are created before the next timestep calculation begins.

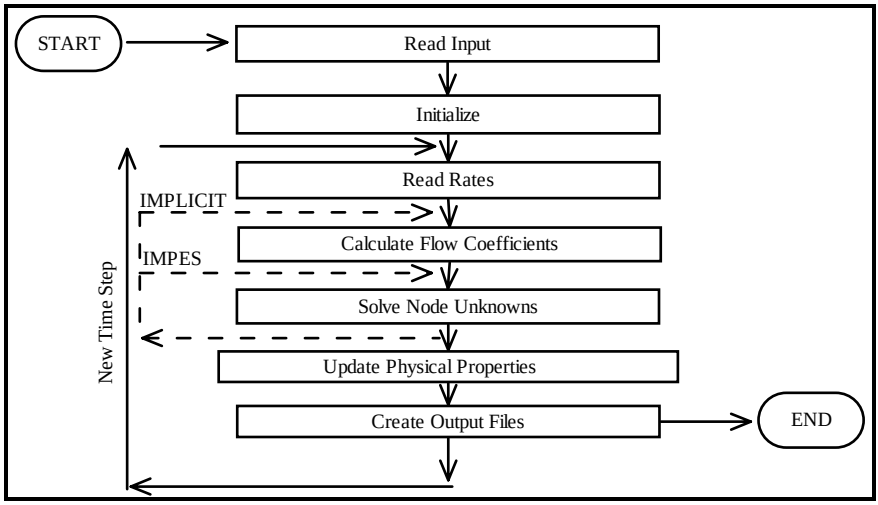

Figure 10-1. Typical simulator flow chart

Fully implicit techniques do more calculations in a timestep than the IMPES procedure, but are stable over longer timesteps. The unconditional stability of the fully implicit techniques means that a fully implicit simulator can solve problems faster than IMPES techniques by taking significantly longer timesteps.

Adaptive implicit techniques attempt to combine the best elements of both IMPES and fully implicit techniques. An adaptive technique will use the IMPES method in regions of the model domain that have relatively small changes in primary variables, and apply the fully implicit method in regions that have relatively large changes in primary variables. Adaptive techniques can increase timestep size relative to the IMPES method, and reduce computer resource requirements relative to the fully implicit method. Adaptive techniques use computer

resources to determine when and where to apply the appropriate solution technique in the model domain.

Simulators also differ in their robustness, that is, their ability to solve a wide range of physically distinct problems. Robustness appears to depend as much on the coding of the simulator as it does on the formulation technique. The best way to determine simulator robustness is to test the simulator with data sets representing many different types of reservoir management problems. The examples provided with IFLO are designed to demonstrate the robustness, or range of applicability, of the simulator.

In summary, a representation of the reservoir is quantified in the reservoir flow simulator. The representation is validated during the history matching process, and forecasts of reservoir performance are then made from the validated reservoir representation.

10.2 Numerical Dispersion

A problem with large timesteps in the fully implicit technique is the introduction of a numerical effect known as numerical dispersion [Lantz, 1971; Fanchi, 1983]. Numerical dispersion is introduced when the Taylor series approximation is used to replace derivatives with finite differences. The resulting truncation error introduces an error in calculating the movement of saturation fronts that looks like physical dispersion, hence it is called numerical dispersion.

Numerical dispersion arises from time and space discretization that lead to smeared spatial gradients of saturation or concentration [Lantz, 1971] and grid orientation effects [Fanchi, 1983]. The smearing of saturation fronts can impact the modeling of displacement processes. Figure 10-2 presents an illustration of front smearing for a linear Buckley-Leverett waterflood model. The numerical front from an IMPES calculation does not exhibit the same piston-like displacement that is shown by the analytical Buckley-Leverett calculation.

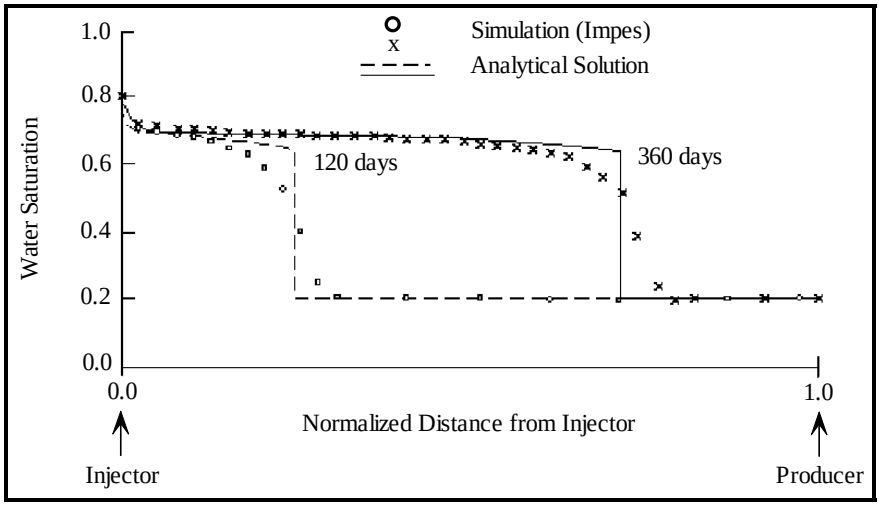

Figure 10-2. Numerical Dispersion (after Fanchi, 1986; reprinted by permission of the Society of Petroleum Engineers)

Total dispersion D^{tot} in a simulator is the sum of physical dispersion D^{phy} and numerical dispersion D^{num}, thus

$$D^{tot} = D^{phy} + D^{num} \tag{10.1}$$

Numerical dispersion in one spatial dimension has the form

$$D^{num} = \frac{v}{2}\left(\Delta x \pm \frac{v\Delta t}{\phi}\right) \tag{10.2}$$

It depends on gridblock size Δx, timestep size Δt, velocity v of frontal advance, porosity ϕ, and numerical formulation. The "+" sign applies to the fully implicit formulation, and the "~" sign applies to IMPES. Notice that an increase in Δt in the fully implicit formulation increases D^{num} while it decreases D^{num} when the IMPES technique is used. Indeed, it appears that a judicious choice of Δx and Δt could eliminate D^{num} altogether in the IMPES method. Unfortunately, the combination of Δx and Δt that yields $D^{num} = 0$ violates a numerical stability criterion. In general, IMPES numerical dispersion is not as large as that associated with fully implicit techniques.

As a rule of thumb, timestep sizes in fully implicit calculations should not exceed a quarter of a year, otherwise numerical dispersion can dominate front modeling. By contrast, the maximum timestep size in an IMPES simulator can be estimated by applying the rule of thumb that throughput in any gridblock should not exceed 10% of the pore volume of the gridblock. Throughput is the volume of fluid that passes through a gridblock in a single timestep. IMPES timestep sizes are often on the order of days.

The IMPES timestep limitation is less of a problem than it might otherwise seem, because it is very common for production data to be reported on a monthly basis. The reporting period often controls the frequency with which well control data is read during a history match. Thus, during the history match phase of a study, simulator timestep sizes are dictated by the need to enter historical data. Large timestep sizes reduce the ability of the model to track variations of rate with time because historical data must be averaged over a longer period of time. As a result, the modeler often has to constrain the fully implicit simulator to run at less than optimum numerical efficiency because of the need to represent more accurately the real behavior of the physical system.

10.3 IFLO Solution Procedure

The solution procedure used in IFLO is outlined below. The multidimensional flow model may be run as a material balance program by setting transmissibility to zero and running the model as a grid with a single gridblock. The formulation of fluid flow equations is presented in more detail by Ammer, et al. [1991] and Fanchi [2000].

10.3.1 Volume Integration and Discretization

The fluid flow equations presented above are discretized using volume integration and finite difference techniques. The volume integration procedure is illustrated by integrating the oil flow equation over a gridblock m with volume V_m; thus

$$\int_{V_m}\left[\nabla\cdot\frac{Kk_{ro}^{e}}{\mu_o^{e}B_o}\nabla\Phi_o-\frac{q_o}{\rho_{osc}}\right]dV=\int_{V_m}\frac{\partial}{\partial t}\left(\phi\frac{S_o}{B_o}\right)dV \tag{10.3}$$

The divergence theorem is used to replace the volume integral over the convection term on the left hand side of Equation (10.3) with a surface integral. Applying the divergence theorem gives

$$\int_{S_{em}}\frac{Kk_{ro}^{e}}{\mu_o^{e}B_o}\nabla\Phi_o\cdot\hat{n}dS-\int_{V_m}\left[\frac{q_o}{\rho_{osc}}\right]dV=\frac{\partial}{\partial t}\int_{V_m}\left(\phi\frac{S_o}{B_o}\right)dV \tag{10.4}$$

where gridblock volume V_m corresponds to the volume V, and the surface S is the external surface S_{em} of the gridblock m. The surface integral represents fluid flow across the gridblock boundaries.

The spatially discretized material balance equation for oil is

$$\frac{dM_o}{dt}+Q_o=\Delta A_o\Delta\Phi_o \tag{10.5}$$

where the volume integral over rate is

$$Q_o=\int_{V_m}\frac{q_o}{\rho_{osc}}dV=\frac{q_o}{\rho_{osc}}V_m \tag{10.6}$$

The volume integral over the accumulation term is

$$M_o=\int_{V_m}\left(\phi\frac{S_o}{B_o}\right)dV=\phi\frac{S_o}{B_o}V_m \tag{10.7}$$

and the surface integral is

$$\Delta A_o\Delta\Phi_o=\int_{S_{em}}\frac{Kk_{ro}^{e}}{\mu_o^{e}B_o}\nabla\Phi_o\cdot\hat{n}dS \tag{10.8}$$

The term A_o represents oil phase transmissibility and oil phase potential is

$$\Delta\Phi_o^{n+1}=\Delta P^{n+1}-\Delta\gamma_o^{n}D \tag{10.9}$$

The variable P is oil phase pressure, D is depth to the center of the gridblock, and γ_o is the specific gravity of the oil phase. The time derivative in Equation (10.5) is replaced with a forward finite difference to obtain

$$\frac{1}{\Delta t}\left[M_o^{n+1} - M_o^{n}\right] + Q_o^{n+1} = \Delta A_o^{n+1}\Delta\Phi_o^{n+1} \qquad (10.10)$$

The superscript n denotes the present time level t^n, and the superscript $n + 1$ denotes the future time level t^{n+1}. Timestep size Δt equals $t^{n+1} - t^n$.

The above formulation is a fully implicit formulation because all variables are assessed at the future time level in Equation (10.10). IMPES is invoked by approximating transmissibilities, capillary pressures and densities at time level $n + 1$ with their values at time level n. The resulting flow equation is

$$\frac{1}{\Delta t}\left[M_o^{n+1} - M_o^{n}\right] + Q_o^{n+1} = \Delta A_o^{n}\Delta\Phi_o^{n+1} \qquad (10.11)$$

Similar equations apply to the other flow equations.

10.3.2 Multi-Variable Newton-Raphson IMPES Procedure

The IMPES equations developed above are solved using an iterative technique that is illustrated by continuing our analysis of the oil flow equation. The residual form of Equation (10.11) is

$$R_o^{\ell} = \frac{1}{\Delta t}\left[M_o^{\ell} - M_o^{n}\right] + Q_o^{\ell} - \Delta A_o^{n}\Delta\Phi_o^{\ell} \qquad (10.12)$$

where the superscript ℓ denotes the iteration level for the variables that are desired at time level $n + 1$. The primary variables for a saturated gridblock are ΔP, ΔS_w, ΔS_g and $\{v_i: I = 1, \ldots, N_s\}$. Gas saturation is replaced by bubble point pressure P_b in the set of primary variables for a saturated gridblock. The variable switching logic used to treat gridblocks undergoing phase transitions is described in Ammer, et al. [1991]. The solution process is designed to find the values of the primary variables which drive the residuals to zero in all gridblocks for all components. Ammer, et al. [1991] refer to the solution procedure as the multivariable Newton-Raphson IMPES method.

10.4 IFLO Transmissibility

Flow between neighboring gridblocks is treated as a series application of Darcy's Law in IFLO. A transmissibility term between two gridblocks is defined using the product of average values of relative permeability $k_{r\ell}$ of phase ℓ, absolute permeability K of each gridblock at the interface, and cross-sectional area A_c of each gridblock at the interface, divided by the product of the viscosity μ_ℓ of phase ℓ and the formation volume factor B_ℓ of phase ℓ in each gridblock. The transmissibility to each phase is determined using a harmonic average calculation of the product of absolute permeability times cross-sectional area at the interface between neighboring gridblocks. An arithmetic average of phase viscosities and formation volume factors is used. The average relative permeability is determined using an upstream weighted averaging technique.

The Darcy transmissibility for the *x*-direction index i is

$$A'_{\ell,i-\frac{1}{2}} = \frac{4\, k_{r\ell(upstream)}}{\left(\mu_{\ell,i-1}+\mu_{\ell,i}\right)\left(B_{\ell,i-1}+B_{\ell,i}\right)} \times \left[\frac{2\left(KA_c\right)_{i-1}\left(KA_c\right)_i}{\Delta x_{i-1}\left(KA_c\right)_i + \Delta x_i\left(KA_c\right)_{i-1}}\right] \tag{10.13}$$

where the j,k indices are suppressed. The *x*-direction length of gridblock i is Δx_i. The finite difference transmissibility for phase ℓ between gridblock $i-1$ and gridblock i is

$$A_{\ell,i-\frac{1}{2}} = A'_{\ell,i-\frac{1}{2}} \frac{\Delta x_i}{\left(\frac{\Delta x' + \Delta x''}{2}\right)} \tag{10.14}$$

where the spatial differences are

$$\Delta x' = x_i - x_{i-1},\ \Delta x'' = x_{i+1} - x_i \tag{10.15}$$

Similar definitions of transmissibility apply in all three coordinate directions.

Fully implicit formulations update relative permeability, viscosity, and formation volume factor as pressure and saturation distributions change during the iterative calculations that occur within a timestep. IMPES formulations update relative permeability, viscosity, and formation volume factor using new pressure and saturation distributions following the completion of a timestep. Some simulators, such as IFLO, have options that let the user update permeability and cross-sectional area as functions of pressure and saturation. For example, cross-sectional area of gridblock i in Eq. (10.13) may be written as

$$\left(A_c\right)_i = \Delta y_i \left(\Delta z_{net}\right)_i \tag{10.16}$$

where Δy_i is the *y*-direction length of gridblock i and $\left(\Delta z_{net}\right)_i$ is the net thickness of gridblock i. The net thickness may shrink as a result of compaction following a decrease in pore pressure. In addition, permeability may change as pore pressure changes. These effects have traditionally been neglected in black oil and compositional simulators, but are becoming more important as modelers recognize that geomechanical effects are needed to understand the production performance of some reservoirs.

Flow simulators are usually programmed with no-flow boundary conditions, that is, fluid is not allowed to flow across the external boundaries of the grid. The no-flow boundary conditions are imposed by setting transmissibility equal to zero across the external boundaries. The user may also impose no-flow boundaries or flow restrictions across user-specified interfaces by directly modifying the appropriate transmissibility. This is useful, for example, when a geologic feature such as a sealing fault needs to be described. In this case, the sealing fault is defined by setting transmissibility equal to zero across the fault boundary. The user needs to understand how the transmissibility adjustment is made in a particular simulator because the transmissibility adjustment applies to the interface between rows, columns, or layers of gridblocks.

10.5 IFLO Well Model

A well model used in many simulators is a variation of Darcy's Law which says that well flow rate is proportional to pressure change. The relationship between flow rate Q_ℓ of phase ℓ and pressure change ΔP may be written as

$$Q_\ell = PI\ \Delta P \tag{10.17}$$

where the proportionality constant is called the productivity index (PI). Rearranging and using Darcy's Law for radial flow into a vertical wellbore, PI can be calculated as

$$PI = \frac{Q_\ell}{\Delta P} = \frac{0.00708 K_e h_{net}}{\mu_\ell B_\ell \left[\ln\left(r_e / r_w\right) + S\right]} \tag{10.18}$$

The meaning and appropriate units of each variable in Eq. (10.18) follow:

μ_ℓ = viscosity of phase ℓ (cp)

B_ℓ = formation volume factor of phase ℓ (RB/STB)

r_e = drainage radius (ft)

r_w = wellbore radius (ft)

S = skin

K_e = effective permeability (md) = $k_{r\ell} K_{abs}$

$k_{r\ell}$ = relative permeability of phase ℓ

K_{abs} = absolute permeability (md)

h_{net} = net thickness (ft)

Q_ℓ = rate of phase ℓ (STB/D)

Most flow simulators calculate PI and pressure change, then flow rate. If the magnitude of the flow rate calculated from the PI and

pressure change is greater than the magnitude of the pressure change input by the user, the flow rate will usually be set at the user specified flow rate. If the magnitude of the flow rate calculated from the PI and pressure change is less than the magnitude of the pressure change input by the user, the flow rate will be the simulator calculated value. The reader should consult the technical documentation of a flow simulator to see the details of well model calculations. Well model features available in IFLO are described here.

10.5.1 IFLO Productivity Index

Some of the terms in the *PI* depend on time-varying pressure and saturation, while other factors change relatively slowly or are constant with respect to time. Relative permeability, viscosity and formation volume factor depend on time-varying pressure and saturation. The remaining variables on the right hand side of Eq. (10.18) change relatively slowly or are constant with respect to time. For example, we separate these terms for the oil phase *PI* to obtain

$$PI = \frac{k_{ro}}{\mu_o B_o} PID \tag{10.19}$$

where the quasistationary factors are collected in the *PID* term, that is,

$$PID = \frac{0.00708 K_{abs} h_{net}}{\left[\ln\left(r_e / r_w\right) + S\right]} \tag{10.20}$$

The IFLO user is expected to provide a *PID* value for each well connection. A connection is a gridblock with a well perforation.

A value of the effective drainage radius for a vertical well in the center of a rectangular gridblock with cross-sectional area $\Delta x \Delta y$ can be estimated from Peaceman's formula [1978]

$$r_e \approx r_o = 0.14\left(\Delta x^2 + \Delta y^2\right)^{1/2} \tag{10.21}$$

Equation (10.21) applies to an isotropic system, that is, a system in which lateral permeability does not depend on direction. For a well in a square gridblock with isotropic permeability, we have $\Delta x = \Delta y$ and

$r_e \approx r_o = 0.2\Delta x$. For a well in a rectangular gridblock and an anisotropic system, the effective permeability can be estimated as

$$K = \sqrt{K_x K_y} \tag{10.22}$$

In this case, lateral permeability depends on direction and the directional components of permeability are not equal; thus $K_x \neq K_y$. The equivalent well gridblock radius for an anisotropic system must account for the dependence of permeability on direction. The effective drainage radius becomes

$$r_e \approx r_o = 0.28 \frac{\left[\left(K_y/K_x\right)^{1/2}\Delta x^2 + \left(K_x/K_y\right)^{1/2}\Delta y^2\right]^{1/2}}{\left(K_y/K_x\right)^{1/4} + \left(K_x/K_y\right)^{1/4}} \tag{10.23}$$

A *PID* value can be estimated for horizontal wells in a manner similar to that for vertical wells by changing variables in Peaceman's equation. Alternatively, a horizontal well model can be used to estimate *PID* values. For example, Joshi's formula [Joshi, 1991] for a horizontal well is

$$PID_k = \frac{\left[0.00708Kh\right]_k}{\left[\ln\left(\frac{a + \sqrt{a^2 - \left(\frac{L}{2}\right)^2}}{L/2}\right) + \frac{h}{L}\ln\left(\frac{h}{2r_w}\right) + S\right]} \tag{10.24}$$

where

$$a = \frac{L}{2}\left[0.5 + \sqrt{0.25 + \left(\frac{2r_{eh}}{L}\right)^4}\right]^{1/2} \tag{10.25}$$

The subscript *k* in Eq. (10.24) denotes the connection in layer *k*. The remaining parameters are defined as:

K = horizontal permeability of connection k (md)

h = thickness of connection k (ft)

L = horizontal well length (ft)

r_{eh} = drainage radius of horizontal well (ft)

10.5.2 IFLO Rate Constraint Representation

In the rate constraint representation, well rates may be specified for injectors or producers. We assume the well may be completed in a total of K connections, and fluid allocation between connections is based on effective mobility λ^e and pressure differential $\Delta P_{wk} = P - P_{wb}$ between the pressure P in the gridblock containing the well connection and the user specified wellbore flowing pressure P_{wb}.

Case 1: Pressure Differential for Specified Oil Production Rate Q_o

The pressure differential for each connection k is

$$\Delta P_{wk} = \frac{Q_o}{\sum_{k=1}^{K} PID_k \left[\lambda_o^e / B_o\right]_k^n} \tag{10.26}$$

where λ_ℓ^e is the effective fluid mobility of phase ℓ and PID is the well productivity index. A PID may be specified for each connection k.

Case 2: Pressure Differential for Specified Water Production Rate Q_w

The pressure differential for each connection k is

$$\Delta P_{wk} = \frac{Q_w}{\sum_{k=1}^{K} PID_k \left[\lambda_w^e / B_w\right]_k^n} \tag{10.27}$$

Case 3: Pressure Differential for Specified Natural Gas Production Rate Q_g

The pressure differential for each connection *k* is

$$\Delta P_{wk} = \frac{Q_g}{\sum_{k=1}^{K} PID_k \left[\lambda_g^e / B_g\right]_k^n} \tag{10.28}$$

Solution gas in both oil and water is neglected when a natural gas production rate is specified. This is a reasonable assumption for wells producing primarily free natural gas. It allows IFLO to model a specified natural gas production rate from natural gas-water systems.

Production rates from each connection are calculated from the pressure differentials as follows:

Oil:

$$Q_{ok} = PID_k \left(\lambda_o^e / B_o\right)_k^n \Delta P_{wk} \tag{10.29}$$

Water:

$$Q_{wk} = PID_k \left(\lambda_w^e / B_w\right)_k^n \Delta P_{wk} \tag{10.30}$$

Natural Gas and Solvent:

$$Q_{ik} = PID_k \left(\lambda_g^e / B_g\right)_k^n \Delta P_{wk} + \left(v_i^n R_{io}^n\right)_k Q_{ok} + \left(v_i^n R_{iw}^n\right)_k Q_{wk} \tag{10.31}$$

where $\{i = g, 1, \ldots, N_s\}$, v_i is the volume fraction of component *i*, and $R_{i\ell}$ is the solubility of component *i* in phase $\{\ell = o, w\}$.

Case 4: Total Production Rate Specified

When the total reservoir voidage rate Q_T is specified, the procedure is similar to the calculation for a specified rate. The expression for pressure differential is

$$\Delta P_{wk} = \frac{Q_T}{\sum_{k=1}^{K} PID_k \left\{\left(\lambda_o^e\right)_k^n + \left(\lambda_w^e\right)_k^n + \left(\lambda_g^e\right)_k^n + \sum_{i=1}^{N_s} \left(\lambda_l^e\right)_k^n\right\}} \tag{10.32}$$

The pressure differential is then used in the rate equations, Eqs. (10.29) through (10.31), to calculate rates.

Case 5: Injection Rate Specified

If the well is an injector, the user must specify the surface injection rate Q_i of component i and a well injectivity index WI_k for each connection. The components that may be injected are water, natural gas, and solvent. The injection rate for each connection is then allocated using the following formulas.

Component $\{i = w, g, 1, \ldots, N_s\}$ Injection Pressure Differential:

$$\Delta P_{wk} = \frac{Q_i}{\sum_{k=1}^{K} \frac{WI_k}{B_{ik}^n} \left\{ \left(\lambda_o^e\right)_k^n + \left(\lambda_w^e\right)_k^n + \left(\lambda_g^e\right)_k^n + \sum_{i=1}^{N_s} \left(\lambda_l^e\right)_k^n \right\}} \tag{10.33}$$

Component $\{i = w, g, 1, \ldots, N_s\}$ Injection Rate:

$$Q_{ik} = \frac{WI_k \Delta P_{wk}}{B_{ik}^n} \left[\left(\lambda_o^e\right)_k^n + \left(\lambda_w^e\right)_k^n + \left(\lambda_g^e\right)_k^n + \sum_{i=1}^{N_s} \left(\lambda_l^e\right)_k^n \right] \tag{10.34}$$

Allocation of injection fluids is based on total mobilities.

10.5.3 Explicit Pressure Constraint Representation

In the explicit pressure constraint representation, pressure differentials are used to calculate flow rates for injectors or producers.

Case 1: Explicit Pressure Constrained Well

The pressure differential for explicit pressure specified wells is given by

$$\Delta P_{wk} = [P^n - P_{wb}]_k \tag{10.35}$$

where $\Delta P_{wk} > 0$ for producers and $\Delta P_{wk} < 0$ for injectors. Rates for production wells are calculated using Eqs. (10.29) through (10.31). Rates for injection wells are calculated using Eq. (10.34).

Case 2: Gas Production Well

The laminar-inertial-turbulent (LIT) method may be used to represent a gas production well. The LIT method entails fitting gas well test data to the equation

$$\Delta\psi = aQ_g + bQ_g^2 = \psi_R - \psi_{wf} \tag{10.36}$$

where

ψ_R = pseudopressure corresponding to shut-in pressure P_R (psia^2/ cp)

ψ_{wf} = pseudopressure corresponding to a specified well flowing pressure P_{wf} (psia^2/cp)

aQ_g = laminar flow

bQ_g^2 = inertial and turbulent flow

IFLO employs user specified values of a, b, P_{wf}, and a table of pseudopressure versus pressure values to compute the total gas well production rate as

$$Q_{ok} = \frac{-a + \sqrt{a^2 + 4b\Delta\psi}}{2b} \tag{10.37}$$

where ψ_R is the pseudopressure corresponding to the nodal pressure P^n. Rates for each phase in connection k are computed using productivity index and mobility allocation.

10.5.4 Implicit Pressure Constraint Representation

In the implicit pressure constraint representation, pressure differentials are used to calculate flow rates for injectors or producers. The pressure differential for explicit pressure specified wells is

$$\Delta P_{wk} = [P^{n+1} - p_{wb}]_k \tag{10.38}$$

where $\Delta P_{wk} > 0$ for producers and $\Delta P_{wk} < 0$ for injectors. The implicit pressure constraint representation differs from the explicit pressure representation by the use of the pressure P^{n+1} for the future time. This pressure must be included in the matrix equations that are solved implicitly for pressure. When P^{n+1} is known, rates for production wells are calculated using Eqs. (10.29) through (10.31), and rates for injection wells are calculated using Eq. (10.34).

10.5.5 Gas-Oil Ratio and Water-Oil Ratio Constraints

Maximum gas-oil ratio (GOR_{max}) and maximum water-oil ratio (WOR_{max}) can be entered by the user for each oil production well. The gas-oil ratio (GOR) for a well is defined as total gas production for all active well completion intervals during the timestep divided by total oil production for all active well completion intervals during the timestep. If GOR for the well exceeds GOR_{max}, then the completion interval (connection) with the highest GOR will be shut in. The procedure is repeated until GOR is less than GOR_{max} or until the well is shut in.

The water-oil ratio (WOR) is defined as total water production for all active well completion intervals during the timestep divided by total oil production for all active well completion intervals during the timestep. If WOR for the well exceeds WOR_{max}, then the completion interval (connection) with the highest WOR will be shut in. The procedure is repeated until WOR is less than WOR_{max} or until the well is shut in.

10.5.6 Fluid Withdrawal Constraints

Fluid withdrawal from explicit pressure controlled production wells can be constrained for primary phases as follows:

A. A minimum production rate QWMIN can be specified.

B. A maximum production rate QWMAX can be specified.

Primary phases subject to fluid production constraints are oil, water, natural gas, and total fluid.

A positive value of QWMIN for a pressure controlled production well is used as the minimum allowed production rate. If the calculated primary phase production rate drops below the minimum allowed value, the well is shut in.

A positive value of QWMAX for a pressure controlled production well is used as the maximum allowed primary phase production rate. If the calculated primary phase production rate exceeds the maximum allowed value, calculated production will be reduced to the allowed value. Production from each connection is proportionally reduced by the ratio of allowed to calculated primary phase production rates.

10.5.7 Fluid Injection Constraints

Fluid injection using explicit pressure controlled injection wells can be constrained for primary phases as follows:

A. A minimum injection rate QWMIN can be specified.

B. A maximum injection rate QWMAX can be specified.

Primary phases subject to fluid injection constraints are water and natural gas.

A negative value of QWMIN for a pressure controlled injection well is used as the minimum allowed injection rate. If the absolute value of the calculated primary phase injection rate drops below the absolute value of the minimum allowed injection rate, the well is shut in.

A negative value of QWMAX for a pressure controlled injection well is used as the maximum allowed primary phase injection rate. If the absolute value of the calculated primary phase injection rate exceeds the absolute value of the maximum allowed injection rate, calculated injection will be reduced to the allowed value. Injection from each connection is proportionally reduced by the ratio of the absolute values of allowed to calculated injection rates.

10.6 IFLO Application: Throughput in a Naturally Fractured Reservoir Model

Simulator users need to understand the formulation of their simulators for very practical reasons. One of the most important reasons is the dependence of maximum allowed timestep size on simulator formulation. In particular, the numerical stability of a simulator depends on the formulation of the simulator and the maximum timestep size selected by the user. The maximum timestep size controls the volume of fluid that can pass through a gridblock in a timestep. Throughput in a timestep depends on the pore volume of the smallest gridblock in the model that is subjected to fluid flow. An estimate of throughput is obtained by calculating pore volume divided by flow rate. A flow simulator with a fully implicit formulation can function properly with timestep sizes corresponding to several pore volumes of throughput per timestep. By contrast, a flow simulator with an IMPES formulation should have a maximum timestep size $\Delta t_{\max}$ that represents approximately 10% pore volume throughput in the smallest gridblock; thus

$$\Delta t_{\max} = \left(0.10 V_P\right)/Q \tag{10.39}$$

where V_P is pore volume and Q is flow rate. Table 10-2 illustrates the importance of throughput on timestep size and presents the calculation of throughput for a naturally fractured reservoir model (data file XS_FRACTURE.DAT).

Table 10-2
IMPES Throughput Calculation

Variable	Fracture		Matrix	
DX	200	ft	200	ft
DY	600	ft	600	ft
Net Thickness	1	ft	47	ft

Porosity	0.01		0.25	
10% Pore Volume	21.4	RB	25100	RB
Flow Rate	100	STB/D	100	STB/D
Oil FVF	1.47	RB/STB	1.47	RB/STB
Δt_{max}	0.3	days	369	days

According to the data presented in Table 10-2, the maximum timestep size calculated from Eq. (10.39) for a fracture gridblock is much smaller than the maximum timestep size calculated for a matrix gridblock. This is typical of naturally fractured reservoir models. One of the motivations for developing fully implicit flow models was to devise a formulation that did not have the maximum timestep size limitation associated with the IMPES formulation.

The value of Δt_{max} for the fracture gridblock is the value that should be used in the flow model. If a value of Δt_{max} greater than the fracture Δt_{max} is used in the flow model, the model can experience numerical difficulties such as oscillations in flow rates or unacceptable material balance errors. The result of using Δt_{max} = 3 days in XS_FRACTURE.DAT leads to the numerical oscillations in water production rate shown in Figure 10-3. This figure should be compared with Figure 6-7, which is the result of using Δt_{max} = .03 days. The rate spike in the first 50 days of Figure 10-3 is an example of model instability, and the abrupt fluctuations in rate shown throughout the simulation period are examples of numerical oscillations. If Δt_{max} in the model is less than fracture Δt_{max}, the rate fluctuations in Figure 10-3 will disappear (see Figure 6-7).

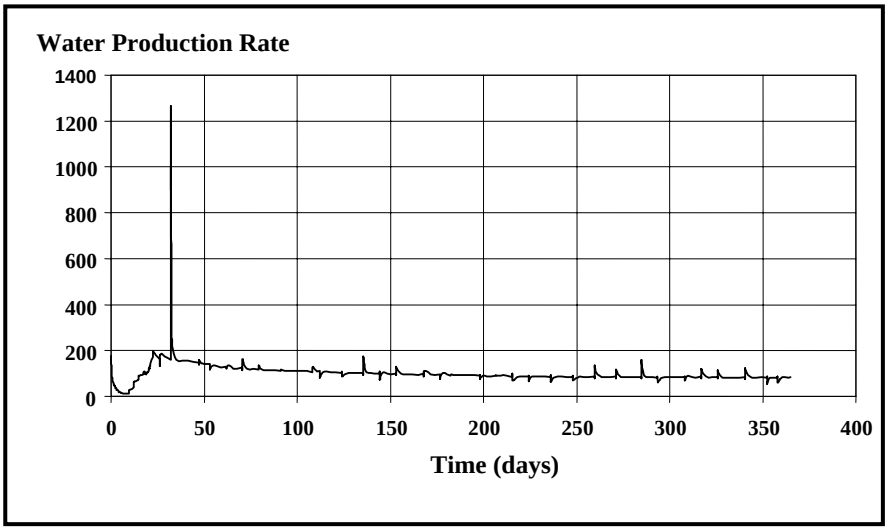

Figure 10-3. Example of Numerical Oscillations

Exercises

Exercise 10.1 Reorder the following steps for a Typical Simulator Flowchart. Note: Disregard any iterative looping in the ordering process.

A. Calculate Flow Coefficients	Step 1.
B. Create Output Files	Step 2.
C. Initialize	Step 3.
D. Solve Node Unknowns	Step 4.
E. Read Rates	Step 5.
F. Update Physical Properties	Step 6.
G. Read Input	Step 7.

Exercise 10.2 Data file EXAM3.DAT can be used to study the numerical dispersion associated with a Buckley-Leverett type waterflood of an undersaturated oil reservoir. Run EXAM3.DAT with constant timesteps of 5 days, 10 days, and 15 days. Plot water saturation (vertical axis) versus *x*-direction gridblock index I (horizontal axis) at 365 days. Note: you

will have to change the time reports are written to a single report at 365 days and set the maximum time of the run to 365 days.

Exercise 10.3 File GOM_UNCONSOLIDATED.DAT represents oil production from a reservoir with properties analogous to an unconsolidated formation in the Gulf of Mexico. For comparison, data file GOM_UNCONSOLIDATED_TRANS.DAT allows permeability and cross-sectional area in the transmissibility calculation to change as pressure and saturation change. Run both files and make the following plots: pore volume weighted average reservoir pressure versus time; oil production rate versus time; cumulative oil production versus time; water production rate versus time; and cumulative water production versus time. Where do the greatest differences appear?

Exercise 10.4 List at least two differences between IMPES and the fully implicit technique.

Exercise 10.5 Data file VFILL3_WF.DAT illustrates the use of well controls in IFLO. Run VFILL3_WF.DAT and rerun it using an oil rate of 150 STBPD. How long do both models run?

Exercise 10.6 Data file EXAM9_LIT.DAT has a gas well under LIT control. Determine the effect of doubling the turbulence factor on reservoir pressure, gas production rate from layers 1 and 2, and water production rate from layer 2 for the LIT controlled gas well.

Exercise 10.7A Suppose gridblock length is 100 ft, velocity of frontal advance is 0.5 ft/day, porosity is 0.2, and timestep size is 30 days. Use Lantz's expression for numerical dispersion to calculate numerical dispersion for both IMPES and fully implicit reservoir simulator formulations.

Exercise 10.7B If water is displacing oil, will water breakthrough occur sooner in an IMPES or a fully implicit model based on the data given above? Why?

Exercise 10.8 Place the wells in the 9 × 9 grid below using the following well data:

Well	**I**	**J**	**Depth (ft)**
W1	3	2	1200
W2	7	3	1220
W3	2	6	1180
W4	6	8	1190

	I:1	2	3	4	5	6	7	8	9
J:1									
2									
3									
4									
5									
6									
7									
8									
9									

Exercise 10.9A Data file XS_FRACTURE.DAT is a model of a naturally fractured reservoir. Most of the flow in this model is through the fractures. Run XS_FRACTURE.DAT and report the cumulative material balance errors for oil, water and gas at the end of the run.

Exercise 10.9B Multiply the maximum timestep in data file XS_FRACTURE.DAT by a factor of ten and run the revised data file. Verify Figure 10-3 and report the cumulative material balance errors for oil, water and gas at the end of the run. Compare the material balance errors from Part B with the material balance errors found in Part A and explain your results.

Chapter 11

Overview of the Modeling Process

The best technology for making reservoir performance predictions today is to model fluid flow in porous media using reservoir flow simulators. The reservoir management process and the systems involved in reservoir modeling are outlined here.

11.1 Prerequisites

Several prerequisites should be satisfied before a model study is undertaken [Coats, 1969]. The most important, from a business perspective, is establishing that the problem has economic importance. At the very least, the objectives of a model study should yield a solution to the economically important problem.

Once the objectives of a study are specified, the modeling team should gather all available data and reports relating to the field. Reservoir characterization and reservoir engineering evaluations are usually performed as standard business practice. Some of the tasks associated with basic reservoir analysis are described in Chapter 2. They provide information that is needed to prepare input data for a simulation study. For example, material balance studies require the acquisition of fluid property data, field pressures, and production volumes. This information

is also needed to conduct a flow model study. Volumetric analyses provide independent appraisals of reservoir volume that can be used to check the original fluid volumes calculated by a reservoir flow model. In addition, basic reservoir analysis can provide an initial concept of the reservoir and associated drive mechanisms. These concepts can be used to design the model study. The modeling team needs to be aware of existing studies and should relate model performance to previous studies whenever possible.

If data that are needed for the flow model are not available, the modeling team should determine if the data can be obtained, either by analogy with other reservoirs or by correlation. Values for all model input data must be obtained because the simulator will not run without a complete set of data. In some cases, it may be necessary to make simplifying assumptions about the reservoir because there is not enough data available to represent the system in greater quantitative detail.

In addition to clearly defined objectives, another prerequisite that must be satisfied before committing to a simulation study is the determination that the objectives of the study cannot be achieved using simpler techniques. If less expensive techniques, such as decline curve analysis or the Buckley-Leverett waterflood displacement algorithm, do not provide adequate results, then more sophisticated and costly methods are justified.

11.2 Major Elements of a Reservoir Simulation Study

The essential elements of a simulation study include matching field history; making predictions, including a forecast based on the existing operating strategy; and evaluating alternative operating scenarios [see, for example, Carlson, 2003; and Ertekin, et al., 2001]. We assume that a decision has been made to conduct a reservoir simulation study and that all relevant data has been acquired. The first phase of the reservoir simulation study is the history matching phase.

History matching is an iterative process that makes it possible to integrate reservoir geoscience and engineering data. History matching is also referred to as model calibration in the literature [Aziz, et al., 2002] because the modeling team should verify and refine the reservoir description during the history match, or model calibration, process. Starting with an initial reservoir description, the model is used to match and predict reservoir performance. If necessary, the modeling team will modify the reservoir description until an acceptable match is obtained.

The history matching process may be considered an inverse problem because an answer already exists. We know how the reservoir performed; we want to understand why. Our task is to find the set of reservoir parameters that minimizes the difference between the model performance and the historical performance of the field. This is a non-unique problem since there is usually more than one way to match the available data.

Once a match of historical data is available, the next step is to make a base case prediction, which is essentially just a continuation of existing operating practice. The base case prediction gives a baseline for comparison with other reservoir management strategies.

Model users should be aware of the validity of model predictions. One way to get an idea of the accuracy of predictions is to measure the success of forecasts made in the past. Lynch [1996] looked at the evolution of the United States Department of Energy price forecast over a period of several years for both oil and gas. Lynch's study showed that there is considerable uncertainty associated with the price forecast. The variation in oil price by a factor of two in the late 1990's illustrates the volatility of economic factors that are needed in cash flow forecasts.

In addition to uncertainty in economic parameters, there is uncertainty in the forecasted production performance of a field. Forecasts do not account for discontinuities in historical patterns that arise from unexpected effects. This is as true in the physical world as it is in the social [Oreskes, et al., 1994]. Simulators do not eliminate uncertainty; they give us the ability to assess and better manage the risk associated with the prediction of production performance.

A valuable but intangible benefit of the process associated with reservoir simulation is the help it provides in managing the reservoir. One of the critical tasks of reservoir management is the acquisition and maintenance of an up-to-date data base. A simulation study can help coordinate activities as a modeling team gathers the resources it needs to determine the optimum plan for operating a field. Collecting input data for a model is a good way to ensure that every important technical variable is considered as data is collected from the many disciplines that contribute to reservoir management. If model performance is especially sensitive to a particular parameter, then a plan should be made to determine that parameter more accurately, for example, from either laboratory or appropriate field tests.

11.3 Reservoir Management Modeling System

A comprehensive reservoir management modeling system can be thought of as four interacting subsystems: the reservoir model, the well model, the wellbore model, and the surface model. Figure 11-1 illustrates the spatial relationship between these models.

Every practical reservoir simulator includes both a reservoir model and a well model. The reservoir model represents fluid flow within the reservoir. The well model is a term in the fluid flow equations that represents the extraction of fluids from the reservoir or the injection of fluids into the reservoir. Full featured commercial simulators also include a wellbore model and a surface facility model. The wellbore model represents flow from the sandface to the surface. The surface model represents constraints associated with surface facilities, such as platform and separator limitations.

The mathematical algorithms associated with each model depend on physical conservation laws and empirical relationships. Computer simulators are based on conservation of mass, momentum, and energy. The most widely used simulators assume the reservoir is isothermal, that is, maintains a constant temperature. If we are modeling a reservoir

where thermal effects matter, such as in a secondary recovery process where heat has been injected in some form, then we need to use a simulator that accounts for temperature variation and associated thermodynamic effects. The set of algorithms is sufficiently complex that high speed computers are the only practical means of solving the mathematics associated with a reservoir simulation study.

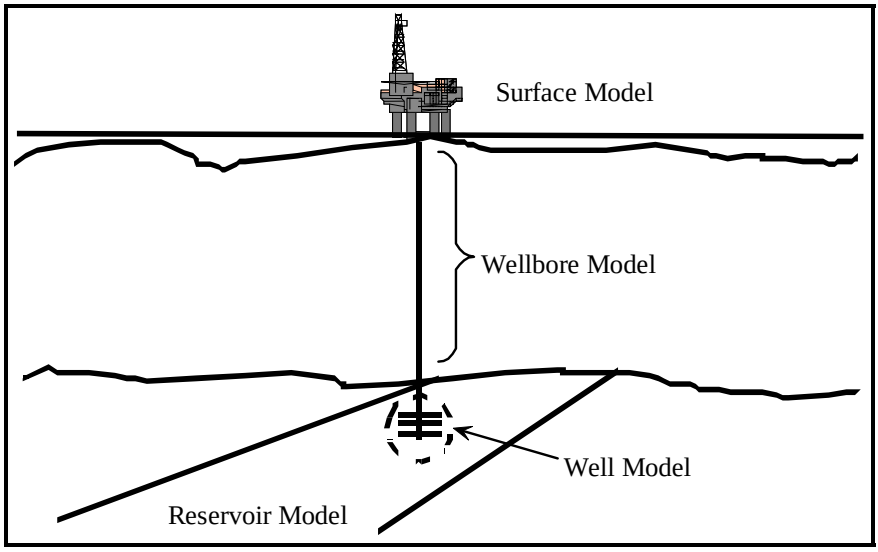

Figure 11-1. Reservoir Management Modeling System

11.3.1 Well and Facilities Modeling

Well and surface facility models are simplified representations of real equipment [for example, see Williamson and Chappelear, 1981; Ertekin, et al., 2001]. The well model, for example, does not account for flow in the wellbore from the reservoir to the surface. This effect can be taken into account by adding a wellbore model. The wellbore model usually consists of a multivariable table relating surface pressure to such parameters as flow rate and gas-oil ratio (GOR). The tables are often calculated using a separate program that performs a nodal analysis of wellbore flow. Well models typically assume that fluid phases are fully dispersed and that the gridblock containing the well is perforated

throughout its thickness. Some commercial simulators will let the user specify a perforation interval under certain conditions.

The different types of well controls include production and injection well controls, and group and field controls for a surface model. The production well model assumes the user specifies one option as the primary control, but may also specify other options as targets for constraining the primary control. For example, if oil rate is the primary control, then the produced GOR may be restricted so that the oil rate is decreased when GOR exceeds a specified value. This provides a more realistic representation of actual field practice.

Injection well controls assume that initial injection well mobility is given by total gridblock mobility. This makes it possible to inject a phase into a gridblock that would otherwise have zero relative permeability to flow.

Allocation of fluids in a well model depends on layer flow capacity and fluid mobility. Simulators can also describe deviated or horizontal wells depending on how the well completions and parameters are specified.

Well, group and field controls can be specified in commercial simulators with a surface facilities model. The user specifies a hierarchy of controls that most realistically represent how the field is being operated. For example, well production may be constrained by platform separator and storage capacity, which in turn is constrained by pipeline flow capacity. The ability to integrate reservoir and surface flow technology using a single simulator is an area of research that is receiving increasing attention [for example, see Heinemann, et al., 1998].

11.4 Wellbore Modeling

The well model may be coupled to a wellbore model to more accurately account for fluid flow in pipes. Figure 11-2 illustrates the system of interest. The purpose of this section is to discuss the coupling of well models with wellbore models. We begin with a description of the physical phenomena, and then discuss simulation technology.

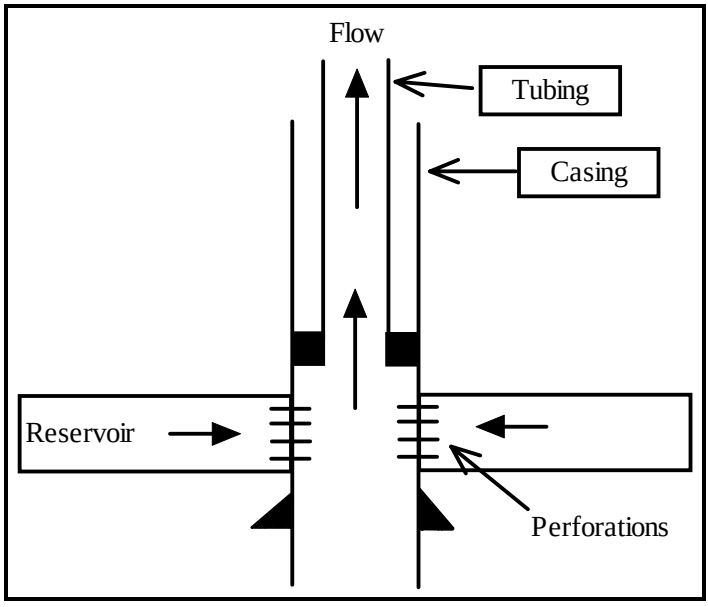

Figure 11-2. Wellbore-Reservoir Coupling

11.4.1 Single Phase Flow in Pipes

Fluid flow in pipes can range from laminar to turbulent flow. Fluid does not move transverse to the direction of bulk flow in laminar fluid flow. By contrast, the velocity components of fluid flow fluctuate in all directions relative to the direction of bulk flow when fluid flow is turbulent. For a fluid with a given density and dynamic viscosity flowing in a tube of fixed diameter, the flow regime is laminar at low flow velocities and turbulent at high flow velocities. One parameter that is often used to characterize fluid flow is Reynolds number N_{Re}.

Reynolds number expresses the ratio of inertial (or momentum) forces to viscous forces. For fluid flow in a conduit, the Reynolds number is

$$N_{\mathrm{Re}} = \frac{\rho v D}{\mu} \tag{11.1}$$

where ρ is fluid density, v is bulk flow velocity, D is tube diameter for flow in a tube, and μ is the dynamic viscosity of the fluid. The choice of

units must yield a dimensionless Reynolds number. In *System Internationale* (SI) units, a dimensionless Reynolds number is obtained if fluid density is in kg/m^3, flow velocity is in m/s, tube diameter is in m, and dynamic viscosity is in Pa·s. Note that 1 cp = 1 mPa·s = 10^3 Pa·s.

We introduce the factors that influence fluid flow in pipe by considering the relatively simple case of single-phase flow in circular pipes [Beggs, 1991; Brill and Mukherjee, 1999]. Laminar flow along the longitudinal axis of a circular pipe is transverse to the cross-sectional area of the pipe. The cross-sectional area A of a circular pipe with internal radius r and internal diameter D is

$$A = \pi r^2 = \pi\left(\frac{D}{2}\right)^2 \tag{11.2}$$

The bulk flow velocity v of a single-phase fluid flowing in the circular pipe is related to volumetric flow rate q by

$$v = \frac{q}{A} = \frac{4q}{\pi D^2} \tag{11.3}$$

The Reynolds number for flow in a circular pipe can be written in terms of volumetric flow rate by substituting Equation (11.3) into (11.1) to give

$$N_{\mathrm{Re}} = \frac{\rho v D}{\mu} = \frac{4\rho q}{\pi \mu D} \tag{11.4}$$

where ρ is fluid density and μ is the dynamic viscosity of the fluid. Fluid flow in circular pipes is laminar if $N_{\mathrm{Re}} < 2000$, and it is considered turbulent at larger values of the Reynolds number.

The relationship between fluid flow velocity and pressure change along the longitudinal axis of the circular pipe is obtained by performing an energy balance calculation. Figure 11-3 shows the geometry of an inclined circular pipe with length L along the longitudinal axis and angle of inclination θ. The single-phase fluid has density ρ and dynamic viscosity μ. It is flowing in a gravity field with acceleration g.

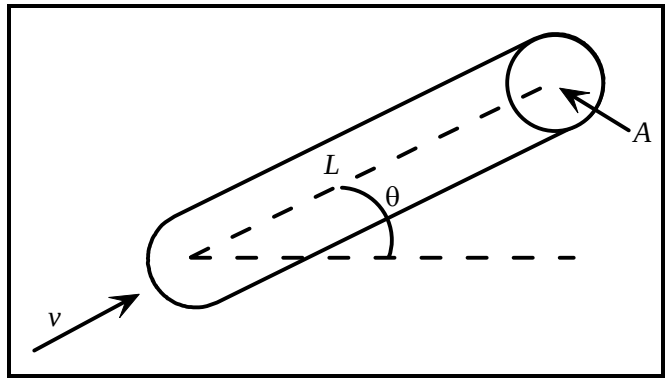

Figure 11-3. Flow in an Inclined Circular Pipe

We make two simplifying assumptions in our analysis that allow us to minimize external factors and consider only mechanical energy terms. We assume that no heat energy is added to the fluid, and that no work is done on the system by its surroundings, e.g. no mechanical devices such as pumps or compressors are adding energy to the system. An energy balance with these assumptions yields the pressure gradient equation

$$\frac{dP}{dL} = \left[\frac{dP}{dL}\right]_{PE} + \left[\frac{dP}{dL}\right]_{KE} + \left[\frac{dP}{dL}\right]_{fric} \tag{11.5}$$

where P is pressure. We have written the pressure gradient along the longitudinal axis of the pipe as the sum of a potential energy term

$$\left[\frac{dP}{dL}\right]_{PE} = \rho g \sin\theta \tag{11.6}$$

a kinetic energy term

$$\left[\frac{dP}{dL}\right]_{KE} = \rho v \frac{dv}{dL} \tag{11.7}$$

and a friction term

$$\left[\frac{dP}{dL}\right]_{fric} = f\,\frac{\rho v^2}{2D} \tag{11.8}$$

that depends on a dimensionless friction factor *f*. If the flow velocity of the fluid does not change appreciably in the pipe, the kinetic energy term can be neglected and the pressure gradient equation reduces to the simpler form

$$\frac{dP}{dL} \approx \rho\, g \sin\theta + f\,\frac{\rho v^2}{2D} \tag{11.9}$$

Equation (11.9) is valid for single-phase, incompressible fluid flow. If we further assume that the right hand side is constant over the length *L* of the pipe, Equation (11.9) can be integrated to give the pressure change

$$\Delta P \approx \rho\, g\, L \sin\theta + f\,\frac{\rho v^2}{2D} L \tag{11.10}$$

The friction factor *f* depends on flow regime. For laminar flow with Reynolds number $N_{\mathrm{Re}} < 2000$, the friction factor is inversely proportional to Reynolds number:

$$f = 16 / N_{\mathrm{Re}} \tag{11.11}$$

For turbulent flow, the friction factor depends on Reynolds number and pipe roughness. Pipe roughness can be quantified in terms of relative roughness ζ which is a fraction defined relative to the inner diameter of the pipe as

$$\zeta = \ell_p / D < 1 \tag{11.12}$$

The length ℓ_p is the length of a protrusion from the pipe wall. Typical values of pipe relative roughness ζ range from 0.0001 (smooth) to 0.05 (rough). The length of protrusions inside the pipe may change during the period that the pipe is in service. For example, buildup of scale or pipe wall corrosion can change the relative roughness of the pipe. An estimate of friction factor for turbulent flow is [Beggs, 1991, page 61]

$$\frac{1}{\sqrt{f}} = 1.14 - 2\log\left[\zeta + \frac{21.25}{N_{\mathrm{Re}}^{0.9}}\right] \tag{11.13}$$

11.4.2 Multiphase Flow in Pipes

The description of single phase fluid flow in pipes presented above is relatively straightforward compared to multiphase flow. In particular, two-phase flow is characterized by the presence of flow regimes or flow patterns [see, for example, Griffith, 1984; Brill, 1987; Brill and Arirachakaran, 1992; Brill and Mukherjee, 1999; Lea, et al., 2003]. The flow pattern represents the physical distribution of gas and liquid phases in the flow conduit. Forces that influence the distribution of phases include buoyancy, turbulence, inertia and surface tension. The relative magnitude of these forces depends on flow rate, the diameter of the conduit, its inclination, and the fluid properties of the flowing phases.

Flow regimes for vertical flow are usually represented by four flow regimes [Brill, 1987; and Brill and Mukherjee, 1999]: bubble flow, slug flow, churn flow, and annular flow. Churn flow and annular flow are referred to as slug-annular transition and annular-mist flow respectively by Lea, et al. [2003]. Figure 11-4 illustrates the four flow regimes. Bubble flow is the movement of gas bubbles in a continuous liquid phase. Slug flow is the movement of slug units; each slug unit consists of a gas pocket, a film of liquid surrounding the gas pocket that is moving downward relative to the gas pocket, and a liquid slug with distributed gas bubbles between two gas pockets. Churn flow is the chaotic movement of distorted gas pockets and liquid slugs. Annular flow is the upward movement of a continuous gas phase in the center of the conduit with an annular film of liquid flowing upward between the central gas phase and the wall of the conduit, and with dispersed liquid droplets being lifted by the gas phase.

Following Beggs and Brill [1973], Brill and Mukherjee [1999] represent multiphase flow in horizontal conduits using the seven flow regimes shown in Figure 11-5. These flow regimes are not universally

accepted. For example, Brill and Arirachakaran [1992] used a similar set of flow regimes that were organized in terms of stratified flow, intermittent flow, annular flow, and dispersed bubble flow. More recently, Petalas and Aziz [2000] used the following set of flow regimes to represent multiphase flow in pipes: dispersed bubble flow, stratified flow, annular-mist flow, bubble flow, intermittent flow, and froth flow. Froth flow was described as a transition zone between dispersed bubble flow and annular-mist flow, and between annular-mist flow and slug flow.

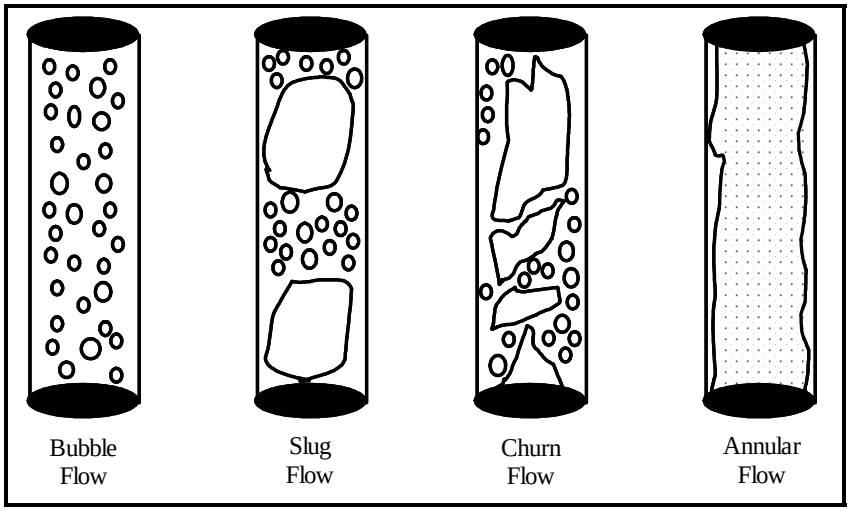

Figure 11-4. Flow regimes for vertical, two-phase flow (adapted from Brill and Mukherjee [1999, Figure 4.21 and AIChE])

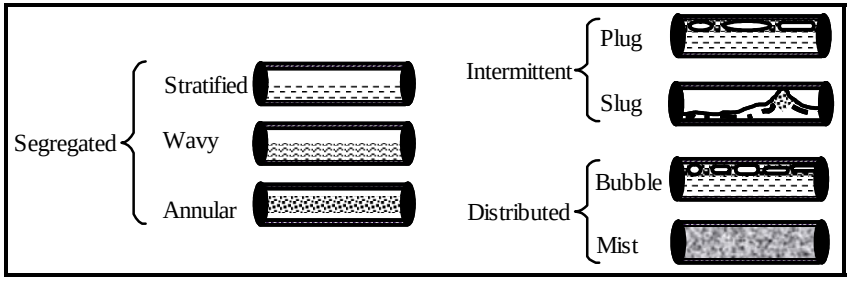

Figure 11-5. Flow regimes for horizontal, two-phase flow (adapted from Brill and Mukherjee [1999, Figure 4.16])

11.4.3 Modeling Multiphase Flow in Pipes

The identification of qualitative flow regimes discussed above influences the structure of analytical and numerical models used to quantify multiphase flow in conduits. The flow regimes are used to construct flow regime maps, also called flow pattern maps, which are log-log plots of superficial gas velocity versus superficial liquid velocity. Figure 11-6 illustrates a flow pattern map.

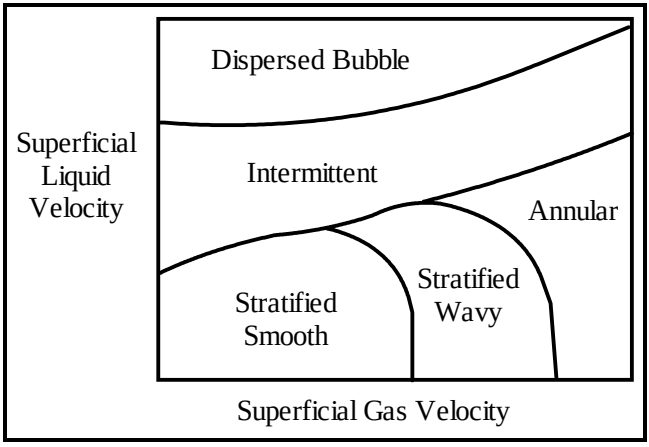

Figure 11-6. Illustration of a flow pattern map (adapted from Brill and Arirachakaran [1992, Figure 2])

Historically, predictions of multiphase flow in pipes began in the 1950's when investigators used data from laboratory test facilities and, to a lesser extent, field data to prepare empirical flow pattern maps [Brill, 1987; Brill and Arirachakaran, 1992]. Early models of multiphase flow were extrapolations of single phase flow models. Single phase terms in the pressure gradient equation introduced above were replaced with mixture variables. Thus, the terms in the pressure gradient equation for single phase flow given by Equation (11.5) become

$$\left[\frac{dP}{dL}\right]_{PE} = \rho_m \, g \, \sin\theta \tag{11.14}$$

for potential energy,

$$\left[\frac{dP}{dL}\right]_{KE} = \rho_m v_m \frac{dv_m}{dL} \tag{11.15}$$

for kinetic energy, and

$$\left[\frac{dP}{dL}\right]_{fric} = f \frac{\rho_m v_m^2}{2D} \tag{11.16}$$

for friction. The subscript *m* attached to variables on the right hand side of Equations (11.14) through (11.16) denotes that the associated variable is calculated for a mixture. Early models tended to neglect the kinetic energy term because the degree of turbulence of flow in wells at the time provided enough mixing of multiphase fluids to let the fluids be treated as homogeneous mixtures with gas and liquid phases moving at comparable velocities. Models based on mixture variables are called homogeneous models.

Decline in the productivity of wells led to the need for more accurate multiphase flow models to represent phenomena such as gas slippage. In addition to homogeneous models, two other approaches are often used: empirical correlations, and mechanistic models. Empirical correlations depend on fitting experimental data and field data to models that contain groups of physical parameters. The empirical correlations approach can yield useful and accurate results quickly, but does not provide a scientific basis for extrapolation to significantly different systems. By contrast, mechanistic models are based on physical mechanisms that describe all significant flow mechanisms. Modern mechanistic modeling still requires some empiricism to determine poorly known or difficult to measure parameters [Brill and Mukherjee, 1999].

Shi, et al. [2003] observed that mechanistic models are the most accurate models, but are not well suited because they can exhibit discontinuities in pressure drop and holdup at the transition between some flow patterns. One way to solve this problem is to use a drift-flux model. The basic drift-flux model was introduced by Zuber and Findlay [1965]. Drift-flux models are modifications of the homogeneous models described above. From the perspective of reservoir simulation, homogeneous models have the advantage that they are relatively simple,

continuous, and differentiable. A significant disadvantage of homogeneous models is that they do not account for slip between fluid phases. Drift-flux models are designed to resolve this deficiency, as well as model countercurrent flow. Countercurrent flow is the movement of heavy and light phases in opposite directions when there is no net fluid flow in the conduit or the fluid flow is slow.

11.4.4 Liquid Loading

Gas wells often produce varying amounts of water depending on reservoir performance and production operations. For example, high flow rate gas wells are able to carry liquids to the surface. If the gas rate decreases due to reservoir pressure depletion, or the volume of liquid entering the wellbore increases relative to the volume of gas, all of the liquid in the wellbore will not be produced and will begin to accumulate in the base of the well. As another example, gas production from water-drive gas reservoirs can result in water coning and liquid accumulation in the wellbore. The accumulation of liquids in the wellbore is called liquid loading.

Liquid loading adversely affects gas well productivity because it results in an increase in flowing bottomhole pressure and an eventual decrease in gas rate. Turner, et al. [1969] conducted one of the first and most extensive investigations to determine the minimum gas rate that would provide continuous removal of liquids. If enough liquid accumulates in the wellbore, the well may be unable to flow and productivity will be completely lost.

Removal of water and hydrocarbon liquids from gas wells is increasingly recognized as an important topic for maintaining gas well productivity. Several techniques have been developed to deliquify gas wells. Lea, et al. [2003], and Lea and Nickens [2004] discuss several deliquification techniques. These techniques include management of well flow rate, reducing the size of tubing, installing downhole pumps such as electric submersible pumps, installing downhole separators, installing surface pumps, implementing plunger lift, and so forth.

11.5 Wellbore-Reservoir Coupling

The above discussion has focused on multiphase flow in wells. The multiphase flow models represent outflow to the surface from the wellbore-reservoir system shown in Figure 11-2. We must also consider inflow into the wellbore from the reservoir.

Wellbore inflow represents fluid flow from the reservoir into the wellbore. Reservoir fluid flow may be modeled using either analytical methods or numerical methods. Analytical methods rely on models of inflow performance relationships (IPR) that were first proposed by Gilbert [1954]. An IPR is the functional relationship between reservoir production rate and bottomhole flowing pressure. Darcy's Law is a simple example of an IPR for single phase liquid flow. The gas well backpressure equation is an example of an IPR for single phase gas flow. Vogel [1968] introduced an IPR for the oil rate from a two-phase reservoir. Vogel's IPR depended on absolute open flow potential, which is the flow rate that is obtained when the bottomhole flowing pressure is equal to atmospheric pressure. Fetkovich [1973] proposed a variation of Vogel's model that does a better job of matching field data from producing oil and gas wells. Joshi [1988] proposed an IPR for horizontal wells.

Figure 11-7 illustrates the relationship between an IPR curve and a Tubing Performance Curve (TPC).

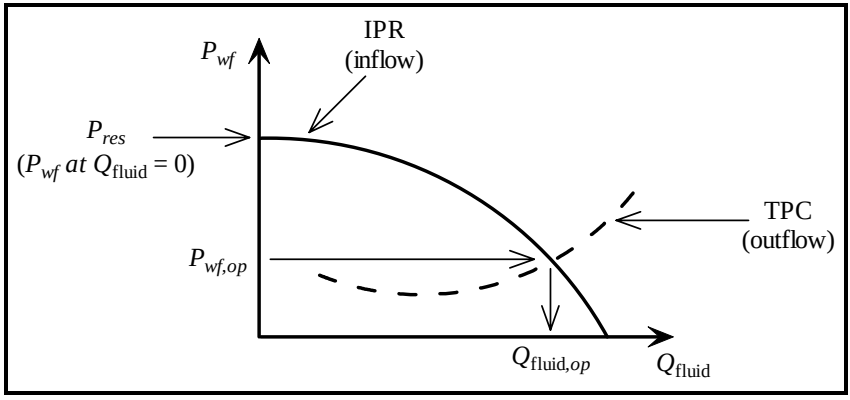

Figure 11-7. Illustration of an IPR versus TPC Plot

The IPR versus TPC plot is a plot of fluid flow rate Q_{fluid} versus bottomhole flowing pressure P_{wf}. Reservoir pressure P_{res} is the pressure at $Q_{fluid} = 0$. The intersection of the IPR and TPC curves identifies the flow rate and bottomhole flowing pressure that simultaneously satisfy inflow into the wellbore from the reservoir and outflow from the wellbore.

The IPRs described above are examples of analytical representations of fluid flow into a wellbore. Another way to calculate inflow into a wellbore is reservoir simulation. Commercial reservoir simulators typically allow the user to specify tubing curves that relate surface pressure to bottomhole flowing pressure. Figure 11-8 illustrates a gridding scheme for a coupled wellbore-reservoir system. Williamson and Chappelear [1981] reviewed the traditional representation of wells in reservoir simulators. Ertekin, et al. [2001], Holmes [2001], and Mlacnik and Heinemann [2003] present more recent discussions of well models in reservoir simulators. Gridding schemes for modeling advanced wells are discussed by Mlacnik and Heinemann [2003], and Holmes [2001].

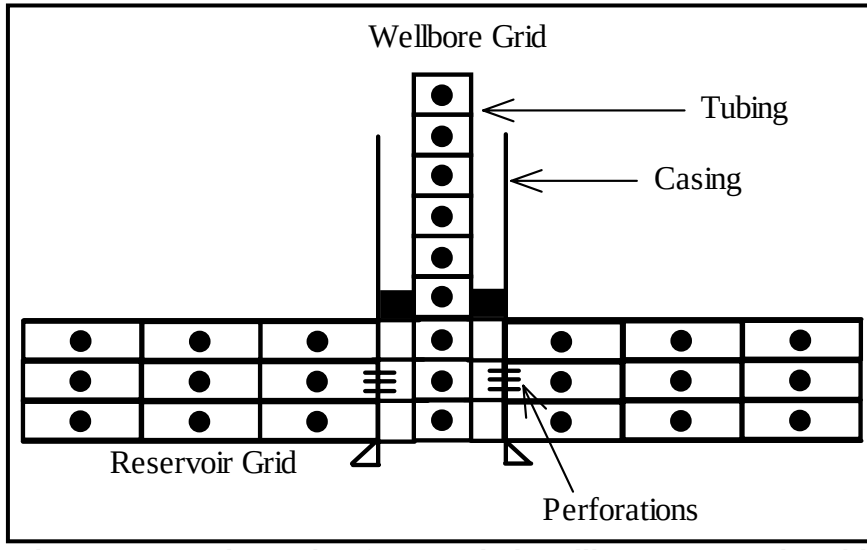

Figure 11-8. Schematic of a Coupled Wellbore-Reservoir Grid

Tubing curves in reservoir simulators allow the user to specify wellhead pressures and then calculate bottomhole flowing pressures. The

tubing curves are typically from empirical correlations, mechanistic models, or drift-flux models. Modelers have found that more sophisticated wellbore models are needed to represent time-dependent (transient) effects in the wellbore. Modern wellbore models are using partial differential equations based on conservation of mass and energy that must be solved numerically in much the same way as flow equations in reservoir simulators.

11.5.1 Industry Practice

The degree of coupling of the wellbore model to the reservoir simulator can be used to classify wellbore-reservoir simulators. The coupling may be sequential or implicit. Sequential coupling solves the wellbore model after the reservoir flow calculation is complete. Implicit coupling simultaneously solves the wellbore and reservoir models. Table 11-1 summarizes the modeling techniques that are commonly used to model wellbore-reservoir coupling.

Table 11-1
Summary of Wellbore-Reservoir Modeling Techniques

Technique	Comment
1	Sophisticated reservoir simulator with production tubing curves
2	Sophisticated wellbore simulator with inflow performance relationship
3	Coupled wellbore-reservoir simulator

Coupled wellbore-reservoir models have been used for a variety of applications. For example, Settari and Aziz [1974] used a coupled reservoir-wellbore simulator to study two-phase coning problems. Winterfeld [1989] introduced a formulation that rigorously coupled a reservoir model with a model of multiphase flow in a wellbore to evaluate pressure transient tests. Some simulators have been designed to couple wellbore and surface facility models to the reservoir model. For

example, Litvak and Darlow [1995] coupled a wellbore model to a compositional simulator that was later used to study the performance of Prudhoe Bay.

11.6 Reservoir-Aquifer Model

A reservoir-aquifer system can be modeled in flow models using two different techniques: as a numerical aquifer model, or as an analytic aquifer model. Each technique is discussed below.

11.6.1 Numerical Aquifer Model

A reservoir-aquifer system can be modeled using small gridblocks to define the reservoir and increasingly larger gridblocks to define the aquifer. This approach has the advantage of providing a numerically uniform analysis of the reservoir-aquifer system. The numerical aquifer model represents aquifer influx by extending the finite difference grid covering the reservoir to include the aquifer (Figure 11-9). Rock and fluid properties for the aquifer gridblocks must be defined. This approach has the disadvantage of requiring more computer storage and computing time because additional gridblocks are needed to model the aquifer. A more time- and cost-effective means of representing an aquifer is to represent aquifer influx with an analytic model.

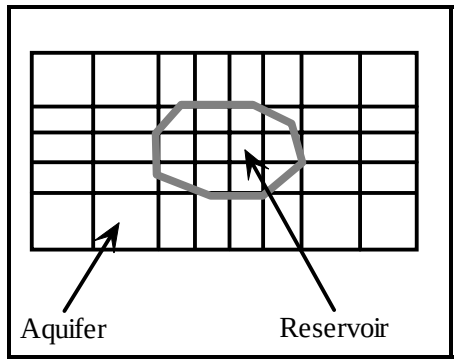

Figure 11-9. Flow Model Grid for Numerical Aquifer Model

11.6.2 Analytic Aquifer Model

Analytic aquifer models represent aquifer influx as a source/sink term in the fluid flow equations. Van Everdinger and Hurst [1949] introduced one of the first analytic aquifer models. Their model could account for unsteady-state aquifer influx into the reservoir using dimensional time and pressure. Carter-Tracy [1960] and Fanchi [1985] modified the van Everdingen-Hurst model to simplify its implementation in reservoir simulators. Fetkovitch [1971] introduced a widely used analytic aquifer model that can represent steady-state and unsteady-state aquifer influx for a variety of aquifer sizes and strengths. An example analytic aquifer model that is available in IFLO is the steady-state aquifer.

The steady-state aquifer model is based on the assumption that the aquifer influx rate q_{wss} is proportional to the pressure difference between the aquifer and the hydrocarbon reservoir. It is further assumed that the aquifer is sufficiently large that it experiences no net pressure change throughout the producing life of the reservoir. With these assumptions, the flow model computes steady-state aquifer influx into a specified gridblock as

$$q_{wss} = -\left[SSAQ \times \left(P^0 - P^n\right)\right]; \; SSAQ \geq 0 \qquad (11.17)$$

where P^n is the gridblock pressure at the present time level n; P^0 is the initial gridblock pressure; and SSAQ is the proportionality constant. The minus sign preceding the bracketed term indicates that water is entering the gridblock when $P^0 > P^n$.

Analytic aquifer models make it unnecessary to cover the entire aquifer with a finite difference grid. Instead, it is sufficient to assign the analytic aquifer to selected gridblocks adjacent to the reservoir. Figure 11-10 shows an analytic aquifer model assigned to gridblocks on the boundary of a reservoir. The modeler can minimize the number of gridblocks needed to represent the aquifer by using analytic aquifer models, but aquifer flow behavior may not include all of the physical effects that would be associated with the finite difference representation of the aquifer.

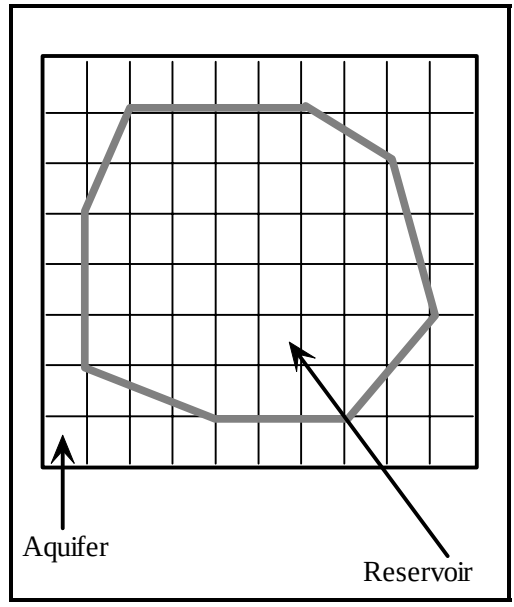

Figure 11-10. Flow Model Grid for Analytic Aquifer Model

Exercises

Exercise 11.1A Darcy's Law in radial coordinates is

$$Q = -0.001127 \frac{2\pi rhK}{\mu B} \frac{dP}{dr}$$

where permeability K is in md, radius r is in ft, net thickness h is in ft, pressure P is in psia, viscosity μ is in cp, formation volume factor B is in reservoir volume per surface volume, and flow rate Q is in STB/day. Treat the derivative as a differential and solve for dP.

Exercise 11.1B Integrate dP from pressure P at wellbore radius r_w to pressure P_e at drainage radius r_e.

Exercise 11.1C Rearrange to find productivity index $PI = Q / \Delta P$.

Exercise 11.1D Estimate the PI for a well in a reservoir that has 10 ft. of net pay, permeability of 50 md, oil with viscosity of 1.5 cp and formation

volume factor (FVF) of 1.4 RB/STB. Assume the wellbore radius is 0.3 ft. and the drainage radius is 500 ft.

Exercise 11.1E What pressure drawdown is required to produce 100 STB/day of oil?

Exercise 11.2 IFLO contains a few fieldwide controls. Data file EXAM4.DAT is a 2-D areal model of an undersaturated oil reservoir undergoing primary depletion. Modify data file EXAM4.DAT so that fieldwide pressure is not allowed to drop below the initial bubble point pressure using the run controls in Section 21.9. What effect does this have on the duration of the run?

Exercise 11.3A What is the difference between laminar and inertial flow?

Exercise 11.3B Does pipe roughness effect fluid flow in a circular pipe?

Exercise 11.4 The Reynold's number for flow in a circular pipe is 2500. Estimate the friction factor for turbulent flow assuming the pipe relative roughness is 0.01.

Exercise 11.5 Kinematic viscosity η in centistokes is related to dynamic viscosity μ in centipoises by the relationship $\eta = \mu/\rho$ where ρ is fluid density in g/cm^3. Suppose a fluid has density = 0.9 g/ cm^3 and dynamic viscosity = 1.05 cp. What is its kinematic viscosity (in centistokes)?

Exercise 11.6A Suppose water is flowing through a circular pipe with volumetric flow rate q = 1000 barrels/day. The water density is ρ = 1 g/ cm^3 = 1000 kg/m^3 and the dynamic viscosity of water is μ = 1 cp = 0.001 Pa·s. The pipe length is 8000 ft and has a 5-inch inner diameter. The relative roughness of the pipe wall is 0.000144. What is the flow regime of the flowing water? Hint: calculate Reynolds number for flow.

Exercise 11.6B What is the friction factor?

Exercise 11.6C Plot pressure gradient dP/dL versus inclination angle θ. Use 10° increments for the inclination angle in the range $-90° \le \theta \le 90°$. Express dP/dL in SI units and θ in degrees.

Exercise 11.6D What is the pressure gradient dP/dL at $\theta = 90°$? Express your answer in psi/ft.

Exercise 11.7 The pressure in a column of water is 1000 psia at a depth of 2300 ft. What is the pressure at a depth of 2200 ft. Assume the density of water is 1 g/cc, the acceleration of gravity is 9.8 m/s^2. Express your answer in psia and kPa.

Exercise 11.8A Data file EXAM8A.DAT is a 3-D model of a gas reservoir undergoing primary depletion. Run EXAM8A.DAT and report the duration of the run. What are the average reservoir pressure, gas rate, water rate, aquifer influx rate and cumulative aquifer influx at the end of the run? Hint: look in ITEMP.TSS or ITEMP.ROF.

Exercise 11.8B Data file EXAM8B.DAT is the same as file EXAM8A.DAT except that an analytic aquifer has been added. Run EXAM8B.DAT and report the duration of the run. What are the average reservoir pressure, gas rate, water rate, aquifer influx rate and cumulative aquifer influx at the end of the run? Explain the differences between Parts A and B.

Chapter 12

Conceptual Reservoir Scales

One of the most important goals of modeling is to reduce the risk associated with making decisions in an environment where knowledge is limited. The validity of data used in the decision-making process depends on the measurement technique used to obtain the data and the appropriate scale of applicability of the technique. Data validity provides information about risk. The integration of scale-dependent data into a cohesive reservoir description can reduce the risk of decision-making. This chapter introduces the concept of scale and discusses Giga Scale information.

12.1 Reservoir Sampling and Scales

We can obtain a sense of just how well we understand the reservoir by considering the fraction of reservoir area sampled by different techniques. As an example, suppose we want to find the size of the area sampled by a wellbore that has a 6-in. radius. If we assume the area is circular, we can calculate the area as πr^2 where r is the sampled radius. The area sampled by a 6-in. radius wellbore is less than a square foot. To determine the fraction of area sampled, we normalize the sampled area with respect to the drainage area of a well. If we assume the drainage area of the well is a modest five acres, the drainage area is 218,000 sq. ft. What fraction of the drainage area is directly sampled by the wellbore?

The fraction of the area sampled by the well is three to four parts in a million. This is a tiny fraction of the area of interest.

A well log signal will expand the area that is being sampled. Suppose a well log can penetrate the formation up to five feet from the wellbore, which is a reasonably generous assumption. The fraction of area that has been sampled is now approximately four parts in ten thousand. The sample size in a drainage area of five acres is still a fraction of a percent.

Core and well log data give a very limited view of the reservoir. A seismic section expands the fraction of area sampled, but the interpretation of seismic data is less precise. Seismic data is often viewed as "soft data" because of its dependence on interpretation. The reliability of seismic interpretation can be improved when correlated with "hard data" such as core and well log measurements.

The range of applicability of measured data depends on the sampling technique. Did we take some core out of the ground, measure an electrical response from a well log, or detect acoustical energy? Figure 12-1 illustrates the ranges. Fayers and Hewett [1992] point out that scale definitions are not universally accepted, but do illustrate the relative scale associated with reservoir property measurements. Scale sizes range from the very big to the microscopic. Variations in the scale of data applicability can be distinguished by defining conceptual scales. Figure 12-2 illustrates the system of reservoir scales that is adopted for use in the following discussion.

The Giga Scale in Figure 12-2 includes information associated with geophysical techniques, such as reservoir architecture. Theories of regional characterization, such as plate tectonics, provide an intellectual framework within which Giga Scale measurement techniques, like seismic and satellite data, can be interpreted. The Mega Scale is the scale of reservoir characterization and includes well logging, pressure transient testing, and 3-D seismic analysis. The Macro Scale focuses on data sampling at the level of core analysis and fluid property analysis. The Micro Scale includes pore scale data obtained from techniques such as thin section analysis and measurements of grain-size distribution. Each of these scales contributes to the final reservoir flow model.

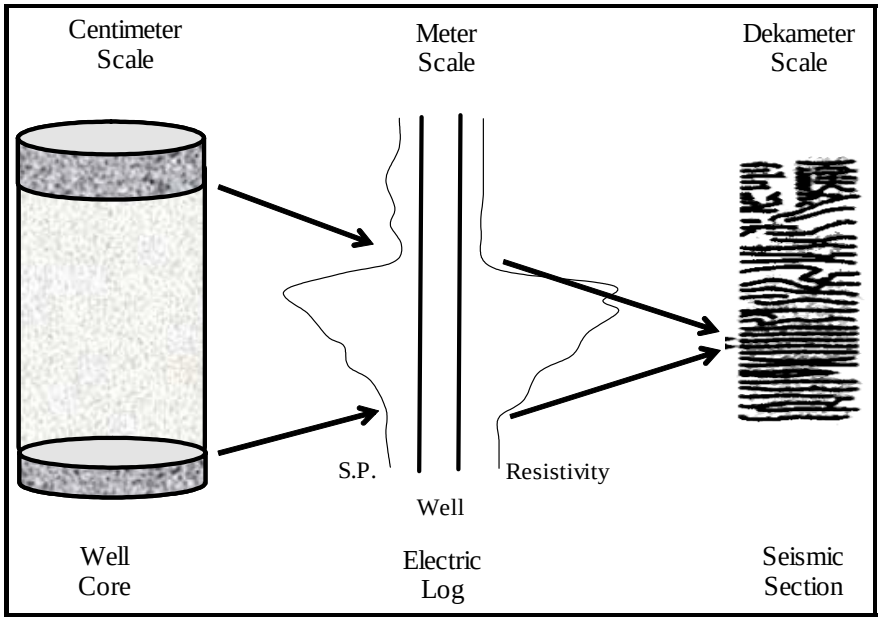

Figure 12-1. Range of Data Sampling Techniques (after Richardson, et al. [1987a])

Comparing the values of properties obtained using methods at two different scales demonstrates the sensitivity of important physical parameters to the scale at which they are measured. For example, rock properties such as porosity and permeability can be obtained from Mega Scale measurements such as well logs and well tests, and by direct measurement in the laboratory. Ideally there will be good agreement between the two scales; that is, well log porosity or well test permeability will agree with corresponding values measured in the laboratory. In many cases, however, there are disagreements. Assuming measurement error is not the source of the disagreement, differences in values show that differences in scale can impact the measured value of the physical parameter. Well test permeability, for example, represents an average over an area of investigation that is very large compared to a laboratory measurement of permeability using a core sample. The modeling team often has to make judgments about the relative merits of contradictory

data. The history matching process should recognize this source of uncertainty, as is discussed in subsequent chapters.

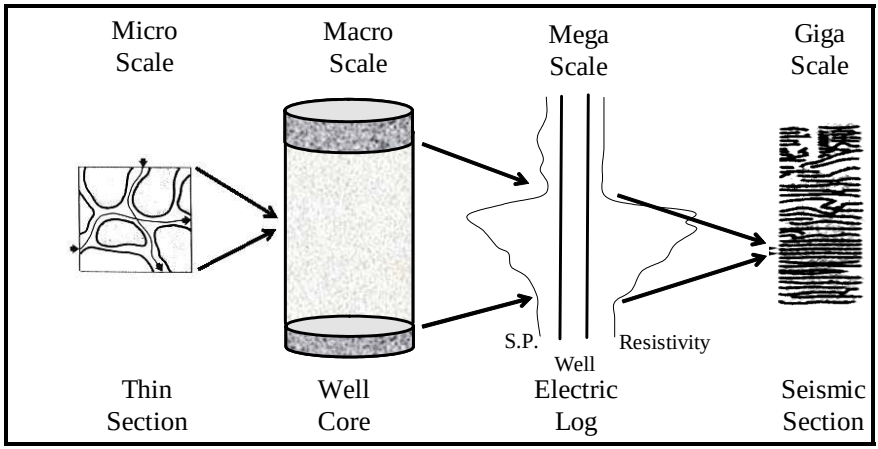

Figure 12-2. Reservoir Scales
(after Haldorsen and Lake [1989])

12.2 Reservoir Geophysics

Seismic measurements discussed by authors such as Ausburn, et al. [1978], McQuillin, et al. [1984], Sheriff [1989], Dorn [1998], and Liner [2004] provide much of the Giga Scale data that can be directly used to characterize a reservoir. Historically, seismic analyses have been of interest primarily as a means of establishing the structural size of the reservoir. People did not believe that seismic data could resolve sufficient detail to provide information beyond overall reservoir structure. But that view has changed with the emergence of time-lapse seismic monitoring and reservoir geophysics [for example, see Richardson, 1989; Ruijtenberg, et al., 1990; Anderson, 1995; He, et al., 1996; Johnston, 1997; Fanchi, et al. 1999; de Waal and Calvert, 2003; Lumley, 2004].

Reservoir geophysics is the application of geophysical techniques to the production of subsurface resources during the producing life of a field. The resolution associated with reservoir geophysics tends to be more quantitative than the resolution associated with exploration

geophysics. Exploration geophysics is the application of geophysical techniques to the search for commercial resources in the subsurface. By contrast, reservoir geophysics can use data from measurements in wells to calibrate the processing and interpretation of seismic measurements. The importance of reservoir geophysics to the reservoir management function makes it worthwhile to introduce some basic geophysical concepts.

Seismic waves are vibrations or disturbances that propagate from a source, such as an explosion or a shock wave, through the earth until they encounter a reflecting surface and are reflected into a detector, such as a geophone. Figure 12-3 shows a seismic trace. Each trace represents the signal received by a detector. Geophysical instruments measure the time it takes the seismic wave to propagate from the source to the reflector and then to the receiver. This time is referred to as two-way travel time. It must be converted to depth for use in geological analysis.

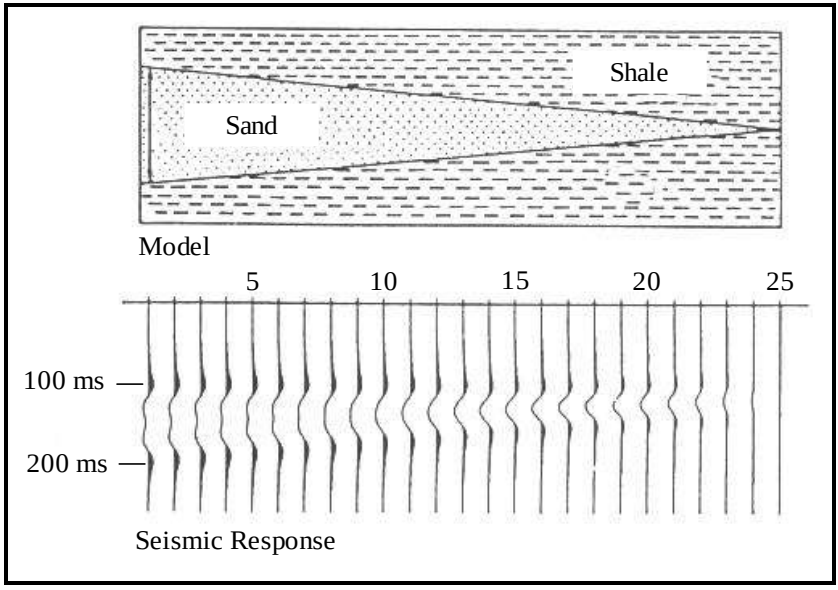

Figure 12-3. Seismic Trace for a Sand Wedge (after Ruijtenberg [1990]; reprinted by permission of the Society of Petroleum Engineers)

One of the central problems in seismic data processing is determining the time to depth conversion which may be considered the point where geology and geophysics meet [Medvin and Rennie, 1996]. When the time to depth conversion is applied to seismic data, it can change the relative depths of seismic amplitudes associated with adjacent traces and require a revision of the original interpretation.

The conversion of travel time data to formation depth requires that the velocity associated with each geologic zone be known or that it can be inferred as the wave evolves with time. Time to depth conversion calculations require models of seismic velocity in different types of materials. Figure 12-4 illustrates the time to depth conversion process for a set of seismic traces in a 3-D volume element. The velocity model in the figure contains seismic velocities that can be used to map time values to depth values. Seismic velocities can be estimated from petrophysical models such as the IFLO petrophysical model described in Section 12.4. Petrophysical models use rock and fluid properties to estimate seismic velocities.

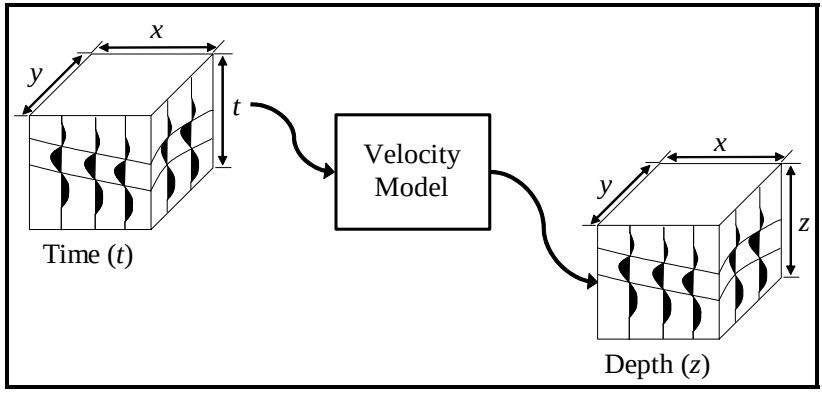

Figure 12-4. Time to Depth Conversion Process

Changes to the direction of propagation of seismic waves occur at reflectors. A seismic reflection occurs at the interface between two regions with different acoustic impedances. Acoustic impedance is a fundamental seismic attribute. Acoustic impedance is defined as

$$Z = \rho V \tag{12.1}$$

where ρ is the bulk density of the medium and V is the compressional velocity of the wave in the medium. Figure 12-5 illustrates a correlation between seismic wave velocity and the bulk density of different types of rock. Further discussion of rock properties and their relationship to seismic variables can be found in the literature [for example, Schön 1996; Mavko, et al., 1998; Tiab and Donaldson, 2003].

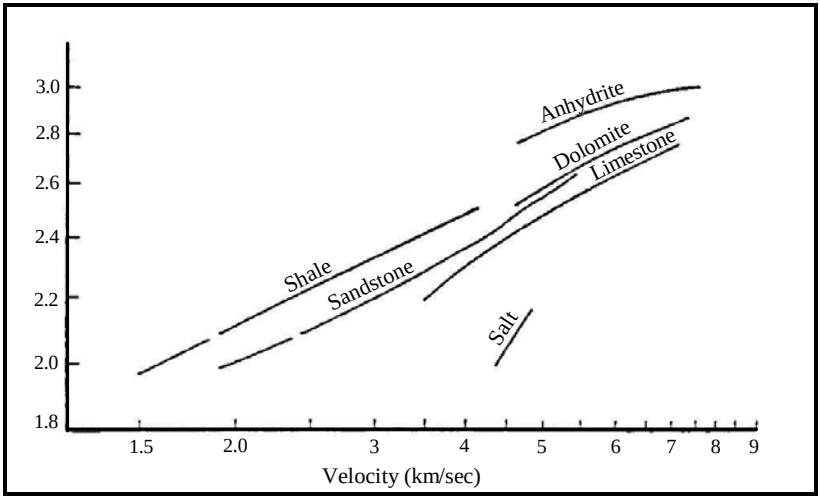

Figure 12-5. Seismic Wave Velocity and Bulk Density of Rock (after Telford, et al. [1976]; reprinted by permission of Cambridge University Press; after Gardner, et al. [1974])

A change in acoustic impedance will cause a reflection of the sound wave. The ability to reflect a sound wave by a change in acoustic impedance is quantified in terms of the reflection coefficient. The reflection coefficient R at the interface between two contiguous layers is defined in terms of acoustic impedances as

$$R = \frac{Z_2 - Z_1}{Z_2 + Z_1} = \frac{\rho_2 V_2 - \rho_1 V_1}{\rho_2 V_2 + \rho_1 V_1} \tag{12.2}$$

where subscripts 1 and 2 refer to the contiguous layers.

Table 12-1 illustrates the reflection coefficient magnitudes for typical subsurface interfaces. Values of reflection coefficients at the sandstone-limestone interface show that reflection coefficients can be relatively small. In addition to the reflection coefficient, a transmission coefficient can be defined. The transmission coefficient is one minus the reflection coefficient.

Table 12-1
Typical Reflection Coefficients

Interface	Reflection Coefficient
Sandstone on limestone	0.040
Limestone on sandstone	− 0.040
Ocean bottom	0.11 (soft) to 0.44 (hard)

Nonzero reflection coefficients occur when a wave encounters a change in acoustic impedance, either because the compressional velocity of the wave changes as it propagates from one medium to another, or because the bulk densities of the media differ. If the change in acoustic impedance is large enough, the reflection can be measured at the surface. That is why gas tends to show up as bright spots on seismic data – there is a big change in the density of the fluid. By contrast, the presence of an oil/water contact is harder to observe with seismic measurements because density differences between the oil and water phases are relatively small and result in small changes in acoustic impedance.

Figure 12-6 compares the amplitude and wavelength of a seismic wave with a sonic log response. The sonic log response shown in Figure 12-6 illustrates the relationship between the scale of the seismic wave and the scale of the sonic log. Seismic wave deflections to the right of the zero line are shaded to facilitate visual analysis of seismic traces. Sonic logs are typically used to calibrate seismic data when seismic data are used in reservoir characterization. The sonic log response in Figure 12-6 delineates the top and base of a geologic section.

The wavelength of the seismic wave is the velocity of the wave divided by its frequency. Alternatively, the wavelength is the velocity in a given medium times the period of the wave. The frequency of the wave

is a measure of the energy of the wave and is conserved as the wave propagates from one medium to another. The wavelength, however, can vary from one medium to another.

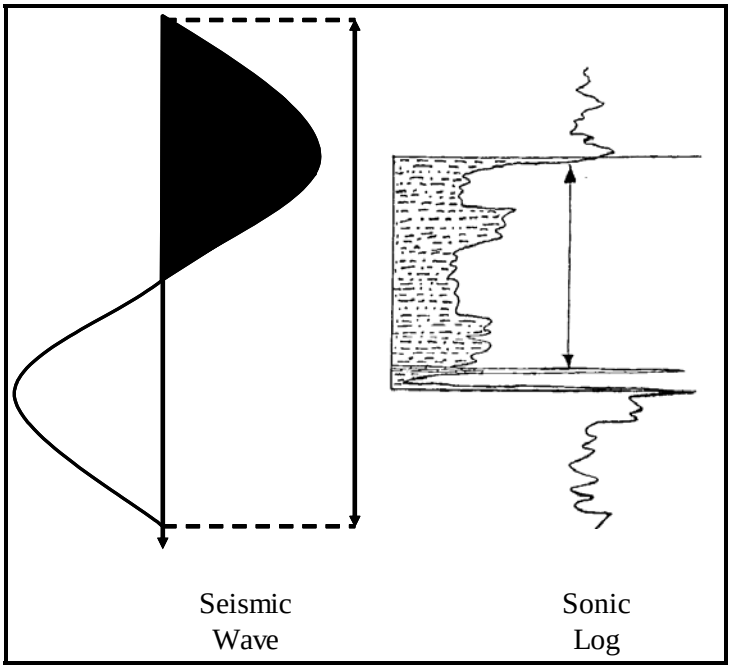

Figure 12-6. Seismic Wave and Sonic Log Response [after de Buyl, et al., 1988]

When waves overlap – or superpose – they create a wavelet, as shown in Figure 12-7. The time duration associated with the wavelet disturbance is denoted Δt. The wavelet has a velocity V in a medium, and the period $T=\Delta t$ is the width of the wavelet when plotted as a trace on a time-map of seismic data. The length of the wave is equal to the velocity V times the period T. Thus, if the wavelet has a 10 millisecond period and the velocity is 5000 feet per second in a particular medium, then the length L of that wavelet is 50 feet.

If seismic data has enough resolving power to show the reflecting boundaries of a geologic layer, then the amplitudes of seismic waves may be useful for further characterizing the petrophysical properties of

the reservoir. For example, suppose a reservoir region is characterized by porosity ϕ, permeability K, net thickness h_{net}, and oil saturation S_o. It may be possible to correlate seismic amplitude with rock quality (for example, Kh_{net} or ϕkh_{net}) or oil productive capacity (for example, $S_o\phi kh_{net}$). When a correlation does exist between seismic amplitude and a grouping of petrophysical parameters, the correlation may be used to help guide the distribution of reservoir properties in areas between wells.

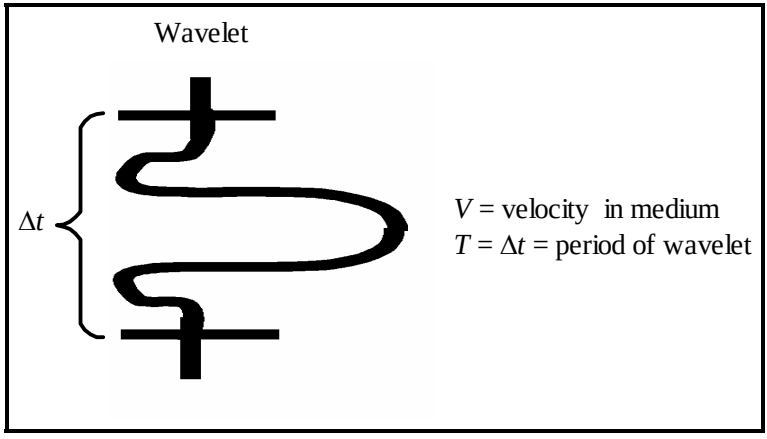

Figure 12-7. Seismic Wavelet

Figures 12-8a and 12-8b show two approaches to contouring a set of values at control points. The smooth contour lines shown in Figure 12-8a can be replaced by the irregular contour lines in Figure 12-8b if the irregular contour lines are supported by additional data. Seismic correlations can be used to justify the more heterogeneous contouring style shown in Figure 12-8b. A growing body of literature provides additional discussion of this application in the context of reservoir geophysics. For example, see de Buyl, et al. [1988], Evans [1996], Blackwelder, et al. [1996], Beasley [1996], Jack [1998], Waal and Calvert [2003], and Lumley [2004].

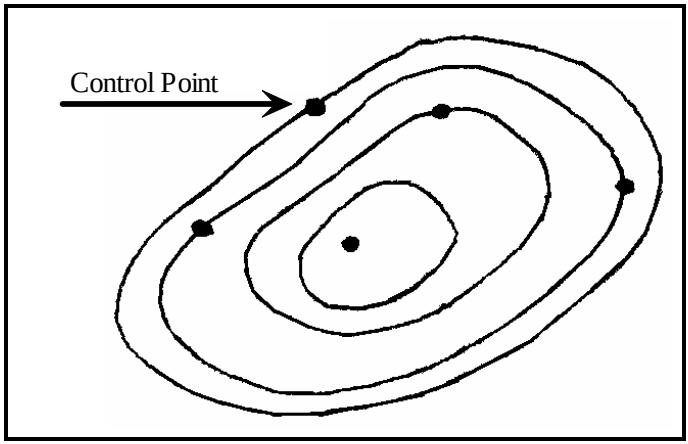

Figure 12-8a. Smooth Contour Lines

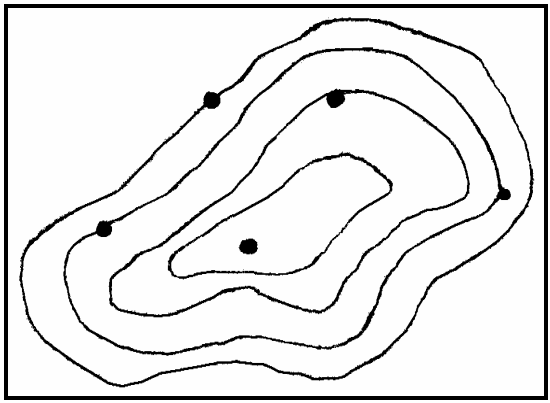

Figure 12-8b. Irregular Contour Lines

12.3 Correlating Reservoir Properties to Seismic Data

Reservoir geophysics has the potential to image important reservoir parameters in regions between wells. The reservoir geophysical procedure requires the correlation of seismic data with reservoir properties. Correlations are sought by making crossplots of seismic data with reservoir properties. The following are some correlation pairs:

- Seismic Amplitude versus Rock Quality
  - Rock Quality equals a parameter group such as kh_{net} or ϕkh_{net},.
- Seismic Amplitude versus Oil Productive Capacity (OPC)
  - OPC equals a parameter group such as $S_o \phi kh_{net}$
- Acoustic Impedance versus Porosity

If a statistically significant correlation is found, it can be used to guide the distribution of reservoir properties between wells. Ideally, the property distribution procedure will preserve reservoir properties at wells.

De Buyl, et al. [1988] used reservoir geophysics to predict the reservoir properties of two wells. They correlated well log-derived properties with seismically controlled properties. One such property is porosity. They then used the correlation to distribute properties. Maps drawn from seismically controlled distributions exhibited more heterogeneity than conventional maps drawn from well log-derived properties. Heterogeneity based on seismically controlled distributions represents spatial variations in reservoir properties determined by direct observation, albeit observation based on interpreted seismic data.

Table 12-2 gives an indication of the technical success of the reservoir geophysical technique. Actual values of reservoir parameters at two well locations are compared with values predicted using both well log-derived properties and seismically controlled properties. This work by De Buyl, et al. [1988] is notable because it scientifically tests the seismic method: it makes predictions and then uses measurements to assess their validity. In this particular case, a reservoir characterization based on seismically controlled properties yielded more accurate predictions of reservoir properties than predictions made using a reservoir characterization based only on well data.

Although reservoir geophysical techniques are still evolving, it is possible to make some general statements about the relative value of this emerging technology. Table 12-3 summarizes the advantages and concerns associated with reservoir geophysics.

Table 12-2
Predictions at New Wells from Seismic and Well Data
[de Buyl, et al., 1988]

Well	Property	Measured Values	Seismic Data Predicted	Well Data Predicted
I	Top of Reservoir (m)	-178.0	-175.0	-181.0
	Gross Porosity (vol %)	15.0	15.5	15.4
	Net ϕh (m)	1.78	1.53	1.96
J	Top of Reservoir (m)	-182.0	-179.0	-174.0
	Gross Porosity (vol %)	13.9	10.6	8.0
	Net ϕh (m)	1.08	1.05	0.15

Table 12-3
Reservoir Geophysics

Advantages	Concerns

➢ Ability to "see" between wells
➢ Single realization enhances
  ➢ communication
  ➢ understanding
	➢ Cost of
	  ➢ data acquisition
	  ➢ analysis
	➢ Time to build reservoir model
	➢ Limited applicability
	➢ Uncertainty of realization (unknown without sensitivity analysis)

Data management and the integration of disciplines will play an increasingly important role in the future of reservoir flow modeling [Thakur, 1996]. Many modelers have predicted that the integration of disciplines will manifest itself in reservoir flow modeling as finer 3-D models with more seismic and geological detail [He, et al., 1996; Kazemi, 1996; Uland, et al., 1997]. This prediction is being borne out with growing interest in shared earth models [Tippee, 1998; Fanchi, 2002a], model-centric working environments [Tobias, 1998], and reservoir flow

models with a million or more gridblocks [Dogru, 2000; Lasseter and Jackson, 2004].

12.4 IFLO Petrophysical Model

The petrophysical model in IFLO can be used to estimate both seismic attributes. Seismic attributes include compressional and shear velocities, and acoustic impedances. The IFLO petrophysical model is described here.

12.4.1 Compressional and Shear Velocities

Seismic compressional velocity and shear velocity are often calculated from the expressions [Mavko, et al., 1998]:

$$V_P = \sqrt{\frac{K_{sat} + \frac{4\mu}{3}}{\rho_B}} \tag{12.3}$$

and

$$V_S = \sqrt{\frac{\mu}{\rho_B}} \tag{12.4}$$

where

V_P = compressional velocity

V_S = shear velocity

K_{sat} = saturated bulk modulus of porous medium

μ = shear modulus of porous medium

ρ_B = bulk density = $(1-\phi)\rho_m + \phi\rho_f$

The expressions for compressional velocity and shear velocity are generalized in the integrated flow model (IFM) to the functional form

$$V_P = \sqrt{\frac{K^* + \frac{4\mu^*}{3}}{\rho^*}} \tag{12.5}$$

and

$$V_S = \sqrt{\frac{\mu^*}{\rho^*}} \tag{12.6}$$

where

V_P = compressional velocity functional

V_S = shear velocity functional

K^* = IFM bulk modulus

μ^* = IFM shear modulus

ρ^* = IFM bulk density = $(1-\phi)\rho_m + \phi\rho_f$

ρ_m = density of rock matrix grains

ρ_f = fluid density = $\rho_o S_o + \rho_w S_w + \rho_g S_g$

ϕ = porosity

The functions K^*, μ^* and ρ^* are determined by a number of techniques, such as matching laboratory data or using idealized models.

12.4.2 Models of Bulk and Shear Moduli

The IFLO petrophysical algorithm lets the user express moduli as functions of porosity ϕ, effective pressure P_e, and clay content volume fraction C. Effective pressure is the difference between confining (overburden) pressure and pore pressure P

$$P_{eff} = P_{con} - \alpha P \tag{12.7}$$

with the Biot coefficient correction factor

$$\alpha = 1 - (1 - \phi)\left(\frac{K^*}{K_m}\right)^n \tag{12.8}$$

The bulk modulus K^* and the grain modulus K_m are estimated at time level n. Confining pressure P_{con} may be entered by the user or estimated from an average overburden gradient γ_{OB} so that $P_{con} = \gamma_{OB}\, z$ where z is the depth to the gridblock midpoint.

The IFM bulk modulus has the form

$$K^* = K_{IFM} + \frac{\left[1 - \dfrac{K_{IFM}}{K_m}\right]^2}{\dfrac{\phi}{K_f} + \dfrac{1-\phi}{K_m} - \dfrac{K_{IFM}}{K_m^2}} \tag{12.9}$$

where

K_{IFM} = IFM dry frame bulk modulus

K_m = bulk modulus of rock matrix grains

K_f = bulk modulus of fluid = $1/c_f$

c_f = fluid compressibility = $c_o S_o + c_w S_w + c_g S_g$

Fluid compressibility for the extended black oil formulation is

$$c_f = c_T - c_r \tag{12.10}$$

where c_T is total compressibility and c_r is porosity compressibility.

The IFM dry frame bulk modulus has the functional dependence

$$K_{IFM} = a_0 + a_1 P_e^{e_1} + a_2\phi + a_3\phi^2 + a_4\phi P_e^{e_2} + a_5\sqrt{C} \tag{12.11}$$

with model coefficients $\{a_0, a_1, a_2, a_3, a_4, a_5, e_1, e_2\}$. Rock matrix grain modulus K_m is calculated from IFM dry frame bulk modulus K_{IFM} when porosity equals zero, thus

$$K_m = a_0 + a_1 P_e^{e_1} + a_5\sqrt{C} \tag{12.12}$$

The functional dependence of shear modulus is

$$\mu^* = \alpha_0 + \alpha_1 P_e^{\varepsilon_1} + \alpha_2\phi + \alpha_3\phi^2 + \alpha_4 P_e^{\varepsilon_2} + \alpha_5\sqrt{C} \tag{12.13}$$

with model coefficients $\{\alpha_0, \alpha_1, \alpha_2, \alpha_3, \alpha_4, \alpha_5, \varepsilon_1, \varepsilon_2\}$.

Rock matrix grain density ρ_m may be expressed as the following quadratic function of clay content

$$\rho_m = b_0 + b_1 C + b_2 C^2 \tag{12.14}$$

with regression coefficients $\{b_0, b_1, b_2\}$.

12.4.2.1 Constant Moduli (Gassmann) Model

Bulk modulus is calculated from Gassmann's [1951] equation as follows [Schön, 1996; McQuillin, et al., 1984]:

$$K^* = K_{sat} = K_{dry} + \frac{\left[1 - \dfrac{K_{dry}}{K_m}\right]^2}{\dfrac{\phi}{K_f} + \dfrac{1-\phi}{K_m} - \dfrac{K_{dry}}{K_m^2}}, \tag{12.15}$$

$$\mu^* = \mu,$$

$$\rho^* = \rho_B$$

where

K_{sat} = saturated bulk modulus

K_{dry} = dry frame bulk modulus

K_m = bulk modulus of rock matrix grains

K_f = bulk modulus of fluid = $1/c_f$

c_f = fluid compressibility = $c_o S_o + c_w S_w + c_g S_g$

μ = shear modulus

ρ_B = Bulk density = $(1-\phi)\rho_m + \phi\rho_f$

The user must enter K_{dry}, K_m, ϕ, and ρ_m as arrays of constant values. Grain modulus K_m equals dry frame bulk modulus K_{dry} when porosity equals zero. Moduli in this model are not allowed to depend on effective pressure or clay content. Porosity and compressibility depend on pore pressure.

12.4.2.2 Han-Eberhart-Phillips Moduli

Table 12-4 presents regression model coefficients for the Han-Eberhart-Phillips (HEP) moduli [Fanchi, 2003a].

Table 12-4
Regression Model Coefficients for HEP Moduli*

K_{dry} Coefficient	Regression Value	μ* Coefficient	Regression Value
a_0	5.2001×10^6	α_0	4.2958×10^6
a_1	2.9300×10^4	α_1	5.3952×10^4
a_2	-1.4307×10^7	α_2	-1.4952×10^7
a_3	6.9014×10^6	α_3	1.3948×10^7
a_4	5.7684×10^2	α_4	-2.2544×10^4
a_5	-1.1936×10^6	α_5	-2.6009×10^6
e_1	1/3	ε_1	1/3
e_2	1/3	ε_2	1/3

* For K_{dry}, μ* and P_e in psia; ϕ a fraction; and C a volume fraction. Calculated moduli have units of psia.

12.4.3 Acoustic Impedance and Reflection Coefficients

Acoustic impedance Z for compressional waves is defined as

$$Z = \rho_B V_P \tag{12.16}$$

The reflection coefficient RC at the interface between two layers with acoustic impedances Z_1 and Z_2 is

$$R = \frac{Z_2 - Z_1}{Z_2 + Z_1} \tag{12.17}$$

12.5 IFLO Application: Scheduling Time-Lapse Seismic Surveys

IFLO can be used to schedule time-lapse seismic surveys to optimize the acquisition of reservoir management information. Time-lapse seismology, also known as 4-D seismic, compares one 3-D seismic survey with another 3-D seismic survey taken in the same geographic location but at a different time. Differences between the two 3-D seismic surveys arise from changes in reservoir properties such as pressure and saturation distributions. As an illustration of 4-D seismic monitoring, we consider the issue of scheduling two time-lapse seismic surveys with the goal of maximizing the acquisition of information that can be used in a reservoir management study.

The fluid properties in the first Society of Petroleum Engineers (SPE) comparative solution project [Odeh, 1981] are used with the reservoir characterization described in the second SPE comparative solution project [Weinstein, et al., 1986]. A cross section of an undersaturated oil reservoir with 15 layers is modeled. Permeability is isotropic and vertical permeability is assumed to be one tenth of horizontal permeability.

Layer 9 of the 15 layer cross section is the best oil target. The lowermost layer (layer 15) is a thick, water bearing aquifer layer. Gas is injected into the upper layers (layers 1 through 3) of the undersaturated oil reservoir cross section while oil is being produced from the lower layers (layers 9 through 12). All layers are in vertical communication. The per cent difference in acoustic response is relatively small in this example (less than 1% for the P-wave velocity to S-wave velocity ratio V_P/V_S), nevertheless the acoustic response for this example illustrates the following important features of time-lapse seismic monitoring.

The advance of the injected gas into the cross section is considered at 180 days and 270 days. The gas front is highlighted by displaying

the change in gas saturation from the beginning of the flood to the current time. The corresponding change in the ratio of compressional to shear velocities is also considered (Figure 12-9). Gas is injected in the upper left hand corner of Figure 12-9 and oil is produced from the lower layers on the right hand side of the figure. The presence of injected gas shows up clearly at both 180 days and 270 days. In addition, the presence of a cone of gas appears at 270 days in the layers above the perforated interval of the oil production well. The appearance of the cone is explained by looking at the pressure distribution in the reservoir relative to the bubble point pressure.

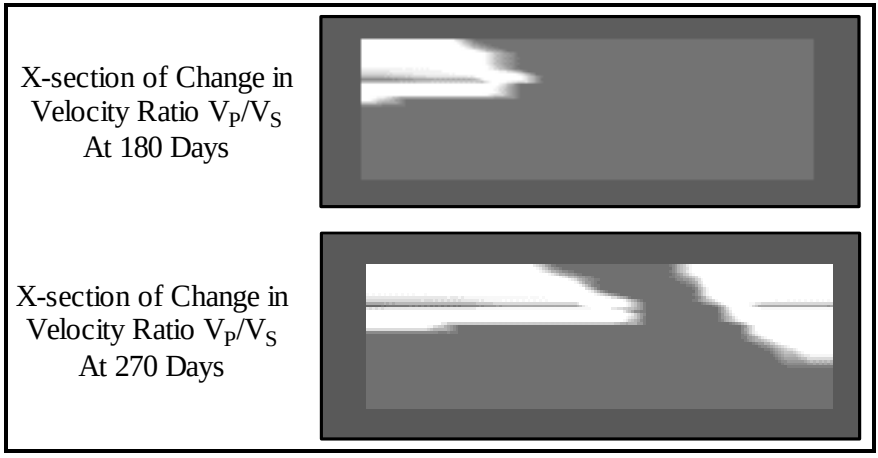

Figure 12-9. Gas Injection in Layered Oil Reservoir

The difference in reservoir pressure relative to bubble point pressure shows the appearance of a cone of free gas that is coming out of solution as reservoir pressure in the vicinity of the production well drops below the bubble point pressure of the oil. A seismic survey at 180 days would see the gas front advance but not the gas cone, while a seismic survey at 270 days would see both the gas front advance and the gas cone. The later seismic survey would provide more information for use in a history match.

Exercises

Exercise 12.1A Run EXAM1.DAT and record the final time, final pressure and initial oil volume.

Exercise 12.1B Multiply the volume of the reservoir in EXAM1.DAT by 0.5, 10 and 100. This can be done by altering the gridblock size (see Section 21.1). Make a table showing the final time, final pressure, and initial oil volume for each case.

Exercise 12.1C How does the change in volume affect the pressure performance of the model as a function of time?

Exercise 12.2 Repeat Exercise 12.1, but make the volume changes by modifying the grid dimensions using the pore volume modification option in IFLO.

Exercise 12.3 What is the seismic reflection coefficient R at the interface between two formations with equal acoustic impedances?

Exercise 12.4A Effective bulk modulus K^* can be written in terms of porosity ϕ, dry rock bulk modulus K_B, grain modulus K_G and fluid modulus K_F as

$$K^* = K_B + \frac{\left[1-b\right]^2}{\dfrac{\phi}{K_F} + \dfrac{1-\phi-b}{K_G}}, \; b = \frac{K_B}{K_G}$$

Solve the above equation exactly for b and show your result. Hint: set $K_B = bK_G$ in K^* and solve for b. The term K_B should not appear in your solution.

Exercise 12.4B Using data from sonic log and laboratory measurements shown in the following table, calculate K_B.

Parameter	Value
V_P (ft/s)	18,736
V_S (ft/s)	10,036
V_P / V_S	1.87
μ^* (psia)	3.61×10^6
K^* (psia)	7.30×10^6
K_G (psia)	9.70×10^6
K_B (psia)	
K_F (psia, brine)	2.97×10^5
ϕ (fraction)	0.15

where

V_P = Compressional velocity

V_S = Shear velocity

K^* = Effective bulk modulus

μ^* = Shear modulus

Exercise 12.5A IFLO calculates *P*-wave and *S*-wave velocities using

$$V_P = \sqrt{\frac{K^* + \frac{4}{3}\mu^*}{\rho^*}}, V_S = \sqrt{\frac{\mu^*}{\rho^*}}$$

where

V_P = Compressional velocity

V_S = Shear velocity

K^* = *IFM* bulk modulus

μ^* = *IFM* shear modulus

ρ^* = *IFM* bulk density

The IFM bulk modulus has the form

$$K^* = K_{IFM} + \frac{\left[1 - \frac{K_{IFM}}{K_m}\right]^2}{\frac{\phi}{K_F} + \frac{1-\phi}{K_m} - \frac{K_{IFM}}{K_m^2}}$$

where

V_P = Compressional velocity

K_{IFM} = *IFM* dry bulk modulus

K_m = Bulk modulus of matrix grains

K_F = Bulk modulus of fluid = $1/c_F$

c_F = Fluid compressibility = $c_o S_o + c_w S_w + c_g S_g$

Use the above information to estimate the minimum value that V_P/V_S can have.

Exercise 12.5B Fill in the following table.

Parameter	Value
V_P / V_S	
μ* (psia)	3.61×10^6
K^* (psia)	7.30×10^6
K_m (psia)	9.70×10^6
K_F (psia, brine)	2.97×10^5
ϕ (fraction)	0.15

Exercise 12.6A Run XS-SPE2.DAT and record the time, pressure, oil rate and gas rate at the end of the run.

Exercise 12.6B Use 3DView to create Figure 12-9.

Chapter 13

Flow Units

Giga Scale information helps define reservoir architecture, but is too coarse to provide the detail needed to characterize the reservoir enough to design a reservoir management plan. The Mega Scale is the scale at which we begin to integrate well log and pressure transient test data into a working model of the reservoir. This chapter introduces the role of well log and pressure transient test data in reservoir modeling. We then discuss the concept of flow unit.

13.1 Well Log Data

Well logs provide valuable information about the formation within a few feet of the wellbore. A thorough discussion of well logging is beyond the scope of this book. We describe several concepts that are applicable to reservoir modeling. For more information, the interested reader should consult references such as Brock [1986], Bassiouni [1994], and Asquith and Krygowski [2004].

Well logs are obtained by running a tool into the wellbore. The tool can detect physical properties such as temperature, electrical current, radioactivity, or sonic reflections. Logging tools are designed to function best in certain types of environments. The environment depends on a variety of factors, including temperature, lithology, and fluid content. The theoretical analysis of log signals is usually based on the assumption

that the formation is infinite in extent with homogeneous and isotropic properties. Tool performance will not be optimal in other environments.

Table 13-1 illustrates the type of information that can be obtained at the Mega Scale level from well log data. The most common interpretations of each log response are included in the table. For example, a high gamma ray response implies the presence of shales, while a low gamma ray response implies the presence of clean sands or carbonates.

The depth of investigation of a well log is a measure of the volume of the formation that is primarily responsible for the well log signal. If we assume the formation has a uniform cylindrical shape for a formation with thickness h, then the volume investigated is $\phi r^2 h$ where the radius r is the depth of investigation into the formation, and ϕ is porosity. Depth of investigation can range from a few inches to several feet.

Table 13-1
Well Log Response

Log	Variable	Response
Gamma ray	Rock type	➢ Detects shale from in situ radioactivity. ➢ High gamma ray ⇒ shales ➢ Low gamma ray ⇒ clean sands or carbonates
Resistivity	Fluid type	➢ Measures resistivity of formation water. ➢ High resistivity ⇒ hydrocarbons ➢ Low resistivity ⇒ brine
Density	Porosity	➢ Measures electron density by detecting Compton scattered gamma rays. Electron density is related to formation density. Good for detecting hydrocarbon (HC) gas with low density compared to rock or liquid. ➢ Small response ⇒ low HC gas content ➢ Large response ⇒ high HC gas content

Acoustic (sonic)	Porosity	➢ Measures speed of sound in medium. Speed of sound is faster in rock than in fluid. ➢ Long travel time ⇒ slow speed ⇒ large pore space ➢ Short travel time ⇒ high speed ⇒ small pore space
Neutron	Hydrogen content	➢ Collisions slow fast neutrons to thermal energies. Thermal neutrons are captured by nuclei, which then emit detectable gamma rays. Note: Hydrogen has a large capture cross section for thermal neutrons. Good for detecting gas. ➢ Large response ⇒ high hydrogen content ➢ Small response ⇒ low hydrogen content
Spontaneous potential (SP)	Permeable beds	➢ Measures electrical potential (voltage) associated with movement of ions. ➢ Small response ⇒ impermeable shales ➢ Large response ⇒ permeable beds

Porosity and saturation can be obtained from well logs. For example, the porosity of a logged interval from the formation density log is given by

$$\phi = \frac{\rho_{ma} - \rho_b}{\rho_{ma} - \rho_f} \tag{13.1}$$

where ϕ is porosity, and ρ_{ma}, ρ_b and ρ_f are rock matrix density, bulk density and fluid density, respectively. Bulk density ρ_B of the medium is

$$\rho_b = (1-\phi)\rho_{ma} + \phi\rho_f \tag{13.2}$$

The wetting phase saturation in a formation can be estimated from a resistivity log as

$$S_w = \left(\frac{FR_w}{R_t} \right)^{1/n} \tag{13.3}$$

where R_t is the resistivity of a porous medium that is partially saturated by an electrically conducting wetting phase with saturation S_w, and R_w is the resistivity of the electrically conducting wetting phase. The formation resistivity factor F can be estimated from the empirical relationship

$$F = a\phi^{-m} \tag{13.4}$$

where the cementation exponent *m* varies from 1.14 to 2.52 and the coefficient *a* varies from 0.35 to 4.78 [Bassiouni, 1994] for sandstones. Both parameters *a* and *m* depend on pore geometry: *a* depends on tortuosity and *m* depends on the degree of consolidation of the rock. Equation (13.3) is Archie's equation for wetting phase saturation, which is often water saturation.

Porosity and saturation estimates are often accompanied by the specification of porosity and saturation cutoffs. A cutoff specifies the minimum value of the parameter that is considered a part of the productive formation. Cutoffs may be used for permeability in addition to porosity and saturation. Worthington and Cosentino [2005] discuss the role of cutoffs in reservoir studies.

Two of the most important uses of well logs are the determination of formation thickness and lateral continuity. Correlations between wells are used to define formations and productive intervals. An example of a correlation technique is the fence diagram. A fence diagram is prepared by aligning well logs in their proper spatial position and then drawing lines between well logs that show the stratigraphic correlation. Fence diagrams illustrate correlations between wells and can show formation pinchouts, unconformities, and other geologic discontinuities.

A combination of well logging tools is usually needed to minimize ambiguity in log interpretation, as discussed by Brock [1986]. For example, the combination neutron-density log is a combination log that consists of both neutron log and density log measurements. Possible gas producing zones can be identified by the log traces of the combination

neutron-density log. The presence of gas increases the density log porosity and decreases the neutron log porosity [Bassiouni, 1994, pg. 329]. If a sonic log is added to the log suite, quantitative information about lithology can be estimated using crossplots, and the log suite can be used to calibrate seismic data.

Sonic log interpretation depends on lithology. In particular, the interval transit time in carbonates depends on the relative amount of primary and secondary porosity. Primary porosity is associated with the matrix, and secondary porosity is associated with features such as fractures and vugs. Subtracting sonic porosity from total porosity recorded using neutron or density logs gives an estimate of secondary porosity.

One more log, the gamma ray log, is usually added to the suite of logs used to evaluate gas bearing formations. The gamma ray log measures natural radioactivity in a formation. It provides a measurement of shale content, and can be used for identifying lithologies, correlating zones and correcting porosity log results in formations containing shale.

13.2 Pressure Transient Test Data

Pressure transient testing uses pressure changes measured at a well that are induced by changes in the flow rate of one or more wells. The variation in pressure is recorded as a function of time using pressure gauges. The information from pressure transient tests can be combined with data from other sources to obtain additional reservoir parameters. Analysis of the pressure response provides information that can be used to infer reservoir parameters such as flow capacity, average reservoir pressure in the drainage area, reservoir size, boundary and fault locations, wellbore damage and stimulation, and well deliverability. We describe several concepts in this section that are applicable to reservoir modeling. Additional information about pressure transient testing can be found in such references as Matthews and Russell [1967], Earlougher [1977], Sabet [1991], Horne [1995], Chaudhry [2003a, b], and Brown and Hawkes [2005].

Table 13-2 from Kamal, et al. [1995] illustrates the type of information that can be obtained at the Mega Scale level from pressure transient test data. The table also notes the time in the life of the project when the pressure transient test is most likely to be run. It is usually necessary to run a variety of pressure transient tests as the project matures. These tests help refine the operator's understanding of the field and often motivate changes in the way the well or the field is operated.

Tables 13-1 and 13-2 illustrate a few of the methods used to gather Mega Scale information. Advances in technology periodically add to a growing list of transient tests and well log tools [for example, see Kamal, 1995; Felder, 1994; Chu [2000], and Brown and Hawkes, 2005]. In many cases, budgetary constraints will be the controlling factor in determining the number and type of tests run. The modeling team must work with whatever information is available. Occasionally, an additional pressure transient test or well log will need to be run, but the expense and scheduling make it difficult to justify acquiring new well log or pressure transient test information once a simulation study is underway.

Table 13-2
Reservoir Properties Obtainable from Pressure Transient Tests

Type of Test	Properties	Development Stage
Drill stem tests	• Reservoir behavior • Permeability • Skin • Fracture length • Reservoir pressure • Reservoir limit • Boundaries	Exploration and appraisal wells
Repeat formation tests / Multiple formation tests	Pressure profile	Exploration and appraisal wells

Drawdown tests	• Reservoir behavior • Permeability • Skin • Fracture length • Reservoir limit • Boundaries	Primary, secondary and enhanced recovery
Buildup tests	• Reservoir behavior • Permeability • Skin • Fracture length • Reservoir pressure • Reservoir limit • Boundaries	Primary, secondary, and enhanced recovery
Falloff tests	• Mobility in various banks • Skin • Reservoir pressure • Fracture length • Location of front • Boundaries	Secondary and enhanced recovery
Interference and pulse tests	• Communication between wells • Reservoir type behavior • Porosity • Interwell permeability • Vertical permeability	Primary, secondary, and enhanced recovery

Layered reservoir tests	• Properties of individual layers • Horizontal permeability • Vertical permeability • Skin • Average layer pressure • Outer boundaries	Throughout reservoir life
Step-rate tests	• Formation parting-pressure • Permeability • Skin	Secondary and enhanced recovery

In addition to providing information about individual well performance, wellbore damage, reservoir pressure, and reservoir fluid flow capacity, pressure transient testing can also provide information that can be used to estimate the distance to reservoir boundaries, structural discontinuities, and communication between wells. For example, the radius of investigation for a pressure transient test in an oil well is the distance the pressure transient moves away from the oil well in the time interval following the change in flow rate. Assuming single-phase, radial flow, the radius of investigation may be estimated from a pressure buildup test in an oil well using the equation

$$r_i = 0.029\sqrt{\frac{Kt}{\phi\mu c_T}} \tag{13.5}$$

where the variables and units are defined in Table 13-3. For comparison, the radius of investigation for a pressure transient test in a gas well is an estimate of the distance the pressure transient moves away from the gas well in a specified time. It may be estimated from a pressure buildup test in a gas well using

$$r_i = 0.0325\sqrt{\frac{Kt}{\phi\mu c_T}} \tag{13.6}$$

where the variables and units are defined in Table 13-3. A comparison of Eq. (13.5) with Eq. (13.6) shows that the radius of investigation for gas wells has the same functional dependence as the radius of investigation for oil wells, but the numerical coefficient is larger for gas than for oil.

Table 13-3
Radius of Investigation Variables

r_i	radius of investigation (ft)
t	shut-in time (hr)
K	permeability (md)
ϕ	porosity (fraction)
μ	viscosity (cp)
c_T	total compressibility (1/psia)

The radius of investigation yields an approximate distance to reservoir features that cause the slope of the pressure transient response to change. Consequently, the radius of investigation can be used to estimate the distance to no-flow barriers such as sealing faults or permeability pinch outs. This type of information should be compared with the geological concept of the reservoir and geophysical indications of structural discontinuities. The most accurate characterization of the reservoir is usually the one that provides a realization of the reservoir that is consistent with all available data from engineering, geology, geophysics, and petrophysics. The resulting characterization is an integrated representation of the reservoir. It may also be viewed as a shared earth model.

13.3 Pressure Correction

When pressures are matched in a model study, the calculated and observed pressures should be compared at a common datum. In addition, pressures from well tests should be corrected for comparison with model gridblock pressures. A widely used pressure correction is Peaceman's correction [1978, 1983].

Figure 13-1 illustrates a pressure buildup curve (PBU) as a function of radial distance from the center of a wellbore with radius r_w. To obtain a well gridblock pressure P_o from a PBU, Peaceman used a Cartesian grid to model the PBU performance of a well to find an equivalent well gridblock radius r_o. Figure 13-2 illustrates a Horner plot of a PBU test. The dashed line in Figure 13-2 is a sketch of the data, and the solid line is the slope.

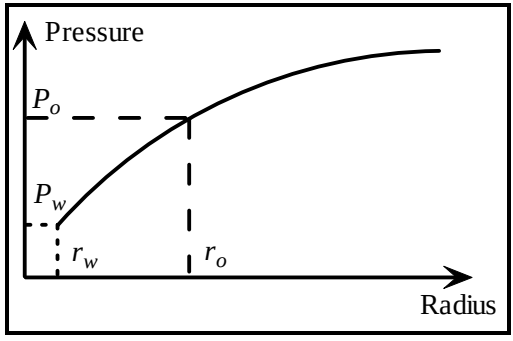

Figure 13-1. Pressure Buildup

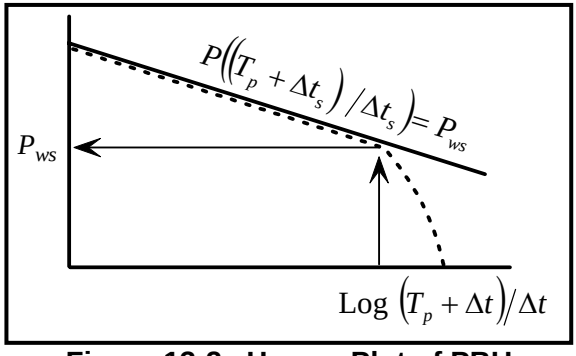

Figure 13-2. Horner Plot of PBU

Peaceman showed that the shut-in pressure P_{ws} of an actual well equals the simulator well gridblock pressure P_o at a shut-in time Δt_s given by

$$\Delta t_s = \frac{1688\phi\mu c_T r_o^2}{K} \tag{13.7}$$

where K is permeability, ϕ is porosity, μ is viscosity, and c_T is total compressibility. The relationship between gridblock pressure P_o and flowing pressure P_{wf} at the wellbore is

$$P_{wf} = P_o - 141.2\frac{QB\mu}{Kh}\left[\ln\frac{r_o}{r_w} + S\right] \tag{13.8}$$

where Q is the flow rate, B is formation volume factor, and S is skin. Shut-in time can be masked by wellbore storage effects. If it is, the shut-in pressure P_{ws} may have to be obtained by extrapolating another part of the curve, such as the radial flow curve. Table 13-4 summarizes the parameters involved in Peaceman's correction for a consistent set of units. Odeh [1985] extended Peaceman's work with 2-D models to 3-D models.

Table 13-4
Oilfield Units for Peaceman's Correction

Parameter	Unit	Parameter	Unit
B	RB/STB	r_o, r_w	ft
c_T	$psia^{-1}$	S	fraction
h	ft	Δt_s	hr
K	md	Δx, Δy	ft
P_o, P_{wf}, P_{ws}	psia	ϕ	fraction
Q	STB/day	μ	cp

The equivalent well gridblock radius depends on the permeability isotropy of the reservoir. An isotropic reservoir in the horizontal plane is a reservoir in which *x*-direction permeability equals *y*-direction permeability ($K_x = K_y$). In this case, the equivalent well gridblock radius is given in terms of the gridblock lengths $\{\Delta x, \Delta y\}$, thus

$$r_o = 0.14\left(\Delta x^2 + \Delta y^2\right)^{1/2} \tag{13.9}$$

13.4 Integrating Scales: The Flow Unit

All of the information collected at various scales must be integrated into a single, comprehensive, and consistent representation of the reservoir. The integration of data obtained at different scales is a difficult issue that is often referred to as the upscaling or scaleup problem [for example, see Oreskes, et al., 1994]. Attempts to relate data from two different scales can be difficult. For example, permeability is often obtained from both pressure transient testing and routine core analysis. The respective permeabilities, however, may appear to be uncorrelated because they represent two different measurement scales. An important task of the scaleup problem is to develop a detailed understanding of how measured parameters vary with scale. The focus on detail in one or more aspects of the reservoir flow modeling process can obscure the fundamental reservoir concept in a model study. One way to integrate available data within the context of a "big picture" is to apply the flow unit concept.

A flow unit is defined as "a volume of rock subdivided according to geological and petrophysical properties that influence the flow of fluids through it" [Ebanks, 1987]. Table 13-5 shows typical geologic and petrophysical properties. A classic application of the flow unit concept is presented in a paper by Slatt and Hopkins [1990].

A reservoir is modeled by subdividing its volume into an array of representative elementary volumes (REV). The REV concept is not the same as the flow unit concept. A flow unit is a contiguous part of the reservoir that has similar flow properties as characterized by geological

and petrophysical data. Several flow unit identification techniques are proposed in the literature, such as the modified Lorenz plot used by Gunter, et al. [1997].

Table 13-5
Properties Typically Needed to Define a Flow Unit

Geologic	Petrophysical
Texture Mineralogy Sedimentary Structure Bedding Contacts Permeability Barriers	Porosity Permeability Compressibility Fluid Saturations

A simplified variation of the modified Lorenz plot technique is to identify a flow unit by plotting normalized cumulative flow capacity as a function of depth. Normalized cumulative flow capacity F_m is calculated as

$$F_m = \frac{\sum_{i=1}^{m} k_i h_i}{\sum_{i=1}^{n} k_i h_i}; \; m = 1, \ldots, n \tag{13.10}$$

where n is the total number of reservoir layers k_i is the permeability of layer i, and h_i is the net thickness of layer i. The layers are numbered in order from the shallowest layer $i = 1$ to the deepest layer $i = m$ for a normalized cumulative flow capacity F_m at depth

$$Z_m = Z_0 + \sum_{i=1}^{m} h_i \tag{13.11}$$

where Z_0 is the depth to the top of layer 1 from a specified datum. A flow unit will appear on the plot as a line with constant slope. In Figure 13-3, a change in slope is interpreted as a change from one flow unit to another. Slope changes in Figure 13-3 occur at depths of 36 feet, 76 feet,

92 feet, 108 feet, 116 feet, 124 feet, 140 feet, 152 feet, and 172 feet. The largest slope is between 108 feet and 116 feet, and corresponds to a high permeability zone. It is followed immediately by a low permeability zone at a depth of approximately 120 feet.

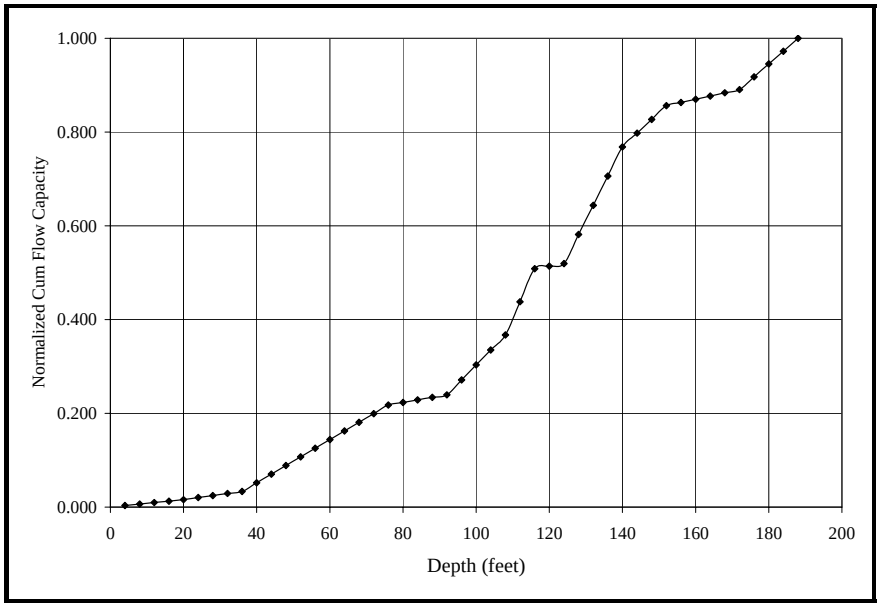

Figure 13-3. Identifying flow units

Another plot that can be used to identify flow units is a plot of normalized cumulative flow capacity F_m versus a cumulative storage capacity Φ_m defined by

$$\Phi_m = \frac{\sum_{i=1}^{m} \phi_i h_i}{\sum_{i=1}^{n} \phi_i h_i}, m = 1, \ldots, n \qquad (13.12)$$

where n is the total number of reservoir layers and ϕ_i is the porosity of layer i. Again, the layers are numbered in order from the shallowest layer $i = 1$ to the deepest layer $i = m$. The analyst again looks for changes in slope in the plot of F_m versus Φ_m.

Flow units usually contain one or more REVs. By contrast, the REV is the volume element that is large enough to provide statistically significant average values of parameters describing flow in the contained volume, but small enough to provide a meaningful numerical approximation of the fundamental flow equations [for example, see Bear, 1972]. As noted by Fayers and Hewett [1992], "It is somewhat an act of faith that reservoirs can be described by relatively few REV types at each scale with stationary average properties." Stolz and Graves [2003] have reviewed different flow unit definition techniques and demonstrated that fluid flow in a layered system is sensitive to the defined flow unit.

The flow unit concept is an effective means of managing the growing base of data being provided by geoscientists. Increasing refinement in geological models gives flow modelers more detail than they can use. Even today, with one hundred thousand to one million gridblock flow models, modelers cannot routinely use all of the information that is provided by computer-based geologic models. Computer-based geologic models often have in excess of one million grid points. It is still necessary to coarsen most detailed geologic models into representative flow units. A notable exception to this observation is the flow modeling work by Aramco modelers [Dogru, 2000; Dogru, et al., 2002]. They have shown that flow models that are created on the same scale as geoscience models can significantly reduce the number of runs needed to achieve a history match.

An understanding of the big picture, even as a simple sketch, is a valuable resource for validating the ideas being quantified in a model. Richardson, et al. [1987b] sketched several common types of reservoir models: a deepwater fan; a sand-rich delta; a deltaic channel contrasted with a deltaic bar, and so forth. Their sketches illustrate what the reservoir might look like for a specified set of assumptions. A sketch such as that in Figure 13-4 is a good tool for confirming that people from different disciplines share the same concept of a reservoir; it is a simple visual aid that enhances communication. In many cases, especially the case of relatively small fields, the best picture of the reservoir may only be a qualitative picture. When a more detailed study begins, the qualitative

picture can be upgraded by quantifying parameters such as gross thickness in the context of the conceptual sketch of the reservoir.

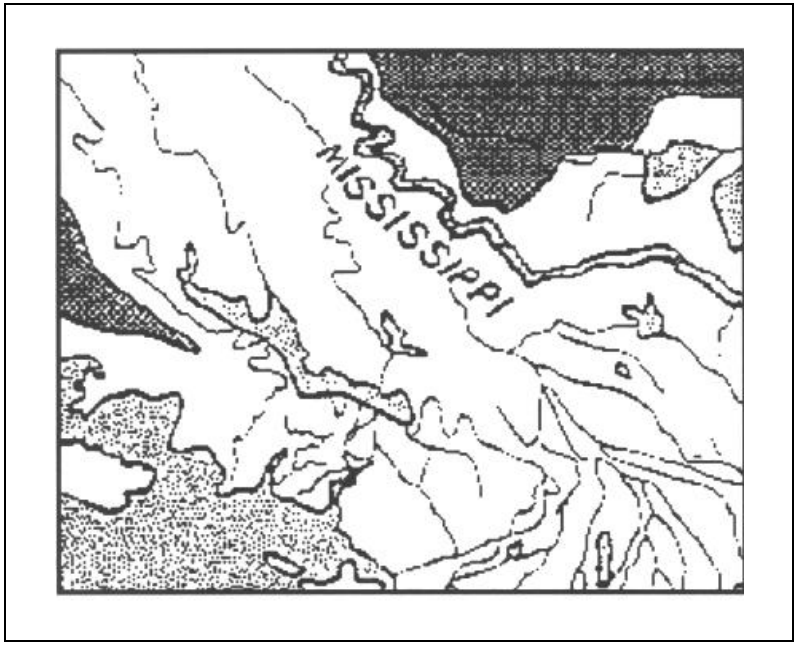

Figure 13-4. Mississippi Delta

Confidence in model performance is acquired by using the model to match historical field performance. History matching and model validation are discussed in greater detail in Chapter 18. From a technical perspective, flow models should be updated and refined as additional information is obtained from the field. In practice, the frequency of model updates depends on the importance of the resource being modeled to the enterprise.

13.5 IFLO Application: Valley Fill Waterflood

A valley fill reservoir is formed by the incision and fluvial erosion of an existing facies. The valley is formed during a fall in relative

sea level. The receding sea level exposes older deposits to incisement by drainage. The base of the incised valley is a sequence boundary that is referred to as the LSE, or lowstand surface of erosion.

If the sea level starts to rise again, the initial deposition into the incised valley is typical of flooded systems. During this period of transgression, the incised valley is filled by a variety of fluvial, estuarine and marine environments. When the period of transgression ends, the surface of the filled valley is covered by a new depositional layer associated with flooding. The top of the valley fill is a second sequence boundary that is referred to as the TSE, or transgressive surface of erosion. A typical incised valley is characterized by a set of fluvial system tracts bounded below by an LSE and above by a TSE. The LSE and TSE are key surfaces in the description of the geologic system.

The Valley Fill reservoir in this application is a meandering channel sand [Fanchi, 2002a]. The incised valley has a regional dip. Six producing wells are located in the channel along with two downstructure water injection wells. The reservoir is subjected to a year of depletion before the water injection begins. The injected water displaces oil toward the upstructure production wells. Figure 13-5 is a cross section that shows the waterflood movement for a geologic representation that uses three model layers. Each layer has the same permeability.

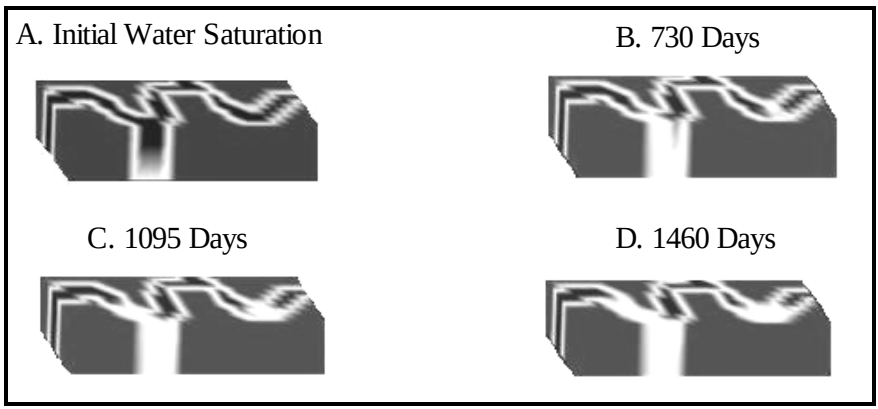

Figure 13-5. Waterflood of Valley Fill Reservoir

Rather than using constant values of permeability for a layered system, a flow unit analysis can provide permeabilities for each layer. For example, suppose a flow unit analysis provides the layer permeabilities given in Table 13-6. The heterogeneous layer permeabilities shown in Table 13-6 have both a high permeability layer (layer 2) and a low permeability layer (layer 3). Rerunning the model shows that the permeability distribution in Table 13-6 results in earlier water production than the constant permeability case (see Exercise 13.5).

Table 13-6
Permeability for Valley Fill Model

Layer	Permeability (md)		
	***x*-direction**	***y*-direction**	***z*-direction**
1	100	100	10
2	300	300	30
3	50	50	5

Exercises

Exercise 13.1A Use the data in the following table to make a porosity-permeability crossplot on semilogarithmic paper. Permeability should be plotted on the vertical, logarithmic axis and porosity should be plotted on the horizontal axis. Is the permeability distribution log-normal?

Flow Unit Exercise: Data from Table 5.35 of Wilhite [1986] for the Hiram No. 17 Well

	Depth				Permeability to air
Layer	Top	Bottom	h	Porosity	
	(ft)	(ft)	(ft)	(%)	(md)
1	2880	2881	1.00	28.9	1271
2	2881	2882	1.00	28.5	1239
3	2882	2883	1.00	28.1	1184

4	2883	2884	1.00	28.8	1891
5	2884	2885	1.00	27.9	1500
6	2885	2886	1.00	29.2	1271
7	2886	2887	1.00	29.0	1565
8	2887	2888	1.00	29.7	1325
9	2888	2889	1.00	27.4	967
10	2889	2890	1.00	27.8	717
11	2890	2891	1.00	28.0	728
12	2891	2892	1.00	22.2	554
13	2892	2893	1.00	20.3	130
14	2893	2894	1.00	21.5	218
15	2894	2895	1.00	25.5	466
16	2895	2896	1.00	24.9	684
17	2896	2897	1.00	27.2	600
18	2897	2898	1.00	23.7	336
19	2898	2899	1.00	21.9	150
20	2899	2900	1.00	22.0	277
21	2900	2901	1.00	19.4	78
22	2901	2902	1.00	17.4	101
23	2902	2903	1.00	18.4	82
24	2903	2904	1.00	16.7	82
25	2904	2905	1.00	16.9	49
26	2905	2906	1.00	17.1	36
27	2906	2907	1.00	15.9	23
28	2907	2908	1.00	16.5	20

29	2908	2909	1.00	13.0	0.1
30	2909	2910	1.00	16.8	56
31	2910	2911	1.00	17.3	49
32	2911	2912	1.00	17.8	26
33	2912	2913	1.00	17.8	33
34	2913	2914	1.00	15.6	26
35	2914	2915	1.00	17.4	36
36	2915	2916	1.00	17.3	42
37	2916	2917	1.00	16.8	33
38	2917	2918	1.00	16.6	39
39	2918	2919	1.00	17.2	52
40	2919	2920	1.00	16.9	56
41	2920	2921	1.00	15.2	33
42	2921	2922	1.00	16.1	46
43	2922	2923	1.00	17.4	36
44	2923	2924	1.00	14.8	29
45	2924	2925	1.00	15.7	33
46	2925	2926	1.00	15.7	23
47	2926	2927	1.00	15.6	33

Exercise 13.1B Plot normalized cumulative flow capacity versus depth on Cartesian paper.

Exercise 13.1C Complete the table below for up to ten flow units. List the depth to top and base of each flow unit that you identify from the plot in Part B.

Flow Unit	Depth to Top (ft)	Depth to Base (ft)
1		
2		
3		
4		
5		
6		
7		
8		
9		
10		

Exercise 13.2A Use Eq. (13.9) to calculate the equivalent well gridblock radius of a gridblock with $\Delta x = \Delta y = 300$ ft.

Exercise 13.2B Estimate shut-in time for Peaceman's correction using Eq. (13.7). Assume $\phi = 0.15$, $c_T = 1 \times 10^{-5}$ psia^{-1}, $\mu = 2$ cp and $K = 10$ md.

Exercise 13.3 Suppose the following physical properties apply to a pressure transient test in an oil well:

K = permeability = 150 md

ϕ = porosity = 0.20

μ = viscosity = 1.0 cp

c_T = total compressibility = 10×10^{-6} psia^{-1}

Calculate the radius of investigation at shut-in times of 0.5 day, 1 day, and 2 days.

Exercise 13.4 Suppose the following physical properties apply to a pressure transient test on a gas well:

K = permeability = 1.1 md

ϕ = porosity = 0.14

μ = viscosity = 0.016 cp

c_T = total compressibility = 5.4×10^{-4} $psia^{-1}$

Calculate the radius of investigation at shut-in times of 0.5 day, 1 day, and 2 days.

Exercise 13.5A Run VFILL3_WF.DAT. Report the oil, water and gas production rates and cumulative oil, water and gas production at the end of the run.

Exercise 13.5B Modify VFILL3_WF.DAT to use the permeabilities given in Table 13-6 and run the revised model. Report pressure; oil, water and gas production rates; and cumulative oil, water and gas production at 1460 days.

Exercise 13.5C Does the flow unit analysis have an affect?

Exercise 13.6A What is the equivalent radius of a gridblock with lateral permeabilities $K_x = K_y$ = 100 md and gridblock sizes $\Delta x = \Delta y$ = 200 ft.?

Exercise 13.6B Use the data in Part A to estimate the shut-in time for Peaceman's correction. Assume that porosity = 0.25, viscosity = 0.64 cp, and total compressibility = 1×10^{-4} /psia.

Chapter 14

Rock Properties

Rock properties significantly influence the production of hydrocarbons from porous media. For example, oil production from unconsolidated sandstone reservoirs in the Gulf of Mexico depends on the relationship between permeability and fluid pressure. One way to approximate this effect in a flow model is to combine porosity-permeability models with porosity-fluid pressure relationships. This chapter describes the role of rock properties in reservoir flow modeling.

14.1 Porosity

One of the most fundamental properties of rock that a reservoir flow model must include is porosity, which is the fraction of a porous medium that is void space. The bulk volume V_B of a porous medium is the sum of pore volume V_P and grain volume V_G, thus

$$V_B = V_P + V_G \tag{14.1}$$

Porosity is the ratio of pore volume to bulk volume:

$$\phi = V_P / V_B \tag{14.2}$$

Dividing Eq. (14.1) by V_B and using the definition of porosity expresses the grain volume in terms of porosity as

$$\frac{V_G}{V_B} = 1 - \phi \tag{14.3}$$

If the void space in a porous medium is connected and communicates with a wellbore, it is referred to as effective porosity. Void space that cannot communicate with the wellbore is considered ineffective porosity. The original porosity resulting from sediment deposition is called primary porosity. Secondary porosity is an incremental increase in primary porosity due to the chemical dissolution of reservoir rocks, especially carbonates. Primary and secondary porosity can be both effective and ineffective. Total porosity is a combination of ineffective porosity and effective (interconnected) porosity.

Porosity values depend on rock type, as shown in Table 14-1. There are two basic techniques for directly measuring porosity: core analysis in the laboratory and well logging. Laboratory measurements tend to be more accurate, but sample only a small fraction of the reservoir. Also, changes in rock properties can occur when the core is brought from the reservoir to the surface. Well log measurements sample a much larger portion of the reservoir than core analysis, but typically yield less accurate values. Ideally, a correlation can be established between *in situ* measurements such as well logging and surface measurements such as core analysis.

Table 14-1
Dependence of Porosity on Rock Type

Rock Type	Porosity Range (%)	Typical Porosity (%)
Sandstone	15-35	25
Unconsolidated sandstone	20-35	30
Carbonate		
• Intercrystalline limestone	5-20	15
• Oolitic limestone	20-35	25
• Dolomite	10-25	20

Porosity compressibility is a measure of the change in porosity ϕ as a function of fluid pressure P. It is defined as

$$c_\phi = \frac{1}{\phi}\frac{d\phi}{dP} \tag{14.4}$$

If ϕ_0 is porosity at pressure P_0 and ϕ is porosity at pressure P, the integral of Eq. (14.4) yields the relationship

$$\phi = \phi_0 \exp\left[\int_{P_0}^{P} c_\phi dP\right] \tag{14.5}$$

If porosity compressibility is constant with respect to pressure, the integral in Eq. (14.5) can be evaluated and gives

$$\phi = \phi_0 \exp\left[c_\phi \Delta P\right] \tag{14.6}$$

where $\Delta P = P - P_0$. The first order approximation to Eq. (14.6) is

$$\phi \approx \phi_0\left[1 + c_\phi \Delta P\right] = \phi_0\left[1 + c_\phi\left(P - P_0\right)\right] \tag{14.7}$$

Equation (14.7) is used in many reservoir flow simulators, including IFLO, to calculate the change in porosity with respect to changes in fluid pressure.

14.2 Permeability

The basic equation describing fluid flow in porous media is Darcy's Law. Darcy's equation for linear, horizontal, single-phase flow is

$$Q = -0.001127\frac{KA}{\mu}\frac{\Delta P}{\Delta x} \tag{14.8}$$

The physical variables are defined in oilfield units as

Q volume flow rate (bbl/day)

K permeability (md)

A cross-sectional area (ft^2)

ΔP change in pressure (psi)

μ fluid viscosity (cp)

Δx length (ft)

Equation (14.8) shows that the movement of a single-phase fluid through a porous medium depends on cross-sectional area, pressure difference ΔP, length Δx of the flow path, and viscosity of the flowing fluid. The minus sign indicates that the direction of fluid flow is opposite to the direction of increasing pressure: the fluid flows from high pressure to low pressure in a horizontal (gravity-free) system. The proportionality constant in Eq. (14.8) is permeability.

Darcy's Law correctly describes laminar flow, and may be used as an approximation of turbulent flow. Permeability calculated from Darcy's Law is less than true rock permeability at turbulent flow rates. The linearity of Darcy's Law is an approximation that is made by virtually all commercial simulators. Fluid flow in a porous medium can have a nonlinear effect that is represented by the Forchheimer equation [Govier, 1978]. The nonlinear effect becomes more important in high flow rate environments such as some gas wells and in hydraulic fracturing [Barree and Conway, 2005].

Permeability is a measure of the connectivity of pore spaces. If we perform a dimensional analysis, we see that permeability has dimensions of L^2 where L is a unit of length. The areal unit (L^2) is physically related to the cross-sectional area of pore throats in rock.

A Micro Scale measurement of grain-size distribution shows that different grain sizes and shapes affect permeability. Permeability may be viewed as a mathematical convenience for describing the statistical behavior of a given flow experiment. In this context, transient testing gives the best measure of permeability over a large volume. Despite their importance to the calculation of flow, permeability and its distribution will not be known accurately. Seismic data can help define the distribution of permeability between wells if a good correlation exists between seismic amplitude and a rock quality measurement that includes permeability.

Permeability depends on rock type. The two most common reservoir rock types are clastic reservoirs and carbonate reservoirs. The

permeability in a clastic reservoir depends on pore size and is seldom controlled by secondary solution vugs. Compacted and cemented sandstone rocks tend to have lower permeabilities than clean, unconsolidated sands. Productive sandstone reservoirs usually have permeabilities in the range of 10 md to 1000 md. The permeability in tight gas and coalbed methane reservoirs is less than 1 md.

Carbonate reservoirs are generally less homogeneous than clastic reservoirs and have a wider range of grain size distributions. The typical matrix permeability in a carbonate reservoir tends to be relatively low. Significant permeability in a carbonate reservoir may be associated with secondary porosity features such as vugs and oolites.

The presence of clay can adversely affect permeability. Clay material may swell on contact with fresh water, and the resulting swelling can reduce a rock's permeability by several orders of magnitude.

In many cases vertical permeability is not measured and must be assumed. A rule of thumb is to assume that vertical permeability is approximately one tenth of horizontal permeability. This is a reasonable assumption when there is no data to the contrary.

Natural or manmade fractures can significantly increase flow capacity in both carbonate and clastic reservoirs. An extensive natural fracture system can provide high flow capacity conduits for channeling flow from the reservoir matrix to a wellbore. Naturally fractured reservoirs are usually characterized by relatively high permeability, low porosity fractures and relatively low permeability, high porosity matrix. Most of the fluid is stored in the matrix, while flow from the reservoir to the wellbore is controlled by permeability in the fracture system.

14.2.1 Directional Permeability

Permeability can be a complex function of spatial location and orientation. Spatial and directional variations of a function are described in terms of homogeneity, heterogeneity, isotropy, and anisotropy. If the value of a function does not depend on spatial location, it is called homogeneous. The function is heterogeneous if its value changes from one

spatial location to another. If the value of a function depends on directional orientation, i.e. the value is larger in one direction than another, than the function is anisotropic. The function is isotropic if its value does not depend on directional orientation. Permeability is a function that can be both heterogeneous and anisotropic. To account for heterogeneity and anisotropy, the simple 1-D form of Darcy's Law must be generalized. The discussion below closely follows the presentation in Chapter 4 of Fanchi [2000].

In general, flow occurs in dipping beds. To account for the effect of gravity, we define a variable called the potential of phase as

$$\Phi = P - \gamma\,(\Delta z) \tag{14.9}$$

where Δz is depth from a datum, P is the pressure of phase and γ is the pressure gradient associated with the gravity term. If we write Darcy's Law for single phase flow in the form

$$q = -\frac{0.001127KA}{\mu}\frac{d\Phi}{dz} \tag{14.10}$$

we find that no vertical movement can occur when $d\Phi/dz = 0$. Thus, Eq. (14.10) expresses the movement of fluids in a form that accounts for gravity equilibrium.

Darcy's Law in one dimension says that rate is proportional to pressure gradient. This can be extended to three dimensions using vector notation. Darcy's Law for single phase flow in three dimensions is

$$\begin{aligned} q_x &= -0.001127K\frac{A}{\mu}\frac{\partial\Phi}{\partial x} \\ q_y &= -0.001127K\frac{A}{\mu}\frac{\partial\Phi}{\partial y} \\ q_z &= -0.001127K\frac{A}{\mu}\frac{\partial\Phi}{\partial z} \end{aligned} \tag{14.11}$$

where the gradient of potential accounts for gravity effects. In vector notation we have

$$q = -0.001127K\frac{A}{\mu}\nabla\Phi \tag{14.12}$$

Equation (14.11) can be written in matrix notation as

$$\begin{bmatrix} q_x \\ q_y \\ q_z \end{bmatrix} = -0.001127K\frac{A}{\mu}\begin{bmatrix} \partial\Phi/\partial x \\ \partial\Phi/\partial y \\ \partial\Phi/\partial z \end{bmatrix} \tag{14.13}$$

where permeability K and cross-sectional area A are treated as constants with respect to direction. A more general extension of Eq. (14.13) is

$$\begin{bmatrix} q_x \\ q_y \\ q_z \end{bmatrix} = -0.001127\frac{A}{\mu}\begin{bmatrix} K_{xx} & K_{xy} & K_{xz} \\ K_{yx} & K_{yy} & K_{yz} \\ K_{zx} & K_{zy} & K_{zz} \end{bmatrix}\begin{bmatrix} \partial\Phi/\partial x \\ \partial\Phi/\partial y \\ \partial\Phi/\partial z \end{bmatrix} \tag{14.14}$$

where permeability is now treated either as a 3×3 matrix with nine elements or as a tensor of rank two [Fanchi, 2006]. The diagonal permeability elements $\{K_{xx}, K_{yy}, K_{zz}\}$ represent the usual dependence of rate in one direction on pressure differences in the same direction. The off-diagonal permeability elements $\{K_{xy}, K_{xz}, K_{yx}, K_{yz}, K_{zx}, K_{zy}\}$ account for the dependence of rate in one direction on pressure differences in orthogonal directions. Expanding Eq. (14.14) gives the corresponding set of equations that demonstrates this dependence:

$$\begin{aligned} q_x &= -0.001127\frac{A}{\mu}\left[K_{xx}\frac{\partial\Phi}{\partial x} + K_{xy}\frac{\partial\Phi}{\partial y} + K_{xz}\frac{\partial\Phi}{\partial z}\right] \\ q_y &= -0.001127\frac{A}{\mu}\left[K_{yx}\frac{\partial\Phi}{\partial x} + K_{yy}\frac{\partial\Phi}{\partial y} + K_{yz}\frac{\partial\Phi}{\partial z}\right] \\ q_z &= -0.001127\frac{A}{\mu}\left[K_{zx}\frac{\partial\Phi}{\partial x} + K_{zy}\frac{\partial\Phi}{\partial y} + K_{zz}\frac{\partial\Phi}{\partial z}\right] \end{aligned} \tag{14.15}$$

In many practical situations it is mathematically possible to find a coordinate system $\{x', y', z'\}$ in which the permeability tensor has the diagonal form

$$\begin{bmatrix} K_{x'x'} & 0 & 0 \\ 0 & K_{y'y'} & 0 \\ 0 & 0 & K_{z'z'} \end{bmatrix}$$

The coordinate axes $\{x', y', z'\}$ are called the principal axes of the tensor and the diagonal form of the permeability tensor is obtained by a principal axis transformation. The flow equations along the principal axes are

$$\begin{aligned} q_{x'} &= -0.001127 \frac{A}{\mu}\left[K_{x'x'}\frac{\partial \Phi}{\partial x'}\right] \\ q_{y'} &= -0.001127 \frac{A}{\mu}\left[K_{y'y'}\frac{\partial \Phi}{\partial y'}\right] \\ q_{z'} &= -0.001127 \frac{A}{\mu}\left[K_{z'z'}\frac{\partial \Phi}{\partial z'}\right] \end{aligned} \tag{14.16}$$

The principal axes in a field can vary from one point of the field to another because of permeability heterogeneity.

The form of the permeability tensor depends on the properties of the porous medium. The medium is said to be anisotropic if two or more elements of the diagonalized permeability tensor are different. The permeability of the medium is isotropic if the elements of the diagonalized permeability tensor are equal, that is

$$K_{x'x'} = K_{y'y'} = K_{z'z'} = K \tag{14.17}$$

If the medium is isotropic, permeability does not depend on direction. If the isotropic permeability does not change from one position in the medium to another, the medium is said to be homogeneous in permeability. On the other hand, if the values of the elements of the permeability tensor vary from one point in the medium to another, both the permeability tensor and the medium are considered heterogeneous. Virtually all reservoirs exhibit some degree of anisotropy and heterogeneity, but the flow

behavior in many reservoirs can be approximated as homogeneous and isotropic. In Figure 14-1, Part A is a sketch of the drainage area of four production wells with isotropic permeability, and Part B is a sketch of the drainage area of four production wells with anisotropic permeability.

When a model is being designed, the modeling team should account for the direction associated with permeability. In principle, simulators can take all of these effects into account. In practice, however, the tensor permeability discussed in the literature by, for example, Bear [1972], Lake [1988] or King and Mansfield [1999], is seldom included in a reservoir simulator. The usual assumption is that permeability is aligned along one of three orthogonal directions known as the principal axes of the tensor. This assumption has implications for model studies that should be considered when assessing model results (see Fanchi [1983]).

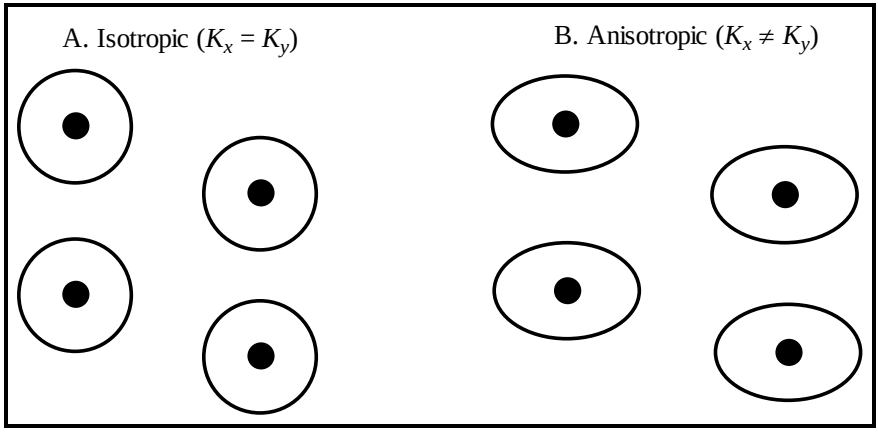

Figure 14-1. Illustration of the Effect of Permeability Anisotropy on Drainage Area

14.3 Porosity-Permeability Models

Models relating permeability to porosity are often based on networks of capillary tubes or the concept of hydraulic radius. This section reviews examples of porosity-permeability models from the literature and then generalizes them for use in a reservoir simulator.

14.3.1 Capillary Tube Model

Flow of a fluid with viscosity μ through a capillary tube with radius r, porosity ϕ, cross-sectional area A and length L is given by Poiseuille's equation for viscous flow in a circular conduit. The permeability K_{cap} of the capillary tube is

$$K_{cap} = \phi \frac{r^2}{8} \tag{14.18}$$

14.3.2 Hydraulic Radius Model

Hydraulic radius r_h is the ratio of pore volume V_P to pore surface area S_P:

$$\begin{aligned} r_h &= V_P / S_P \\ &= \phi V_B / S_P \end{aligned} \tag{14.19}$$

where V_B is the bulk volume of the sample [Guéguen and Palciauskas, 1994]. Defining specific surface area S as the pore surface area divided by the sample bulk volume,

$$S = S_P / V_B \tag{14.20}$$

the hydraulic radius becomes

$$r_h = \phi / S \tag{14.21}$$

If we assume the permeability of the medium can be approximated as a capillary tube with radius r_h, then we can use Eq. (14.18) to write

$$\begin{aligned} K &= B\phi r_h^2 \\ &= B\frac{\phi^3}{S^2} \end{aligned} \tag{14.22}$$

where B is a constant that represents the model geometry. For a cylindrical tube that satisfies Poiseuille's equation we have $B = 1/8$.

14.3.3 Kozeny- Carman Model

The relationship between K and ϕ^3 in Eq. (14.22) is an example of a Kozeny-Carman relation. If we assume the porous medium is a packing of spheres with diameter d, we have [Mavko, et al., 1998]

$$S = \frac{3}{2}\frac{(1-\phi)}{d} \tag{14.23}$$

and Eq. (14.22) becomes

$$K = B'\frac{\phi^3 d^2}{(1-\phi)^2} \tag{14.24}$$

where the constant 3/2 is absorbed in the new proportionality constant B'.

According to the percolation model, porosity below a percolation porosity ϕ_c does not contribute to flow. The percolation effect is taken into account by replacing ϕ with ϕ - ϕ_c in the Kozeny-Carman relation. The result is

$$K = B''(\phi - \phi_c)^3 d^2 \tag{14.25}$$

where B'' is a new proportionality constant.

Equations (14.18), (14.24) and (14.25) suggest that permeability and porosity are related by the proportionality

$$K \propto \phi^n \tag{14.26}$$

where n has been observed to vary from $n \leq 2$ to $n \geq 7$. Equation (14.26) is a power law relationship between permeability and porosity that is suitable for use in a reservoir simulator. A more generalized algorithm relating porosity and permeability is presented below.

14.3.4 Porosity-Permeability Crossplots

The permeability models described above are idealized physical models. Measurements of porosity and permeability distributions in fields around the world have shown that porosity and permeability are

correlated. The statistical distribution of porosity is often the normal (or Gaussian) distribution, and the statistical distribution of permeability is often log normal. Two empirical relationships between porosity and permeability have been observed and are widely used: the semilog crossplot, and the log-log crossplot. The plot of porosity versus permeability is often referred to as a phi-k crossplot.

It is often necessary to use linear regression to quantify the straight line segments of a phi-k crossplot because there is a considerable amount of scatter in data plotted from real fields. The log-log model is obtained by fitting a regression line to a plot of the logarithm of porosity versus a logarithm of permeability. Permeability is related to porosity in the log-log model by

$$K = \alpha_1 \phi^{b_1} \tag{14.27}$$

with regression constants α_1 and b_1. If we specify a permeability K_0 corresponding to a porosity ϕ_0, Eq. (14.27) becomes

$$K_0 = \alpha_1 \phi_0^{b_1} \tag{14.28}$$

Dividing Eq. (14.27) by (14.28) shows that the log-log model satisfies

$$\frac{K}{K_0} = \left(\frac{\phi}{\phi_0} \right)^{b_1} \tag{14.29}$$

Equation (14.29) is a power law relationship similar to Eq. (14.26). The use of a reference permeability K_0 and porosity ϕ_0 lets us replace the proportionality in Eq. (14.26) with the equality in Eq. (14.29).

The semilog model is obtained by fitting a regression line to a plot of porosity versus the logarithm of permeability. In the semilog model, permeability is related to porosity by

$$K = \alpha_2 \exp\left(b_2 \phi\right) \tag{14.30}$$

where α_2 and b_2 are constants determined by the regression analysis. If we specify a permeability K_0 corresponding to a porosity ϕ_0, Eq. (14.30) becomes

$$K_0 = \alpha_2 \exp\left(b_2 \phi_0\right) \tag{14.31}$$

Dividing Eq. (14.30) by (14.31) shows that the semilog model satisfies

$$\frac{K}{K_0} = \exp\left[b_2\left(\phi - \phi_0\right)\right] \tag{14.32}$$

Equations (14.29) and (14.32) can be represented in a single algorithmic form as

$$\frac{K}{K_0} = a_1\left(\frac{\phi}{\phi_0}\right)^{b_1} + a_2 \exp\left[b_2\left(\phi - \phi_0\right)\right] \tag{14.33}$$

where K_0 is the permeability corresponding to porosity ϕ_0, and the coefficients $\{a_1, a_2, b_1, b_2\}$ are determined empirically. Equation (14.33) is a generalized porosity-permeability relationship.

14.4 Permeability-Porosity-Fluid Pressure Relationships

The dependence of permeability on fluid pressure is specified through the dependence of porosity on fluid pressure. Beginning with fundamental definitions, we obtain a relationship between porosity and fluid pressure that is similar to the result obtained by McKee, et al. [1988]. The porosity-fluid pressure relationship of interest here is

$$\phi = \phi_0 \frac{\exp \int_{P_0}^{P} \left(\frac{c_\phi}{1-\phi}\right) dP}{1 - \phi_0\left[1 - \exp \int_{P_0}^{P} \left(\frac{c_\phi}{1-\phi}\right) dP\right]} \tag{14.34}$$

If porosity compressibility and porosity change slowly with respect to fluid pressure, Eq. (14.34) may be written as

$$\phi = \phi_0 \frac{\exp[c_\phi (P - P_0)]}{1 - \phi_0\{1 - \exp[c_\phi (P - P_0)]\}} \tag{14.35}$$

Equation (14.35) can be written to first order in the pressure change as

$$\begin{aligned}\phi &= \phi_0 \frac{\exp[c_\phi (P - P_0)]}{1 - \phi_0 \{1 - \exp[c_\phi (P - P_0)]\}} \\ &\approx \phi_0 \exp\left[c_\phi \left(P - P_0\right)\right] \approx \phi_0 \left[1 + c_\phi \left(P - P_0\right)\right]\end{aligned} \tag{14.36}$$

Notice that Eq. (14.36) is in agreement with Eq. (14.7). By calculating changes in porosity as a function of changes in fluid pressure, we can use porosity-permeability relationships such as Eq. (14.33) to estimate the change in permeability as a result of a change in fluid pressure. Authors such as McKee, et al. [1988], Soares, et al. [2002], Reyes and Osisanya [2002], Raghavan and Chin [2004], and Schutjens, et al. [2004] provide additional discussion of the dependence of permeability on stress. Many porosity-permeability relationships have been published in the literature. For example, Nelson [2004] describes a catalog of porosity-permeability data sets for sandstones, and Jennings and Lucia [2003] present porosity-permeability relationships for carbonates.

14.5 IFLO Geomechanical Model

The geomechanical model in IFLO can be used to estimate geomechanical parameters. The calculation of geomechanical parameters makes it possible to include pressure-dependent changes to permeability in well and transmissibility calculations. This section describes the IFLO geomechanical model.

14.5.1 Poisson's Ratio and Young's Modulus

Poisson's ratio ν is calculated as

$$\nu = \frac{0.5 V_P^2 - V_S^2}{V_P^2 - V_S^2} \tag{14.37}$$

where V_P is compressional or *P*-wave velocity, and V_S is shear or *S*-wave velocity. Young's modulus *E* is calculated from Poisson's ratio as

$$E = 2(1+\nu)\mu \tag{14.38}$$

where μ is shear modulus.

Dynamic measurements of Young's modulus and Poisson's ratio are approximations of the static values needed for geomechanical calculations. To obtain static values for Young's modulus and Poisson's ratio, a conversion calculation must be made [Wang, 2000; Tiab and Donaldson, 2003]. The dynamic to static conversion algorithm for Young's modulus E is

$$\begin{aligned} E_s &= aE_d^b + c \\ a &= a_1 + a_2 \log(P_e) \\ b &= b_1 + b_2 \log(P_e) \end{aligned} \tag{14.39}$$

where subscript s denotes static and subscript d denotes dynamic. The coefficients $\{a, a_1, a_2, b, b_1, b_2, c\}$ are empirical fit parameters, and P_e is effective pressure. An analogous dynamic to static conversion algorithm may be specified for Poisson's ratio.

14.5.2 Uniaxial Compaction, Horizontal Stress and Fracture Gradient

Uniaxial compaction Δh is estimated using

$$\Delta h = \frac{1}{3}\left(\frac{1+\nu}{1-\nu}\right)\phi c_\phi h_{net} \Delta P \tag{14.40}$$

where h_{net} is net thickness, ϕ is porosity, c_ϕ is porosity compressibility, and the change in pore pressure is $\Delta P = P - P_{init}$. Pore pressure is set equal to the fluid pressure being used as a primary variable in the solution of the fluid flow equations.

Total horizontal stress σ_H is estimated as

$$\sigma_H = \frac{\nu}{1-\nu}(P_{con} - \alpha P) + \alpha P \tag{14.41}$$

with the Biot coefficient correction factor

$$\alpha = 1 - (1 - \phi)\left(\frac{K^*}{K_m}\right)^n \tag{14.42}$$

Fracture gradient γ_F is estimated as [Tiab and Donaldson, 2003]

$$\gamma_f = \frac{\nu}{1+\nu}\frac{P_{con}}{z} \tag{14.43}$$

14.5.3 Permeability-Porosity-Fluid Pressure Algorithm

The dependence of permeability on fluid pressure is made explicit by substituting Eq. (14.36) into Eq. (14.33) to obtain

$$\frac{K}{K_0} = a_1\left[1 + c_\phi\left(P - P_0\right)\right]^{b_1} + a_2 \exp\left[b_2\phi_0 c_\phi\left(P - P_0\right)\right] \tag{14.44}$$

The coefficients $\{a_1, a_2, b_1, b_2\}$ are determined empirically. Equation (14.44) is an algorithm that relates permeability, porosity and fluid pressure. The effect of pressure on permeability may be included in the calculation of well productivity index and transmissibility.

14.6 IFLO Application: Geomechanics and Compaction

Geomechanical properties give us insight into the behavior of the structure of the reservoir and the impact of structural changes on fluid flow. The conventional approach to coupling geomechanics and fluid flow is to solve two sets of nonlinear equations representing fluid flow and geomechanical deformation [Settari, et al., 2001; Settari [2002]; Yale, 2002; Tran, et al., 2002; Dean, et al., 2003]. The solution techniques range from full coupling in which both sets of equations are solved simultaneously at each timestep to varying degrees of partial coupling.

The relative merits of coupled versus uncoupled formulations have been discussed in the literature. Yale [2002] argues that tight coupling between geomechanical and fluid flow models can more accurately account for the effect of heterogeneity, anisotropy and inelastic deformation on fluid flow if there is enough information to properly characterize the algorithms used in a tightly coupled fluid flow simulator. Dean, et al. [2003] evaluated the degree of coupling for four sample problems and concludes that the "coupling techniques produce similar results and one's selection of a technique is determined by ease of implementation, program availability, numerical stability, and computational efficiency. No technique worked best on all four problems."

An important practical problem with the routine inclusion of geomechanical calculations in reservoir management studies is that conventional geomechanical simulators require a substantial increase in computer processing time to perform both geomechanical calculations and fluid flow calculations. Furthermore, geomechanical algorithms require input data that may not be available. Geomechanical calculations made by the integrated flow model IFLO minimize these issues because the IFLO geomechanical algorithm requires little incremental computer processing time and requires minimal additional input data [Fanchi, 2003a, 2003c]. To achieve these objectives, the IFLO compaction calculation relies on simplifying physical assumptions. Conventional geomechanical models include the compacting reservoir deformation effects shown in the upper half of Figure 14-2, namely surface extension, compression, and reservoir compaction. The IFLO compaction model approximates all of these effects as uniaxial compaction of the reservoir, which is sketched in the lower half of Figure 14-2. The goal of this application is to discuss the validity of the IFLO compaction model approximation.

The traditional formulation of a flow simulator with a pressure dependent porosity does include the calculation of geomechanical effects associated with the effect of changing pressure on porosity. This calculation depends on the rock compressibility term. The traditional formulation of a black oil simulator assumes that rock compressibility is satisfactorily represented by porosity compressibility. The IFM solution

technique is an explicit coupling technique that uses information from the flow equations to calculate geomechanical properties. An indication of the accuracy of the explicitly coupled geomechanical calculation in the integrated flow model (IFM) is determined by comparing IFM results with results reported by Dean, et al. [2003].

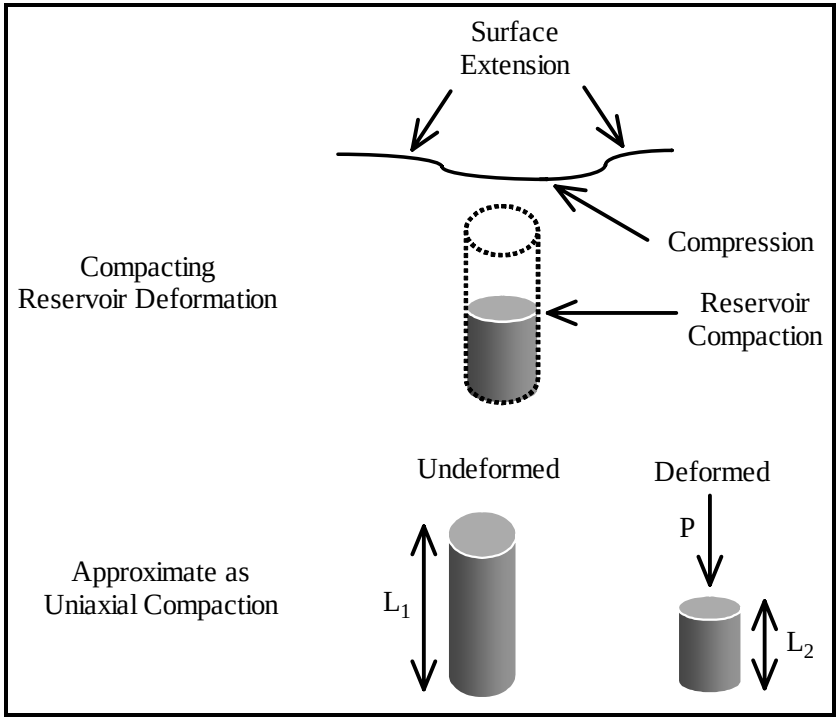

Figure 14-2. Schematic of Reservoir Compaction Features

14.6.1 ACRES

Dean, et al [2003] compared three techniques for coupling flow in porous media and geomechanical displacements associated with changes in stress in the system. The three techniques are explicit coupling, iterative coupling and full coupling. The explicit coupling technique calculates fluid flow every timestep, but geomechanical displacements only during selected timesteps. This allows flow calculations to be performed on a shorter time scale than geomechanical displacement

calculations. The iterative coupling technique performs a sequential calculation of fluid flow and geomechanical displacement. The fully coupled technique simultaneously calculates fluid flow and geomechanical displacements. All three coupling options were contained in the ARCO Comprehensive Reservoir Simulator (ACRES), that was provided to Dean, et al. by BP. ACRES used an IMplicit Pressure Explicit Mass (IMPEM) calculation procedure.

14.6.2 Comparison Problem

The comparison problem considered here is Problem 4 in Dean, et al. [2003]. This problem is a waterflood of an initially undersaturated oil reservoir that does not have enough pressure support to prevent the formation of a mobile, free gas phase. A three-phase, black oil simulator must be used to model all of the flow mechanisms that occur in the system.

The flow model covers one quadrant of a 5-spot pattern. A vertical oil production well is in one corner of the grid and a vertical water injection well is in the diagonally opposite corner (Figure 14-3). The grid contains 21×21×11 gridblocks. The lengths of each side of the gridblock are $\Delta x = \Delta y = 60\,\text{ft}$, $\Delta z = 20\,\text{ft}$. The top of the grid is at a depth of 4000 ft.

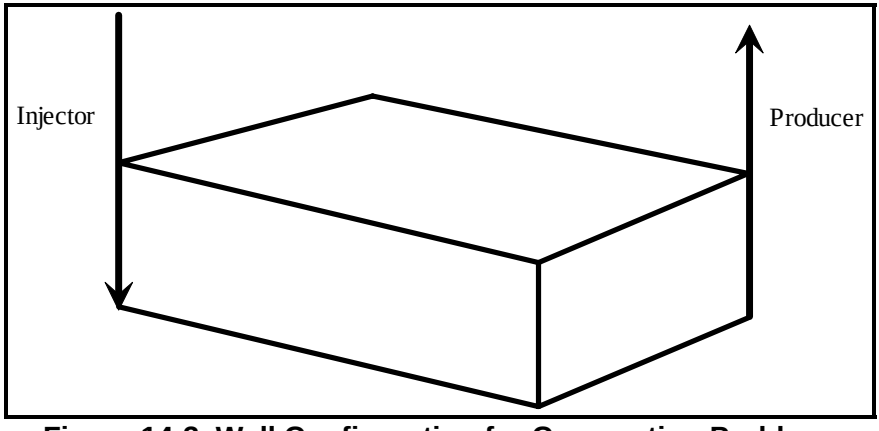

Figure 14-3. Well Configuration for Compaction Problem

Dean, et al. [2003] defined the following petrophysical parameters for this problem: Poisson's ratio ν is 0.35, elastic (Young's) modulus E is 5×10^4 psia, and grain density is 2.7 g/cc. Rock compressibility is 4.15×10^{-5} / psia. Dry frame bulk modulus was calculated using

$$K = E\left[\frac{1-\nu}{(1+\nu)(1-2\nu)}\right] - \frac{4}{3}\mu \tag{14.45}$$

where shear modulus μ was calculated as

$$\mu = \frac{E}{2(1+\nu)} \tag{14.46}$$

The dry frame bulk modulus for the IFLO petrophysical algorithm was calculated to be 5.56×10^4 psia, and the corresponding shear modulus is 1.85×10^4 psia. Although the IFLO calculation can use fluid substitution, conventional geomechanical flow simulators cannot, so grain modulus was set equal to dry frame bulk modulus in IFLO for this application.

14.6.3 Initial Conditions

Reservoir pressure is 3010 psi at a depth of 4010 ft. Reservoir porosity is 30%. Reservoir permeability varies by layer. Starting at the top layer, horizontal permeability for each layer is 5 md, 100 md, 20 md, 20 md, 20 md, 100 md, 20 md, 20 md, 100 md, 20 md and 20 md. Vertical permeabilities are 0.01 times horizontal permeabilities.

The reservoir is undersaturated with oil, water and gas saturations equal to 80%, 20% and 0% respectively. The bubble point pressure of the oil is 3000 psi. Details of fluid properties and rock-fluid interaction properties are presented in Dean, et al. [2003].

The water injection well in the model had a prescribed water injection rate of 500 STB/day and the production well in the Dean, et al. model had a prescribed liquid production rate of 750 STB/day. IFLO does not have a liquid production rate option, but it does have a fluid production rate option. Consequently, the IFLO model used a prescribed fluid production rate of 750 STB/day. The two production well options

are equivalent as long as mobile water production is negligible. Therefore, the different models were compared for the equivalent period of time prior to water breakthrough at the production well, which was approximately 4000 days.

14.6.4 Model Results

Results presented by Dean, et al. [2003] showed that reservoir pressure declined from the beginning of the run. The pressure decline caused the reservoir pressure to go quickly below bubble point pressure, even though water injection began immediately. Consequently, a free gas phase appeared early in the production period. Figures 14-4 and 14-5 compare model pressure and gas-oil ratio (GOR). IFLO results are identified in the figures by the acronym "IFM". The figures show that the flow calculations for each of the simulators match during the 4000-day production period prior to water breakthrough at the production well.

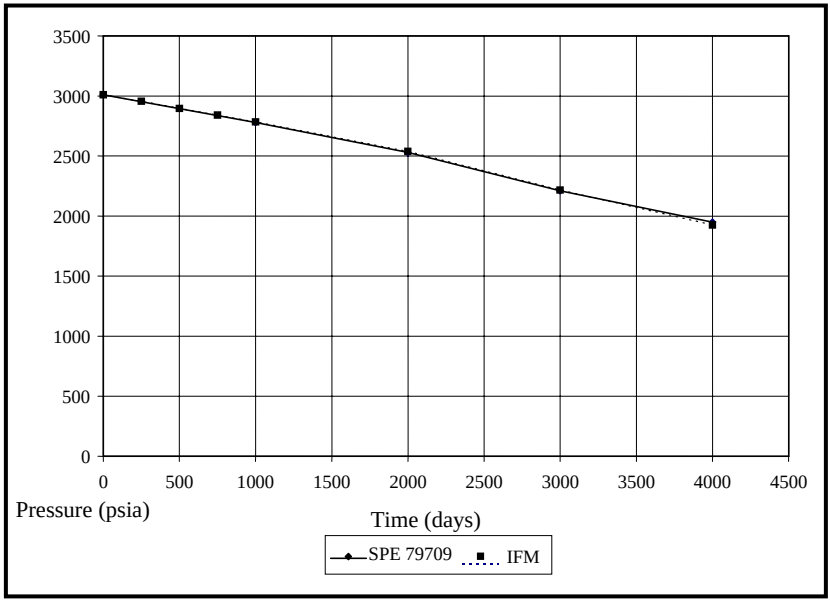

Figure 14-4. Comparison of Model Pressure

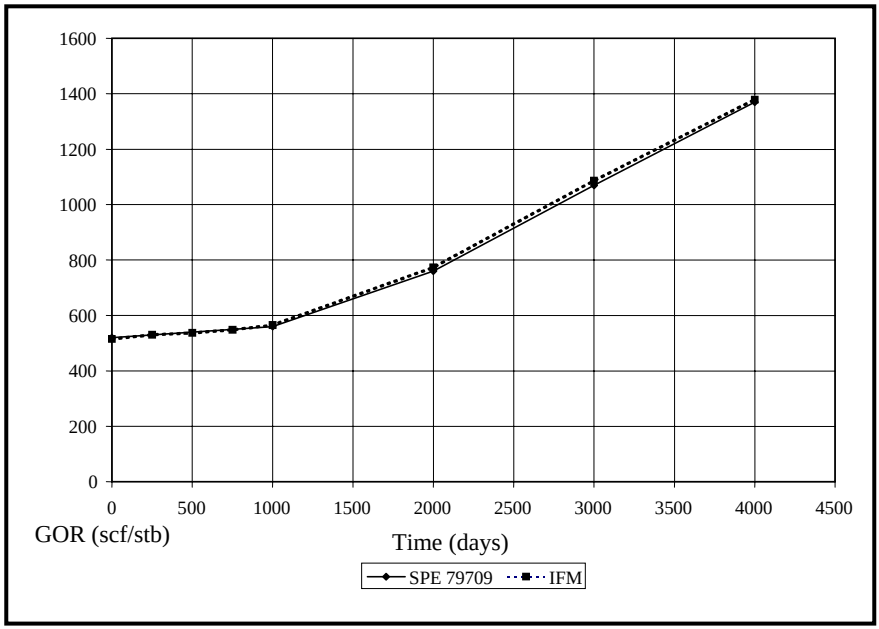

Figure 14-5. Comparison of Model GOR

Figure 14-6 compares model calculated compaction for the production well column [private communication from R.H. Dean, 7 March 2004]. The IFLO compaction in the production well column is approximately 80% of the compaction calculated by ACRES after 4000 days of production.

The average compaction of each layer of gridblocks in IFLO is calculated as the average compaction of all gridblocks in the layer. The sum of these layer average compaction values gives the average compaction calculated by IFLO. Figure 14-7 compares the average compaction of IFLO to the uniaxial compaction calculated using Eq. (14.40), the set of constant petrophysical parameters defined by Dean, et al. [2003], and pore volume weighted average reservoir pressure from IFLO. IFLO compaction results are comparable to results that would be calculated using a uniaxial compaction approximation.

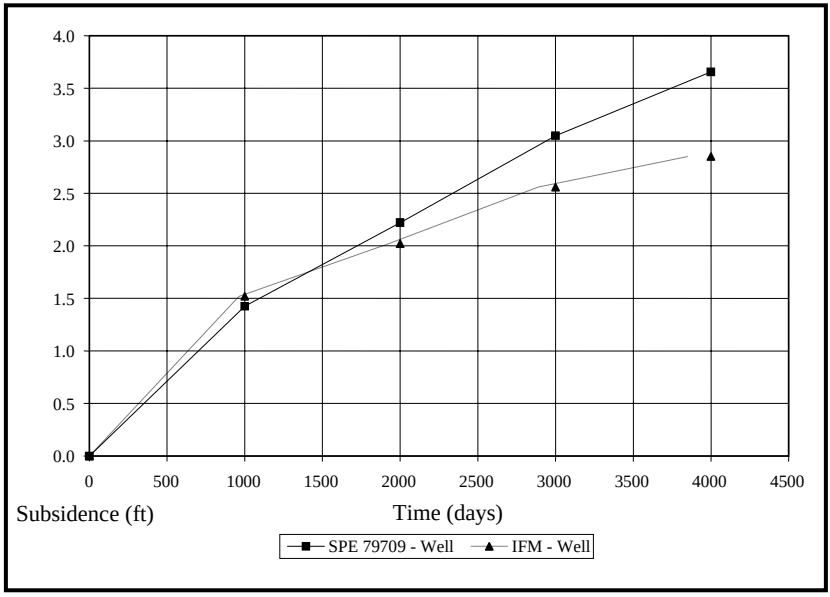

Figure 14-6. Comparison of Compaction of the Production Well Column

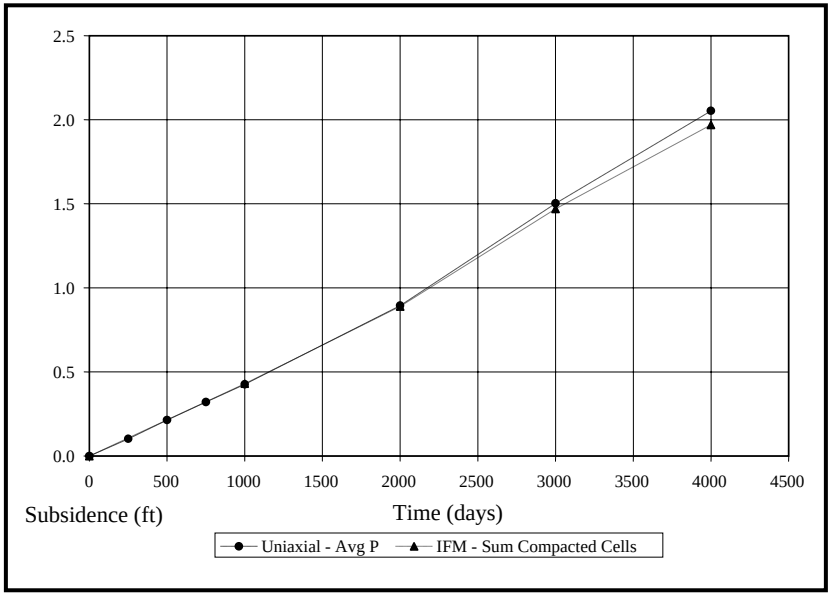

Figure 14-7. Uniaxial Compaction

Exercises

Exercise 14.1 Derive Eq. (14.5).

Exercise 14.2 A sandstone core sample is cleanly cut and carefully measured in a laboratory. The cylindrical core has a length of 3 inches and a diameter of 0.75 inch. The core is dried and weighed. The dried core weighs 125.00 grams. The core is then saturated with fresh water. The water saturated core weighs 127.95 grams. Determine the porosity of the sandstone core. Neglect the weight of air in the dried core and assume the density of water is 1 g/cc.

Exercise 14.3A Consider a cylindrical core plug that has a radius of 0.5 in. and a length of 2 in. Suppose the core is flooded with an oil that has viscosity = 0.5 cp, formation volume factor = 1.0 RB/STB, and a measured flow rate = 0.1 BOPD (barrel of oil per day). If the pressure drop from the inlet to the outlet is 20 psia, what is the permeability of the plug? Hint: Express area A in sq. ft. and length L in ft. Solve Darcy's Law for permeability. Recall that Darcy's Law is

$$Q = \frac{0.001127\, k\, A \Delta P}{L\, \mu\, B}$$

where permeability k is in md, area A is in sq. ft., pressure P is in psia, length L is in ft, viscosity μ is in cp, formation volume factor B is in reservoir volume per surface volume, and flow rate Q is in BOPD.

Exercise 14.3B Suppose that water (viscosity = 1.0 cp, FVF = 1.0 RB/STB) was used instead of oil in Part A. Use the permeability calculated in Part A to estimate the water flow rate. We are assuming that the permeability to single phase flow of water is the same as the permeability to single phase flow of oil.

Exercise 14.4 The pressure at an injection well is 3000 psia and the pressure at a production well is 1500 psia. The injection well and production well are separated by a distance of 1000 ft. Mobile fluid in the reservoir

between the injection well and the production well has a viscosity of 0.9 cp. The net thickness of the reservoir is 15 ft and the effective width of the reservoir is 500 ft. Use Darcy's Law to fill in the following table.

Permeability	**Flow Rate from Injector to Producer**
(md)	**(bbl/day)**
1	
10	
100	
1000	

Exercise 14.5A Problem # 4 in Dean, et al. [2003] is an eleven-layer model. The model layers have the following thicknesses and permeabilities:

Layer	**Thickness (ft)**	**Permeability (md)**
1	20	5
2	20	100
3	20	20
4	20	20
5	20	20
6	20	100
7	20	20
8	20	20
9	20	100
10	20	20
11	20	20

A simple method for coarsening (or upscaling) the eleven-layer model to four layers is to treat the layers as parallel beds. We can then estimate the

average permeability of each coarsened layer using the thickness weighted average

$$K_{avg} = \frac{\sum_k h_k K_k}{\sum_k h_k}$$

where K_k is the permeability of layer k and h_k is the net thickness of layer k. Use the above information to fill in the following table:

Layer	**Thickness (ft)**	**Average Permeability (md)**
1	55	
2	55	
3	55	
4	55	

Exercise 14.5B Calculate the averages and standard deviations of the permeabilities in the eleven-layer model and in the four-layer model. Compare the averages and standard deviations of the permeabilities for the two models.

Exercise 14.6 File GEOMECH_COARSE.DAT is a four-layer version of Problem # 4 in Dean, et al. [2003]. Run input data file GEOMECH_COARSE.DAT. Report average reservoir pressure, oil production rate, water production rate, gas production rate, and uniaxial compaction in the production well column (I = 21, J = 21) at 4000 days. Is compaction important in this problem?

Exercise 14.7 File GEOMECH_PID.DAT is the same as file GEOMECH_COARSE.DAT except that file GEOMECH_PID.DAT also allows the permeability in the well productivity index calculation to depend on pressure. Run input data file GEOMECH_PID.DAT. Report average reservoir pressure, oil production rate, water production rate, gas

production rate, and uniaxial compaction in the production well column ($I = 21$, $J = 21$) at 4000 days. Is pressure-dependent permeability important in this problem?

Chapter 15

Distributing Rock Properties

Reservoir rock properties are distributed by contouring and digitizing geologic maps. The mapping-contouring process is the point where the geological and geophysical interpretations have their greatest impact on the final representation of the reservoir. This chapter discusses methods for distributing rock properties.

15.1 Types of Flow Models

The distribution of rock properties depends on the type of flow model that will be used. Flow models may be classified into three different types: full field models, sector or window area models, and conceptual models. Full field models are used to match performance of the entire field. They take into account the interaction between all wells and layers. The disadvantage of using full field models is that the number of gridblocks may need to be large or the grid size may need to be relatively coarse to include the entire field.

Sector or window area models are designed to look at smaller areas of the field. In the following, we use the term *window area model* as a synonym for both sector models and window area models. Window area models are often constructed from a full field description. They allow finer grid resolution or shorter turnaround time if the model runs faster than a full field model. The window area models are useful for

studying recovery mechanisms and for determining reasonable grid preparation criteria for use in full field models, especially with regard to layering. Full field models require sufficient layering to track fluid contact movement or other depth dependent information that is needed to achieve study objectives. Window area models have the disadvantage of not being able to model flux accurately across window area boundaries. This means that effects of wells outside the window area are not accounted for except through boundary conditions. Some commercial simulators will output time-dependent boundary conditions for use in window area models. Although this information is helpful, the process is does not necessarily yield accurate results. Field history can be used to guide development of the window area model, but has only limited utility as a criterion for validating window model performance. Heinemann [1995] has discussed further concepts and applications of a dynamic windowing technique that is designed to minimize the difficulties of preparing and applying window area models in conjunction with full field models.

One of the most useful types of models is the conceptual model. Conceptual models can be built quickly and require only an approximate description of the part of the reservoir that is relevant to the conceptual study. Computer resource requirements are relatively small when compared with full field or window area models. Results of the conceptual model are qualitative and best used for comparing concepts such as vertical layering. They can also be used to prepare pseudo curves for use in full field or window area models. For example, the saturation of a gridblock in a model with a transition zone depends on the depth of the centerpoint of the gridblock. As a result, a grid that is vertically coarse may have only a rough approximation of the transition zone. More accurate modeling of saturation gradient in a transition zone requires vertical grid refinement or use of pseudo curves. Conceptual models are useful for preparing such pseudo curves. The disadvantage to conceptual models is that their results do not apply directly to the description of a particular field. Since there is no history match, conceptual model results should be viewed as qualitative rather than quantitative estimates of field

performance. They do provide useful qualitative information that can be applied to specific fields in window area and full field models.

15.2 Traditional Mapping

The different parameters that must be digitized for use in a grid include elevations or structure tops, permeability in three orthogonal directions, porosity, gross thickness, net-to-gross thickness, and where appropriate, descriptions of faults, fractures, and aquifers. The resulting maps are digitized by overlaying a grid on the maps and reading a value for each gridblock. The digitizing process is sketched in Figures 15-1a through 15-1d. Several authors have discussed mapping and reservoir characterization, including Harris [1975], Harpole [1985], Haldorsen and Damsleth [1993], Uland, et al. [1997], and Tearpock, et al. [2002].

The resolution of the model depends on the resolution of the grid. A fine grid divides the reservoir into many small gridblocks. It gives the most accurate numerical representation, but has the greatest computational expense. A coarse grid has fewer gridblocks, but the coarse gridblocks must be larger than the fine gridblocks to cover the same model volume. As a result, the coarse grid is less expensive to run than a fine grid, but it is also less accurate numerically. The loss of accuracy is most evident when a coarse grid is used to model the interface between phases such as fluid contacts and displacement fronts. Thus, fine grid modeling is often the preferred choice to achieve maximum numerical accuracy. It is important to recognize, however, that a fine grid covering an area defined by sparse data can give the illusion of accuracy. Sensitivity studies can help quantify the uncertainty associated with the model study.

The gridding process is most versatile when used with an integrated 3-D reservoir mapping package. Modern mapping techniques include computer generated maps that can be changed relatively quickly once properly set up. The next section introduces computer generated mapping techniques.

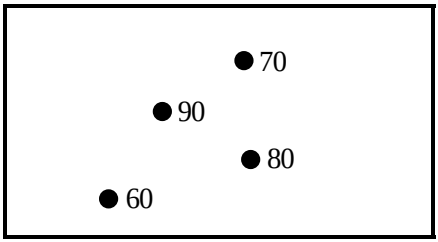

Figure 15-1a. Gather data

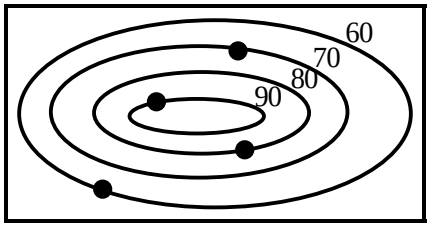

Figure 15-1b. Contour data

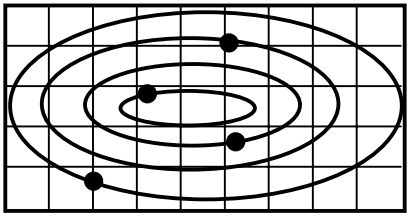

Figure 15-1c. Overlay grid

60	60	60	65	65	65	60	60	60
60	60	75	80	82	80	75	67	60
65	75	85	90	90	86	80	70	64
60	70	75	77	78	77	74	65	60
60	60	60	65	66	65	62	60	60

Figure 15-1d. Digitize data

15.3 Computer Generated Mapping

An important function of geologic maps is to present values for a spatially distributed property at any point on a surface or within a layer that were estimated from control point values. Control point values correspond to property values measured at wells or determined by seismic

methods that apply to the surface or layer of interest. Control points can also be imposed by a mapper using soft data such as seismic indications of structure boundaries. Maps of spatially distributed properties can be generated by computer using a variety of techniques.

After an algorithm has computed a surface, mappers may want to edit the surface. An easy method is to add data points to force a contour to move to a certain location. More complex computer programs allow the imposition of trends onto the data. The character of the reservoir conceptualized by the mapper should be adequately represented in the final computer generated map.

Computer generated maps may not include all of the detailed interpretations a geologist might wish to include in the model, particularly with regard to faults, but the maps generated by computer in a 3-D mapping program do not have the problems so often associated with the stacking of 2-D plan view maps, namely physically unrealistic layer overlaps. Layer overlaps need to be corrected before the history match process begins. Dahlberg [1975] presented one of the first analyses of the relative merits of hand drawn and computer generated maps.

Another problem with computer generated maps is the amount of detail that can be obtained. Computer generated maps can describe a reservoir with a much finer grid than the resolution typically used in a flow model. For example, a computer mapping program such as that described by Englund and Sparks [1991] or Pannatier [1996] may use a grid with a million or more cells to represent the reservoir, yet reservoir simulation grids are often one hundred thousand gridblocks or fewer. This means that the reservoir representation in the computer mapping program must be upscaled, or coarsened, for use in a reservoir simulator.

Many attempts have been made to find the most realistic process for upscaling data, but there is no widely accepted scaleup method in use today [for example, see Slatt and Hopkins, 1990; Christie, 1996; King and Mansfield, 1999; Dogru, 2000; Lasseter and Jackson, 2004; Stern, 2005]. Christie and Blunt [2001] present a comparison of upscaling techniques in the tenth Society of Petroleum Engineers (SPE) comparative solution project. Chawathé and Taggart [2004] discuss upscaling using streamlines. Ates, et al. [2005] present a field example that used stream-

line models to upscale geostatistical reservoir models. Hui, et al. [2005] introduce an upscaling technique for miscible processes.

The techniques described in this section are relatively simple examples of technology that can be used to generate geologic maps using computer programs. More sophisticated computer mapping techniques exist and can be used to prepare 2-D, 3-D and 4-D maps of spatially distributed parameters. Geostatistics is an example of a more sophisticated mapping technology that is based on the spatial distribution of statistically correlated properties. It is discussed in the next section.

15.3.1 Inverse Distance Weighting

One of the simplest algorithms that can be coded in a computer program to generate a map is to distribute property values over a surface or within a layer by using inverse distance weighting of all applicable control point values. The formula for inverse distance weighting is

$$V_x = \frac{\sum_{i=1}^{N} \left(V_i / d_i \right)}{\sum_{i=1}^{N} \left(1 / d_i \right)} \tag{15.1}$$

where V_x is the value of the property at x calculated from N known values $\{V_i\}$ of the property at distances $\{d_i\}$ from x. Inverse distance weighting assigns more weight to control points close to location x and less weight to control points further away. The weighting factor is the inverse of control point distance from x. For example, the value at a point x that is at the distances $\{d_A, d_B\}$ from two known values $\{V_A, V_B\}$ is

$$V_x = \frac{\frac{V_A}{d_A} + \frac{V_B}{d_B}}{\frac{1}{d_A} + \frac{1}{d_B}} \tag{15.2}$$

Figure 15-2 illustrates the inverse distance weighting example in Equation (15.2) with two control points. If only one value V_C is known (N = 1), then $V_x = V_C$ for all values of x.

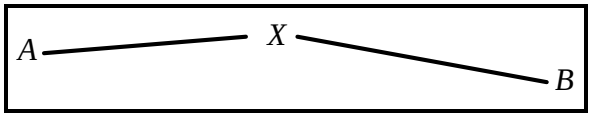

Figure 15-2. Inverse Distance Weighting with Two Control Points {A, B}

15.3.2 Weighted Averaging

Inverse distance weighting is an example of a technique that uses control points in the neighborhood of an unknown point to estimate the property value at the point. A more general expression for distributing an attribute using a weighted average is

$$Z_{avg} = \frac{\sum_{i=1}^{N} W(r_i, R) \bullet Z_i}{\sum_{i=1}^{N} W(r_i, R)} \tag{15.3}$$

where

Z_{avg} = weighted average value of attribute Z

Z_i = value of attribute Z at control point i

W = weighting function

r_i = distance from the interpolated point to control point i

R = user specified search radius

N = number of control points

The search radius R constrains the number of control points N that are used to determine the weighted average of the attribute. An example of a

weighting function is that in Eq. (15.1), namely $1/d_i$. Another example of a weighting function with a search radius is

$$W(r,R)=\left(1-\frac{r}{R}\right)^2 \bullet \left(\frac{R}{r}\right)^x \tag{15.4}$$

where the value of the exponent x is entered by the user.

15.3.3 Trend Surface Analysis

A technique for determining the spatial distribution of a property by computer is to fit a surface through the control points. This technique is referred to as *trend surface analysis*. Linear trend surface analysis uses regression to fit a line through all control point values in a given direction. The regression model for linear trend surface analysis is

$$Z_{obs} = a_0 + a_1 x_{loc} + a_2 y_{loc} \tag{15.5}$$

where Z_{obs} is the observed value of attribute Z at the control point, $\{x_{loc}, y_{loc}\}$ are the $\{x\text{-axis}, y\text{-axis}\}$ locations of the control point, and $\{a_0, a_1, a_2\}$ are regression coefficients. Equation (15.5) can be extended to be a quadratic function of control point location. Quadratic trend surface analysis can fit a curved surface to data, and is therefore useful for representing geologic structures such as anticlines or synclines.

15.4 Geostatistics and Kriging

The spatial distribution of rock properties is a fundamental aspect of the reservoir characterization process. Two modern methods for spatially distributing rock properties are reservoir geophysics (see Chapter 12) and geostatistics. Information obtained from reservoir geophysics is improving our ability to "see" between wells in a deterministic sense. By contrast, geostatistics provides a reservoir characterization that is statistical. Many modelers view geostatistics as the method of choice for sophisticated reservoir flow modeling [for example, see Lieber, 1996;

Haldorsen and Damsleth, 1993; and Rossini, et al., 1994]. Are these methods competing or complementary? This section presents several points about geostatistics that can help answer this question.

Geostatistics is a branch of "applied statistics" that attempts to describe the distribution of a property in space. Geostatistics is also known as spatial statistics. It assumes that a spatially distributed property exhibits some degree of continuity. Porosity and permeability are examples of spatially dependent properties that are suitable for geostatistical description. Much of our discussion of geostatistics is based on publications by Isaaks and Srivastava [1989], Hirsche, et al. [1997], Deutsch and Journel [1998], Chambers, et al. [2000], and Clark and Harper [2002].

Geostatistics consists of a set of mathematical tools which employ the assumption that properties are correlated in space and are not randomly distributed. The geological context of the data must be considered in addition to spatial relationships between data. Geostatistical algorithms provide formalized methods for integrating data of diverse type, quality and quantity.

A geostatistical analysis has several goals, including:

- Acquiring an understanding of the spatial relationships and correlations between reservoir properties;
- Modeling those relationships with mathematical expressions;
- Developing an understanding of the uncertainty associated with the reservoir properties and the conceptual geologic model; and
- Determining if a deterministic or stochastic approach is appropriate for the creation of a reservoir model.

A deterministic model is a single realization, or representation, of reservoir geology. The uncertainty associated with a deterministic model can be estimated by estimating the sensitivity of the model to uncertainties in available data.

A stochastic model is a set of realizations obtained from the probability distributions developed during the geostatistical analysis of data. The shape of a probability distribution is defined by the proximity

and quality of local data within the context of a spatial correlation model. By its nature, stochastic modeling propagates the uncertainty of the input parameters.

Stochastic modeling has two goals. The first goal is to preserve the heterogeneity inherent in a geological system as a means of creating more realistic and useful simulation models. The second goal is to quantify the uncertainty in the geologic model by generating many possible realizations. The stochastic model should incorporate multiple data types with varying degrees of quality and quantity. The data should represent different measurement scales.

The process of preparing a geologic model requires the development of a structural and stratigraphic framework using available seismic and well data. Multiple realizations may be generated and used to quantify uncertainty in the geologic model. The process of translating point observations to a conceptual geologic model is a sequential process. It is also an iterative process if a match of time-dependent (dynamic) data is included in the preparation of the final reservoir model. Once the framework exists, a lithofacies model and petrophysical properties can be incorporated in the flow model.

15.4.1 Geostatistical Modeling

Geostatistical modeling refers to the procedure for determining a set of reservoir realizations. The realizations depend on both the spatial relationships between data points and their statistical correlation as a function of separation in space.

The spatial relationship(s) associated with data are computed and then modeled. This process is analogous to (1) plotting data on a cross-plot (computing) and then (2) fitting a line to the data with linear regression (modeling). The plotted points make up the experimental semi-variogram, and the line that is fit to the data points is called the semi-variogram model. Figure 15-3 illustrates a fit to data by a semi-variogram model.

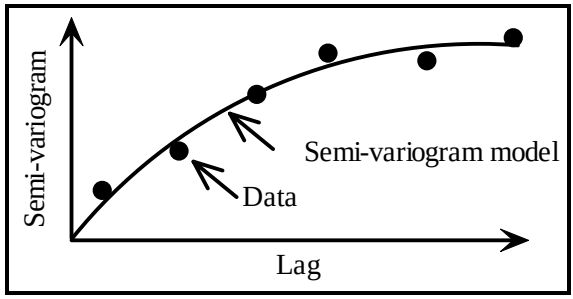

Figure 15-3. Semi-variogram

A semi-variogram is a plot of semi-variance versus range. Semi-variance is a measure of the degree of dissimilarity between the values of a parameter Z at two different locations, or points in space. The semi-variance $\gamma(h)$ is a function of lag h, or the distance of separation, between two observations $Z(x)$ and $Z(x + h)$ of the parameter Z, thus

$$\gamma(h) = \frac{1}{2N(h)} \sum_{i=1}^{N(h)} \left[Z(x_i) - Z(x_i + h) \right]^2 \qquad (15.6)$$

where $N(h)$ is the number of data pairs that are approximately separated by the lag h.

Figure 15-4 illustrates three important features of the semi-variogram. The sill is the maximum value of the semi-variogram for the parameter Z. The sill is also the variance σ^2 of the measured data, where σ is the standard deviation.

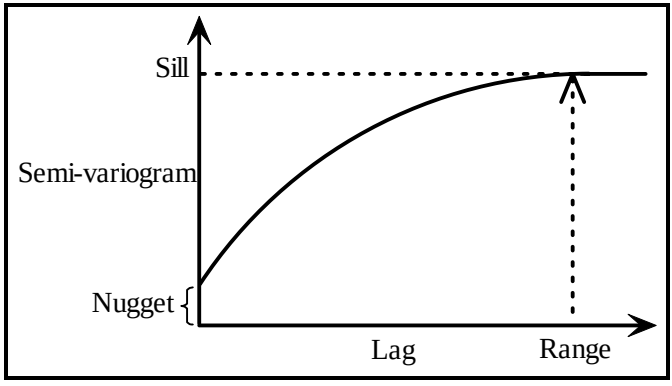

Figure 15-4. Characterizing a Semi-variogram

The nugget in Figure 15-4 is the value of the semi-variance at zero lag. A nonzero value of the nugget is due to factors such as sampling error and short range variability of the parameter. In fact, the term "nugget" refers to the observation that the lag for a finite size gold nugget can never equal zero.

The range in Figure 15-4 is an estimate of the maximum correlation length between two points at a separation distance *h*. A spatial correlation between values of parameter *Z* exists at values of the lag less than the range.

Several types of semi-variogram models exist. For example, the exponential model is

$$\gamma(h) = C_0 + C_1\left\{1 - \exp\left(-\frac{h}{a}\right)\right\} \tag{15.7}$$

and the Gaussian model is

$$\gamma(h) = C_0 + C_1\left\{1 - \exp\left(-\frac{h^2}{a^2}\right)\right\} \tag{15.8}$$

where $h \geq 0$ is lag, C_0 is the nugget, C_1 is the sill, and a is the range of influence.

Semi-variogram modeling is performed by fitting a semi-variogram model to experimental data as in Figure 15-3. The resulting semi-variogram is a measure of the spatial dependence of reservoir attributes such as porosity, permeability and net thickness. The semi-variogram model is used to predict values of the modeled attribute at unsampled locations.

One widely used estimation technique is kriging. Kriging is named after the South African mining engineer D.G. Krige who helped pioneer the development of geostatistical methods in the 1950's. Kriging is a linear weighted average method. The weights used in kriging are based on the semi-variogram model of spatial correlation. It is instructive to make these points explicit.

The kriging equation for estimating the value of attribute Z_P at point P from a set of n control points with attribute values $\{Z_i : i = 1,2,\ldots,n\}$ is

$$Z_P = \sum_{i=1}^{n} w_i Z_i \tag{15.9}$$

The attribute Z_P may be a rock property such as porosity or permeability. The weights $\{w_i : i = 1,2,\ldots,n\}$ are calculated from the set of n equations

$$\begin{aligned} &w_1\gamma(h_{11}) + w_2\gamma(h_{12}) + \cdots + w_n\gamma(h_{1n}) + \lambda = \gamma(h_{1P}) \\ &w_1\gamma(h_{21}) + w_2\gamma(h_{22}) + \cdots + w_n\gamma(h_{2n}) + \lambda = \gamma(h_{2P}) \\ &\vdots \\ &w_1\gamma(h_{n1}) + w_2\gamma(h_{n2}) + \cdots + w_n\gamma(h_{nn}) + \lambda = \gamma(h_{nP}) \end{aligned} \tag{15.10}$$

The semi-variogram $\gamma(h_{ij})$ is the semi-variogram at lag distance h_{ij} between two points (P_i, P_j). The semi-variogram $\gamma(h_{iP})$ is the semi-variogram at lag distance h_{iP} between control point P_i and the point P where attribute Z_P is being estimated. The constant λ is the Lagrange multiplier for the "unbiased" constraint

$$\sum_{i=1}^{n} w_i = 1 \tag{15.11}$$

Equation (15.9) is considered the "best linear unbiased estimate" (BLUE) of Z_P, and the procedure for solving the above set of equations is considered ordinary kriging. Universal kriging combines ordinary kriging and trend surface analysis.

15.4.2 Technical Note

The ordinary kriging equations in Eq. (15.10) and (15.11) are $n+1$ equations for the n weights $\{w_i : i = 1,2,\ldots,n\}$ and the Lagrange

multiplier λ. These equations can be written as a matrix equation and solved using matrix solution techniques. It is worth noting that many matrix solution techniques depend on a nonzero diagonal, which can be a problem if the diagonal terms are the semi-variograms $\gamma(h_{ii})$ because $\gamma(h_{ii})$ are the nuggets of the semi-variogram and may be zero. Numerical matrix solvers that are designed to use the diagonal elements as pivot elements will not work if the diagonal elements are zero. This problem can be avoided by rewriting Eq. (15.10) as

$$\begin{aligned}
&\lambda + w_1\gamma(h_{11}) + w_2\gamma(h_{12}) + \cdots + w_n\gamma(h_{1n}) = \gamma(h_{1P}) \\
&\lambda + w_1\gamma(h_{21}) + w_2\gamma(h_{22}) + \cdots + w_n\gamma(h_{2n}) = \gamma(h_{2P}) \\
&\vdots \\
&\lambda + w_1\gamma(h_{n1}) + w_2\gamma(h_{n2}) + \cdots + w_n\gamma(h_{nn}) = \gamma(h_{nP})
\end{aligned} \tag{15.12}$$

so that the Lagrange multiplier is the first element of the column vector of unknowns. The resulting matrix equation for both Eq. (15.12) and Eq. (15.11) is

$$\begin{bmatrix}
1 & \gamma(h_{11}) & \gamma(h_{12}) & \cdots & \gamma(h_{1n}) \\
1 & \gamma(h_{21}) & \gamma(h_{22}) & \cdots & \gamma(h_{2n}) \\
\vdots & \vdots & \vdots & & \vdots \\
1 & \gamma(h_{n1}) & \gamma(h_{n2}) & \cdots & \gamma(h_{nn}) \\
0 & 1 & 1 & \cdots & 1
\end{bmatrix}
\begin{bmatrix}
\lambda \\ w_1 \\ w_2 \\ \vdots \\ w_n
\end{bmatrix}
=
\begin{bmatrix}
\gamma(h_{1P}) \\ \gamma(h_{2P}) \\ \vdots \\ \gamma(h_{nP}) \\ 1
\end{bmatrix} \tag{15.13}$$

The diagonal elements of the $n \times n$ matrix on the left hand side of Eq. (15.13) are nonzero and can be used as pivot elements for numerical matrix solvers.

15.4.3 Kriging Accuracy

One method of determining the accuracy of the values obtained by ordinary kriging is to calculate the variance σ^2_{OK} of the ordinary kriging estimate. The variance is

$$\sigma_{OK}^2 = \sum_{i=1}^{n} w_i \gamma(h_{iP}) + \lambda - \gamma(h_{PP}) \tag{15.14}$$

where the Lagrange multiplier is

$$\lambda = \sum_{i=1}^{n} w_i \gamma(h_{iP}) - \sum_{i=1}^{n} \sum_{j=1}^{n} w_i w_j \gamma(h_{ij}) \tag{15.15}$$

Equations (15.14) and (15.15) can be solved once the weights have been calculated. Equation (15.15) can be used to check the value of the Lagrange multiplier obtained by solving Eq. (15.13).

Another method of determining the accuracy of the values obtained by an estimation technique is to treat a sampled (known) data point as an unknown point at the test location. The estimation technique is used to calculate the parameter at the test location and the resulting value is compared with the known data point. The accuracy of the estimation process can be quantified by calculating the semi-variance of actual values relative to the estimated values. The resulting semi-variance provides a cross-validation of the original semi-variogram model and provides information about the quality of the estimation technique. Notice that this model cross-validation procedure could be applied to any computer based estimation technique.

15.4.4 The Use and Abuse of Geostatistics

Hirsche, et al. [1997; page 259] have pointed out that “geostatistical reservoir characterization should not be done in isolation.” Geostatistics is like other reservoir characterization techniques: the technique is most successful when all available data is incorporated into the reservoir characterization process.

The violation of basic geostatistical assumptions can lead to the creation of an inaccurate reservoir model. Inaccuracies in the model appear as errors in associated maps. Limited well control and biased sampling of well information are examples of real world constraints that can violate the underlying assumptions of geostatistics. Abrupt changes

in reservoir features, such as faults and high permeability channels, are difficult to identify using geostatistics [Fanchi, et al., 1996].

Geostatistics and stochastic modeling can be used to integrate data, provide a realistic representation of reservoir heterogeneity, and quantify uncertainty. On the other hand, the existence of multiple realizations can be confusing and more expensive than the construction of a single deterministic representation of the reservoir. In addition, the stochastic images may look realistic but actually do a poor job of representing flow in the actual reservoir. The process of validating the reservoir model is made more complicated by the existence of multiple realizations.

15.5 Geostatistical Case Study

An example of a full field model study using a geostatistical reservoir realization is the reservoir management study of the N.E. Nash Unit in Oklahoma [Fanchi, et al., 1996]. The goal of the study was to prepare a full field reservoir flow model that could be used to identify unswept parts of the field. We knew from the history of the field that water was breaking through at several wells. The study was designed to look for places where an additional production well could be economically drilled.

The N.E. Nash Unit has a gradual dip from north to south. The Misener sandstone reservoir is bounded above by the Woodford shale, on the flanks by the Sylvan shale, and below by the Viola limestone. The Viola limestone does allow some aquifer support for the Misener sandstone.

One of the primary tasks of the study was to map the N.E. Nash Unit. Two sets of maps were prepared: conventional hand-drawn maps, and a set of maps based on a geostatistical analysis of the field. The hand-drawn maps correspond to the deterministic approach in which a single realization is used, while the geostatistical maps correspond to a stochastic image of the reservoir.

A geostatistical analysis was performed using forty-two well control points to calculate structural tops, gross thickness, net-to-gross ratio, and porosity. A crossplot between porosity and core permeability yielded a relationship for calculating permeability from porosity. From this data, directional semi-variograms were prepared to describe the spatial continuity of each parameter.

When two sets of maps were compared, the hand-drawn maps were found to be more homogenous than the geostatistical maps. The geostatistical maps exhibited the large scale trends shown in the hand-drawn maps, but contained more local variability. This was not surprising, since additional heterogeneity is expected to arise as a result of geostatistical mapping.

The choice of final maps was based on management priorities: minimize the risk of drilling a dry hole on the flanks of the field, and complete the study before water breakthrough occurred in the remaining oil producers. The geostatistical model satisfied both of these criteria. The main flow path in the reservoir was narrower in the geostatistically generated maps than in the hand-drawn maps, and the geostatistical realization could be modified more quickly than hand-drawn maps.

Once a set of maps was chosen, the history matching process could begin. Tracer information in the form of salinity changes helped identify sources of injection water as the water was produced. This was valuable in defining flow channels that could not otherwise be inferred. In some areas, transmissibility and porosity changes were needed to match water cut and reservoir pressure.

The geostatistical realization used in the N.E. Nash study was just a single realization. It was selected because it satisfied constraints imposed by previous volumetric and material balance studies. If these constraints had not been available or had been less reliable, which would be the case early in the life of a field, a geostatistical study would require the use of multiple realizations to characterize the reservoir. This raises the question of how many realizations are necessary.

Figure 15-5 shows a random sampling from a discrete probability distribution. A running average is calculated as the average of all preceding trials. For example, the running average at trial 10 is obtained

by averaging the first 10 trial results. The running average shown in Figure 15-5 does not stabilize, or approach a constant value, until at least twenty trials have been completed. This is a large number of realizations if history matching is needed for each realization. Indeed, it would be an unacceptably large number of realizations, in most cases, because of the time it takes to perform a history match. Most studies are usually based on the assumption that a single history match will be sufficient.

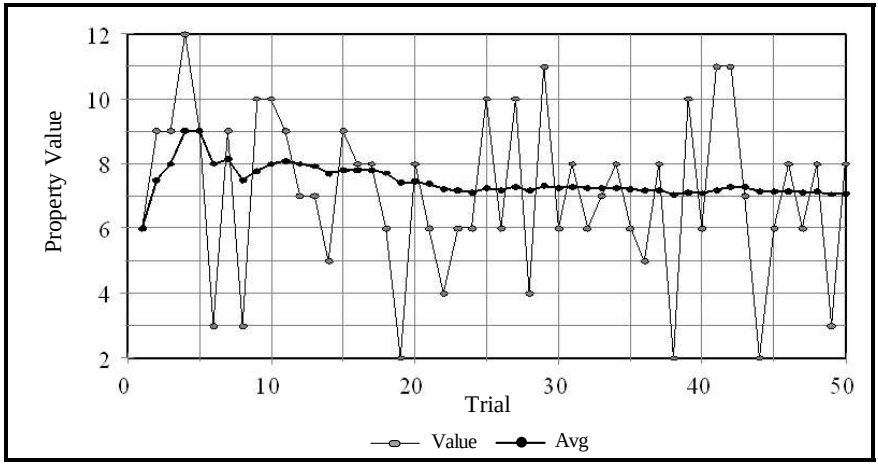

Figure 15-5. Running Average

Multiple realizations can also confuse people who are not closely involved with the modeling process because they do not have a single picture of the reservoir. On the other hand, the use of multiple realizations makes it possible to quantify the uncertainty associated with our limited knowledge of properties distributed spatially throughout the field.

Table 15-1 summarizes the advantages and concerns associated with geostatistics. There is no established procedure for selecting one or more realizations for history matching from a set of geostatistically derived realizations. Examples of procedures are described by Rossini, et al. [1994] and Gilman, et al. [2002]. Applications of reservoir geostatistics in the context of a multidisciplinary study are presented by several authors, such as Wang, et al. [1998] and Dubrule [2003].

Table 15-1
Geostatistics

Advantages	Concerns
➢ Realism ➢ Quantification of uncertainty	➢ Multiple realizations entail cost and confusion ➢ History matching still necessary to account for model discontinuities such as channeling ➢ History matching complicated by factors such as probabilistically generated heterogeneity

Exercises

Exercise 15.1 Sketch the model grids for data files EXAM1.DAT, EXAM2.DAT, EXAM3.DAT, EXAM5.DAT, and EXAM7.DAT using the information from each data file.

Exercise 15.2 Sketch the model grids for case study data files CS-MB.DAT, CS-VC.DAT, and CS-XS.DAT using the information from each data file.

Exercise 15.3 Modify the grid in EXAM3.DAT so that it has only ten gridblocks in the x direction, but the model volume is unchanged. Be sure to relocate the wells relative to the grid to keep them in their appropriate physical locations and correct the PID index. How does the coarser grid affect the model?

Exercise 15.4 Modify the grid in EXAM2.DAT so that it has $5 \times 5 \times 4$ gridblocks. The well should be in the center of the reservoir and the reservoir volume should be unchanged by the redefinition of the grid. Correct the PID index. How does the finer grid affect model performance when the model is run for three years?

Exercise 15.5 Roll a pair of dice 50 times and record the results. Calculate a running average by calculating a new average after each trial (roll of dice). Plot the running average for each trial. How many trials are necessary before the average stabilizes, that is, the average approaches a constant value?

Exercise 15.6 Plot the exponential semi-variogram as a function of lag distance in the range $0 \le h \le 2000$ for nugget = 0, sill = 500, and range = 200.

Exercise 15.7A The effect of different spatial distribution techniques is illustrated here for a permeability distribution in an areal model. File KRIGE_A.DAT is an areal model with aquifer support and an average lateral permeability of 75 md. Vertical permeability is one tenth of lateral permeability. Run KRIGE_A.DAT and record pressure, well PID in layer K = 1, and producing water-oil ratio (WOR) in layer K = 3 of the well at 2920 days.

Exercise 15.7B File KRIGE_B.DAT is the same as file KRIGE_A.DAT except that lateral permeability is from contouring in each layer, thus:

	I = 1	2	3	4	5	6	7	8	9
J = 1	60	60	60	65	65	65	60	60	60
2	60	60	75	80	82	80	75	67	60
3	65	75	85	90	90	86	80	70	64
4	60	70	75	77	78	77	74	65	60
5	60	60	60	65	65	65	62	60	60

Run KRIGE_B.DAT and record pressure, well PID in layer K = 1, and producing WOR in layer K = 3 of the well at 2920 days.

Exercise 15.7C File KRIGE_C.DAT is the same as file KRIGE_A.DAT except that lateral permeability is from ordinary kriging in each layer, thus:

	$I = 1$	2	3	4	5	6	7	8	9
$J = 1$	74.7	75.4	76.4	76.1	73.5	72.1	73.5	74.0	74.2
2	74.7	76.1	79.5	80.9	75.7	73.1	73.9	74.2	74.3
3	74.0	75.0	79.9	84.1	78.6	76.5	75.1	74.6	74.4
4	72.5	70.5	71.9	76.3	77.8	78.2	75.6	74.7	74.5
5	71.6	66.8	65.8	72.6	75.2	75.8	75.2	74.7	74.4

Run KRIGE_C.DAT and record pressure, well PID in layer $K = 1$, and producing WOR in layer $K = 3$ of the well at 2920 days.

Exercise 15.7D Explain the differences between the models.

Exercise 15.8A The data used to prepare the permeability distributions in Parts B and C of Exercise 15.7 are given in the following table:

Well	**Permeability (md)**	***x*-Location (ft)**	***y*-Location (ft)**
1	70	1020	200
2	90	640	440
3	80	1040	660
4	60	420	860

What are the average and standard deviation of the permeabilities in the table?

Exercise 15.8B What are the averages and standard deviations of the permeability distributions in Parts B and C of Exercise 15.7?

Exercise 15.9 Files RIM_2D.DAT and RIM_SYMMETRIC.DAT are 2-D models of gas production from an anticlinal gas reservoir with an oil rim. Run both files and use 3DView to view the structure. Are there any differences between the structures in the two files? Confirm your analysis by looking at the structure tops in the data files.

Chapter 16

Fluid Properties

Properties of petroleum fluids must be quantified in a reservoir simulator. The range of applicability of a reservoir simulator is defined, in part, by the types of fluids that can be modeled using the mathematical algorithms coded in the simulator. This chapter discusses the general types of fluids that may be encountered in a commercial reservoir environment and that are suitable for flow modeling. For additional information, see Amyx, et al. [1960], Pedersen, et al. [1989], Koederitz, et al. [1989], McCain [1990, 1991], Towler [2002], and Walsh and Lake [2003].

16.1 Fluid Types

The elemental composition (by mass) of petroleum is approximately 84% to 87% carbon, 11% to 14% hydrogen, 0.6% to 8% sulphur, 0.02% to 1.7% nitrogen, 0.08% to 1.8% oxygen, and 0% to 0.14% metals. The composition of petroleum shows that petroleum fluids are predominantly hydrocarbons. The most common hydrocarbon molecules are paraffins, napthenes, and aromatics because of the relative stability of the molecules. A paraffin is a saturated hydrocarbon, that is, it has a single bond between carbon atoms. Examples include methane and ethane.

Paraffins have the general chemical formula C_nH_{2n+2}. Napthenes are saturated hydrocarbons with a ringed structure, as in cyclopentane. They have the general chemical formula C_nH_{2n}. Aromatics are unsaturated hydrocarbons with a ringed structure that have multiple bonds between the carbon atoms as in benzene. The unique ring structure makes aromatics relatively stable and nonreactive.

A general fluid property diagram of a pure substance displays phase behavior as a function of pressure, volume, and temperature (PVT). The diagram is usually referred to as a *PVT diagram*. The types of properties of interest from a reservoir engineering perspective can be conveyed in a pressure-temperature (P-T) diagram of phase behavior like the one shown in Figure 16-1. Most reservoir fluids do not exhibit significant temperature effects *in situ*, although condensate reservoirs in thick sands may display a compositional gradient that can influence condensate yield as a function of the depth of well perforations.

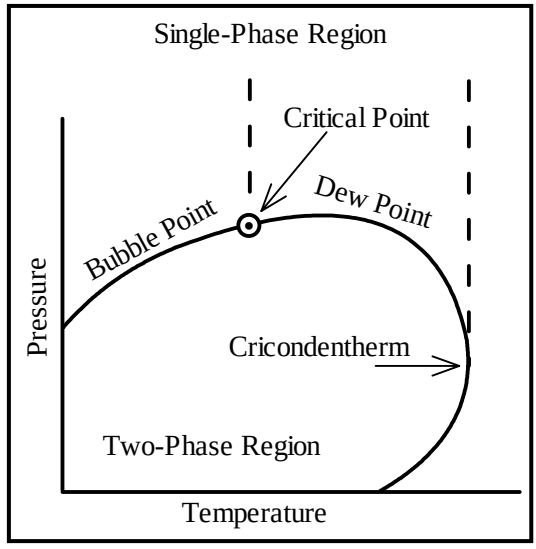

Figure 16-1. P-T Diagram [after Craft, et al., 1991]

The P-T diagram includes both single-phase and two-phase regions. The line separating the single-phase region from the two-phase region is called the phase envelope. The black oil region is found at low

temperature and in the high pressure region above the bubble point curve separating the single-phase and two-phase regions. If we consider pressures in the single-phase region and move to the right of the diagram by letting temperature increase towards the critical point, we encounter volatile oils. At temperatures above the critical point but less than the cricondentherm – the maximum temperature of the phase envelope – reservoir fluids behave like condensates. When reservoir temperature is greater than the cricondentherm, we encounter only the gas phase.

Table 16-1 summarizes fluid types. Notice that separator gas-oil ratio (GOR) is a useful indicator of fluid type.

Table 16-1
Rules of Thumb for Classifying Fluid Types

Fluid Type	Separator GOR (MSCF/STB)	Pressure Depletion Behavior in Reservoir
Dry gas	No surface liquids	Remains gas
Wet gas	> 100	Remains gas
Condensate	3 − 100	Becomes gas with liquid drop out
Volatile oil	1.5 − 3	Becomes liquid with significant gas
Black oil	0.1 − 1.5	Becomes liquid with some gas
Heavy oil	~ 0	Exhibits negligible gas formation

Let us consider a reservoir containing hydrocarbons that are at a pressure and temperature corresponding to the single-phase black oil region. If reservoir pressure declines at constant temperature, the reservoir pressure will eventually cross the bubble point pressure curve and enter the two-phase gas-oil region. Similarly, starting with a single-phase condensate and letting reservoir pressure decline at constant temperature, the reservoir pressure will cross the dew point pressure curve to enter the two-phase region. In this case, a free-phase liquid drops out of the condensate gas. Once liquid drops out, it is very difficult to recover. One

recovery method is dry gas cycling, but the recovery efficiency will be substantially less than 100%. If we drop the pressure even further, it is possible to encounter retrograde condensation for some hydrocarbon compositions.

The P-T diagram also applies to temperature and pressure changes in a wellbore. In the case of wellbore flow, the fluid moves from relatively high reservoir temperature and pressure to relatively low surface temperature and pressure. As a result, it is common to see fluids that are single-phase in the reservoir become two-phase by the time they reach the surface.

The P-T diagram in Figure 16-2 compares two-phase envelopes for four types of fluids. A reservoir fluid can change from one fluid type to another depending on how the reservoir is produced. A good example is dry gas injection into a black oil reservoir. Dry gas injection increases the relative amount of low molecular weight components in the black oil. The two-phase envelope rotates counterclockwise in the P-T diagram as the relative amount of lower molecular weight components increases. Similarly, dry gas injection into a condensate can make the phase envelope transform from one fluid type to another. Thus, the way the reservoir is operated has a significant impact on fluid behavior in the reservoir and at the surface.

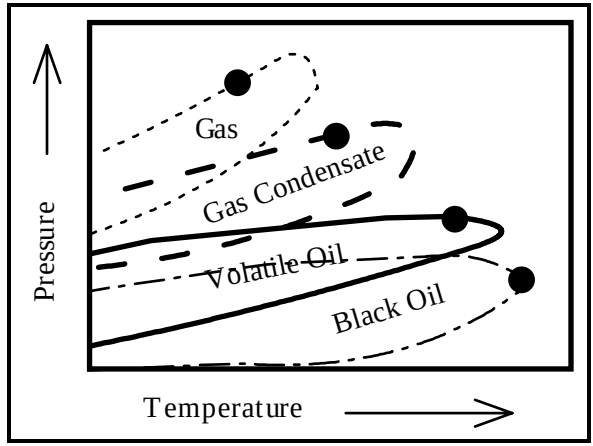

Figure 16-2. Typical Two-phase P-T Envelopes for Different Fluid Types

Table 16-2 shows different compositions for typical fluid types. Dry gas usually contains only the lower molecular weight components. Gas condensates start to add higher molecular weight components. Volatile oils continue to add higher molecular weight components. Black oils result from the addition of higher molecular weight components and the reduction of lower molecular weight components. If we monitor methane content (C_1), we see that it tends to decrease as fluids change from dry gas to black oil.

Table 16-2
Typical Molar Compositions of Petroleum Fluid Types
[after Pedersen, et al., 1989]

Component	Gas	Gas Condensate	Volatile Oil	Black Oil
N_2	0.3	0.71	1.67	0.67
CO_2	1.1	8.65	2.18	2.11
C_1	90.0	70.86	60.51	34.93
C_2	4.9	8.53	7.52	7.00
C_3	1.9	4.95	4.74	7.82
iC_4+nC_4	1.1	2.00	4.12	5.48
iC_5+nC_5	0.4	0.81	2.97	3.80
iC_6+nC_6	C_{6+}: 0.3	0.46	1.99	3.04
C_7		0.61	2.45	4.39
C_8		0.71	2.41	4.71
C_9		0.39	1.69	3.21
C_{10}		0.28	1.42	1.79
C_{11}		0.20	1.02	1.72
C_{12}		0.15	C_{12+}: 5.31	1.74
C_{13}		0.11		1.74
C_{14}		0.10		1.35
C_{15}		0.07		1.34
C_{16}		0.05		1.06
C_{17}		C_{17+}: 0.37		C_{17+}: 12.10

16.2 Fluid Modeling

In general, fluid behavior is best modeled using an equation of state. Table 16-3 shows some cubic equations of state (EoS) used in commercial compositional simulators. In addition to pressure (P), volume (V), and temperature (T), the EoS contains the gas constant R and a set of adjustable parameters $\{a, b\}$ which may be functions of temperature. The EoS in Table 16-3 are called "cubic" because they yield a cubic equation for the compressibility factor $Z = PV/RT$. In the case of an ideal gas, $Z = 1$.

Table 16-3
Examples of Cubic Equations of State

Redlich-Kwong	$P = \dfrac{RT}{V-b} - \dfrac{a/T^{1/2}}{V(V+b)}$
Soave-Redlich-Kwong	$P = \dfrac{RT}{V-b} - \dfrac{a(t)}{V(V+b)}$
Peng-Robinson	$P = \dfrac{RT}{V-b} - \dfrac{a(t)}{V(V+b)+b(V-b)}$
Zudkevitch-Joffe	$P = \dfrac{RT}{V-b} - \dfrac{a(T)/T^{1/2}}{V[V+b(T)]}$

Equations of state are valuable for representing fluid properties in many situations. For example, suppose we want to model a system in which production is commingled from more than one reservoir with more than one fluid type. In this case the most appropriate simulator would be a compositional simulator because a black oil simulator would not provide as accurate a representation of fluid behavior.

The two most common types of reservoir fluid models are black oil models and compositional models. Black oil models are based on the assumption that the saturated phase properties of two hydrocarbon

phases (oil and gas) depend on pressure only. Compositional models also assume two hydrocarbon phases, but they allow the definition of many hydrocarbon components. Unlike a black oil simulator, which can be thought of as a compositional simulator with two components, a compositional simulator often has six to ten components. By comparison, process engineering simulators that are used to model surface facilities typically require up to twenty components or more. The cost of running a compositional simulator increases dramatically with increases in the number of components modeled, but the additional components make it possible to model complex fluid phase behavior more accurately. If compositional model results are to be used in a process engineering model, it is often necessary to compromise on the number of components to be used for each application.

Equations of state must be used to calculate equilibrium relations in a compositional model. This entails tuning parameters such as EoS parameters $\{a, b\}$ in Table 16-3. Several regression techniques exist for tuning an EoS. They usually differ in the choice of EoS parameters that are to be varied in an attempt to match lab data with the EoS. The use of equations of state in compositional simulation is discussed by several authors, such as Whitson and Brulé [2000], Wang and Pope [2001], and Thomas, et al. [2002].

Figures 16-3 and 16-4 show typical fluid property behavior of gas and oil properties for a black oil model. Gas phase properties are gas formation volume factor (B_g), gas viscosity (μ_g), and liquid yield (r_s). Oil phase properties are oil formation volume factor (B_o), oil viscosity (μ_o), and solution GOR (R_{so}). Both saturated and undersaturated curves are included as functions of pressure only. Phase changes occur at the saturation pressures. Single-phase oil becomes two-phase gas-oil when pressure drops below the bubble point pressure (P_b), and single-phase gas becomes two-phase gas condensate when pressure drops below the dew point pressure (P_d).

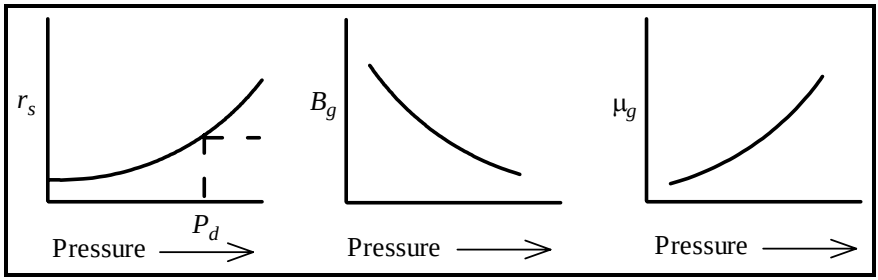

Figure 16-3. Gas Phase Properties

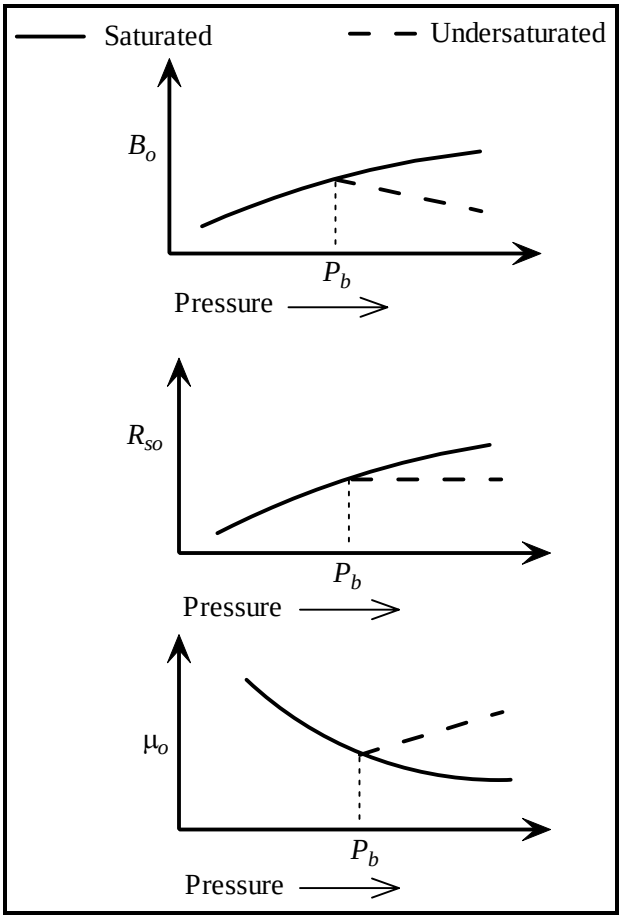

Figure 16-4. Oil Phase Properties

Simulators run most efficiently when fluid property data are smooth curves. Any discontinuity in a curve can cause numerical difficulties. Ordinarily, realistic fluid properties are smooth functions of pressure except at points where phase transitions occur. As a practical matter, it is usually wise to plot input PVT data to verify the smoothness of the data. Most simulators reduce the nonlinearity of the gas formation volume factor B_g by using the inverse $b_g = 1/B_g$ to interpolate gas properties.

Water properties must also be entered in a simulator. Ideally water properties should be measured by performing laboratory analyses on produced water samples. If samples are not available, correlations are often sufficiently accurate to describe the behavior of water.

In the absence of reliable fluid data for one or more of the reservoir fluids, it may be necessary to use correlations. McCain [1991] reviewed the state of the art in the use of correlations to describe fluid properties. New correlations for estimating bubble point pressure, formation volume factor, and isothermal oil compressibility have been proposed by Levitan and Murtha [1999].

16.2.1 Oil Property Correction

Flow in the reservoir is a relatively slow process that corresponds to a differential process in the laboratory. A differential process is one in which pressures are allowed to change in relatively small increments. For comparison, a flash process allows pressures in the experiment to change by relatively large increments. The production of oil up the wellbore to surface facilities is considered a flash process. Black oil property measurements from a testing laboratory will generally entail a differential liberation study coupled with a separator study. A correction procedure is often applied to oil property data from the laboratory to adjust the data to more adequately represent fluids as they flow differentially in the reservoir prior to being flashed to surface conditions.

The following procedure [Amyx, et al., 1960; Moses, 1986] corrects differential liberation data to flash values at field separation

conditions. If the separator formation volume factor for oil B_o and solution gas-oil ratio R_{so} are known, the conversion equations are:

$$B_o(P) = B_{od}(P)\frac{B_{ofbp}}{B_{odpb}} \tag{16.1}$$

and

$$R_{so}(P) = R_{sofbp} - \left(R_{sodbp} - R_{sod}(P)\right)\frac{B_{ofbp}}{B_{odpb}} \tag{16.2}$$

where the variable P is pressure. The subscripts in the equations are defined as follows: *d* refers to differential liberation data; *f* refers to flash data; and *bp* refers to values at the bubble point pressure. The corrections alter solution gas-oil ratio and oil formation volume factor so that they may be used in black oil simulation. Alternative procedures for adjusting differential liberation data to separator conditions are discussed by Poetmann and Thompson [1986], McCain [2002], Walsh and Lake [2003], and Al-Marhoun [2003].

16.3 Fluid Sampling

All laboratory measurements of fluid properties and subsequent analyses are useless if the fluid samples do not adequately represent *in situ* fluids. The goal of fluid sampling is to obtain a sample that is representative of the original fluid in the reservoir. It is often necessary to condition the well before the sample is taken. A well is conditioned by producing any nonrepresentative fluid, such as drilling mud, from within and around the wellbore until it is replaced by original reservoir fluid flowing into the wellbore. Fluid samples may then be taken from either the surface or subsurface.

Subsurface sampling requires lowering a pressurized container to the production interval and subsequently trapping a fluid sample. This is routinely accomplished by drill stem testing, especially when access to surface facilities is limited. Downhole fluid sampling is most effective when fluids flow into the well as a single phase and the fluid samples are

obtained early in the life of the well. It is generally cheaper and easier to take surface samples from separator gas and oil.

If a surface sample is taken, the original *in situ* fluid, that is, the fluid at reservoir pressure and temperature, must be reconstituted by combining separator gas and separator oil samples. The recombination step assumes that measurements of flow data at the surface are accurate, especially gas-oil ratio. Subsurface sampling from a properly conditioned well avoids the recombination step, but is more difficult and costly than surface sampling, and usually provides a smaller volume of sample fluid. The validity of fluid property data depends on the quality of the fluid sampling procedure.

16.4 IFLO Fluid Model

The multicomponent, pseudomiscible simulator IFLO uses the extended fluid properties model described by Ammer, et al. [1991]. It is an adaptation of Chase and Todd's [1984] mixing parameter method. See Ammer, et al. [1991] or Fanchi [2000] for additional details. Bubble point tracking and the gas property correlation option implemented in IFLO are outlined below.

16.4.1 Bubble Point Tracking

The technique of variable switching [Thomas, et al., 1976] is used to track bubble point pressure in IFLO [Ammer, et al. 1991]. The primary variables that specify the state of a gridblock depend on the condition of the gridblock. The saturated condition of the gridblock is determined at the beginning of an iteration by comparing oil phase pressure and bubble point pressure. At the end of the iteration, saturated gridblocks are tested for a change of state. If gas saturation is positive in the saturated gridblock, bubble point pressure P_b is set equal to gridblock pressure P. If gas saturation is negative, gas saturation is set to zero and P_b is set slightly below the oil phase pressure. This makes the gridblock slightly undersaturated as it enters the next iteration. Undersaturated

gridblocks do not require any special switching logic. The next iteration is then performed.

16.4.2 Gas PVT Correlation Option

The Benedict-Webb-Rubin [1940] eight-parameter equation of state is used to express the *Z*-factor as a function of pseudocritical temperature T_r and pseudocritical pressure P_r, thus $Z = Z(P_r,T_r)$. Once Z is known, the gas formation volume factor is easily determined for a given temperature and pressure using the real gas law.

The isothermal gas compressibility c_g is

$$c_g = \frac{1}{P_c}\left[\frac{1}{P_r} - \frac{1}{Z}\left(\frac{\partial Z}{\partial P_r}\right)_{T_r}\right] \tag{16.3}$$

where P_c is the critical pressure (psia).

Real gas viscosities are computed using the Carr, Kobayashi, and Burrows [1954] hydrocarbon gas viscosity determination procedure.

16.4.3 Pseudopressure Calculations

Pseudopressures are defined by

$$\psi(P) = 2\int_{P_o}^{P} \frac{P'}{\mu_g Z}\, dP' \tag{16.4}$$

where

P' = dummy integration variable with pressure units (psia)

P_o = reference pressure = 14.7 psia

P = specified pressure (psia)

μ_g = gas viscosity (cp)

Z = gas compressibility factor

The pseudopressure $\psi(P)$ is often written as $m(P)$. Since μ_g and Z depend on P', evaluation of Eq. (16.4) is accomplished by numerical integration using the trapezoidal rule and a user-specified pressure increment dP'.

16.4.4 Correlation Range Limits

The following range limits apply to correlations used in calculating gas Z-factors, compressibilities and viscosities:

$$\begin{aligned} 1.05 &< \frac{T}{T_c} < 3.0 \\ 0.01 &< \frac{P}{P_c} < 15.0 \\ 0.55 &< SPG < 1.5 \\ 40 &< T < 400 \end{aligned} \tag{16.5}$$

where

T_c = pseudocritical temperature (^{o}R)

P_c = pseudocritical pressure (psia)

T = temperature (^{o}R)

P = pressure (psia)

SPG = gas specific gravity

No values of T, P, or SPG should be used that exceed the above correlation ranges. If the range limit is exceeded, a fatal error will occur.

16.5 Rock-Fluid Interaction

Small scale laboratory measurements of fluid flow in porous media show that fluid behavior depends on the properties of the solid material. Laboratory measurements provide information at the core scale (Macro Scale) and, in some cases, at the microscopic scale (Micro Scale). The interaction between rock and fluid is modeled using a variety

of physical parameters that include relative permeability and capillary pressure [Collins, 1961; Dake, 1978; Koederitz, et al., 1989]. They are the subject of the present section.

16.5.1 Relative Permeability

Relative permeability was defined in Chapter 3. In the absence of measured data, correlations such as Honarpour, et al. [1982] provide a reasonable starting point for estimating relative permeability. Alternatively, relative permeability can be represented empirically using the saturation exponent method. The relative permeability of phase ℓ is approximated by the equation

$$k_{r\ell} = k_{r\ell}^{\max} S_{n\ell}^{e_\ell} \tag{16.6}$$

where

S_ℓ = saturation of phase ℓ

$S_{n\ell}$ = normalized saturation of phase ℓ

e_ℓ = exponent of phase ℓ

$k_{r\ell}^{\max}$ = maximum relative permeability of phase ℓ.

Table 16-4 presents equations for calculating the normalized saturation. End point saturation values in Table 16-4 are

S_{orw} = residual oil saturation in the presence of water

S_{org} = residual oil saturation in the presence of gas

S_{gc} = critical gas saturation

S_{wc} = connate water saturation

Saturation end points for relative permeability curves are used to establish initial fluids-in-place in addition to modeling multiphase flow behavior.

Table 16-4
Normalized Saturations for Relative Permeability

Normalized Water Saturation for k_{rw} Calculation	$S_{nw} = (S_w - S_{wc})/(1 - S_{orw})$ $k_{rw} = 0 \text{ if } S_w \le S_{wc}$ $k_{rw} = k_{rw}^{\max} \text{ if } S_w \ge 1 - S_{orw}$
Normalized Oil Saturation for k_{row} Calculation	$S_{now} = (S_o - S_{orw})/(1 - S_{wc})$ $k_{row} = 0 \text{ if } S_o \le S_{orw}$ $k_{row} = k_{row}^{\max} \text{ if } S_o \ge 1 - S_{wc}$
Normalized Oil Saturation for k_{rog} Calculation	$S_{nog} = (S_o - S_{org})/(1 - S_{gc} - S_{wc})$ $k_{rog} = 0 \text{ if } S_o \le S_{org}$ $k_{rog} = k_{rog}^{\max} \text{ if } S_o \ge 1 - S_{gc} - S_{wc}$
Normalized Gas Saturation for k_{rg} Calculation	$S_{ng} = (S_g - S_{gc})/(1 - S_{org} - S_{wc})$ $k_{rg} = 0 \text{ if } S_g \le S_{gc}$ $k_{rg} = k_{rg}^{\max} \text{ if } S_g \ge 1 - S_{org} - S_{wc}$

In practice, relative permeability is one of the most useful physical quantities available for performing a history match. The curves that are initially entered into a reservoir flow model are often modified during the history matching process. The rationale for changing relative permeability curves is based on the observation that they are usually obtained by flooding core in the laboratory. Laboratory floods correspond to a much smaller scale than flow through the drainage area of a well. Therefore, it can be argued that relative permeability curves measured in the laboratory are not representative of multiphase flow on the reservoir scale. In addition, the modeling team needs to realize that the relative permeability curves used in a flow model are most representative of the type of experiment that was used to measure the curves. Applying these

curves to another type of displacement mechanism can introduce significant error.

16.5.2 IFLO Three-Phase Relative Permeability

Three-phase relative permeability should be used when oil, water, and gas are flowing simultaneously. As a practical matter, three-phase relative permeabilities are difficult to measure and correlations are used instead of direct measurements. IFLO contains a correlation for computing a three-phase oil relative permeability curve using two-phase water-oil and gas-oil relative permeability curves. The three-phase oil relative permeability algorithm in IFLO is based on the assumptions that:

1. The water relative permeability curve (k_{rw}) obtained for a water-oil system depends only on water saturation, and
2. The gas relative permeability curve (k_{rg}) obtained for a gas-oil system depends only on gas saturation.

Given these assumptions, k_{rw} and k_{rg} for water-oil and gas-oil systems, respectively, are also valid for a water-gas-oil system. The three-phase oil relative permeability k_{ro3} is calculated as

$$k_{ro3} = k_{rom}\left(\frac{k_{row}}{k_{rom}} + k_{rw}\right)\left(\frac{k_{rog}}{k_{rom}} + k_{rg}\right) - \left(k_{rw} + k_{rg}\right) \qquad (16.7)$$

where

k_{row} = oil relative permeability for water-oil system,

k_{rog} = Oil relative permeability for gas-oil system,

k_{rom} = oil relative permeability at zero gas saturation and irreducible water saturation.

Equation (16.7) is based on the work by Stone [1973], and Dietrich and Bondor [1976]. Other models of three-phase relative permeability are discussed by Blunt [1999] and Fanchi [2000].

When the three-phase calculation is activated, the user must be sure the input water-oil and gas-oil relative permeability curves are realistic. For example, if we write irreducible water saturation as S_{wr}, the

relative permeability constraint k_{row} (1 - S_{wr}) = k_{rog} (S_o + S_w = 1.0) must be satisfied since S_g = 0 in both cases.

16.5.3 Capillary Pressure

Capillary pressure is often included in reservoir simulators to help establish the initial distribution of fluids. Capillary pressure is also used in fractured reservoir flow models for controlling the flow of fluids between the fracture and the rock matrix. The role of capillary pressure in flow model initialization is discussed in more detail in the next chapter.

The capillary pressure concept is also used to simplify the handling of the phase pressures and potentials in the flow equations. The differences in phase pressures

$$P_{cow} = P_o - P_w \tag{16.8}$$

and

$$P_{cgo} = P_g - P_o \tag{16.9}$$

are the capillary pressures for oil-water and gas-oil systems, respectively. Experimentally P_{cow} and P_{cgo} have been observed to be functions of water and gas saturations, respectively. Equations (16.8) and (16.9) are used to replace the phase pressures in fluid flow equations with a single phase pressure.

16.5.4 Capillary Pressure and Transition Zones

Capillary pressure data is used for determining initial fluid contacts and transition zones. The relationship between capillary pressure and elevation is used to establish the initial transition zone in the reservoir. The oil-water transition zone, for example, is the zone between water only flow and oil only flow. It represents that part of the reservoir where 100% water saturation grades into oil saturation with irreducible water saturation. Similar transition zones may exist at the interface between any pair of immiscible phases.

If capillary pressure is neglected, transition zones are not included in the model. Figure 16-5 illustrates a dipping reservoir with fluid contacts and no transition zones. Figure 16-6 shows the effect of neglecting capillary pressure when a grid is used to represent the reservoir. The fluid content of the gridblock is determined by the location of the gridblock midpoint relative to a contact between two phases. The gridblock midpoint is shown as a dot in the center of the gridblocks in Figure 16-6. Thus, if the gridblock midpoint is above the gas-oil contact (GOC), the entire gridblock is treated as a gas cap gridblock (single-phase gas with irreducible water saturation), even if much of the gridblock extends into the oil column. A more accurate representation may be obtained by decreasing the thickness of the gridblocks and increasing the number of gridblocks, but this often results in a substantial increase in the cost of making computer runs. Some simulators initialize saturation in the gridblock by splitting the gridblock into a group of thin layers and calculating a thickness weighted average saturation. The resulting saturation is then applied to the user-specified gridblock thickness. The thin layers are not used in the flow calculation. The relative benefits of incremental accuracy versus incremental cost should be considered when modeling transition zones.

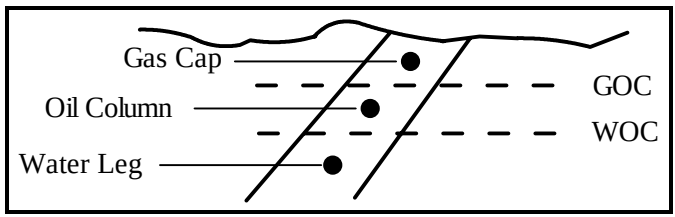

Figure 16-5. Case 1: Neglect Transition Zones

The inclusion of a transition zone in the model requires specifying a capillary pressure (P_c) curve as a function of saturation for whatever transition zone is being modeled: oil-water, gas-oil, or gas-water. The height h_{tz} of the transition zone above the free water level (the level corresponding to P_c = 0 psia) is proportional to the capillary pressure and inversely proportional to the density difference between the two

fluids (see Chapter 3). The height of the transition zone is a function of saturation because capillary pressure depends on saturation. The oil-water transition zone is typically the thickest transition zone because the density difference between oil and water is less than the density difference between gas and an immiscible liquid.

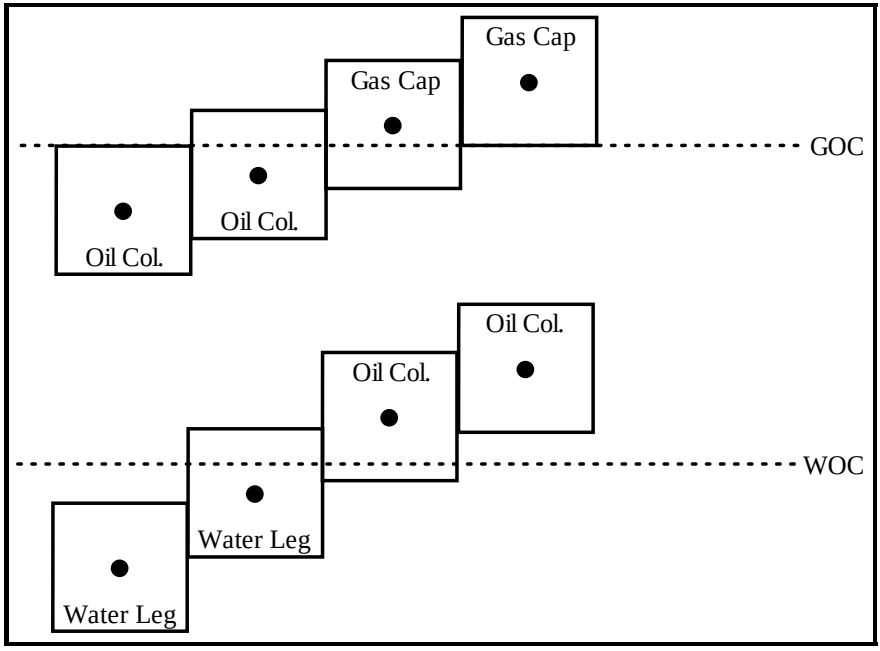

Figure 16-6. Initial Fluid Distribution in Model without Transition Zone

Figures 16-7 and 16-8 illustrate the initialization of a model containing a nonzero capillary pressure curve. First, the height h_{tz} above a specified contact, such as the water-oil contact (WOC), is calculated from P_c and the difference in fluid densities at the contact. The saturation of a gridblock with a midpoint at height h_{tz} above the contact is then calculated from the relationship between capillary pressure and saturation.

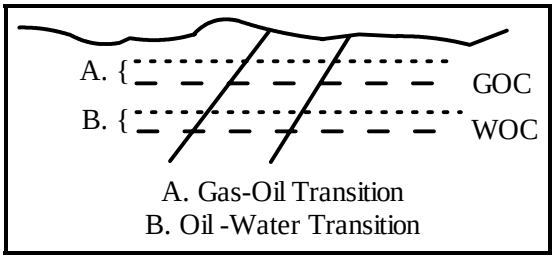

Figure 16-7. Case 2: Include Transition Zone in Model

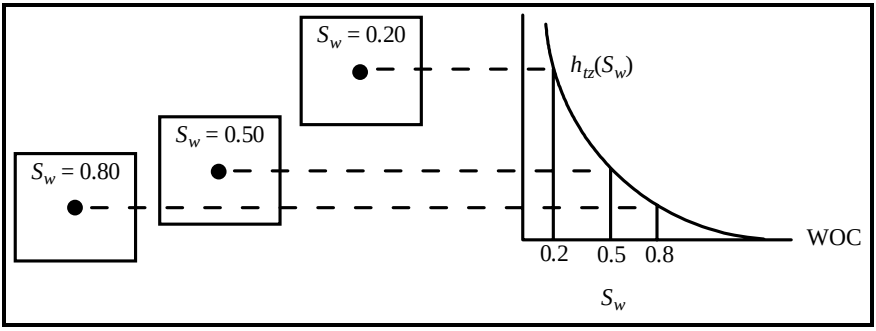

Figure 16-8. Initial Gridblock Saturations in Model with Transition Zone

Transition zones complicate the identification of fluid contacts because the definition of fluid contact is not universally accepted. For example, WOC may be defined as the depth at which the capillary pressure is zero (the free water level). The WOC depth can be identified using a repeat formation test (RFT) by finding the point of intersection between the oil-phase pressure and the water-phase pressure. By contrast, the WOC may be defined as the deepest point in the reservoir at which a well can still produce water-free oil. The different definitions of contact result in differences in the transition zone model, so it is important to know which definition is applicable. In some cases, it may be necessary to prepare models with both definitions. One definition is treated as the base case and the other definition is a sensitivity case.

Exercises

Exercise 16.1A Suppose the bubble point pressure is 2400 psia in a reservoir with 30% irreducible water saturation. Is the reservoir saturated or undersaturated at an initial reservoir pressure of 2515 psia?

Exercise 16.1B List the fluid phases that are present at initial conditions.

Exercise 16.2A The pressure at the GOC in a gas reservoir with an oil rim is equal to the bubble point pressure. Suppose gas is produced from the gas cap. Will the resulting pressure at the GOC be above or below the bubble point pressure?

Exercise 16.2B Suppose the bubble point pressure of oil in a reservoir simulator gridblock is 2514 psia prior to depletion. If the gridblock pressure drops to 2500 psia, will the gridblock contain any free gas?

Exercise 16.3 A gas condensate reservoir has a dew point pressure of 2500 psia. If condensate drops out at the rate of 500 STB/psia drawdown below the dew point pressure, how much condensate will drop out if the reservoir pressure declines from 2600 psia to 2300 psia?

Exercise 16.4A Using data in the file CS_HM.DAT, calculate the oil formation volume factor in a gridblock that has a pressure of 4014.7 psia. Note: based on the bubble point pressure in the data file, the gridblock is undersaturated.

Exercise 16.4B Is there free gas in the gridblock?

Exercise 16.4C Run file CS_HM.DAT and report the total initial fluid volumes in place in the reservoir. Do the model results support your answer to Part B?

Exercise 16.5A Using data in the file CS_HM.DAT, calculate oil viscosity in a gridblock that has a pressure of 4014.7 psia. Note: based on the bubble point pressure in the data file, the gridblock is undersaturated.

Exercise 16.5B Using data in the file CS_HM.DAT, calculate the solution gas-oil ratio in a gridblock that has a pressure of 4014.7 psia. Note: based on the bubble point pressure in the data file, the gridblock is undersaturated.

Exercise 16.6A Use the real gas law $PV = ZnRT$ to find a general expression for gas formation volume factor B_g. Use subscripts "*s*" and "*r*" to denote surface conditions and reservoir conditions, respectively.

Exercise 16.6B Calculate B_g using $\{P_s = 14.7$ psia, $T_s = 60^oF$, $Z_s = 1\}$ and $\{P_r = 2175$ psia, $T_r = 140^oF$, $Z_r = 0.9\}$. Express B_g as reservoir cubic feet per standard cubic feet (RCF/SCF).

Exercise 16.6C Calculate B_g using $\{P_s = 1$ atm, $T_s = 20^oC$, $Z_s = 1\}$ and $\{P_r = 15$ MPa, $T_r = 60^oC$, $Z_r = 0.9\}$. Express B_g as reservoir cubic meters per standard cubic meter (Rm^3/Sm^3).

Exercise 16.6D What is the difference between the calculation in Part B and the calculation in Part C?

Exercise 16.7A Data file EXAM9_PSI models depletion of a gas reservoir with aquifer support. Initial reservoir pressure is approximately 1947 psia. Run the model at a temperature of 226°F and record time, pressure, gas rate and water rate at the end of the run. Report the gas viscosity in the gas PVT table at 2015 psia pressure.

Exercise 16.7B Repeat Part A at a temperature of 150°F.

Exercise 16.7C Explain the differences in model performance. For this example, neglect the temperature dependence of water properties.

Exercise 16.8A A reservoir gridblock has a length of 1000 ft, a width of 2000 ft, and a gross thickness of 15 ft. What is the bulk volume of the gridblock? Express your answer in ft^3, bbl, and m^3.

Exercise 16.8B If the reservoir gridblock porosity is 0.2 and the net-to-gross ratio is 0.8, what is the pore volume of the gridblock? Express your answer in ft^3, bbl, and m^3.

Exercise 16.8C If the reservoir gridblock has a gas saturation of 0.7, what is the volume of gas in the gridblock? Express your answer in ft^3, bbl, and m^3.

Exercise 16.9A Calculate the pore volume of a gridblock with $\Delta x = 200$, $\Delta y = 200$ ft, $\Delta z = 80$ ft, $\phi = 0.20$, and net-to-gross ratio = 0.9. Express your answer in reservoir barrels. Note: 1 bbl = 5.6146 cu ft.

Exercise 16.9B If initial oil saturation is 0.7 and residual oil saturation is 0.25, what is the volume of mobile oil in the gridblock? Express your answer in reservoir barrels (RB).

Exercise 16.9C If a well produces 500 RB oil/day from the gridblock, how long does it take to produce all of the mobile oil in the gridblock?

Chapter 17

Model Initialization

The flow model is considered initialized when it has all the data it needs to calculate fluids in place. The reservoir must be characterized in a format that can be used by a simulator. Reservoir characterization includes the selection of a grid and the distribution of reservoir properties in the grid. It may also require the study of multiple reservoir realizations in the case of a geostatistical model study [for example, see Chambers, et al., 2000; Kelkar, 2000; Deutsch and Journel, 1998; Pannatier, 1996; Lieber, 1996; Rossini, et al., 1994; Englund and Sparks, 1991; Haldorsen and Damsleth, 1990; and Isaaks and Srivastava, 1989]. All fluid data corrections must be completed during the model initialization process. Another aspect of model initialization is equilibration which depends on the definition of the grid, and is the point at which fluid contacts are established and fluid volumes are calculated. Each of these topics is discussed below.

17.1 Grid Definition

Flow model grids may be defined in several different ways. Several authors discuss different types of grids, including Aziz [1993], Verma and Aziz [1997], Heinemann and Heinemann [1998], Ertekin, et al. [2001], Dogru, et al. [2002], Carlson [2003], Mlacnik and Heinemann [2003], and Mlacnik, et al. [2004]. Definitions of grid coordinate system

orientation vary from one simulator to another and must be clearly defined for effective use in a simulator. Reservoir grids can often be constructed in one-, two-, or three-dimensions, and in Cartesian or cylindrical coordinates. Horizontal 1-D models are used to model linear systems that do not include gravity effects. Examples of horizontal 1-D models include core floods and linear displacement in a horizontal layer. Core flood modeling has a variety of applications, including the determination of saturation-dependent data such as relative permeability curves. A dipping 1-D reservoir is easily defined in a model by specifying structure top as a function of distance from the origin of a grid.

Figure 17-1 shows an example of a 2-D grid. Grids in 2-D may be used to model areal and cross-sectional fluid movement. Grid orientation in 2-D is illustrated by comparing Figure 15-1c and Figure 17-1. Although Figure 15-1c has fewer gridblocks, which is computationally more efficient, Figure 17-1 may be useful in some circumstances. For example, Figure 17-1 is more useful than Figure 15-1c if the boundary of the reservoir is not well known or an aquifer needs to be attached to the flanks of the reservoir to match reservoir behavior.

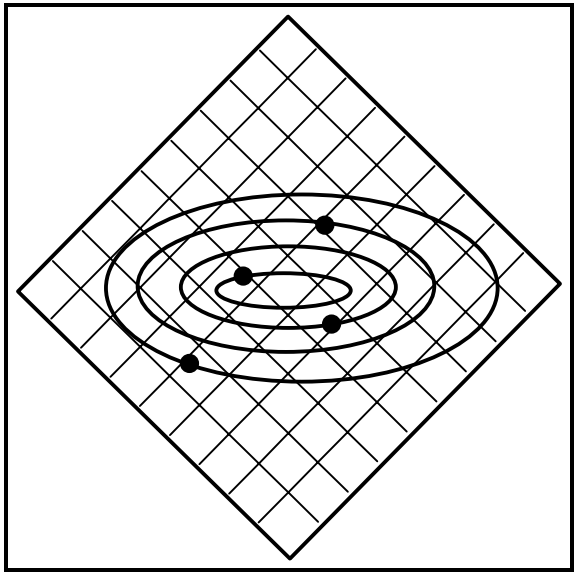

Figure 17-1. Grid Orientation

The use of 2-D grids for full field modeling has continued to be popular even as computer power has increased and made large 3-D models practical. Figure 17-2 shows a simple 3-D grid that is often called a "layer cake" grid. Techniques are available for approximating the vertical distribution of fluids in 2-D cross-sectional and 3-D models by modifying relative permeability and capillary pressure curves. The modified curves are called pseudo curves. An example of a pseudoization technique is the vertical equilibrium (VE) approximation. The principal VE assumption is that fluid segregation in the vertical dimension is instantaneous. This assumption is approximated in nature when vertical flow is rapid relative to horizontal flow. This situation occurs when the vertical permeability of the reservoir is comparable in magnitude to its horizontal permeability, and when density differences are significant, such as in gas-oil or gas-water systems. For more discussion of specific pseudoization techniques, see authors such as Taggart, et al. [1995], Ertekin, et al. [2001], Walsh and Lake [2003], and Carlson [2003] and their references.

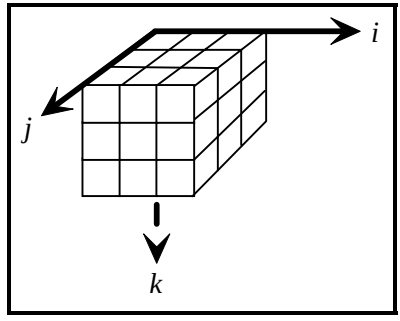

Figure 17-2. Example of a 3-D "layer cake" grid

One reason for the continuing popularity of 2-D grids is that the expectation of what is appropriate grid resolution has changed as simulation technology evolved. Thus, even though 3-D models can be used today with the grid resolution that was considered acceptable a decade ago for 2-D models, modern expectations often require that even finer grids be used for the same types of problems. This is an example of a task expanding to fit the available resources. Increased grid resolution

does not guarantee better reservoir management decisions. Indeed, it can be argued that the technological ability to add complexity is making it more difficult for people to develop a "big picture" understanding of the system being studied because they are too busy focusing on the details of a complex model. Once again, a judicious use of Ockham's Razor is advisable in selecting a reservoir grid. The grid should be appropriate for achieving study objectives.

In many cases, simple conceptual models may be useful in selecting a final grid for the model study, especially when determining the number of layers. As an illustration, suppose we want to track flood front movement in a very large field. In this case, we want as much areal definition as possible (at least three to five gridblocks between each gridblock containing a well), but this may mean loss of vertical definition. A way to resolve the problem is to set up one or more cross-section models representing different parts of the field. Vertical conformance effects in these regions are modeled in detail by calculating flow performance with the cross-section models. The flow performance of a detailed cross-section model is then matched by adjusting relative permeability curves in a model with fewer layers. The resulting pseudorelative permeability curves are considered acceptable for use in an areal model.

17.1.1 Non-Cartesian Grids

Near-wellbore coning models may be either 2-D or 3-D grids, but are defined in cylindrical rather than Cartesian coordinates. Coning (or radial) models are designed to study rapid pressure and saturation changes. Figure 17-3 shows an example of a radial grid. High throughput, that is, large flow rate through relatively small, near-wellbore gridblocks is most effectively simulated by a fully implicit formulation. Implicit pressure – explicit saturation (IMPES) can be used to model coning, but timesteps must be very small. Small timesteps are not a problem if the duration of the modeled history is short, as it would be in the case of a pressure transient test.

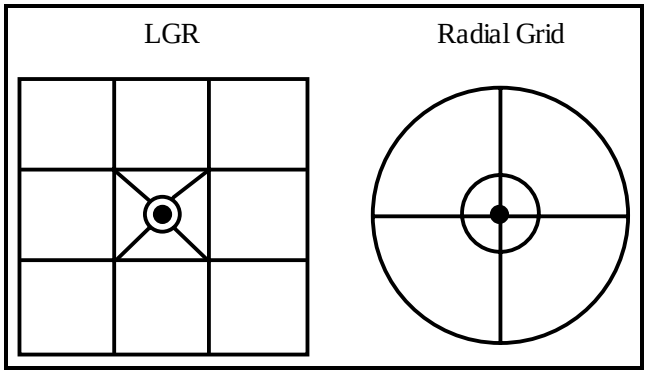

Figure 17-3. LGR and Radial Grids

Local grid refinement (LGR) is used to provide additional grid definition in a few selected regions of a larger grid. Raleigh [1991] compared LGR with a radial grid (Figure 17-3) and showed that the results are comparable. An LGR grid is an example of a flexible or unstructured grid. A flexible grid is made up of polygons in 2-D (polyhedra in 3-D) whose shape and size vary from one subregion to another in the modeled region. The LGR grid shown in Figure 17-3 is an example of a hybrid grid [Evans, 2004]. Hybrid grids are a combination of two different types of grids. In this case, it is the combination of a radial grid and a Cartesian grid.

Although many grid preparation options are available, improving grid preparation capability is an ongoing research and development topic. For example, some flow simulators are based on control volume finite element formulations that use triangular meshes in 2-D (tetrahedral meshes in 3-D). Finite difference grids typically display global orthogonality in which the grid axes are aligned along orthogonal coordinate directions. Examples of globally orthogonal coordinate systems include the Cartesian *x*-*y*-*z* system and the cylindrical *r*-θ-*z* system. Grids with global orthogonality may be distorted to fit local irregularities such as faults using corner point geometry as described below. By contrast, finite element grids display orthogonality in which gridblock boundaries are perpendicular to lines joining gridblock nodes on opposite sides of each boundary. An example of a locally orthogonal grid is a perpendicular

bisector (PEBI) grid. Aziz [1993], Chin [1993], Heinemann [1994], Verma and Aziz [1997], and Heinemann and Heinemann [1998] provide additional discussion. Mlacnik, et al. [2004] review the state-of-the-art in windowing techniques which allow the replacement of the grid or a part of the grid with another grid during the flow simulation. Dogru, et al. [2002] describe a technique for routinely solving megacell flow models using parallel processors.

17.1.2 Corner Point Geometry

Gridblocks may be defined in terms of corner point geometry or gridblock centered geometry (Figure 17-4). Gridblock centered geometry is the most straight forward technique, but corner point geometry has gained popularity because it yields more visually realistic representations of reservoir architecture. This is valuable when making presentations to people who are nonspecialists.

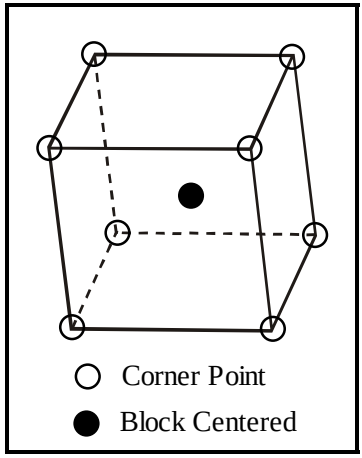

Figure 17-4. Gridblock Representation

Figure 17-5a-c illustrates the different geometric representations for a two-layer dipping reservoir. Although corner point geometry is visually more realistic, it is easier to define a grid with gridblock centered geometry. Gridblock centered geometry requires the specification

of the lengths of each side of the gridblock and the gridblock center or top. Corner point geometry requires the specification of the location of all eight corners of the gridblock. This is most readily accomplished with a computer program.

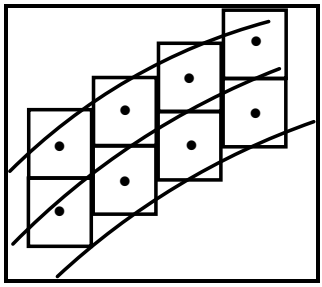

Figure 17-5a. Conventional Grid with Rectangles

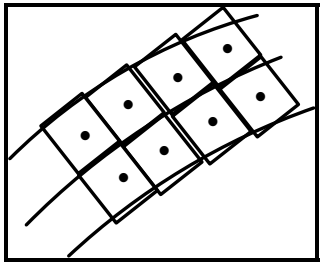

Figure 17-5b. Dip-aligned Grid with Rectangles

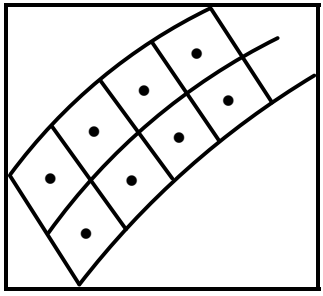

Figure 17-5c. Conventional Grid with Parallelograms

There is little computational difference between the results of corner point and gridblock centered geometry. One caution should be noted with respect to corner point geometry. It is possible to define very

irregularly shaped grids using corner points. This can lead to the distortion of flood fronts and numerical stability problems. Flood front distortions caused by gridding are an example of the grid orientation effect discussed by many authors, including Aziz and Settari [1979], Mattax and Dalton [1990], and Ertekin, et al. [2001].

17.2 Grid Orientation Effect

The grid orientation effect is exhibited by looking at a displacement process in 2-D (Figure 17-6). Each producer is equidistant from the single injector in a model that has uniform and isotropic properties. If grid orientation did not matter, the symmetry of the problem would show that both wells would produce injected water at the same time. The figure shows that production is not the same. Injected fluids preferentially follow the most direct grid path to the producer. Thus, even though the producers are symmetrically located relative to the injector and each other, the grid orientation alters the expected flow pattern.

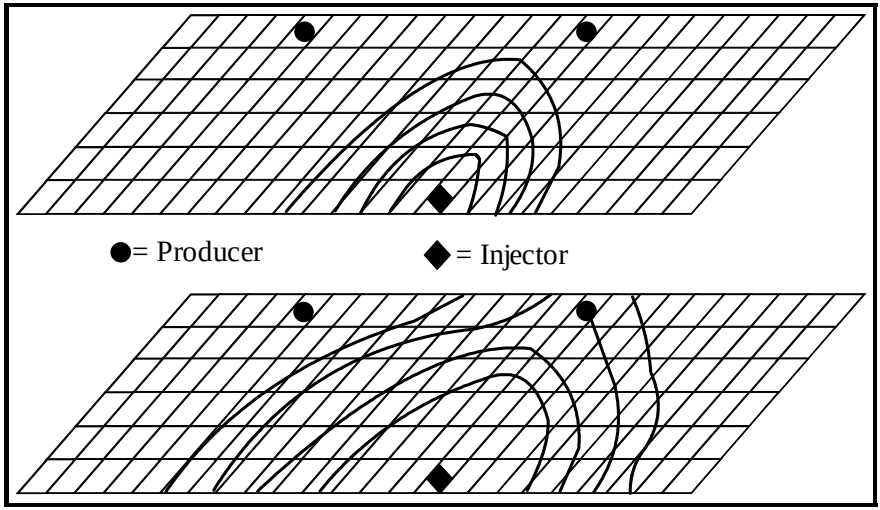

Figure 17-6. Grid Orientation Effect (after Hegre, et al. [1986]; reprinted by permission of the Society of Petroleum Engineers)

Figure 17-6 shows the effect on frontal advance. In this case, the front arrives sooner at the producer in the upper right than the producer in the upper left. If these results are incorporated in a reservoir management plan, they can reduce its overall effectiveness.

Another example of the grid orientation effect arises in connection with the modeling of pattern floods. Figure 17-7 illustrates two grids that can be used to model flow in a five-spot pattern. The parallel grid results in earlier breakthrough of injected fluids than the diagonal grid. This effect can be traced to the finite difference representation of the fluid flow equations.

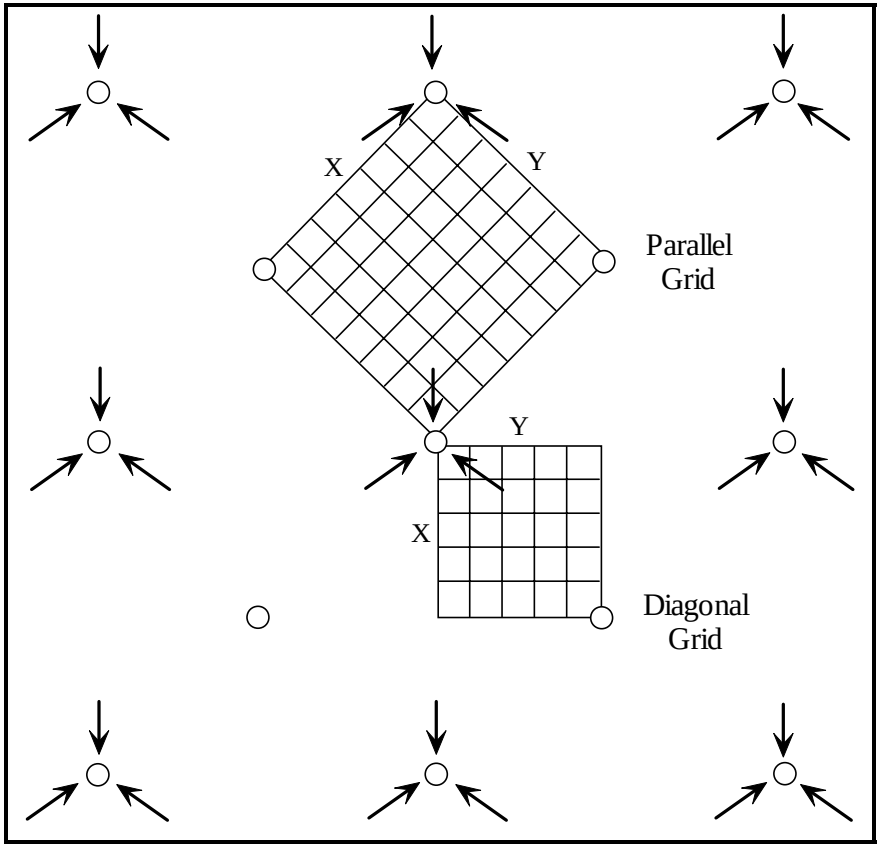

Figure 17-7. Parallel and Diagonal Grids (after Todd, et al. [1972]; reprinted by permission of the Society of the Petroleum Engineers)

Most finite difference simulators only account for flow contributions from gridblocks that are nearest neighbors to the central gridblock along orthogonal Cartesian axes. In Table 17-1, the central gridblock is denoted by "C" and the nearest neighbor gridblock contributing to the standard finite difference calculation in 2-D is denoted by an asterisk. The five gridblocks denoted by "C" and "*" are used in the five-point differencing scheme associated with a 2-D Cartesian grid.

Table 17-1
Finite Difference Stencils

Gridblock	***I* - 1**	***I***	***I* + 1**
***J* - 1**	9	*	9
J	*	C	*
***J* + 1**	9	*	9

Reservoir simulators are usually formulated with the assumption that diagonal gridblocks do not contribute to flow into gridblock "C". Diagonal gridblocks are denoted by "9" in Table 17-1. In most simulators, the mathematical formulation of the fluid flow equations assumes that the grid is aligned along the principal axes of the permeability tensor. This assumption and the use of the five-point finite difference stencil result in the neglect of contributions to flow from diagonal gridblocks.

Grid orientation effects can be minimized, at least in principle, if the diagonal gridblocks are included in the nine-point finite difference formulation [for example, see Young, 1984; Hegre, et al., 1986: Lee, et al., 1997]. The nine-point finite difference stencil includes all nine gridblocks shown in Table 17-1. The nine gridblocks are used to calculate flow into and out of the central gridblock in a 2-D Cartesian grid. The option of using a nine-point finite difference stencil is available in some commercial simulators. In 3-D models, the number of gridblocks needed to represent all adjacent gridblocks, including diagonal terms, is twenty-seven. By contrast, only seven gridblocks are used in the conventional formulation of a 3-D finite difference model.

17.3 IFLO Initialization Model

An equilibrium initialization algorithm and a gravity segregation algorithm are available as options in IFLO. These options are described below.

17.3.1 Equilibrium Initialization

Suppose a gridblock has a gas-oil contact (GOC) and a water-oil contact (WOC) as shown in Figure 17-8. The pressure at GOC is PGOC. Similarly, PWOC is the pressure at WOC. The initial oil phase pressure assigned to the gridblock in Figure 17-8 is determined by PWOC, PGOC and the depth of the node (midpoint) relative to the respective contact elevations. The equilibrium initialization algorithm is described in detail by Ammer, et al. [1991]. We closely follow their presentation here.

The oil density RO_{WOC} and water density RW_{WOC} at WOC are calculated using the pressure PWOC. The water-oil capillary pressure PCOW is calculated for the gridblock at the midpoint elevation EL using the densities at WOC, thus:

$$\mathrm{PCOW} = \frac{1}{144}\left(\mathrm{RW}_{\mathrm{WOC}} - \mathrm{RO}_{\mathrm{WOC}}\right)\cdot\left(\mathrm{WOC} - \mathrm{EL}\right) \qquad (17.1)$$

The initial water saturation SWI for the gridblock is calculated at the midpoint elevation using PCOW and the following algorithm:

1. If PCOW ≥ PCOW at irreducible water saturation S_{wr}, set SWI = S_{wr}.
2. If PCOW ≤ PCOW at water saturation $S_w = 1$, set SWI = 1.
3. If PCOW($S_w = 1$) < PCOW < PCOW($S_w = S_{wr}$), then interpolate the value of SWI from the user-input water-oil capillary pressure curve.

The notation PCOW($S_w = 1$) should be read as the variable PCOW is evaluated at $S_w = 1$ since PCOW is a function of S_w. Similarly, the notation PCOW($S_w = S_{wr}$) says that the variable PCOW is evaluated at $S_w = S_{wr}$.

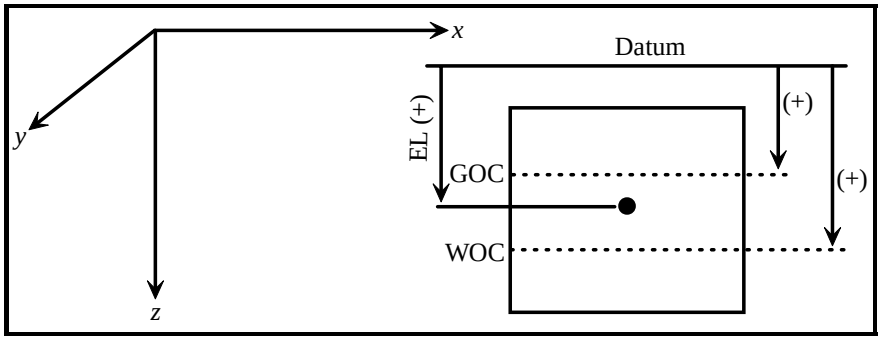

Figure 17-8. Depths for Initialization Algorithm

A similar calculation is performed to determine initial oil phase pressure at the GOC using gas and oil densities. The gas density RG_{GOC} and oil density RO_{GOC} at GOC are calculated using the pressure PGOC. The gas-oil capillary pressure PCGO is calculated for the gridblock at the midpoint elevation EL using the densities at GOC, thus:

$$\mathrm{PCGO} = \frac{1}{144}\left(\mathrm{RO}_{\mathrm{GOC}} - \mathrm{RG}_{\mathrm{GOC}}\right)\cdot\left(\mathrm{GOC} - \mathrm{EL}\right) \qquad (17.2)$$

The initial gas saturation (SGI) and initial oil saturation (SOI) for the gridblock are calculated at the midpoint elevation using PCGO, the previous calculation of SWI, and the following algorithm:

a, If PCGO ≤ PCGO at total liquid saturation $S_L = 1$, set SGI = 0.

b. If PCGO ≥ PCGO at $S_L = S_{wr}$, set SGI = 1 - SWI.

c. If PCGO(S_L = 1) < PCGO < PCGO ($S_L = S_{wr}$), then interpolate the value of SGI from the user-input water-oil capillary pressure curve.

The notation PCGO(S_L = 1) should be read as the variable PCGO is evaluated at S_L = 1 since PCGO is a function of S_L. Similarly, the notation PCGO($S_L = S_{wr}$) says that the variable PCOW is evaluated at $S_L = S_{wr}$.

Oil saturation is obtained from the constraint $S_o + S_w + S_g = 1$.

The initial oil phase pressure *P* is calculated using the saturations determined above to define the appropriate pressure gradient. The algorithm for calculating *P* follows:

Case 1: If SWI = 1, then

$$P = \mathrm{PWOC} + \frac{1}{144}\left(\mathrm{RW}_{\mathrm{WOC}}\right)\cdot\left(\mathrm{EL} - \mathrm{WOC}\right) + \mathrm{PCOW}(S_w = 1) \tag{17.3}$$

Case 2: If SOI > 0, then

$$P = \mathrm{PWOC} - \frac{1}{144}\left(\mathrm{RO}_{\mathrm{WOC}}\right)\cdot\left(\mathrm{WOC} - \mathrm{EL}\right) \tag{17.4}$$

Case 3: If SGI > 0 and SOI = 0, then

$$P = \mathrm{PWOC} + \frac{1}{144}\left(\mathrm{RO}_{\mathrm{WOC}}\right)\cdot\left(\mathrm{EL} - \mathrm{WOC}\right) + \frac{1}{144}\left(\mathrm{RO}_{\mathrm{GOC}}\right)\cdot\left(\mathrm{GOC} - \mathrm{EL}\right) + \frac{1}{144}\left(\mathrm{RG}_{\mathrm{GOC}}\right)\cdot\left(\mathrm{EL} - \mathrm{GOC}\right) - \mathrm{PCGO}(S_g = 1) \tag{17.5}$$

A natural gas-water system can be initialized by setting PWOC = PGOC and WOC = GOC + ε where ε is an incremental displacement such as 1 ft.

The oil-water transition zone thickness is given by

$$H_{owTZ} = \frac{\mathrm{PCWO}\left(\mathrm{SW} = S_{wr}\right) - \mathrm{PCWO}\left(\mathrm{SW} = 1\right)}{\left|\gamma_w - \gamma_o\right|} \tag{17.6}$$

where γ_o and γ_w are the oil and water pressure gradients in psia/ft. A similar calculation is performed to determine the gas-oil transition zone thickness.

17.3.2 Gravity Segregated Saturation Initialization

A simple model of a gravity segregated saturation distribution is calculated using the following algorithm. The algorithm assumes no solvent exists in the reservoir at the beginning of the run. We define reservoir geometry for depths increasing downward using the cases shown in Table 17-2.

Table 17-2
Algorithm for Gravity Segregated Saturation Initialization

Case 1	GOC ____ TOP ____ BOT _____ WOC _____	$S_g = 0$ S_o = SOI S_w = 1 - SOI	
Case 2	TOP ____ GOC ____ } f_g WOC ____ BOT ____ } f_w	f_g= GTHICK/THICK f_w=WTHICK/THICK $S_g = f_g \times$ SGI $S_o = (1 - f_g - f_w) \times$ SOI $S_w = 1 - S_o - S_g$	*If* $S_o < S_{or}$, *then* $S_o = 0$ $S_g = (f_g \times$ SGI*)/*(f_g+f_w) $S_w = 1 - S_g$
Case 3	TOP _____ GOC ____ } f BOT ____ WOC ____	f=1-(GTHICK/THICK) $S_o = 1 -$ SOI $\times f$ $S_g = (1 - f) \times$ SGI $S_w = 1 - S_o - S_g$	If $S_o < S_{or}$, then $S_o = 0$ S_w = 1 - SGI S_g = SGI
Case 4	GOC ____ TOP ____ } f WOC ____ BOT ____	$f = 1$-(WTHICK/THICK) $S_g = 0$ $S_w = 1 -$ SOI $\times f$ $S_o =$ SOI $\times f$	If $S_o < S_{or}$, then $S_o = 0$ $S_w = 1$
Case 5	TOP _____ BOT _____ GOC _____ WOC_____	$S_o = 0$ S_w = 1 - SGI S_g = SGI	
Case 6	GOC_____ WOC_____ TOP _____ BOT _____	$S_o = S_g = 0$ $S_w = 1$	

Gridblock elevations and thicknesses are calculated using the relationships

$$\text{Gridblock BOT} = \text{EL} + 0.5 * \text{DZ}$$

$$\text{Gridblock THICK} = \text{DZ}$$

$$\text{Gridblock TOP} = \text{BOT} - \text{THICK}$$

Water zone thickness

$$\text{WTHICK} = \text{BOT} - \text{WOC}$$

Gas zone thickness

$$\text{GTHICK} = \text{GOC} - \text{TOP}$$

The user must specify the initial oil saturation (SOI) for an oil-water system and the initial gas saturation (SGI) for a water-gas system. Given the initial saturations SOI and SGI, the algorithm in Table 17-2 is applied. Water saturation is calculated as $S_w = 1 - S_o - S_g$ in all cases. Cases 2 through 4 require the user to enter residual oil saturation S_{or}.

17.4 Case Study: Introduction

We introduce a case study in this chapter that is designed to increase your understanding of the reservoir simulation process, and to give you experience applying a simulator to a realistic model study. The case study is introduced in this chapter, and continued in Chapters 18 and 19.

17.4.1 Reservoir Management Objective

The first step in a study is to identify its objectives. The reservoir management objective of this case study is to ***optimize production from a dipping, undersaturated oil reservoir***. Constraints imposed on the case study objective are presented after we review some background information about the field of interest. The background information should be sufficient to initialize the flow model.

17.4.2 Reservoir Structure

Figure 17-9 shows a seismic line through an east-west cross section of the field. The single well (P-1) has been producing from what appears to be a fault block bounded upstructure and to the east by an unconformity; downstructure and to the west by a fault or aquifer; and to the north and south by sealing faults.

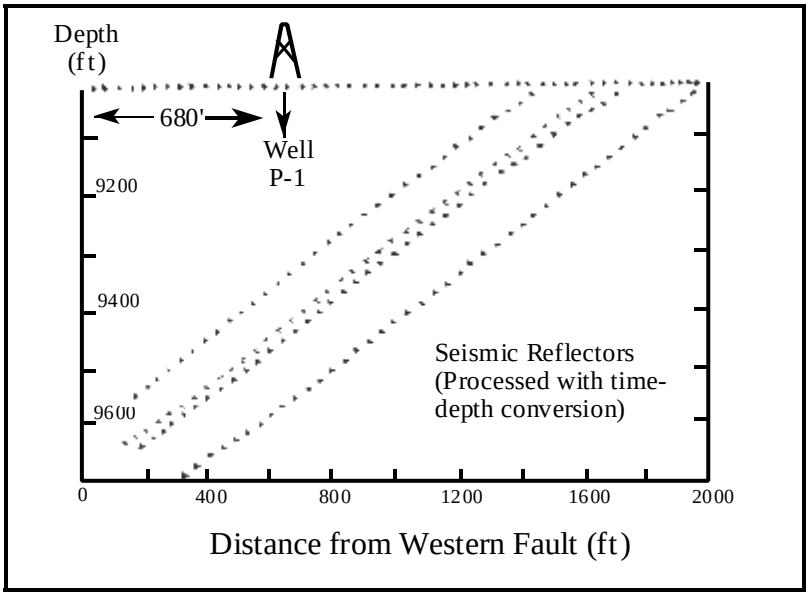

Figure 17-9. East-West Seismic Line

Figure 17-10 shows a well log trace. An analysis of the well log data shows that two major sands are present and are separated by a shale section. The lower sand includes streaks of shale. Well log measurements are presented in Table 17-3. The table headings refer to porosity ϕ, water saturation S_w, gross thickness h, and net-to-gross ratio NTG. The gross thickness of the upper pay zone is thinner than the gross thickness of the lower pay zone. Porosity is greater in the lower pay zone than in the upper pay zone. Both the upper and lower pay zones have comparable water saturation. Combining porosity and net thickness (gross thickness times net-to-gross ratio) shows that the lower pay zone has more storage capacity than the upper pay zone.

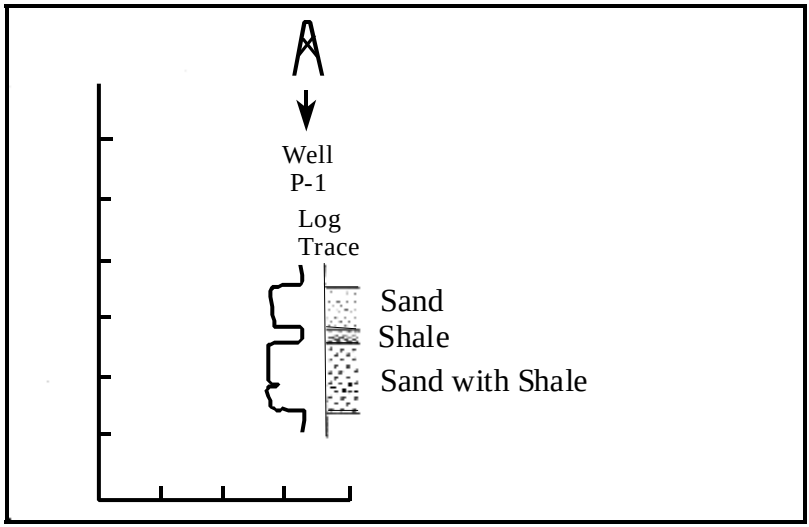

Figure 17-10. Well Log Trace

Table 17-3
Well Log Analysis Summary

Lithology (from cuttings)	Depth (ft) to Top of Formation	ϕ (fr.)	S_w (fr.)	h (ft)	NTG (fr.)
Sandstone	9330	0.20	0.30	80	0.9
Shale	9410	—	—	20	—
Sandstone with Shale Stringer	9430	0.25	0.30	120	0.8

Figure 17-11 is a conceptual sketch of the reservoir cross section. We have adopted an unconformity as our geologic model. This is an assumption that is subject to validation during the history matching stage of the reservoir management study. In some cases it may be necessary to hypothesize a different geologic model if we have problems obtaining a history match.

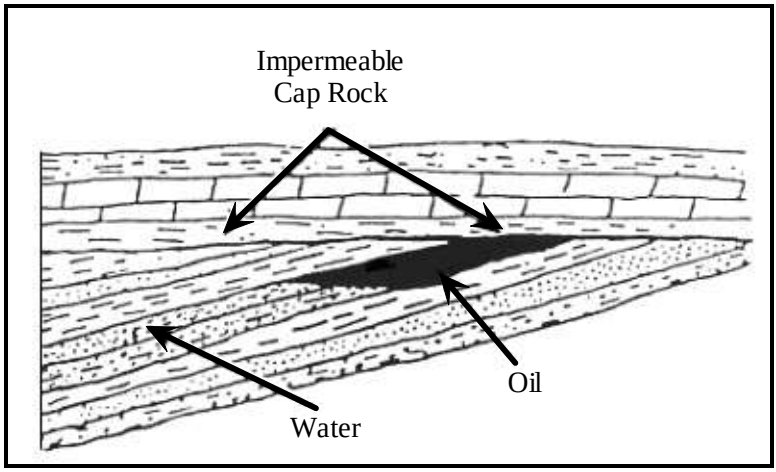

Figure 17-11. Conceptual Sketch of Reservoir Cross Section (after Clark [1969]; reprinted by permission of the Society of Petroleum Engineers)

17.4.3 Drill Stem Test

Well P-1 logs and cores show the presence of two major sands. A drill stem test (DST) run in both major sands yielded the information summarized in Table 17-4.

Table 17-4
Summary of Well P-1 DST Results

Wellbore Radius	0.25 ft
Wellbore Skin	-0.5
Initial Pressure	3936 psia at 9360 ft
No-Flow Boundary	Within 700 ft

Permeability is estimated from the DST data for both sands. Table 17-5 presents the results, together with average water saturation (S_w) values and oil saturation (S_o) values, for both major sands.

Table 17-5
Saturation and Permeability Values for Two Major Sands

Sand	S_w	$S_o = 1 - S_w$	Permeability (md)
1	0.3	0.7	75
2	0.3	0.7	250

17.4.3.1 DST Radius of Investigation

The radius of investigation for the DST as a function of shut-in time is

$$r_i = 0.029\sqrt{\frac{K\Delta t}{\phi\mu c_T}} \tag{17.7}$$

where K is permeability in md, ϕ is fractional porosity, μ is viscosity in cp, c_T is total compressibility in 1/psia, and Δt is shut-in time in hours. Table 17-6 summarizes the physical properties of the case study DST.

Table 17-6
Summary of DST Properties

K	Permeability	250 md
ϕ	Porosity	0.228
μ	Viscosity	0.71 cp
c_T	Total compressibility	13×10^{-6} psia^{-1}

An interpretation of the DST shows that a no-flow boundary exists within approximately 700 ft of production well P-1. This interpretation is consistent with our picture of the reservoir as a fault block bounded above by an unconformity. The no-flow boundary is indicating the distance to one of the lateral edges of the fault block. The presence of a no-flow boundary implies that the fault is sealing.

17.4.4 Fluid Properties

In addition to pressure, flow capacity, and boundary information, the DST provides a fluid sample. Table 17-7 presents fluid properties from a laboratory analysis of the DST fluid sample.

Table 17-7
Fluid Properties

Pressure	Oil		Rso	Gas		Water	
	Vis	FVF		Vis	FVF	Vis	FVF
psia	cp	RB/ STB	SCF/ STB	cp	RCF/ SCF	cp	RB/ STB
14.7	1.040	1.062	1	0.0080	0.9358	0.5000	1.0190
514.7	0.910	1.207	150	0.0112	0.0352	0.5005	1.0175
1014.7	0.830	1.295	280	0.0140	0.0180	0.5010	1.0160
1514.7	0.765	1.365	390	0.0165	0.0120	0.5015	1.0145
2014.7	0.695	1.435	480	0.0189	0.0091	0.5020	1.0130
2514.7	0.641	1.500	550	0.0208	0.0074	0.5025	1.0115
3014.7	0.594	1.550	620	0.0228	0.0063	0.5030	1.0100
4014.7	0.510	1.600	690	0.0260	0.0049	0.5040	1.0070
5014.7	0.450	1.620	730	0.0285	0.0040	0.5050	1.0040
6014.7	0.410	1.630	760	0.0300	0.0034	0.5060	1.0010

Initial reservoir pressure from the DST is 3936 psia at a depth of 9360 ft below sea level. This pressure is over 1400 psia greater than the laboratory measured bubble point pressure of 2514 psia and implies that the reservoir is initially undersaturated. Consequently, we do not expect a free gas saturation to exist in the reservoir. Initial gas production should be due to solution gas that comes out of solution at surface conditions.

17.4.4.1 Black Oil PVT Correction

The corrections for adjusting laboratory-measured differential liberation and separator data to a form suitable for use in a black oil simulator are given by the conversion equations:

$$B_o(p) = B_{od}(p)\frac{B_{ofbp}}{B_{odbp}}$$
$$R_{so} = R_{sofbp} - \left[R_{sodbp} - R_{sod}(p)\right]\frac{B_{ofbp}}{B_{odbp}} \tag{17.8}$$

where B_o is the oil formation volume factor and R_{so} is the solution GOR. The subscripts are defined as *d* represents differential liberation data; *f* represents flash data; and *bp* represents bubble point. For the case study, laboratory measurements include a flash from 6000 psig to 0 psig. Table 17-8 presents separator test conditions and results.

Table 17-8
Separator Test (Flash)

Separator P (psig)	GOR (SCF/STB)	FVF (RB/STB)
100	572	
0		
0	78	
Total GOR = 650		1.5

17.4.4.2 Undersaturated Oil Properties

Table 17-9 presents undersaturated oil properties. The slopes for undersaturated oil properties are discussed in Section 21.6. They are needed to calculate oil properties at undersaturated reservoir conditions. We do not show the slope of the solution gas-oil ratio at undersaturated

conditions because solution gas-oil ratio is constant when reservoir pressure is greater than bubble point pressure.

Table 17-9
Undersaturated Oil Properties

Pressure (psia)	Corrected B_{opb} (RB/STB)	μ_o (cp)	Remarks
2515	1.3800	0.641	Bubble Point
3935	1.3473	0.706	Undersaturated Values

17.4.5 Reservoir Management Constraints

Table 17-10 presents reservoir management constraints. In this case, for example, it is considered important to keep water-oil ratio (WOR) less than five STB water per STB oil. In addition, only one additional well may be drilled. These constraints are typically formulated by decision makers who have considered issues ranging from technical to commercial. The constraints are especially important in the prediction phase of the study.

Table 17-10
Reservoir Management Constraints

- One additional well may be drilled.
- Completion interval in existing well may be changed.
  - The well is presently completed in entire pay interval.
- Target oil rate is 1000 STB/day
- Water is available for injection if desired.
- WOR should not exceed five STB water per STB oil
- Minimum allowed BHP is 2600 psia
- Maximum allowed injection pressure is 5000 psia
- Minimum economic oil rate is 100 STB/day

Exercises

Exercise 17.1 Use the properties in Table 17-6 to fill in the following table for shut-in times of 0.25 day, 0.5 day, and 1 day.

Estimating the DST Radius of Investigation

Shut-in Time		Radius of Investigation (ft)
days	**hours**	
0.25	6	
0.50	12	
1.00	24	

Exercise 17.2 Apply the differential to flash conversion to the black oil data and verify that the PVT values are properly entered in data file CS_MB.DAT. What is the bubble point pressure in the model?

Exercise 17.3 Calculate the rate of change of oil FVF with respect to pressure and the rate of change of oil viscosity with respect to pressure for the undersaturated oil using data in Table 17-9.

Exercise 17.4A Data file CS_VC4.DAT is a vertical column model with four layers. Layers K = 1, 3, 4 are pay zones, and layer K = 2 is a shale layer. The data file is a model of primary depletion of an initially undersaturated oil reservoir. Run CS_VC4.DAT for three years and show gas saturation in all four layers at the end of the run. You should see gravity segregation and the formation of a gas cap in layer K = 3. The reporting times should be changed to 365 days, 730 days, and 1095 days. What are the original fluids in place in the model?

Exercise 17.4B By referring to file ITEMP.DAT, determine which model layers are being depleted through wellbore perforations.

Exercise 17.5 Replace solution gas-oil ratio in CS_VC4.DAT with the following data. Run the modified data file for a period of three years, and then compare the results with the results of Exercise 17.4.

Pressure (psia)	**Solution Gas-Oil Ratio (SCF/STB)**
14.7	1.0
514.7	54.0
1014.7	105.0
1514.7	209.0
2014.7	292.0
2514.7	357.0
3014.7	421.0
4014.7	486.0
5014.7	522.0
6014.7	550.0

Exercise 17.6 Run the data file prepared in Exercise 17.5 with the assumption that no fluids can flow between model layers (multiply *z*-direction transmissibility by zero).

Exercise 17.7 Run data file CS_VC4.DAT for three years with the bubble point pressure reduced by 500 psia. The reporting times should be changed to 365 days, 730 days, and 1095 days. What effect does this have on original solution gas-oil ratio and model performance?

Chapter 18

History Matching

Project objectives help define the level of detail that will be incorporated in a reservoir flow model. Once objectives are defined, it is helpful to think of the study proceeding in three stages: the history matching stage; a calibration stage, which provides a smooth transition between the first and third stages; and the prediction stage. The first step of the history matching stage is the collection and analysis of data.

18.1 Data Preparation

Data must be acquired and evaluated with a focus on its quality and the identification of relevant drive mechanisms that should be included in the model [for example, see Crichlow, 1977; Saleri, et al., 1992; Raza, 1992; Carlson, 2003]. Given that information, it is possible to select the type of model that will be needed for the study: conceptual, window area, or full field model. In many cases all three of these model types may be required, as Fanchi, et al. [1996] have illustrated. Data must be acquired for each model.

Some of the data that is required for a model study can be found in existing reports. The modeling team should find as many reports as it can from as many disciplines as possible. Table 18-1 lists the types of data that are needed in a model study. A review of geophysical, geological, petrophysical, and engineering reports provides a background on

how the project has been developed and what preconceived interpretations have been established. During the course of the study, it may be necessary to develop not only a new view of the reservoir, but also to prepare an explanation of why the new view is superior to a previously approved interpretation. If significant gaps exist in the reports, particularly regarding the historical performance of the field, it is wise to update them.

Table 18-1
Data Required for a Simulation Study

Property	Sources
Permeability	Pressure transient testing, Core analyses, Correlations, Well performance
Porosity, Rock compressibility	Core analyses, Well logs
Relative permeability and capillary pressure	Laboratory core flow tests
Saturations	Well logs, Core analyses, Pressure cores, Single well tracer tests
Fluid property (PVT) data	Laboratory analyses of reservoir fluid samples
Faults, boundaries, fluid contacts	Seismic, Pressure transient testing
Aquifers	Seismic, Material balance calculations, Regional exploration studies
Fracture spacing, orientation, connectivity	Core analyses, Well logs, Seismic, Pressure transient tests, Interference testing, Wellbore performance
Rate and pressure data, completion and workover data	Field performance history

The pressure range associated with fluid property data should cover the entire range of pressures expected to be encountered over the life of the field. The data should be smooth to enhance computational efficiency and to ensure data consistency. A check on data consistency is a calculation of fluid compressibility. If negative compressibility is encountered, the data should be corrected. The problem of negative compressibility occurs most often when data is extrapolated beyond measured pressure ranges.

Flow units should be determined by reviewing geological and petrophysical data. It is possible to represent the behavior of a flow unit by defining a set of PVT and Rock property tables for each flow unit. PVT property tables contain data that describe fluid properties, while Rock property tables represent relative permeability and capillary pressure effects. Each set of PVT or Rock property tables applies to a particular region of gridblocks, hence the collection of gridblocks to which a particular set of PVT or Rock property tables applies is referred to as a PVT or Rock region. The number of flow units, and the corresponding number of PVT and Rock regions, should be kept to the minimum needed to achieve the objectives of the study.

One of the essential tasks of the data acquisition stage is determining the history of field performance and select data that should be matched during the history matching process. For example, if a gas-water reservoir is being modeled, gas rate is usually specified and water production is matched. By contrast, if an oil reservoir is being modeled, oil rate is specified and water and gas production are matched.

A review of available data may identify gaps or errors in the data. If it does, additional data should be obtained when possible. This may require special laboratory tests, depending on the objectives of the study. If additional field tests are needed, they should be requested and incorporated into the study schedule. Due to project costs and operating constraints, it may be difficult to justify the expense of acquiring more data or delaying the study while additional data is obtained. If measured data cannot be obtained during the scope of the study, then correlations or data from analogous fields will have to be used. Values must be entered into the simulator, and it is necessary to select values that can be

justified. The modeling team should take care to avoid underestimating the amount of work that may be needed to prepare an input data set. It can take as long to collect and prepare the data as it does to do the study.

18.2 Illustrative History Matching Strategies

There is no single, universally accepted strategy for performing a history match. Several authors have presented history matching guidelines, including Crichlow [1977], Thomas [1982], Mattax and Dalton [1990], Saleri, et al. [1992], and Carlson [2003]. Carlson [2003] pointed out that the guidelines suggested by two or more authors may actually contradict each other. Nevertheless, there are some general guidelines that can help move a history match toward successful completion. Table 18-2 presents one set of history matching guidelines. The first two steps in the table take precedence over the last two steps. If the first two steps cannot be achieved, there is a good chance that the model is inadequate and revisions will be necessary. An inadequate model may be due to a variety of problems: for example, the wrong model was selected, the reservoir is poorly characterized, or field data is inaccurate or incomplete.

Among the data variables matched in a typical black oil or gas study are pressure, production rate, water-oil ratio (WOR), gas-oil-ratio (GOR), and tracer data if it is available. More specialized studies, such as compositional or thermal studies, should also match data unique to the process, such as well stream composition or the temperature of produced fluids.

The pressure is usually the first dynamic variable to be matched during the history matching process. A comparison of estimated reservoir pressures obtained from well tests of a single well on successive days shows that errors in reported historical pressures can be up to 10 percent of pressure drawdown. This error may be larger than Peaceman's correction. As a first approximation, it is sufficient to compare uncorrected historical pressures directly with model pressures, particularly if your initial interest is in pressure trends and not in actual pressure values.

Pressure corrections should be applied when fine tuning the history match.

Table 18-2
Suggested History Matching Procedure

Step	Remarks
I	Match volumetrics with material balance and identify aquifer support.
II	Match reservoir pressure. Pressure may be matched both globally and locally. The match of average field pressure establishes the global quality of the model as an overall material balance. The pressure distribution obtained by plotting well test results at given points in time shows the spatial variation associated with local variability of field performance.
III	Match saturation dependent variables. These variables include water-oil ratio (WOR) and gas-oil ratio (GOR). WOR and GOR are often the most sensitive production variables in terms of both breakthrough time and the shape of the WOR or GOR curve.
IV	Match well flowing pressures.

Production rates are usually from monthly production records. The modeler specifies one rate or well pressure, and then verifies that the rate is entered properly by comparing observed cumulative production with model cumulative production. After the rate of one phase is specified, the rates of all other phases must be matched by model performance. In many cases, observed rates will be averaged on a monthly or quarterly basis and then compared with model calculated rates. If the history of reservoir performance is extensive, then it is often wise to place a greater reliance on the validity of the most recent field data when performing a history match.

Phase ratios, such as GOR and WOR, are sensitive indicators of model performance. Matching ratios provides information about pressure depletion and front movements. Tracers are also useful for modeling

fluid fronts. Tracers need not be expensive chemicals; they can even be changes in the salinity of produced water. Salinity changes can occur as a result of mixing when injected brine and *in situ* brine have different salinities. Water sample analysis on a periodic basis is useful for tracking salinity variation as a function of time. For a review of advances in interwell tracer analysis, see Guan, et al. [2005].

An emerging history matching strategy is to combine time-lapse seismic reservoir monitoring with traditional flow modeling in a process referred to as seismic history matching [Lumley and Behrens, 1997]. Seismic history matching is an iterative process, as illustrated in Figure 18-1.The ovals in the figure represent model preparation, while the rectangles correspond to the history matching process.

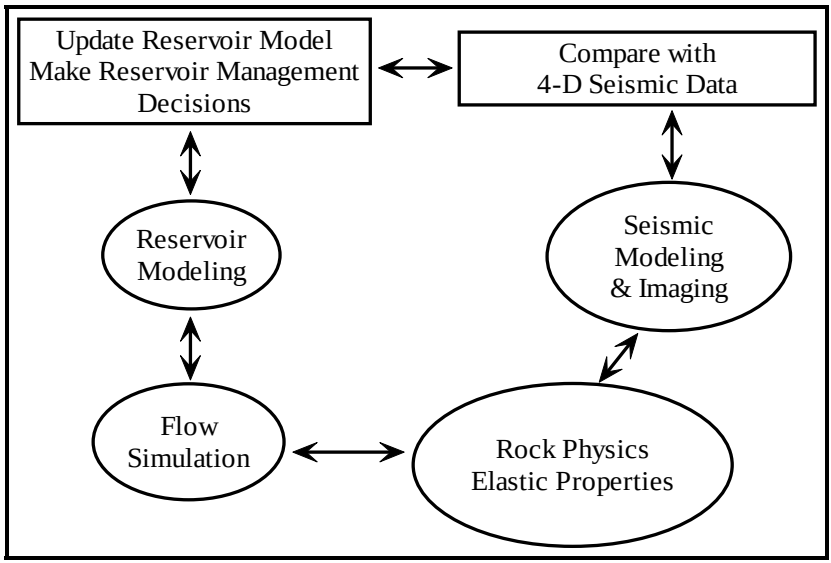

Figure 18-1. Seismic History Matching
[after Lumley and Behrens, 1997]

The seismic history matching process includes steps for incorporating time-lapse seismic monitoring information. Time-lapse seismic monitoring compares two or more 3-D seismic surveys over the same region at different points in time. IFLO includes algorithms for providing information that can facilitate all of the tasks shown in Figure 18-1. This

has been made possible by the inclusion of a petrophysical model in the flow simulator.

18.3 Key History Matching Parameters

A fundamental concept in history matching is the *hierarchy of uncertainty* which is a ranking of model input data quality. The modeler uses the hierarchy of uncertainty to rank data from most reliable to least reliable. Changes to model input data are then constrained by the principle that the least reliable data should be changed first. The question is: which data are least reliable?

Data reliability is determined when data are collected and evaluated for completeness and validity. This is such an important step in establishing a feel for the data that the modeler should be closely involved with the review of data. Relative permeability data are typically placed at the top of the hierarchy of uncertainty because they are modified more often than other data. Relative permeability curves are often determined from core floods. As a consequence, the applicability of the final set of curves to the rest of the modeled region is always in doubt.

Initial fluid volumes may be modified by changing a variety of input parameters, including relative permeability endpoints and fluid contacts. Model calculated, original fluid volumes in place are constrained by independent techniques like volumetrics and material balance studies.

Attempts to match well data may require changing the producing interval or the productivity index (PI) of a perforation interval. If it is difficult to match well performance in a zone or set of zones, the modeler needs to look at a variety of possibilities, including unexpected completion and wellbore problems. In one study, for example, an unexpectedly high GOR from a perforation interval that was known to be below the gas-oil contact was due to gas flow in the annulus between the tubing and the casing. This result was confirmed by running a cement bond log and finding a leak in the wellbore interval adjacent to the gas cap. Gas cap gas was entering the wellbore and causing greater than expected

production GOR. This effect can be modeled by a variety of options, depending on the degree of accuracy desired: for example, it could be modeled by altering productivity index (PI) in the well model or by designing a near wellbore conceptual model and preparing pseudorelative permeability curves. The choice of method will influence the predictive capability of the model. Thus, a pseudorelative permeability model will allow for high GOR even if the well is recompleted, whereas the PI could be readily corrected at the time of well recompletion to reflect the improvement in wellbore integrity.

Map adjustments may also be necessary. This used to be considered a last resort change because map changes required substantial effort to digitize the modified maps and prepare a revised grid. Preprocessing packages and computer-aided geologic modeling are making map changes a more acceptable history match method. In the case of geostatistics, a history matching process may actually involve the use of several different geologic models. Each geologic model is called a stochastic image or realization.

Toronyi and Saleri [1988] present a detailed discussion of their approach to history matching. It is noteworthy because they provide guidance on how changes in some history match parameters affect matches of saturation and pressure gradients. A summary is presented in Table 18-3 which shows, for example, that a change in pore volume can affect pressure as it changes with time. As another example, relative permeability changes are useful for matching saturation variations in time and space. Notice that fluid property data are seldom changed to match field history. This is because fluid property data tend to be more accurately measured than other model input data.

History matching must not be achieved by making incorrect parameter modifications. For example, matching pressure may be achieved by adjusting rock compressibility, yet the final match value should be within the set of values typically associated with the type of rock in the formation. In general, modified parameter values must be physically meaningful.

Table 18-3
Influence of Key History Matching Parameters

Parameter	Pressure Match	Saturation Match
Pore volume	ΔP versus Δt	*
Permeability thickness	ΔP versus Δx	ΔS versus Δx
Relative permeability	Not used	ΔS versus Δx and ΔS versus Δt
Rock compressibility	*	Not used
Bubble point pressure	ΔP versus Δt *	*
*Avoid changing if possible		

18.4 Evaluating the History Match

One way to evaluate the history match is to compare observed and calculated parameters. Typically, observed and calculated parameters are compared by making plots of pressure versus time, cumulative production (or injection) versus time, production (or injection) rates versus time, and GOR, WOR, or water cut versus time. Other comparisons can and should be made if data are available. They include, for example, model saturations versus well log saturations, and tracer concentration (such as salinity) versus time. In the case of compositional simulation, dominant components (typically methane) should be plotted as a function of time.

In many studies, the most sensitive indicators of model performance are plots of GOR, WOR, or water cut versus time. These plots can be used to identify problem areas. For example, suppose we plot all high and low WOR and GOR wells or plot all high and low pressure wells. A review of such plots may reveal a grouping of wells with the same problem. This can identify the presence of a systematic error or flaw in the

model that needs to be corrected. If the distribution is random, then local variations in performance due to heterogeneity should be considered.

18.4.1 Deciding on a Match

There are several ways to decide if a match is satisfactory. In all cases, a clear understanding of the study objectives should be the standard for making the decision. If a coarse study is being performed, the quality of the match between observed and calculated parameters does not need to be as accurate as it would need to be for a more detailed study. For example, pressure may be considered matched if the difference between calculated and observed pressures is within ±10% drawdown. The tolerance of ±10% is determined by estimating the uncertainty associated with measured field pressures and the required quality of the study. A study demanding greater reliability in predictions may need to reduce the tolerance to ± 5% or even less, but it is unrealistic to seek a tolerance of less than 1%. The uncertainty applies not to individual well gauge pressures, which may be measured to a precision of less than one percent, but to estimates of average field or region pressure from two or more well tests. The latter error is generally much larger than that of a single well test. In any event, model calculated pressure trends should match field or region pressure performance.

Another sensitive indicator of the quality of a history match is the match of WOR, GOR, or water cut. Three factors need to be considered: breakthrough time, the magnitude of the difference between observed and calculated values, and trends. Adjustments in the model should be made to improve the quality of each factor. Saleri [1993] has observed that a match of the field is more easily obtained than a match of individual well performance. Indeed, he notes that matching every well is virtually impossible. As a rule of thumb, the field match may be valid for a year or more without updating, and we can expect the well match to be valid for up to six months without updating. Deviations from this rule will vary widely, and will depend on the type of system modeled and the alignment of the interpreted model with reality. Indeed, gas reservoirs

without aquifer influx may be accurately modeled for the life of the field, while a gas reservoir with complex lithology and water influx may never be satisfactorily matched.

Modelers must resist succumbing to the "one more run" syndrome. This occurs when a modeler (or member of the study team) wants to see "just one more run" to try an idea that has not yet been tried. In practice, a final match is often declared when the time or money allotted for the study is depleted.

18.4.2 Test of Reasonableness

A model may be considered reasonable if it does not violate any known physical constraints. In many cases, a model may be acceptable if it is reasonable. In other situations, not only must physical constraints be satisfied, but approved processes for evaluating data must also be followed. Thus a model may be reasonable, but if it is based on an innovative technique that is reasonable but not approved, the model will be unacceptable. The modeler may use a method that is in the literature, but the commissioner of the study may have a philosophical or empirical objection to the method. Window area or sector modeling is a good example of a method that may be reasonable but not acceptable because failure to describe flux across model boundaries adequately can yield poor results. Similarly, the modeler needs to be aware that some modeling methods are not universally accepted. At the very least, alternative methods may be needed to corroborate the disputed method as part of a sensitivity analysis or model validation exercise.

18.4.3 History Match Limitations

History matching (or model calibration) may be thought of as an inverse problem. An inverse problem exists when the dependent variable is the best known aspect of a system and the independent variable must be determined [Oreskes, et al., 1994]. For example, the "dependent variable" in oil and gas production is the production performance of the

field. Production performance depends on input variables such as permeability distribution and fluid properties. The goal of the history match is to find a set of input variables that can reconstruct field performance.

In the context of an inverse problem, the history matching problem is solved by finding a set of reasonable reservoir parameters that minimizes the difference between model performance and the historical performance of the field. As usual, we must remember that we are solving a nonunique problem whose solution is often as much art as science. The uniqueness problem arises from many factors. Most notable of these are unreliable or limited field data, interpretation errors, and numerical effects. Advances in hardware and software technology have made it possible to minimize the effects of numerical problems, or at least estimate their influence on the final history match solution. Data limitations are more difficult to resolve because the system is inherently underdetermined: we do not have enough data to be sure that our final solution is correct. In many instances, observed data can be inaccurate. Kabir and Young [2004] present a case study that discusses how they handled production data uncertainty.

The goal of history matching is to prepare a flow model that can contribute to reservoir management decision making. The modeling team needs to avoid the mistake of preparing a history matched model "at all costs." The modeling team should pay attention to data from all sources, and use the level of complexity that is needed to satisfy reservoir management objectives.

18.5 Case Study: Data Analysis and Grid Preparation

This section presents more data from the case study introduced in Chapter 17 and subjects that data to reservoir engineering analysis. The analysis includes a geologic estimate of volumetrics and a material balance determination of initial fluids in place. A geologic interpretation guides the preparation of a reservoir grid.

18.5.1 Production History

Well P-1 has produced for a year. Tables 18-4 and 18-5 show its production history. The historical data in Tables 18-4 and 18-5, especially rates, show some variability. The GOR is relatively constant. This implies that the reservoir is undersaturated; that is, reservoir pressure is above bubble point pressure and there is no free gas phase initially. Only one hydrocarbon phase – the liquid phase – is produced at reservoir conditions from an undersaturated reservoir. The fact that GOR has not changed significantly over the life of the field is interpreted to mean that the reservoir was undersaturated at initial conditions and is still undersaturated after one year of production.

Table 18-4
Production Rate History

TIME	RATES			GOR	WOR
	OIL	GAS	WATER		
Days	STB/day	MSCF/day	STB/day	SCF/STB	
1	506	227	0	449	0
91	508	228	1	450	0
183	493	229	2	465	0
274	504	228	3	452	0
365	494	226	5	458	0

A review of the water production rate in Table 18-4 shows that there is no initial water production. Water production does begin after three months of oil production, and the water production rate continues to increase for the rest of the production rate history. Cumulative water production is relatively low, but the presence of water production raises the possibility that the fault block is in communication with an aquifer. The material balance analysis below examines this possibility.

Table 18-5
Pressure and Cumulative Production History

TIME	AVG RES PRESSURE	CUM PROD		
		OIL	GAS	WATER
DAYS	PSIA	MSTB	MMSCF	MSTB
1	3942	0.5	0.2	0.0
91	3830	46	21	0.0
183	3825	91	42	0.1
274	3823	137	63	0.4
365	3820	183	83	0.7

18.5.2 Volumetrics

A volumetric estimate of oil volume is a useful number for checking the accuracy of the numerical representation of the reservoir geology in a reservoir flow model. The volume of oil in the reservoir is the product of bulk volume V_B, porosity ϕ, and oil saturation S_o. Taking the product of thickness-weighted average porosity (ϕ_{ave} = 0.228) and bulk volume gives the following estimate of pore volume: ft

$$V_P = \phi_{ave} V_B \approx 9.18 \times 10^7 \,\text{ft}^3 \approx 16.4 \times 10^6 \,\text{RB} \qquad (18.1)$$

The product of oil saturation and pore volume gives an estimate of oil volume in reservoir barrels. Dividing this volume by oil formation volume factor B_o for the reservoir gives an estimate of oil volume in stock tank barrels. The value of oil formation volume factor at an initial average reservoir pressure of 3942 psia is 1.3472 RB/STB. This value is obtained from laboratory data and has been corrected for use in a reservoir simulator. The resulting oil volume for initial oil saturation of 70% (Table 17-5) is

$$V_o = \frac{S_o V_P}{B_o} \approx \frac{0.7 V_P}{B_o} \sim \frac{11.5 \times 10^6 \,\text{RB}}{1.3472 \,\text{RB/STB}} \sim 8.5 \times 10^6 \,\text{STB} \quad (18.2)$$

18.5.3 Material Balance

Volumetrics provides one measure of the original fluids in place in a reservoir flow model. Another estimate of original fluids in place can be obtained from a material balance study if a reasonable amount of production data is available, including historical pressure and production data.

Our analysis so far has let us surmise that the reservoir was initially undersaturated. The presence of a few barrels of water during the latter months of the first year of production indicates that mobile water is present, but its source is unknown. The volume of produced water is small enough to be water mobilized by swelling as reservoir pressure declines, or it could be the first indication of water production from aquifer influx. Both of these scenarios can be assessed if we consider the possibilities of depletion with and without aquifer influx.

We begin by deriving a material balance equation for depletion of an undersaturated oil reservoir with water influx. The derivation is simplified by assuming that formation compressibility is negligible and then setting the decrease in oil volume at reservoir conditions equal to the increase in water volume at reservoir conditions as oil is produced and reservoir pressure decreases. In this case, rock compressibility is 3×10^{-6} psia^{-1}. For comparison, total compressibility for the DST discussed in Section 17.4 was 13×10^{-6} psia^{-1}. The change in volume due to rock compressibility is considered negligible for the pressure decline range shown in Table 18-5. The material balance equations derived below conserve volume and neglect volume changes associated with rock compressibility. A more detailed material balance study should include rock compressibility effects.

1. Calculate the decrease in oil volume ΔV_o (RB) given

N = original oil in place = OOIP (STB)

B_{oi} = oil FVF (RB/STB) at initial pressure P_i

N_p = oil produced (STB) at pressure P and time t

B_o = oil FVF (RB/STB) at pressure P and time t

The change in oil volume is

$$\Delta V_o = NB_{oi} - \left(N - N_p\right)B_o \tag{18.3}$$

with

NB_{oi} = OOIP (RB) at initial reservoir pressure P_i

$(N - N_p)\, B_o$ = OIP (RB) at pressure P and time t

2. Calculate the increase in water volume ΔV_w (RB) given

W = original water in place = OWIP (RB) at initial pressure P_i

B_w = water FVF (RB/STB) at pressure P and time t

W_p = water produced (STB) at pressure P and time t

W_e = water influx (RB)

The change in water volume is

$$\Delta V_w = \left(W + W_e - W_p B_w\right) - W = W_e - W_p B_w \tag{18.4}$$

with

$W_p B_w$ = cumulative water produced (RB) at pressure P and time t

3. The assumption that the volume of the reservoir remains constant implies $\Delta V_o = \Delta V_w$. Combining results from steps 1 and 2 above gives the material balance equation for depletion of an incompressible, undersaturated oil reservoir with aquifer influx:

$$NB_{oi} - \left(N - N_p\right)B_o = W_e - W_p B_w \tag{18.5}$$

The two unknowns in the equation are N and W_e.

The simplest production scenario is to assume that water influx is negligible, that is, $W_e = 0$. If we further observe that water production W_p is insignificant, we have

$$N = \frac{N_p B_o}{B_o - B_{oi}} \tag{18.6}$$

where B_{oi} = 1.3472 RB/STB at P_i = 3942 psia. The corrected oil FVF is used in this calculation. Table 18-6 presents the results of the calculation.

Table 18-6
Results Assuming No Water Influx

TIME	AVG RES PRESSURE	B_o	N_p	N
DAYS	PSIA	RB/STB	MMSTB	MMSTB
1	3942	1.3472	0.0005	
91	3830	1.3497	0.0456	23.9
183	3825	1.3499	0.0913	45.8
274	3823	1.3499	0.1369	67.5
365	3820	1.3500	0.1825	87.8

The value of N increases at each time. This implies that the material balance model does not account for all of the pressure support and suggests that an aquifer influx model should be considered.

If we use a volumetric estimate of N, namely N_{vol} = 8.5 MMSTB, we can calculate W_e. Again recognizing that $W_p \approx 0$, the material balance equation becomes

$$W_e = N\left(B_{oi} - B_o\right) + N_p B_o \tag{18.7}$$

Table 18-7 shows results of the calculation. Notice that W_e increases as a function of time. The values in parentheses are IFLO values when the correct aquifer model is used.

Table 18-7
Results Assuming Water Influx with Volumetric OOIP

TIME	AVG RES PRESSURE	B_o	N_p	W_e
DAYS	PSIA	RB/STB	MMSTB	MMSTB
1	3942	1.3472	0.0005	
91	3830	1.3497	0.0456	0.0397 (0.0396)
183	3825	1.3499	0.0913	0.1004 (0.0998)
274	3823	1.3499	0.1369	0.1615 (0.1608)
365	3820	1.3500	0.1825	0.2225 (0.2217)

18.5.4 Relative Permeability

As we continue our preparation of a 3-D simulation model, we observe that not all of the data needed by the simulator is available. Since we cannot ignore data and still perform a credible model study, we must complete the data set. Several options are available, such as ordering additional measurements or finding reasonable correlations or analogies for the missing data. In this case, our commercial interests are best served by moving the project forward without additional expense or delays.

We do not have laboratory measured relative permeability data. We could attempt to construct relative permeability data from production data, but our production history is essentially single-phase oil. Since we must specify relative permeability to run the model, we can turn to analogous reservoirs or correlations for guidance. We choose the Honarpour, et al. [1982] correlation for water-wet sandstone as a starting point

for determining relative permeability curves. Well logs provide some information about saturation end points such as initial and irreducible water saturation. Core floods and capillary pressure measurements could provide information about residual hydrocarbon saturations, but they are not available. For that reason, end points like residual oil saturation must be estimated. Results of the calculation are included in the case study input data files (data files that begin with "CS"). If our choice of relative permeability correlations does not match field performance, we will have to change the relative permeability curves. In any event, we recognize that in this case study relative permeability is poorly known and should be considered uncertain.

18.5.5 Fluid Contacts

A water-oil contact (WOC) was not seen on either well logs or in seismic data. The production of a small amount of water suggests that there may be a WOC in the vicinity of the reservoir. The data are not compelling, however. We could assume that the oil zone extends well below the bottom depth of our well, but this would be an optimistic assumption that could prove to be economically disastrous. In the interest of protecting our investment, let us make the more conservative assumption that a WOC does exist and is just beyond the range of our observations, that is, our well log and seismic data. We assume WOC $\approx$ 9600 ft, which is near the bottom of the seismically observed reservoir structure. The pressure at this WOC depth is estimated to be about 4000 psia.

18.5.6 Grid Preparation

Figure 18-2 is a sketch of the well location relative to the interpreted reservoir boundaries. Based on seismic data shown in Section 17.4, the reservoir is thought to be bounded to the east by a facies change.

A cross section through points B and B′ shows that the sides of the reservoir appear to be bounded by faults. Without evidence to the contrary, we assume that the faults are sealing. This assumption is subject to verification during the history match phase of the study.

A cross section through points A and A′ (see Figure 18-2) illustrates the dip of the reservoir and the layering. The structure of the reservoir is based on well log and seismic interpretation. The downdip fault is speculative. It is based on the assumption that the fault shown on the western side of Figure 18-2 extends down through the formation. This is not obvious from seismic data. Indeed, if the reservoir is receiving aquifer support, the aquifer influx will come from lower in the reservoir as reservoir pressure declines. Bear in mind, however, that both the fault and the aquifer may be present. This could happen, for example, if the fault is not sealing. The fault could be providing a flow path for water influx from another horizon.

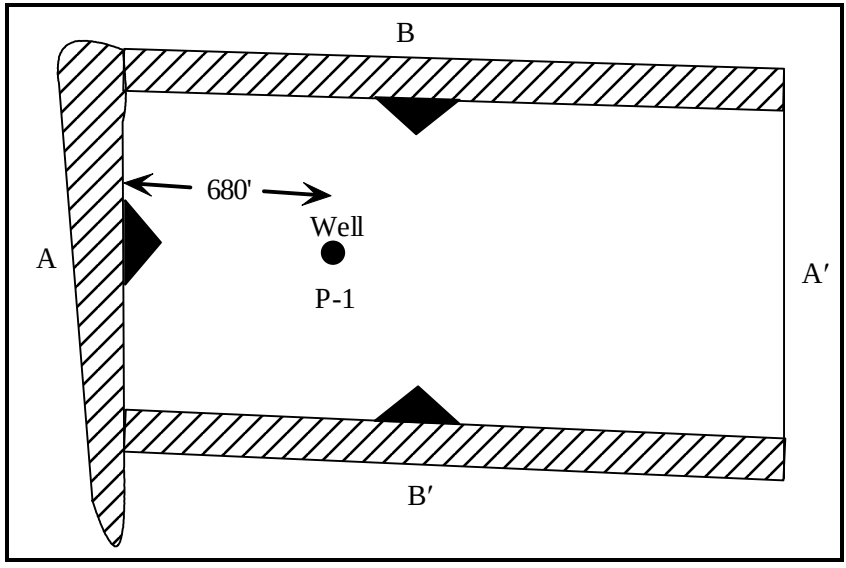

Figure 18-2. Plan View

Exercises

Exercise 18.1 Calculate the pore volume of the reservoir given Δx = 2000' and Δy = 1200' from maps, and Δz = 72' + 96' = 168' from well logs. Use thickness weighted average porosity.

Exercise 18.2A Suppose a well is completed in a gridblock with the following properties: $\Delta x = \Delta y$ = 200 ft, net thickness = 64 ft, and porosity = 0.25. What is the pore volume of the gridblock in reservoir barrels? Note: 1 bbl = 5.6146 cu ft.

Exercise 18.2B If the well is producing 500 RB/day of fluid, what percentage of the gridblock pore volume is being produced in a 5-day timestep?

Exercise 18.3 Data file CS_MB.DAT is an input file for a material balance analysis of the case study. It represents the reservoir as a single gridblock, or "tank" model. The tank model is equivalent to a material balance calculation. Run IFLO with the file CS_MB.DAT. Verify that the original volume of oil in the model agrees with the volumetric estimate in Section 18.5.

Exercise 18.4 Use data file CS_MB.DAT to study the effect of aquifer influx on material balance performance. This is done by modifying the input data file to include an aquifer model, then adjusting aquifer parameters until model pore volume weighted average reservoir pressures match historical pressures. Note: Section 21.10 contains details on how to set up an analytic aquifer. For an example of a data file with an analytic aquifer model, see data file CS_HM.DAT.

Exercise 18.5 Data file CS_VC4.DAT is a vertical column model of the case study. Sketch the grid to scale, locate the contacts on the sketch, and match reservoir pressure. You may need to include an analytic aquifer as in Exercise 18.4.

Exercise 18.6 Repeat Exercise 18.5 beginning with the cross section model data file CS_XS.DAT.

Chapter 19

Predictions

The previous chapters have shown how to build a working model of the reservoir and establish a level of confidence in the validity of model results. It is time to recall that modeling was undertaken to prepare a tool that would help us develop recommendations for a reservoir management program. The commercial impact of the simulation study is the preparation of a cash flow prediction from projected field performance. Thus, the model study is often completed by making field performance predictions for use in economic analysis of possible operating strategies. This chapter discusses the role of flow models as forecasting tools.

19.1 Prediction Process

The prediction process begins with model calibration. It is usually necessary to ensure continuity in well rate when the modeler switches from rate control during the history match to pressure control during the prediction stage of a study. In Figure 19-1, the solid curve represents the predicted rate based on the productivity index (PI) used in the history match. A clear discontinuity in rate is observed between the end of history and the beginning of prediction. The rate difference usually arises because the actual well PI, especially skin effect, is not

accurately modeled by the model PI. An adjustment to model PI needs to be made to match final historical rate with initial predicted rate.

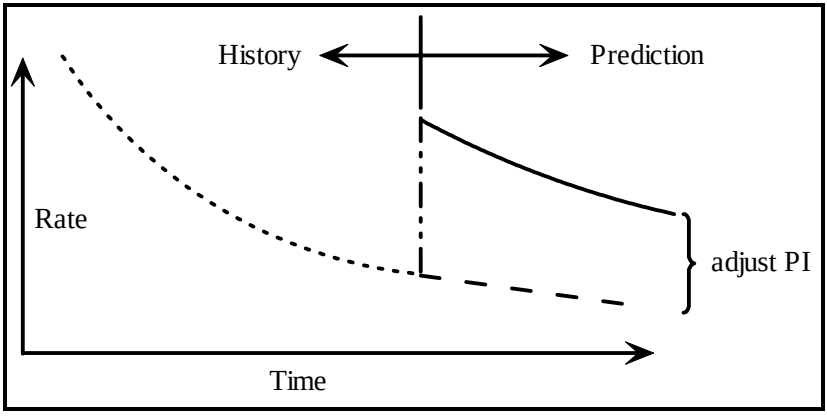

Figure 19-1. Model calibration

The next step is to prepare a base case prediction. The base case prediction is a forecast that assumes existing operating conditions apply. For example, the base case for a newly developed field that is undergoing primary depletion should be a primary depletion case that extends to a user-specified economic limit. By contrast, if the field was being waterflooded, the waterflood should be the base case and alternative strategies might include gas injection and WAG (water alternating gas).

The base case prediction establishes a basis from which to compare changes in field performance resulting from changes in existing operating conditions. In addition, a sensitivity analysis should be performed to provide insight into the uncertainty associated with model predictions. A procedure for conducting a sensitivity analysis is outlined below.

19.2 Sensitivity Analyses

Sensitivity analyses are often needed in both the history matching and prediction stages [for example, see Crichlow, 1977; Mattax and Dalton, 1990; Saleri, 1993; Fanchi, et al., 1996; Carlson, 2003]. Any

method that quantifies the uncertainty or risk associated with selecting a particular prediction case may be viewed as a sensitivity analysis. Conceptual modeling is an example of a sensitivity analysis technique that is cost-effective in moving a history match forward. It can be used to address very specific questions, such as determining the impact of fluid contact movement on hydrocarbon recovery. Similarly, window models that study such issues as the behavior of a horizontal well in a fault block provide useful information on the sensitivity of a model to changes in input parameters.

Another example of a sensitivity analysis technique is risk analysis. Murtha [1997] defines risk analysis as "any form of analysis that studies and hence attempts to quantify risks associated with an investment." Risk in this context refers to a potential "change in assets associated with some chance occurrences." Risk analysis generates probabilities associated with changes in model input parameters. The parameter changes must be contained within ranges that are typically determined by the range of available data, information from analogous fields, and the experience of the modeling team. Each model run using a complete set of model input parameters constitutes a trial. A large number of trials can be used to generate probability distributions. Alternatively, the results of the trials can be used in a multivariable regression analysis to generate analytical expressions, as described below.

One of the most widely used techniques for studying model sensitivity to input parameter changes is to modify model input parameters in the history matched model. The following procedure combines multivariable regression and the results of model trials to generate an analytical expression for quantifying the effect of changing model parameters.

Assume a dependent variable F has the form

$$F = \kappa \prod_{j=1}^{n} X_j^{e_j} \tag{19.1}$$

where $\{X_j\}$ are n independent variables and κ is a proportionality constant that depends on the units of the independent variables. Examples of X_j are well separation, saturation end points, and aquifer strength. Taking

the logarithm of the defining equation for F linearizes the function F and makes it suitable for multivariable regression analysis, thus

$$\ln F = \ln \kappa + \sum_{j=1}^{n} e_j \ln X_j \tag{19.2}$$

A sensitivity model is constructed using the following procedure:

1. Run a model with different values of $\{X_j\}$
2. Obtain values of F for each set of values of $\{X_j\}$

The constants κ, $\{e_j\}$ are obtained by performing a multivariable regression analysis using values of F calculated from the model runs as a function of $\{X_j\}$.

In addition to quantifying behavior, the regression procedure provides an estimate of fractional change of the dependent variable F when we make fractional changes to the independent variables $\{X_j\}$. The fractional change in F is given by

$$\frac{dF}{F} = \sum_{j=1}^{n} e_j \frac{dX_j}{X_j} \tag{19.3}$$

This lets us compare the relative importance of changes to the independent variables. Notice that the proportionality constant κ has been factored out of the expression dF/F for the fractional change in F. Thus, the quantity dF/F does not depend on the system of units used in the sensitivity study.

19.3 Prediction Capabilities

Performance predictions are valuable for a variety of purposes. Predictions can be used to better interpret and understand reservoir behavior and they provide a means of determining model sensitivity to changes in input data. This sensitivity analysis can guide the acquisition of additional data for improving reservoir management.

Predictions enable people to estimate project life by predicting recovery versus time. Project life depends not only on the flow behavior of the reservoir, but also on commercial issues. Models let the user impose a variety of economic constraints on future reservoir performance during the process of estimating project life. These constraints reflect a range of economic criteria that will interest management, shareholders, and prospective investors.

Commercial interests are clearly important to the future of a project, as are technical issues. It is often necessary to compare different recovery processes as part of a study. Since there is only one field, it is unrealistic to believe that many different recovery processes can be evaluated in the field, even as small scale pilot projects. Pilot projects tend to be substantially more expensive to run than simulation studies. In some cases, however, it might be worthwhile to confirm a simulation study with a pilot project. This is especially true with expensive processes such as chemical and thermal flooding.

Yet another use for model predictions is the preparation of a reservoir management plan. Reservoir management plans have been discussed in previous sections. Their preparation is often the single most important motivation for performing a simulation study.

19.3.1 Economic Analysis

In addition to providing technical insight into fluid flow performance, model predictions are frequently combined with price forecasts to estimate how much revenue will be generated by a proposed reservoir management plan. The revenue stream is used to pay for capital and operating expenses, and the economic performance of the project depends on the relationship between revenue and expenses [see, for example, Chorn and Croft, 2000; Seba, 1998; Bradley and Wood, 1994; Mian, 1992; Thompson and Wright, 1985].

In a very real sense, the reservoir flow model determines how much money will be available to pay for wells, compressors, pipelines, platforms, processing facilities, and any other items needed to implement

the plan represented by the model. For this reason, the modeling team may be expected to generate flow predictions using a combination of reservoir parameters that yield better recoveries than would be expected if a less "optimistic" set of parameters had been used. The sensitivity analysis is a useful process for determining the likelihood that a set of parameters will be realized. Indeed, modern reserves classification systems are designed to present reserves estimates in terms of their probability of occurrence. The probabilistic representation of forecasts gives decision-making bodies such as corporate managements and financial institutions the information they need to make informed decisions.

19.4 Validity of Model Predictions

Saleri [1993] studied the validity of model predictions by comparing actual field performance with predicted performance. The overall match of field performance, such as total rate and pressure performance, is reasonable. The field match is somewhat deceptive however, because the validity of individual well performance forecasting varies widely. Indeed, Saleri deemed the match of water and gas performance for about half of the wells a "bust" by the author. This is not unusual in a model study. Saleri arrived at the following conclusions:

- "Barring major geologic and/or reservoir data limitations, fieldwide cumulative production forecast accuracies would tend to range from 10% to 40%." [Saleri, 1993]
- "Well performance forecasts are bound to be less successful than fieldwide predictions." [Saleri, 1993]

These points underscore the need to recognize that the history match process does not yield a unique solution. Forecasts of reservoir behavior depend on the validity of the history match.

Despite the uncertainty associated with simulator-based forecasts, reservoir simulation continues to be the most reliable method for making performance predictions, particularly for reservoirs that do not have an extensive history or for fields that are being considered as candidates for a change in reservoir management strategy. Other methods,

such as decline curve analysis and material balance analysis, can generate performance forecasts, but not to the degree of detail provided by a reservoir flow model study. As Saleri [1993] noted,

> ➢ "While a 10% to 40% forecast uncertainty may appear alarming in an absolute sense, the majority of reservoir engineering decisions require choices based solely on comparative analyses (for example, peripheral vs. pattern flood). Thus, in selecting optimum management strategies, finite difference models still offer the most effective tools."

Saleri's view is similar to that of Oreskes, et al. [1994]. Even though models are nonunique representations of nature, they still have many uses. In summary, models can be used to

- Corroborate or refute hypotheses about physical systems
- Identify discrepancies in other models
- Perform sensitivity analyses

19.5 Case Study: History Match and Prediction

The history match is now well under way. The models discussed in the exercises in Chapter 18 are conceptual models designed to provide you with a sense of how fluids move in the reservoir. This is the art of modeling. As you work with various models of the reservoir, you should begin to develop a knowledge base for determining how changes to model parameters will help achieve a match for a particular physical variable. This knowledge base is valuable as you develop your feel for the study.

The previous chapters set the stage for preparing a 3-D model of the case study reservoir. A 3-D model should provide enough reservoir definition to let us make meaningful performance predictions. Before matching the 3-D model, we discuss how to incorporate well information into the model. Once the well model has been prepared, we proceed to history matching and performance predictions.

19.5.1 Well Model Preparation

Well model calculations require estimates of productivity index and flowing bottomhole pressure. This section illustrates these calculations.

19.5.1.1 Productivity Index Estimate

Well model calculations in IFLO need to have the quasistationary productivity index factor (*PID*) specified by the user. *PID* is estimated from the expression

$$PID = \frac{0.00708 K_{abs} h_{net}}{\ln\left(r_e / r_w\right) + S} \tag{19.4}$$

where

r_e = drainage radius (ft)

r_w = wellbore radius (ft)

S = skin

K_e = $k_{ro} K_{abs}$ = effective permeability (md)

h_{net} = net thickness (ft)

Given S = -0.5, r_w = 0.25 ft and

$$r_o \cong 0.14\left(\Delta x^2 + \Delta y^2\right)^{1/2} \cong 40\,\text{ft} \tag{19.5}$$

with $\Delta x = \Delta y$ = 200 ft., we find

$$PID = 1.55 \times 10^{-3} K_{abs} h_{net} \tag{19.6}$$

where $r_e \approx r_o$. Table 19-1 presents the calculation of *PID* for each layer identified by well log analysis. Notice that the second model layer has no flow capacity because the model layer represents impermeable shale. The upper sand is represented by the first model layer, and the lower sand is represented by the third and fourth model layers.

Table 19-1
Estimate of *PID* by Layer

Layer	K_{abs} (md)	h_{net} (ft)	*PID*
1	75	72	8.4
2	0	20	0
3	250	64	24.8
4	250	32	12.4

19.5.1.2 Oil Well FBHP Estimate

The production well model needs a flowing bottomhole pressure (*FBHP*). Assuming an oil column in the wellbore, we can prepare a quick estimate of *FBHP* for a single-phase oil well that is completed at a 9500 ft depth by assuming *FBHP* oil head. Consequently, oil head is approximated by

$$\gamma_o \Delta z \approx FBHP \tag{19.7}$$

where γ_o is the oil pressure gradient and Δz is the height of the oil column. An estimate of average oil pressure gradient for the oil column is found by averaging the pressure gradient at surface and reservoir conditions:

- Approximate pressure gradient at surface conditions:

$$\rho_s = 46.244 \frac{\text{lb}}{\text{ft}^3} = 0.321 \frac{\text{psia}}{\text{ft}} \tag{19.8}$$

where oil density at surface conditions (ρ_s) is 46.244 lbm/SCF. psia

- Approximate pressure gradient at reservoir conditions:

$$\rho_R = \frac{\rho_s}{B_o} = 34.3 \frac{\text{lb}}{\text{ft}^3} = 0.238 \frac{\text{psia}}{\text{ft}} \tag{19.9}$$

where oil FVF (B_o) at bottomhole conditions is 1.3482 RB/STB.

The resulting *FBHP* for use in IFLO is

$$\begin{aligned} \text{FBHP} &= \frac{1}{2}\left[0.321\frac{\text{psia}}{\text{ft}} + 0.238\frac{\text{psia}}{\text{ft}}\right] \times 9500\,\text{ft} \\ &\approx 2660\text{psia} \end{aligned} \tag{19.10}$$

A more accurate estimate can be obtained from wellbore correlations or nodal analysis as discussed by such authors as Brown and Lea [1985].

19.5.1.3 Well Gridblock Pressure from PBU

A correction is needed to properly relate the pressure buildup (PBU) curve to simulator well gridblock pressures. To illustrate this correction, suppose a well is in a gridblock with grid dimensions Δx = 200 ft and Δy = 200 ft. We want to compare the simulator well gridblock pressure with a pressure from a PBU. According to Peaceman's correction [1978, 1983], shut-in pressure P_{ws} of the actual well should equal the simulator well gridblock pressure P_o at a shut-in time Δt_s given by

$$\Delta t_s = \frac{1688\phi\mu c_T r_o^2}{K} \tag{19.11}$$

For an isotropic reservoir in which horizontal permeability does not depend on direction, that is, $K_x = K_y$, we estimate the equivalent radius of a well in the center of a gridblock as

$$r_o = 0.14\left(\Delta x^2 + \Delta y^2\right)^{1/2} \tag{19.12}$$

The shut in time Δt_s at which the PBU pressure should be obtained is calculated from the following physical parameters:

c_r	3×10^{-6} psia^{-1}
c_o	13×10^{-6} psia^{-1}
c_w	3×10^{-6} psia^{-1}
S_o	0.7

S_w	0.3
μ_o	0.71 cp
ϕ	0.20
K	75 md

The equivalent radius of the well gridblock is estimated to be $r_o \approx 0.14\ (200^2 + 200^2)^{½} = 39.6$ ft, while the total compressibility is given by $c_T = c_r + S_o\, c_o + S_w\, c_w = 3 \times 10^{-6} + 0.7\ (13 \times 10^{-6}) + 0.3\ (3 \times 10^{-6}) \approx 13 \times 10^{-6}$ psia^{-1}. The PBU shut in time corresponding to these values is

$$\Delta t_s = 1688 \frac{(0.20)(0.71)(13 \times 10^{-6})(39.6)^2}{75} \qquad (19.13)$$

$$= 0.065 \text{ hr} = 4 \text{ min}$$

This early time part of the PBU curve could be masked by wellbore storage effects. Since the shut in pressure P_{ws} of the actual well equals the simulator well gridblock pressure P_o at a shut in time Δt_s, the shut in pressure P_{ws} may have to be obtained by extrapolation of the radial flow curve.

19.5.1.3.1 Throughput Estimate

Model timestep size is estimated by calculating pore volume throughput from well flow rates. In our case, pore volume throughput is given by

$$V_{PT} = \frac{Q\Delta t}{V_P}(5.6146) \qquad (19.14)$$

where

$V_P = \phi\, \Delta x\, \Delta y\, \Delta z$ = pore volume (ft^3)

Q = volumetric flow rate at reservoir conditions (RB/day)

Δt = timestep size (day)

Timesteps for an IMPES simulator should correspond to about 10% throughput or less. The maximum timestep is estimated as follows.

Suppose ϕ = 22.5%, $\Delta x = \Delta y$ = 200 ft, $\Delta z = h_{net}$, and Q = 400 RB/day. Then Δt is found by setting $V_{PT} = 0.10$ and rearranging the pore volume throughput equation to give

$$\Delta t = \frac{(0.1)V_P}{5.6146Q} = (0.1)\frac{\phi \Delta x \Delta y \Delta z}{5.6146Q} = 0.4h_{net}(\text{days}) \qquad (19.15)$$

If h_{net} = 100 ft, then $\Delta t \approx 40$ days is an estimate of the maximum IMPES timestep size.

19.5.2 Full Field (3-D) Model History Match

Data file CS_HM.DAT is the 3-D model used to match the production history. It uses the areal grid shown in Figure 19-2 to model the reservoir. Production well P-1 and its location in the grid are also shown in Figure 19-2. Each gridblock is a square with lengths $\Delta x = \Delta y$ = 200 ft. The dark areas of the grid are outside the reservoir area. The pore volume in the dark area is made inactive in data file CS_HM.DAT by using porosity multipliers.

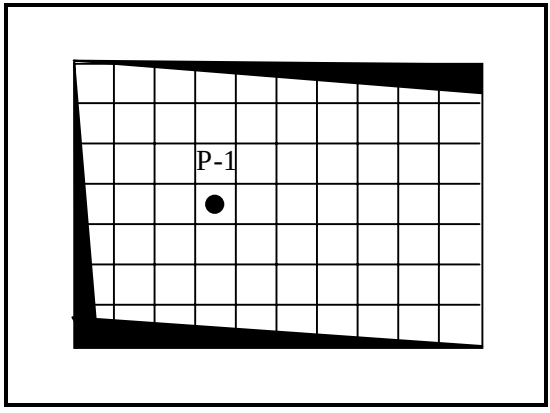

Figure 19-2. Plan View of Grid

The depth and thickness of each gridblock depend on reservoir architecture. The model grid should approximate the structure depicted in Figure 17-9. The dip of the reservoir is included by specifying the tops of each gridblock. The gridblock length modifications are designed to cut off those parts of the gridblock that continue the grid beyond the surface of the unconformity sketched.

Transmissibility multipliers in the vertical direction are set to zero to simulate impermeable shale barriers. This includes the shale streak that divides the second major sand into two thinner sands with a shale break. The interpretation of seismic data was unable to resolve this feature, but the well log shown in Figure 19-3 does indicate the presence of a shale streak.

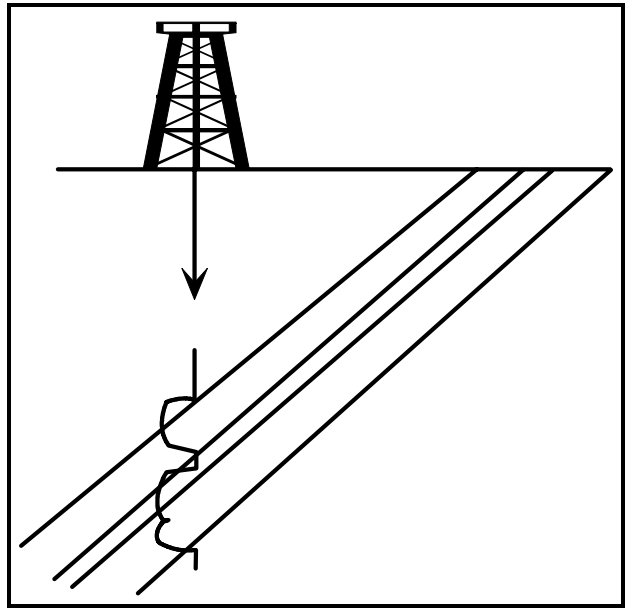

Figure 19-3. Overlay of Seismic and Well Log Data

The water-oil contact is at 9600 ft. A steady-state aquifer is in communication with all three oil layers at this depth. It is the source of water production shown in the production history.

19.5.3 Predictions

Predictions can be made once a history match model is adopted. The first step in the prediction stage is to establish a base case prediction. A frequently used base case is one that assumes that there will be no changes in operating strategy. Given a base case prediction, several runs should be made to optimize reservoir performance within the constraints imposed by the commissioners of the study and to evaluate the sensitivity of predictions to data limitations. In our case, the predictions should satisfy the reservoir management constraints in Table 17-10. Production forecasts can then be combined with price forecasts to predict cash flow, and provide valuable economic information to decision makers.

Exercises

Exercise 19.1 Repeat the shut in time Δt_s calculation in Section 19.5.1 using Δx = 1000 ft and Δy = 1000 ft.

Exercise 19.2A Run data file CS_XS.DAT and estimate the average timestep size of the run. Is there an analytic aquifer in the model?

Exercise 19.2B What are the average reservoir pressure and water production rate at the end of the run? How do these results compare with the historical data presented in Section 18.5?

Exercise 19.3A Attach a steady-state analytic aquifer model to both layers in the first (I = 1) column of data file CS_XS.DAT. Set the aquifer strength equal to 2 SCF/day/psia. What is your final average reservoir pressure, water production rate, and aquifer influx rate?

Exercise 19.3B How do your results compare with the historical data presented in Section 18.5 and the results of Exercise 19.2?

Exercise 19.4 Data file CS_HM.DAT was used as the basis of the case study. Run data file CS_HM.DAT and plot average reservoir pressure versus time and water production rate versus time. Verify that the model results match the historical data shown in Tables 18-4 and 18-5.

Exercise 19.5 Several sensitivity runs may be made by varying model parameters and noting reservoir performance. As an example of a sensitivity study, change the water-oil contact to 9500 ft in CS_HM.DAT. How does this change affect water rate and average reservoir pressure during the history matching period?

Exercise 19.6 Run data file CS_HM.DAT for five years with Well P-1 under oil rate control. You should add four years to the existing file. What are the production rates at the end of the run? This run establishes a base case prediction.

Exercise 19.7 Data file CS_PD.DAT represents primary depletion for seven years beyond the first year of historical production. Beginning with data file CS_PD.DAT, maximize oil recovery given the reservoir management constraints for the case study. Two ideas to consider are downdip water injection after drilling an updip producer; and downdip production after drilling an updip gas injector.

Chapter 20

Introduction to IFLO

IFLO is an iterative, implicit pressure-explicit saturation finite difference simulator. It can simulate isothermal, multiphase Darcy flow in up to three dimensions. This chapter outlines procedures for entering data into IFLO, executing IFLO, and obtaining results from IFLO.

20.1 Input Data File

IFLO input data is divided into two parts: initialization data, and recurrent data. Chapter 21 describes initialization data which include data that is set at the beginning of the study and is not expected to change during a model run. Such data includes the reservoir description and fluid properties. Chapter 22 describes recurrent data which include data that are expected to change during the course of a simulation. Such data include well schedules and timestep control information. Appendix B presents an example input data set.

IFLO reads a file called ITEMP.DAT and outputs to files with the prefix ITEMP. The output files are described below. You should copy and rename any files you wish to save because IFLO overwrites the ITEMP.* files each time it runs.

An efficient way to prepare a new data file is to edit an old one. This will give you an example of the formats needed for most options. If

you start with an old data set, make sure that you check all applicable data entries and make changes where appropriate.

20.2 IFLO Execution

You are given the option at the start of an IFLO run to direct output to either the screen or to a set of files. The program IFLO runs the file called ITEMP.DAT. To run a new data set, such as NEWDATA.DAT, copy NEWDATA.DAT to ITEMP.DAT. The File ITEMP.DAT should be in the same folder as the executable IFLO.EXE.

Run IFLO by double-clicking on the IFLO.EXE file. Select option “Y” to write the run output to files. A one-line timestep summary is sent to the screen each timestep so that you can monitor the progress of a run. When the program ends, it will print “STOP.” Close the IFLO window. You do not need to save changes since they are written to file ITEMP.TSS. All output files are in text format.

It is often worthwhile to send output to the screen when first building and debugging a data set. To implement this option, double-click on the IFLO.EXE file and select option “N” to write the run output to the screen. IFLO will abort at the point in the data set where it encounters improperly entered data. For evaluating run results, it is preferable to send output to files.

20.3 IFLO Output Files

All IFLO output files are text files so that they may be read by a variety of commercially available spreadsheets. IFLO output may then be manipulated using spreadsheet options. This is especially useful for making plots or displaying array data. Different output files are defined so that simulator output file sizes are more manageable. The output files are designed to contain information that is logically connected, e.g. well data in one file, timestep information in another file. The different output files are described below.

20.3.1 Timestep Summary File – ITEMP.TSS

A one-line timestep summary is automatically printed to the terminal as a record of the progress of the run. This summary provides you with necessary information for evaluating the stability of the solution as a function of time. For example, significant oscillations in gas-oil ratio (GOR) or water-oil ratio (WOR), or large material balance errors indicate simulation problems and should be corrected. A smaller timestep through the difficult period is often sufficient to correct IMPES instabilities.

The timestep summary is written to file ITEMP.TSS. The output quantities include: cumulative production of oil, water and gas; pore volume weighted average pressure; aquifer influx rate and cumulative aquifer influx; and fieldwide WOR and GOR values. The WOR and GOR are ratios of total producing fluid rates. Consequently these ratios are comparable to observed fieldwide ratios. These quantities are output as functions of time and timestep number.

20.3.2 Run Output File – ITEMP.ROF

Model initialization data and run output information, including well performance, are found in file ITEMP.ROF. IFLO outputs the following initialization data in the text file ITEMP.ROF:

- Gridblock sizes
- Node midpoint elevations
- Porosity distributions
- Permeability distributions
- Rock and PVT region distributions
- Relative permeability and capillary pressure tables
- Petrophysical distributions
- PVT tables
- Slopes calculated from PVT data
- Timestep control parameters

- Analytic aquifer model selection
- Coal gas model selection
- Initial fluid volumes-in-place
- Initial pressure and saturation arrays
- Initial reservoir geophysical attribute arrays
- Initial well information

Other output can be obtained at your request. For example, if a modification option is invoked, you may print out the altered array. It is worthwhile to do this as a check on the input changes.

You may output the following arrays whenever you desire as part of the recurrent data output: pressure, saturations, bubble point pressure, cumulative aquifer influx, acoustic velocities, acoustic impedances, seismic reflection coefficient, Poisson's ratio, Young's modulus, and uniaxial compaction. Output arrays may be used as input pressure and saturation distributions for restarting a run.

It is usually unnecessary to print all of the arrays. To avoid excessive output and correspondingly large output files, you should decide judiciously which arrays to print.

20.3.3 Well Output File – ITEMP.WEL

Well performance data are found in file ITEMP.WEL. The information is provided for easy access and includes production (injection) for each well completion as well as total well production (injection) for all production (injection) wells.

20.3.4 Array File – ITEMP.ARR

Selected parameter arrays are tabulated in ITEMP.ARR. The arrays are displayed as functions of the Cartesian (x, y, z) coordinate locations of each gridblock midpoint. The parameter arrays include pressure, saturations, and acoustic velocity information.

20.3.5 Material Balance Error File – ITEMP.MBE

Material balance errors as a function of time are summarized in ITEMP.MBE.

Chapter 21

Initialization Data

Initialization data records are read once at the beginning of the simulation. They must be read in the order presented below. Title or heading records are read before each major and many minor sections. These records are designed to make the input data file easier to read and edit.

In many cases, codes are read that will specify the type of input to follow and the number of values that will be read. These codes increase the efficiency and flexibility of entering input data. All input data, with the exception of well names, are entered by free format. Data entered on the same line must be separated by a comma or a space.

Tabular data entered by the user should cover the entire range of values expected to occur during a simulation. The table interpolation algorithms in IFLO will return table endpoint values if the independent variable goes outside the range of the input tabular values. No message will be printed if this occurs.

1. **Title** Up to 80 characters. This record will appear as run title.

21.1 Model Dimensions and Geometry

21.1.1 Model Dimensions

1. **Heading** Up to 80 characters.

2. **II, JJ, KK, NWELL, NWCON**

Code	Meaning
II	number of gridblocks in the *x*-direction
JJ	number of gridblocks in the *y*-direction
KK	number of gridblocks in the *z*-direction
NWELL	number of wells
NWELCON	number of connections per well

NOTE: The IFLO simulator assumes a block centered grid with the axes aligned using a right-handed coordinate system with the *z*-axis pointing down. The top layer is labeled by the index K = 1. The second layer K = 2 is below the K = 1 layer, and so on.

3. **Heading** Up to 80 characters.

4. **KDX, KDY, KDZ, KDZNET**

KDX Control code for input of *x*-direction grid size.

KDY Control code for input of *y*-direction grid size.

KDZ Control code for input of *z*-direction gross thickness.

KDZNET Control code for input of *z*-direction net thickness.

Code	Value	Meaning
KDX	-1	The *x*-direction grid dimensions are the same for all gridblocks. Read only one value.
	0	The *x*-direction dimensions are read for each gridblock in the first row (J = 1) of layer one (K = 1). These values are assigned to all other rows and layers. Read II values.
	1	The *x*-direction dimensions are read for each gridblock in layer one (K = 1). These values are assigned to all other layers. Read II × JJ values.
KDY	-1	The *y*-direction grid dimensions are the same for all gridblocks. Read only one value.
	0	The *y*-direction dimensions are read for each gridblock in the first column (I = 1) of layer one (K = 1). These values are assigned to all other columns and layers. Read JJ values.
	1	The *y*-direction dimensions are read for each gridblock in layer one (K = 1). These values are assigned to all other layers. Read II × JJ values.
KDZ	-1	The *z*-direction gross thickness is the same for all gridblocks. Read only one value.
	0	A constant gross thickness is read for each layer; each layer may have a different value. Read KK values.
	1	The *z*-direction gross thickness is read for each gridblock in the grid. Read II × JJ × KK values.
KDZNET	-1	The *z*-direction net thickness is the same for all gridblocks. Read only one value.
	0	A constant net thickness is read for each layer; each layer may have a different value. Read KK values.
	1	The *z*-direction net thickness is read for each gridblock in the grid. Read II × JJ × KK values.

NOTE: If an array of input values must be read, the following input order must be followed. Layer 1 (K = 1) is read first. The data in each layer are read by the rows, starting with row 1 (J = 1). Values of the array element are read for the first row starting with column 1 (I = 1) and proceeding to the end of the row (column I = II). After II values are read, the next row (J = 2) of values are entered. These values must begin on a new line. This data entry procedure is repeated for all rows and, subsequently, for all layers until the complete set of array elements has been entered.

5. **DX**

DX	Gridblock size in *x*-direction (ft).
If KDX =	-1, read one constant value.
If KDX =	0, read II values (one for each row).
If KDX =	+1, read II × JJ values (one for each K = 1 gridblock).

6. **DY**

DY	Gridblock size in *y*-direction (ft).
If KDY =	-1, read one constant value.
If KDY =	0, read JJ values (one for each column).
If KDY =	+1, read II × JJ values (one for each K = 1 gridblock).

7. **DZ**

DZ	Gross gridblock thickness in *z*-direction (ft).
If KDZ =	-1, read one constant value.
If KDZ =	0, read KK values (one for each layer).
If KDZ =	+1, read II × JJ × KK values (one for each gridblock).

8. **DZNET**

DZNET	Net gridblock thickness in *z*-direction (ft).

If KDZNET = -1, read one constant value.
If KDZNET = 0, read KK values (one for each layer).
If KDZNET = +1, read II × JJ × KK values (one for each gridblock).

NOTE: Gridblocks with zero pore volume should be defined by setting DZNET = 0 or porosity = 0. Bulk volume (DX × DY × DZ) should be a nonzero, positive value for every gridblock. The IFLO calculation assumes that all gridblocks have a nonzero pore volume. A gridblock with zero pore volume is treated as a water filled gridblock with a (porosity) × (net-to-gross ratio) = 0.0001. Transmissibilities for these gridblocks are set to zero to prevent flow into or out of the gridblock.

21.1.2 Modifications to Grid Dimensions

1. **Heading** Up to 80 characters.

2. **NUMDX, NUMDY, NUMDZ, NUMDZN, IDCODE**
   - NUMDX — Number of regions where *x*-direction length (DX) is changed.
   - NUMDY — Number of regions where *y*-direction length (DY) is changed.
   - NUMDZ — Number of regions where *z*-direction gross thickness (DZ) is changed.
   - NUMDZN — Number of regions where z-direction net thickness (DZN) is changed.
   - IDCODE — = 0 means do not print the modified distributions;
     = 1 means print the modified distributions.

3. **I1, I2, J1, J2, K1, K2, DX**
   Omit this record if NUMDX = 0.

I1	Coordinate of first region gridblock in I-direction.
I2	Coordinate of last region gridblock in I-direction.
J1	Coordinate of first region gridblock in J-direction.
J2	Coordinate of last region gridblock in J-direction.
K1	Coordinate of first region gridblock in K-direction.
K2	Coordinate of last region gridblock in K-direction.
DX	New value of *x*-direction grid size for region (ft).

NOTE: NUMDX records must be read.

4. **I1, I2, J1, J2, K1, K2, DY**

Omit this record if NUMDY = 0.

I1	Coordinate of first region gridblock in I-direction.
I2	Coordinate of last region gridblock in I-direction.
J1	Coordinate of first region gridblock in J-direction.
J2	Coordinate of last region gridblock in J-direction.
K1	Coordinate of first region gridblock in K-direction.
K2	Coordinate of last region gridblock in K-direction.
DY	New value of *y*-direction grid size for region (ft).

NOTE: NUMDY records must be read.

5. **I1, I2, J1, J2, K1, K2, DZ**

Omit this record if NUMDZ = 0.

I1	Coordinate of first region gridblock in I-direction.
I2	Coordinate of last region gridblock in I-direction.
J1	Coordinate of first region gridblock in J-direction.
J2	Coordinate of last region gridblock in J-direction.
K1	Coordinate of first region gridblock in K-direction.
K2	Coordinate of last region gridblock in K-direction.
DZ	New value of *z*-direction gross thickness for region (ft).

NOTE: NUMDZ records must be read.

6. **I1, I2, J1, J2, K1, K2, DZNET**

Omit this record if NUMDZN = 0.

I1	Coordinate of first region gridblock in I-direction.
I2	Coordinate of last region gridblock in I-direction.
J1	Coordinate of first region gridblock in J-direction.
J2	Coordinate of last region gridblock in J-direction.
K1	Coordinate of first region gridblock in K-direction.
K2	Coordinate of last region gridblock in K-direction.

DZNET New value of *z*-direction net thickness for region (ft).

NOTE: NUMDZN records must be read.

21.1.3 Depths to Top of Gridblocks

The coordinate system used in IFLO is defined so that values in the *z*-direction (vertical) increase as the layer gets deeper. Negative values will be read as heights above the datum.

1. **Heading** Up to 80 characters.

2. **KEL**
   KEL Control code for input of depth values.

KEL	Meaning
0	A single constant value is read for the depth to the top of all gridblocks in layer 1 (horizontal plane). Each layer is contiguous in this option. Depths to the top of gridblocks in layers below layer 1 are calculated by adding the layer thickness to the preceding layer top; thus Top (I, J, K + 1) = Top (I, J, K) + DZ (I, J, K)
1	A separate depth value must be read for each gridblock in layer 1. Read II × JJ values. Each layer is contiguous in this option. Depths to the top of gridblocks in layers below layer 1 are calculated by adding the layer thickness to the preceding layer top; thus Top (I, J, K + 1) = Top (I, J, K) + DZ (I, J, K)
2	A separate depth value is read for each layer. Read KK values. Each layer is horizontal (layer cake) in this option.
3	A separate depth value is read for each gridblock. Read II × JJ × KK values.

3. **ELEV**
   ELEV Depth to top of gridblock (ft).

If KEL = 0, read one constant value.

If KEL = 1, read II × JJ values (one for each gridblock in layer 1).

If KEL = 2, read KK values (one for each layer).

If KEL = 3, read II × JJ × KK values (one for each gridblock).

21.2 Porosity and Permeability Distributions

21.2.1 Porosity and Permeability

1. **Heading** Up to 80 characters.

2. **KPH, KKX, KKY, KKZ**

KPH Control code for input of porosity.

KKX Control code for input of *x*-direction permeability.

KKY Control code for input of *y*-direction permeability.

KKZ Control code for input of *z*-direction permeability.

Code	Value	Meaning
KPH	-1	The porosity is constant for all gridblocks. Read only one value.
	0	A constant value is read for each layer. Read KK values.
	1	A value is read for each gridblock. Read II × JJ × KK values.

KKX	-1	The *x*-direction permeability is constant for all grid-blocks. Read only one value.
	0	A constant value is read for each layer. Read KK values.
	1	A value is read for each gridblock. Read II × JJ × KK values.
KKY	-1	The *y*-direction permeability is constant for all grid-blocks. Read only one value.
	0	A constant value is read for each layer. Read KK values.
	1	A value is read for each gridblock. Read II × JJ × KK values.
KKZ	-1	The *z*-direction permeability is constant for all grid-blocks. Read only one value.
	0	A constant value is read for each layer. Read KK values.
	1	A value is read for each gridblock. Read II × JJ × KK values.

3. **PHI**

PHI Porosity (fraction).
If KPH = -1, read one constant value.
If KPH = 0, read KK values (one for each layer).
If KPH = +1, read II × JJ × KK values (one for each grid-block).

4. **PERMX**

PERMX Permeability in *x*-direction (md).
If KKX = -1, read one constant value.
If KKX = 0, read KK values (one for each layer).
If KKX = +1, read II × JJ × KK values (one for each grid-block).

5. **PERMY**

PERMY	Permeability in *y*-direction (md).
If KKY =	-1, read one constant value.
If KKY =	0, read KK values (one for each layer).
If KKY =	+1, read II × JJ × KK values (one for each grid-block).

6. **PERMZ**

PERMZ	Permeability in *z*-direction (md).
If KKZ =	-1, read one constant value.
If KKZ =	0, read KK values (one for each layer).
If KKZ =	+1, read II × JJ × KK values (one for each grid-block).

21.2.2 Modifications to Porosities and Permeabilities

1. **Heading** Up to 80 characters.

2. **NUMP, NUMKX, NUMKY, NUMKZ, IPCODE**

NUMP	Number of regions where porosity (PHI) is changed.
NUMKX	Number of regions where *x*-direction permeability (PERMX) is changed.
NUMKY	Number of regions where *y*-direction permeability (PERMY) is changed.
NUMKZ	Number of regions where *z*-direction permeability (PERMZ) is changed.
IPCODE	= 0 means do not print the modified distributions; = 1 means print the modified distributions.

3. **I1, I2, J1, J2, K1, K2, VALPHI**
Omit this record if NUMP = 0.

I1	Coordinate of first region gridblock in I-direction.
I2	Coordinate of last region gridblock in I-direction.
J1	Coordinate of first region gridblock in J-direction.
J2	Coordinate of last region gridblock in J-direction.
K1	Coordinate of first region gridblock in K-direction.
K2	Coordinate of last region gridblock in K-direction.
VALPHI	See table.

Code	Value	Meaning
NUMP	> 0	New value of porosity (fr).
	< 0	Multiply porosity by VALPHI.

NOTE: NUMP records must be read.

4. **I1, I2, J1, J2, K1, K2, VALKX**

Omit this record if NUMKX = 0.

I1	Coordinate of first region gridblock in I-direction.
I2	Coordinate of last region gridblock in I-direction.
J1	Coordinate of first region gridblock in J-direction.
J2	Coordinate of last region gridblock in J-direction.
K1	Coordinate of first region gridblock in K-direction.

K2 Coordinate of last region gridblock in K-direction.

VALKX See table.

Code	Value	Meaning
NUMKX	> 0	Specify value of *x*-direction permeability (md).
	< 0	Multiply *x*-direction permeability by VALKX.

NOTE: NUMKX records must be read.

5. **I1, I2, J1, J2, K1, K2, VALKY**

Omit this record if NUMKY = 0.

I1 Coordinate of first region gridblock in I-direction.

I2 Coordinate of last region gridblock in I-direction.

J1 Coordinate of first region gridblock in J-direction.

J2 Coordinate of last region gridblock in J-direction.

K1 Coordinate of first region gridblock in K-direction.

K2 Coordinate of last region gridblock in K-direction.

VALKY See table.

Code	Value	Meaning
NUMKY	> 0	Specify value of *y*-direction permeability (md).
	< 0	Multiply *y*-direction permeability by VALKY.

NOTE: NUMKY records must be read.

6. **I1, I2, J1, J2, K1, K2, VALKZ**

Omit this record if NUMKZ = 0.

I1	Coordinate of first region gridblock in I-direction.
I2	Coordinate of last region gridblock in I-direction.
J1	Coordinate of first region gridblock in J-direction.
J2	Coordinate of last region gridblock in J-direction.
K1	Coordinate of first region gridblock in K-direction.
K2	Coordinate of last region gridblock in K-direction.
VALKZ	See table.

Code	Value	Meaning
NUMKZ	> 0	Specify value of *z*-direction permeability (md).
	< 0	Multiply *z*-direction permeability by VALKZ.

NOTE: NUMKZ records must be read.

21.3 Rock Region Information

21.3.1 Definition of Rock Regions

1. **Heading** Up to 80 characters.

2. **KR3P, NROCK, KPHIMOD**

KR3P	Code specifying desired relative permeability option.

NROCK Number of distinct Rock regions. A separate set of saturation dependent tables must be entered for each Rock region.

KPHIMOD Code specifying desired ϕ-K model for initial permeability calculation and transmissibility updates.

Code	Value	Meaning
KR3P	0	Oil relative permeability calculated from the relative permeability data for the two-phase water-oil system.
	1	Oil relative permeability calculated from the relative permeability data for the two-phase gas-oil system.
	2	Three-phase oil relative permeability based on modified Stone equation
KPHIMOD	0	Do not use ϕ-K model.
	1	Use ϕ-K model to calculate initial permeability. Do not update transmissibility.
	2	Use ϕ-K model to calculate initial permeability and update transmissibility.
	3	Use ϕ-K model to update transmissibility. Do not calculate initial permeability.

3. **Heading** Up to 80 characters.
Omit this record if NROCK = 1.

4. **NUMROK**
Omit this record if NROCK = 1.
NUMROK = 0 Enter Rock region value for each gridblock.
NUMROK > 0 Number of regions where the Rock region default value of 1 is changed.

5. **IVAL**

Omit this record if NROCK = 1 or NUMROK > 0.

IVAL	Array of Rock region values. Read II × JJ × KK values.

6. **I1, I2, J1, J2, K1, K2, IVAL**

Omit this record if NROCK = 1 or NUMROK = 0.

I1	Coordinate of first region gridblock in I-direction
I2	Coordinate of last region gridblock in I-direction
J1	Coordinate of first region gridblock in J-direction
J2	Coordinate of last region gridblock in J-direction
K1	Coordinate of first region gridblock in K-direction
K2	Coordinate of last region gridblock in K-direction
IVAL	Number of the saturation dependent data set to be assigned to this Rock region and IVAL ≤ NROCK

NOTE: NUMROK records must be read.

21.3.2 Porosity-Permeability Model for Transmissibility Calculation

1. **Heading** Up to 80 characters.

Include this record if KPHIMOD > 0.

2. **XKBASE, YKBASE, ZKBASE, PHIBASE**

Include this record if KPHIMOD = 1 or 2.

XKBASE	Base permeability in *x*-direction (md)

YKBASE	Base permeability in *y*-direction (md)
ZKBASE	Base permeability in *z*-direction (md)
PHIBASE	Base porosity (fr)

NOTE: The *x*-direction ϕ-K model is

$$K_x = K_{x,\text{base}}\left\{a_1\left(\frac{\phi}{\phi_{\text{base}}}\right)^{b_1} + a_2 e^{\left[b_2\left(\phi-\phi_{\text{base}}\right)\right]}\right\}$$

Similar models apply to *y*-direction and *z*-direction permeabilities. Coefficients are defined below.

3. **XKPHIA1, XKPHIB1, XKPHIA2, XKPHIB2**
Include this record if KPHIMOD > 0.

XKPHIA1	Coefficient a_1 for ϕ-K model in *x*-direction
XKPHIB1	Coefficient b_1 for ϕ-K model in *x*-direction
XKPHIA2	Coefficient a_2 for ϕ-K model in *x*-direction
XKPHIB2	Coefficient b_2 for ϕ-K model in *x*-direction

4. **YKPHIA1, YKPHIB1, YKPHIA2, YKPHIB2**
Include this record if KPHIMOD > 0.

YKPHIA1	Coefficient a_1 for ϕ-K model in y-direction
YKPHIB1	Coefficient b_1 for ϕ-K model in y-direction
YKPHIA2	Coefficient a_2 for ϕ-K model in y-direction
YKPHIB2	Coefficient b_2 for ϕ-K model in y-direction

5. **ZKPHIA1, ZKPHIB1, ZKPHIA2, ZKPHIB2**
Include this record if KPHIMOD > 0.

ZKPHIA1	Coefficient a_1 for ϕ-K model in *z*-direction
ZKPHIB1	Coefficient b_1 for ϕ-K model in *z*-direction
ZKPHIA2	Coefficient a_2 for ϕ-K model in *z*-direction

ZKPHIB2 Coefficient b_2 for ϕ-K model in *z*-direction

NOTE: Repeat records 1 through 5 a total of NROCK times (one set of records for each Rock Region defined in Section 21.3.1).

21.3.3 Relative Permeability and Capillary Pressure Tables

1. **Heading** Up to 80 characters.

2. **SAT1 KROW1 KRW1 PCOW1**
   ⋮
   SATn KROWn KRWn PCOWn

   SAT Water phase saturation (fr). Set SATn = 1.0
   KROW Oil relative permeability for oil-water system (fr)
   KRW Water relative permeability for oil-water system (fr)
   PCOW Oil-water capillary pressure (psi)

   NOTE: There must be table entries for irreducible water saturation (S_{wr}) and residual oil saturation (S_{orw}). Capillary pressure is defined as PCOW = P_o - P_w where P_o and P_w are the oil and water phase pressures respectively.

   NOTE: Repeat records 1 and 2 a total of NROCK times (one set of records for each Rock Region defined in Section 21.3).

3. **Heading** Up to 80 characters.

4. **SAT1 KROG1 KRG1 PCGO1**
   ⋮
   SATn KROGn KRGn PCGOn

SAT	Gas phase saturation (fr). Set SAT1 = 0.0 and SATn = 1.0
KROG	Oil relative permeability for gas-oil system (fr)
KRG	Gas relative permeability for gas-oil system (fr)
PCGO	Gas-oil capillary pressure (psi)

NOTE: The gas-oil table assumes that irreducible water saturation (S_{wr}) is present. As a matter of consistency, KROG at SAT1 = 0 must equal KROW at S_{wr}. There must be table entries for residual gas saturation (S_{gr}) and residual oil saturation (S_{org}). Capillary pressure is defined as PCGO = P_g - P_o where P_o and P_g are the oil and gas phase pressures respectively. If solvent is included in the model, gas-oil capillary pressure will only be used at gridblocks that have pressures below the miscibility pressure.

NOTE: Repeat records 3 and 4 a total of NROCK times (one set of records for each Rock Region defined in Section 21.3.1).

21.4 Modifications to Pore Volumes and Transmissibilities

1. **Heading** Up to 80 characters.

2. **NUMPV, NUMTX, NUMTY, NUMTZ, ITCODE**

NUMPV	Number of regions where pore volume is changed
NUMTX	Number of regions where *x*-direction transmissibility (TX) is changed
NUMTY	Number of regions where *y*-direction transmissibility (TY) is changed
NUMTZ	Number of regions where *z*-direction transmissibility (TZ) is changed

ITCODE = 0 means do not print the modified distributions
= 1 means print the modified distributions

NOTE: The conventions for gridblock (I, J, K) transmissibility follow:
TX(I, J, K) refers to flow between gridblocks I-1 and I.
TY(I, J, K) refers to flow between gridblocks J-1 and J.
TZ(I, J, K) refers to flow between gridblocks K-1 and K.

3. **I1, I2, J1, J2, K1, K2, VALPV**
Omit this record if NUMPV = 0.

I1	Coordinate of first region gridblock in I-direction
I2	Coordinate of last region gridblock in I-direction
J1	Coordinate of first region gridblock in J-direction
J2	Coordinate of last region gridblock in J-direction
K1	Coordinate of first region gridblock in K-direction
K2	Coordinate of last region gridblock in K-direction
VALPV	Multiplier of pore volume for region

NOTE: NUMPV records must be read.

4. **I1, I2, J1, J2, K1, K2, VALTX**
Omit this record if NUMTX = 0.

I1	Coordinate of first region gridblock in I-direction
I2	Coordinate of last region gridblock in I-direction
J1	Coordinate of first region gridblock in J-direction

J2	Coordinate of last region gridblock in J-direction
K1	Coordinate of first region gridblock in K-direction
K2	Coordinate of last region gridblock in K-direction
VALTX	Multiplier of *x*-direction transmissibility for region

NOTE: NUMTX records must be read.

5. **I1, I2, J1, J2, K1, K2, VALTY**

Omit this record if NUMTY = 0.

I1	Coordinate of first region gridblock in I-direction
I2	Coordinate of last region gridblock in I-direction
J1	Coordinate of first region gridblock in J-direction
J2	Coordinate of last region gridblock in J-direction
K1	Coordinate of first region gridblock in K-direction
K2	Coordinate of last region gridblock in K-direction
VALTY	Multiplier of *y*-direction transmissibility for region

NOTE: NUMTY records must be read.

6. **I1, I2, J1, J2, K1, K2, VALTZ**

Omit this record if NUMTZ = 0.

I1	Coordinate of first region gridblock in I-direction
I2	Coordinate of last region gridblock in I-direction
J1	Coordinate of first region gridblock in J-direction
J2	Coordinate of last region gridblock in J-direction
K1	Coordinate of first region gridblock in K-direction
K2	Coordinate of last region gridblock in K-direction
VALTZ	Multiplier of *z*-direction transmissibility for region

NOTE: NUMTZ records must be read.

21.5 Reservoir Geophysical Parameters

21.5.1 Moduli and Grain Densities

1. **Heading** Up to 80 characters.

2. **KGPMOD, KDSMOD**

KGPMOD	Control code for reservoir geophysical model
KDSMOD	Control code for dynamic to static conversion model

KGPMOD	KDSMOD	Meaning
-1	0	No reservoir geophysical model
0	0	Constant moduli model: enter moduli as arrays of constant values; moduli do not depend on effective pressure, porosity, or clay content
1	0	IFM model: enter moduli as functions of porosity, effective pressure, and clay content; enter model parameters by Rock Region (NROCK values)
1	1	IFM model plus conversion of Young's modulus and Poisson's ratio from dynamic to static conditions; enter model parameters by Rock Region (NROCK values)

3. **Heading** Up to 80 characters.
   Enter this record if KGPMOD = 0.

4. **KKB, KKG, KMU, KRHO**
   Enter this record if KGPMOD = 0.

   KKB Control code for input of the dry frame bulk modulus (evacuated porous rock).

   KKG Control code for input of the grain bulk modulus (solid matrix material).

   KMU Control code for input of the shear modulus (evacuated porous rock).

   KRHO Control code for input of the grain density (solid matrix material).

Code	Value	Meaning
KKB	-1	Dry frame bulk moduli are the same for all grid-blocks. Read only one value.
	0	A constant value of dry frame bulk modulus is read for each layer; each layer may have a different value. Read KK values.
	1	Dry frame bulk moduli are read for each gridblock. Read II × JJ × KK values.
KKG	-1	Grain bulk moduli are the same for all gridblocks. Read only one value.
	0	A constant value of grain bulk modulus is read for each layer; each layer may have a different value. Read KK values.
	1	Grain bulk moduli are read for each gridblock. Read II × JJ × KK values.
KMU	-1	Shear moduli are the same for all gridblocks. Read only one value.
	0	A constant value of shear modulus is read for each layer; each layer may have a different value. Read KK values.
	1	Shear moduli are read for each gridblock. Read II × JJ × KK values.
KRHO	-1	Grain densities are the same for all gridblocks. Read only one value.
	0	A constant value of grain density is read for each layer; each layer may have a different value. Read KK values.
	1	Grain densities are read for each gridblock. Read II × JJ × KK values.

5. **KB**

Enter this record if KGPMOD = 0.

KB Dry frame bulk modulus (psia).

If KKB = -1, read one constant value.

If KKB = 0, read KK values (one for each layer).

If KKB = +1, read II × JJ × KK values (one for each gridblock).

NOTE: In the absence of data, a value of 3×10^6 psia is reasonable.

6. **KG**

Enter this record if KGPMOD = 0.

KG Grain bulk modulus (psia).

If KKG = -1, read one constant value.

If KKG = 0, read JJ values (one for each layer).

If KKG = +1, read II × JJ values (one for each gridblock).

NOTE: In the absence of data, a value of 3×10^6 psia is reasonable.

7. **MU**

Enter this record if KGPMOD = 0.

MU Effective shear modulus (psia).

If KMU = -1, read one constant value.

If KMU = 0, read KK values (one for each layer).

If KMU = +1, read II × JJ × KK values (one for each gridblock).

NOTE: In the absence of data, a value of 3×10^6 psia is reasonable.

8. **RHOMA**

Enter this record if KGPMOD = 0.

RHOMA Grain density (lbf/ft^3).

If KRHO = -1, read one constant value.
If KRHO = 0, read KK values (one for each layer).
If KRHO = +1, read II × JJ × KK values (one for each grid-block).

NOTE: In the absence of data, a value of 168 lbf/ft^3 (corresponding to 2.7 g/cm^3) is reasonable.

21.5.2 IFM Model

1. **Heading** Up to 80 characters.
Enter this record if KGPMOD = 1.

2. **AIKMA, AIKMB, AIKMC, AIKMD, AIKME, AIKMF**
Enter this record if KGPMOD = 1.
AIKMA Dry frame bulk modulus parameter a_0
AIKMB Dry frame bulk modulus parameter a_1
AIKMC Dry frame bulk modulus parameter a_2
AIKMD Dry frame bulk modulus parameter a_3
AIKME Dry frame bulk modulus parameter a_4
AIKMF Dry frame bulk modulus parameter a_5

3. **EXK1, EXK2**
Enter this record if KGPMOD = 1.
EXK1 Dry frame bulk modulus exponent e_1
EXK2 Dry frame bulk modulus exponent e_2

4. **AIMUA, AIMUB, AIMUC, AIMUD, AIMUE, AIMUF**
Enter this record if KGPMOD = 1.
AIMUA Shear modulus parameter α_0
AIMUB Shear modulus parameter α_1
AIMUC Shear modulus parameter α_2
AIMUD Shear modulus parameter α_3

AIMUE	Shear modulus parameter α_4
AIMUF	Shear modulus parameter α_5

5. **EXM1, EXM2**

Enter this record if KGPMOD = 1.

EXK1	Dry frame bulk modulus exponent ε_1
EXK2	Dry frame bulk modulus exponent ε_1

6. **AIRHOA, AIRHOB, AIRHOC**

Enter this record if KGPMOD = 1.

AIRHOA	Rock matrix grain density parameter b_0
AIRHOB	Rock matrix grain density parameter b_1
AIRHOC	Rock matrix grain density parameter b_2

NOTE: Repeat records 1 through 6 a total of NROCK times (one set of records for each Rock Region defined in Section 21.3).

21.5.3 Confining Pressure and Clay Content for IFM Model

1. **KPCON, KCLAY**

Enter this record if KGPMOD = 1.

KPCON	Control code for input of confining pressure.
KCLAY	Control code for input of clay content.

Code	Value	Meaning
KPCON	-1	Confining pressure is the same for all gridblocks. Read only one value.
	0	A constant value of confining pressure is read for each layer; each layer may have a different value. Read KK values.
	1	Confining pressures are read for each gridblock. Read II × JJ × KK values.
	11	Calculate confining pressures from gridblock elevations and overburden pressure gradient.
KCLAY	-1	Clay content is the same for all gridblocks. Read only one value.
	0	A constant value of clay content is read for each layer; each layer may have a different value. Read KK values.
	1	Clay content is read for each gridblock. Read II × JJ × KK values.

2. **PCON**

Enter this record if KGPMOD = 1.

PCON Confining pressure (psia).

If KPCON = -1, read one constant value.

If KPCON = 0, read KK values (one for each layer).

If KPCON = +1, read II × JJ × KK values (one for each gridblock).

If KPCON = +11, read constant values for **OBGRAD, OBDAT**

OBGRAD Overburden pressure gradient (psia/ft)

OBDAT Overburden datum (ft)

NOTE: In the absence of data, values of OBGRAD = 1.0 psia/ft and OBDAT = 0.0 ft are reasonable.

3. **CLAY**

Enter this record if KGPMOD = 1.

CLAY Clay content (volume fraction).

If KCLAY = -1, read one constant value.

If KCLAY = 0, read JJ values (one for each layer).

If KCLAY = +1, read II × JJ values (one for each gridblock).

NOTE: In the absence of data, a value of 0.0 is reasonable.

21.5.4 Modifications to Confining Pressure and Clay Content

1. **Heading** Up to 80 characters.

2. **NUMCON, NUMCLA, IDCODE**

NUMCON Number of regions where confining pressure (PCON) is changed.

NUMCLA Number of regions where clay content (CLAY) is changed.

IDCODE = 0 means do not print the modified distributions;
= 1 means print the modified distributions.

3. **I1, I2, J1, J2, K1, K2, PCON**

Omit this record if NUMCON = 0.

I1 Coordinate of first region gridblock in I-direction.

I2 Coordinate of last region gridblock in I-direction.

J1 Coordinate of first region gridblock in J-direction.

J2	Coordinate of last region gridblock in J-direction.
K1	Coordinate of first region gridblock in K-direction.
K2	Coordinate of last region gridblock in K-direction.
PCON	New value of confining pressure (psia).

NOTE: NUMCON records must be read.

4. **I1, I2, J1, J2, K1, K2, CLAY**
Omit this record if NUMCLA = 0.

I1	Coordinate of first region gridblock in I-direction.
I2	Coordinate of last region gridblock in I-direction.
J1	Coordinate of first region gridblock in J-direction.
J2	Coordinate of last region gridblock in J-direction.
K1	Coordinate of first region gridblock in K-direction.
K2	Coordinate of last region gridblock in K-direction.
CLAY	New value of clay content (volume fraction).

NOTE: NUMCLA records must be read.

21.5.5 Dynamic to Static Conversion of Young's Modulus and Poisson's Ratio

1. **Heading** Up to 80 characters.
Enter this record if KGPMOD = 1 and KDSMOD = 1.

2. **YDSA1, YDSA2, YDSB1, YDSB2, YDSC**

Enter this record if KGPMOD = 1 and KDSMOD = 1.

YDSA1 Coefficient a_1 for dynamic to static Young's modulus conversion.

YDSA2 Coefficient a_2 for dynamic to static Young's modulus conversion.

YDSB1 Coefficient b_1 for dynamic to static Young's modulus conversion.

YDSB2 Coefficient b_2 for dynamic to static Young's modulus conversion.

YDSC Coefficient c for dynamic to static Young's modulus conversion.

NOTE: The dynamic to static conversion algorithm for Young's modulus E is

$$E_s = aE_d^b + c$$
$$a = a_1 + a_2 \log\left(P_e\right)$$
$$b = b_1 + b_2 \log\left(P_e\right)$$

where subscript s denotes static and subscript d denotes dynamic. The coefficients {a, a_1, a_2, b, b_1, b_2, c} are empirical fit parameters, and P_e is effective pressure. An analogous dynamic to static conversion algorithm may be specified for Poisson's ratio.

3. **PDSA1, PDSA2, PDSB1, PDSB2, PDSC**

Enter this record if KGPMOD = 1 and KDSMOD = 1.

PDSA1 Coefficient a_1 for dynamic to static Poisson's ratio conversion.

PDSA2 Coefficient a_2 for dynamic to static Poisson's ratio conversion.

PDSB1 Coefficient b_1 for dynamic to static Poisson's ratio conversion.

PDSB2 Coefficient b_2 for dynamic to static Poisson's ratio conversion.

PDSC Coefficient c for dynamic to static Poisson's ratio conversion.

NOTE: Repeat records 1 through 3 a total of NROCK times (one set of records for each Rock Region defined in Section 21.3).

21.6 Fluid PVT Tables

1. **Heading** Up to 80 characters.

2. **PBO, VOSLP, BOSLP, BWSLP, PMAX**

PBO Initial reservoir oil bubble point pressure (psia). If no oil or natural gas exist, set PBO = 14.7 psia.

VOSLP Slope of the oil viscosity versus pressure curve for undersaturated oil, i.e. for pressures above PBO. The slope ($\Delta\mu_o/\Delta P_o$) should be in cp/psia.

BOSLP Slope of the oil formation volume factor versus pressure curve for undersaturated oil. The slope ($\Delta B_o/\Delta P_o$) should be in RB/STB/psia and should be negative or zero.

BWSLP Slope of the water formation volume factor versus pressure curve for undersaturated water, i.e. for pressures above PBO. The slope ($\Delta B_w/\Delta P_o$) should be in RB/STB/psia and should be negative or zero.

PMAX Maximum pressure entry for all PVT tables (psia).

NOTE: VOSLP, BOSLP and BWSLP are used only for undersaturated oil and water. The slope ($\Delta R_{so}/\Delta P_o$) of the solution

natural gas-oil ratio versus pressure curve for undersaturated oil is assumed to be zero.

3. **Heading** Up to 80 characters; oil table follows.

4. **P1 MUO1 BO1 RSO1**
⋮
PMAX MUO(PMAX) BO(PMAX) RSO(PMAX)

P	Pressure (psia). Pressures must be in ascending order from P1 (normally 14.7 psia) to PMAX. The last table entry must be PMAX.
MUO	Oil viscosity (cp).
BO	Oil formation volume factor (RB/STB).
RSO	Solution natural gas-oil ratio (SCF/STB).

NOTE: Oil properties must be entered as saturated data over the entire pressure range. Saturated oil data is required because of the bubble point pressure tracking algorithm.

5. **Heading** Up to 80 characters; water table follows.

6. **P1 MUW1 BW1 RSW1**
⋮
PMAX MUW(PMAX) BW(PMAX) RSW(PMAX)

P	Pressure (psia). Pressures must be in ascending order from P1 (normally 14.7 psia) to PMAX. The last table entry must be PMAX.
MUW	Water viscosity (cp).
BW	Water formation volume factor (RB/STB).
RSW	Solution natural gas-water ratio (SCF/STB). Water properties must be entered as saturated data over the entire pressure range if RSW in nonzero.

NOTE: It is usually assumed in black oil simulations that the solubility of gas in water can be neglected. In this case, set RSW = 0.0 for all pressures. IFLO includes gas solubility in the water phase to account for CO_2 solubility in water, gas production from geopressured aquifers, or any other case where gas solubility in water can be significant.

7. **Heading** Up to 80 characters.

8. **KGCOR**

Code	Value	Meaning
KGCOR	0	Read gas and rock properties table.
	1	Activate gas correlation option and read rock compressibility versus pressure table.

9. **Heading** Up to 80 characters; gas table follows.
Omit this record if KGCOR = 1.

10. **P1 MUG1 BG1 PSI1 CR1**
⋮
PMAX MUG(PMAX) BG(PMAX) PSI(PMAX) CR(PMAX)
Omit this record if KGCOR = 1.

P	Pressure (psia). Pressures must be in ascending order from P1 (normally 14.7 psia) to PMAX. The last table entry must be PMAX.
MUG	Natural gas viscosity (cp).
BG	Natural gas formation volume factor (RCF/SCF).
PSI	Real gas pseudo-pressure ($psia^2/cp$).
CR	Rock compressibility (1/psia).

11. **KODEA, MPGT, TEM, SPG**

Omit this record if KGCOR = 0.

KODEA — Gas composition option.

MPGT — Number of gas PVT table entries ($1 < MPGT \leq 25$).

TEM — Reservoir temperature (^oF).

SPG — Gas specific gravity (air = 1.0).

KODEA	GAS DESCRIPTION
1	Sweet gas: input 12 component mole fractions as 0. 0. 0. 1. 0. 0. 0. 0. 0. 0. 0. 0.
2	Sour gas: input 12 component mole fractions in the order y_1 y_2 y_3 y_4 0. 0. 0. 0. 0. 0. 0. 0. where y_1 = mole fraction of H_2S, y_2 = mole fraction of CO_2, y_3 = mole fraction of N_2, and $y_4 = 1 - (y_1 + y_2 + y_3)$.
3	Sweet or sour gas with the following 12 component mole fractions read in the following order: H_2S, CO_2, N_2, C_1, C_2, C_3, iC_4, nC_4, iC_5, nC_5, C_6, C_{7+}. The sum of the mole fractions should equal one.
4	Same as KODEA = 3 but also read critical pressure, critical temperature, and molecular weight of C_{7+}.

12. **FRCI**

Omit this record if KGCOR = 0.

FRCI — Component mole fraction of gas. Read 12 entries in the following order.

FRCI(I)	Component I	FRCI(I)	Component I
1	H_2S	7	iC_4
2	CO_2	8	nC_4
3	N_2	9	iC_5
4	C_1	10	nC_5

FRCI(I)	Component I	FRCI(I)	Component I
5	C_2	11	C_6
6	C_3	12	C_{7+}

13. **PRSCI, TEMCI, RMWTI**
Omit this record if KGCOR = 0 or if KODEA ≠ 4.
PRSCI Critical pressure (psia).
TEMCI Critical temperature (^oR).
RMWTI Molecular weight.

14. **Heading** Up to 80 characters.
Omit this record if KGCOR = 0.
NOTE: Rock compressibility table follows.

15. **P1 CR1**
⋮
PMAX CR(PMAX)
Omit this record if KGCOR = 0.

Number of Records	Variable	Meaning
Option 1. Constant rock compressibility		
Enter one record.	PMAX	Maximum table pressure (psia) from record 4.
	CR	Rock compressibility (1/psia)
Option 2. Pressure-dependent rock compressibility		
Enter MPGT records.	P	Pressure (psia). Pressures must be in ascending order from P1 (normally 14.7 psia) to PMAX. The last table entry must be PMAX.
	CR	Rock compressibility (1/psia)

16. **Heading** Up to 80 characters.

17. **RHOSCO, RHOSCW, RHOSCG**

RHOSCO	Stock tank oil density (lbm/cu ft).
RHOSCW	Stock tank water density (lbm/cu ft).
RHOSCG	Gas density at standard conditions (lbm/cu ft). If no natural gas exists, set RHOSCG = 0.

NOTE: At stock tank conditions (14.7 psia and 60 degrees F for oilfield units) pure water has a density of 62.4 lbm/cu ft and air has a density of 0.0765 lbm/cu ft.

21.7 Miscible Solvent Data

1. **Heading** Up to 80 characters.

2. **NSLUGS, NSREAD**

NSLUGS	Number of solvents.
NSREAD	Number of solvent PVT tables to be read (up to 4). NSREAD must be equal to or greater than NSLUGS.

NOTE: NSREAD is provided as a convenience. PVT data for one to four solvents may be left in the input data set for an oil-water-natural gas run by setting NSREAD = 1 to 4 and NSLUGS = 0.

If NSREAD = 0, omit the data in the remainder of this section and proceed to Section 21.8.

3. **Heading** Up to 80 characters.

4. **PBO1, VO1OPE, BO1OPE**

PBO1	Initial base solvent-oil bubble point pressure (psia).
VO1OPE	Undersaturated slope of oil viscosity (cp/psi).
BO1OPE	Undersaturated slope of oil formation volume factor (RB/STB/psi).

5. **Heading** Up to 80 characters.

6. **PBW1, VW1OPE, BW1OPE**

PBW1	Initial base solvent-water bubble point pressure (psia).
VW1OPE	Undersaturated slope of water viscosity (cp/psi).
BW1OPE	Undersaturated slope of water formation volume factor (RB/STB/psi).

7. **Heading** Up to 80 characters.

8. **PMISC, FPMISC, SOMIN, REDK, BETA, SORM, VSMISC**

PMISC	Miscibility pressure (psia).
FPMISC	Fraction of PMISC (fr) for calculating multi-contact miscibility pressure PMCM (psia). PMISC and PMCM are related by PMCM = FPMISC × PMISC.
SOMIN	Minimum oil saturation for solid precipitation (fr). SOMIN > 0 only if SORM = 0.
REDK	Relative permeability reduction factor for solid precipitation (fr).
BETA	Parameter for water blocking function.
SORM	Miscible region residual oil saturation (fr). SORM > 0 only if SOMIN = 0.
VSMISC	Total solvent volume fraction required to obtain full miscibility (fr).

Code	Value	Meaning
SOMIN	0	No solid precipitation.
	> 0	Allow solid precipitation.
BETA	< 0	No water blocking.
	≥ 0	Water blocking on.

NOTE: If the automatic timestep control is on, saturation convergence requires that SOMIN < DSMAX (Section 21.9).

9. **Heading** Up to 80 characters.

10. **OM1, OM2**

OM1 Mixing parameter ω_1 for natural gas-solvent miscibility.

OM2 Mixing parameter ω_2 for oil-gas-solvent miscibility.

NOTE: Only OM1 is used if the gridblock pressure P < PMCM. Only OM2 is used if P > PMISC. Both OM1 and OM2 are used if P is in the multicontact miscibility pressure range PMCM < P < PMISC.

11. **Heading** Up to 80 characters.

12. **RHOSC1, RHOSC2, RHOSC3, RHOSC4**

RHOSC1 Stock tank density of base solvent (lbm/cu ft).

RHOSC2 Stock tank density of solvent 2 (lbm/cu ft).

RHOSC3 Stock tank density of solvent 3 (lbm/cu ft).

RHOSC4 Stock tank density of solvent 4 (lbm/cu ft).

13. **Heading** Up to 80 characters.

14. **Heading** Up to 80 characters.

15.

P1	**MUS1**	**BS1**	**RSOS1**	**RSWS1**	**BO1**	**MUO1**	**BW1**	**MUW1**
⋮	⋮	⋮	⋮	⋮	⋮	⋮	⋮	⋮
PMAX	**MUS1 @ PMAX**	**BS1 @ PMAX**	**RSOS1 @ PMAX**	**RSWS1 @ PMAX**	**BO1 @ PMAX**	**MUO1 @ PMAX**	**BW1 @ PMAX**	**MUW1 @ PMAX**

P	Pressure (psia). Pressures must be in ascending order from P1 (normally 14.7 psia) to PMAX. The last table entry must be PMAX.
MUS1	Viscosity of base solvent (cp).
BS1	Formation volume factor of base solvent (RB/STB).
RSOS1	Solubility of base solvent in oil (SCF/STB).
RSWS1	Solubility of base solvent in water (SCF/STB).
BO1	Formation volume factor of oil with base solvent (RB/STB).
MUO1	Viscosity of oil with base solvent (cp).
BW1	Formation volume factor of water with base solvent (RB/STB).
MUW1	Viscosity of water with base solvent (cp).

NOTE: Base solvent PVT data is required if NSREAD > 0. Base solvent PVT data is used only if NSLUGS > 0. Oil and water properties must be entered as base solvent saturated data over the entire pressure range. Saturated oil and water data are required because of the bubble point pressure tracking algorithm. Oil-base solvent properties should be determined with dead oil that is fully saturated with base solvent at each pressure.

16. **Heading** Up to 80 characters.

17. **Heading** Up to 80 characters.

18. **P1 MUS2 BS2 RSOS2**
⋮
PMAX MUS2(PMAX) BS2(PMAX) RSOS2(PMAX)

P Pressure (psia). Pressures must be in ascending order from P1 (normally 14.7 psia) to PMAX. The last table entry must be PMAX.

MUS2 Viscosity of solvent 2 (cp).

BS2 Formation volume factor of solvent 2 (RB/STB).

RSOS2 Solubility of solvent 2 in oil (SCF/STB).

NOTE: Solvent 2 PVT data is required if NSREAD > 1. Solvent 2 PVT data is used only if NSLUGS > 1.

19. **Heading** Up to 80 characters.

20. **Heading** Up to 80 characters.

21. **P1 MUS3 BS3 RSOS3**
⋮
PMAX MUS3(PMAX) BS3(PMAX) RSOS3(PMAX)

P Pressure (psia). Pressures must be in ascending order from P1 (normally 14.7 psia) to PMAX. The last table entry must be PMAX.

MUS3 Viscosity of solvent 3 (cp).

BS3 Formation volume factor of solvent 3 (RB/STB).

RSOS3 Solubility of solvent 3 in oil (SCF/STB).

NOTE: Solvent 3 PVT data is required if NSREAD > 2. Solvent 3 PVT data is used only if NSLUGS > 2.

22. **Heading** Up to 80 characters.

23. **Heading** Up to 80 characters.

24. **P1 MUS4 BS4 RSOS4**
⋮
PMAX MUS4(PMAX) BS4(PMAX) RSOS4(PMAX)

P Pressure (psia). Pressures must be in ascending order from P1 (normally 14.7 psia) to PMAX. The last table entry must be PMAX.

MUS4 Viscosity of solvent 4 (cp).

BS4 Formation volume factor of solvent 4 (RB/STB).

RSOS4 Solubility of solvent 4 in oil (SCF/STB).

NOTE: Solvent 4 PVT data is required if NSREAD > 3. Solvent 4 PVT data is used only if NSLUGS > 3.

25. **Heading** Up to 80 characters.

26. **NOMOB, MOBCTL, SCI**

NOMOB Number of entries in the mobility control table.

MOBCTL Mobility control switch.

SCI Surfactant concentration index. SCI multiplies the mobility reduction values FRCO2 defined below.

Code	Value	Meaning
MOBCTL	0	No mobility control.
	1	Apply mobility control.

27. **Heading** Up to 80 characters.
Omit this record if MOBCTL = 0.

28. **NSC, FRCO2**

Omit this record if MOBCTL = 0.

NSC	Normalized surfactant concentration (fr).
FRCO2	Reduction of base solvent mobility (fr).

NOTE: NOMOB records must be read.

21.8 Pressure and Saturation Initialization

1. **Heading** Up to 80 characters.

2. **KPI, KSI**

KPI	Pressure initialization code.
KSI	Saturation initialization code.

CodeValues		**Meaning**
KPI	**KSI**	
0	0	Equilibrium pressure and saturation initialization. Enter pressures and depths at the OWC and GOC. This option assumes no solvent present at initialization. Saturations are calculated from capillary pressures.
1		Specify pressure throughout grid. Read II × JJ × KK values of P.
	1	Specify constant initial oil, water and gas saturations; specify constant initial solvent volume fractions.
	2	Specify variable saturations throughout grid. Read II × JJ × KK values of SO, SW, and solvent volume fractions. IFLO sets SG = 1 − SO − SW internally.
0	3	Gravity segregated oil, water and gas saturations. This option assumes no solvent present at initialization.

NOTE: Option {KPI = 1, KSI = 2} may be used to prepare a restart data file.

3. **WOC, PWOC, GOC, PGOC**

Enter this record if KPI = 0.

WOC	Depth to the water-oil contact (ft below datum).
PWOC	Pressure at the water-oil contact (psia).
GOC	Depth to the gas-oil contact (ft below datum).
PGOC	Pressure at the gas-oil contact (psia).

NOTE: Repeat this record a total of NROCK times: one record for each Rock region defined in Section 21.3.

4. **PO**

Enter this record if KPI = 1.

PO	Oil phase pressure (psia). Read II × JJ × KK values.

5. **SOI, SWI, SGI, VS1I, VS2I, VS3I, VS4I**

Enter this record if KSI = 1.

SOI	Initial oil saturation (fr).
SWI	Initial water saturation (fr).
SGI	Initial gas saturation (fr).

Omit the following values if NSLUGS = 0.

VS1I	Initial base solvent volume fraction in the gaseous phase (fr). Enter this value if NSLUGS ≥ 1.
VS2I	Initial solvent 2 volume fraction in the gaseous phase (fr). Enter this value if NSLUGS ≥ 2.
VS3I	Initial solvent 3 volume fraction in the gaseous phase (fr). Enter this value if NSLUGS ≥ 3.
VS4I	Initial solvent 4 volume fraction in the gaseous phase (fr). Enter this value if NSLUGS ≥ 4.

NOTE: The sum of the saturations must satisfy SOI + SWI + SGI = 1 and the sum of the volume fractions must satisfy the constraint VGG + VS1 + VS2 + VS3 + VS4 = 1.0 where VGG is the fraction of natural gas in the gaseous phase.

6. **SO, SW, VS1, VS2, VS3, VS4**

Enter this record if KSI = 2.

SO — Oil saturation (fr). Read II × JJ × KK values.

SW — Water saturation (fr). Read II × JJ × KK values.

Omit the following arrays if NSLUGS = 0.

VS1 — Base solvent volume fraction in the gaseous phase (fr). Read II × JJ × KK values. Enter this array if NSLUGS ≥ 1.

VS2 — Solvent 2 volume fraction in the gaseous phase (fr). Read II × JJ × KK values. Enter this array if NSLUGS ≥ 2.

VS3 — Solvent 3 volume fraction in the gaseous phase (fr). Read II × JJ × KK values. Enter this array if NSLUGS ≥ 3.

VS4 — Solvent 4 volume fraction in the gaseous phase (fr). Read II × JJ × KK values. Enter this array if NSLUGS ≥ 4.

NOTE: If NSLUGS > 0, then the sum of the volume fractions must satisfy the constraint VGG + VS1 + VS2 + VS3 + VS4 = 1.0 where VGG is the fraction of natural gas in the gaseous phase.

7. **SOI, SGI, SOR**

Enter this record if KSI = 3.

SOI — Initial oil saturation (fr) for the oil-water zone. Initial water saturation in the oil-water zone is 1 − SOI.

SGI — Initial gas saturation (fr) for the gas-water zone. Initial water saturation in the gas-water zone is 1 − SGI.

SOR — Irreducible oil saturation (fr). If SOR > 0, set S_o = 0 when S_o < SOR. Water and gas saturations are then renormalized.

NOTE: Repeat this record a total of NROCK times: one record for each Rock region defined in Section 21.3.

21.9 Run Control Parameters

1. **Heading** Up to 80 characters.

2. **KSW1, KSW2, KSW3, KSW4**

   KSW1 Control code for printing material balance information. Information includes the gridblock location with the largest component material balance error, the magnitude of the error, and the elapsed time.

   KSW2 Control code for graphical image orientation.

   KSW3 Control code for printing the number of iterations required for convergence of the iterative solution techniques (SSOR, LSOR, ORTHOMIN).

   KSW4 Control code for printing timestep summary to terminal.

Code	Code Value	Meaning
KSW1	0	Do not print the information
	1	Print the information to file ITEMP.MBE
KSW2	0	Image aligned with grid
	1	Image inverted relative to y-axis
KSW3	0	Do not print the information
	1	Print the information to file ITEMP.MBE
KSW4	0	Print summary at each timestep
	1	Print summary at FTIO times (Section 22.1)

3. **Heading** Up to 80 characters.

4. **NMAX, FACT1, FACT2, TMAX, WORMAX, GORMAX, PAMIN, PAMAX**

   NMAX Maximum number of timesteps per simulation run.

   FACT1 Factor for increasing timestep size using automatic timestep control. FACT1 = 1.0 for fixed timestep size. A common value for FACT1 is 1.25.

   FACT2 Factor for decreasing timestep size using automatic timestep control. FACT2 = 1.0 for fixed timestep size. A common value for FACT2 is 0.5.

   TMAX Maximum elapsed time to be simulated (days); the run will be terminated when the time exceeds TMAX.

   WORMAX Maximum allowed water-oil ratio for a producing oil well (STB/STB).

   GORMAX Maximum allowed gas-oil ratio for a producing oil well (SCF/STB).

   PAMIN Minimum field average pressure (psia).

   PAMAX Maximum field average pressure (psia).

   NOTE: The run will be terminated if producing WOR > WORMAX or producing GOR > GORMAX. GORMAX is the total natural gas plus solvent-oil ratio. PAMIN and PAMAX should be within the range of pressures covered by the fluid PVT tables discussed in Section 21.6. The run will be terminated when the pore volume weighted average reservoir pressure P_{avg} < PAMIN or P_{avg} > PAMAX. Each of the controls {WORMAX, GORMAX, PAMIN, PAMAX} will be ignored if it is set to zero.

5. **Heading** Up to 80 characters.

6. **KSOL, MITR, OMEGA, TOL, NCYCLE, DSMAX, DPMAX, ITMAX, RTOL, NERR**

KSOL	Solution method code.
MITR	For KSOL = 1 or 2: maximum number of SOR iterations for convergence with a typical value of 100. For KSOL = 4: maximum number of conjugate gradient iterations for convergence with a typical value of 50.
OMEGA	For KSOL =1 or 2: initial SOR acceleration parameter. Initial value of OMEGA should be between 1.0 and 2.0. A typical initial value is 1.2. The model will attempt to optimize OMEGA if NCYCLE $\neq 0$.
TOL	For KSOL = 1 or 2: maximum acceptable SOR pressure convergence tolerance with a typical value of 0.001 psia. For KSOL = 4: pressure convergence tolerance with a typical value of 0.001 psia to 0.0001 psia.
NCYCLE	For KSOL = 1 or 2: number of SOR iteration cycles for determining when to change (optimize) OMEGA. A typical value is 12. If NCYCLE = 0, the initial value of OMEGA will be used for the entire run.
DSMAX	Maximum saturation change (fraction) allowed per timestep. The timestep size DT will be reduced by FACT2 if the saturation change of any phase or any component in any gridblock exceeds DSMAX and DT > DTMIN (the user-specified minimum timestep size defined in Section 22.1). If the resulting step size is less than DTMIN, the timestep will be repeated with DT = DTMIN. A typical value of DSMAX is 0.05.

DPMAX Maximum pressure change (psia) allowed per timestep. The timestep size will be reduced by FACT2 if the pressure change in any gridblock exceeds DPMAX and DT > DTMIN. If the resulting step size is less than DTMIN, the timestep will be repeated with DT = DTMIN. A typical value of DPMAX is 100 psia.

ITMAX Maximum number of Newton-Raphson iterations per timestep for convergence. A typical value is 5.

RTOL Maximum allowed residual for Newton-Raphson convergence. A typical value is 0.001. ITMAX overrides RTOL if RTOL is not reached.

NERR Code for controlling material balance error technique. NERR = 1 is recommended.

Code	Value	Meaning
KSOL	1	SSOR: iterative, slice (planar) successive over-relaxation method for 2-D and 3-D models.
	2	LSOR: iterative, line successive over-relaxation method for 0-D, 1-D, 2-D and 3-D models.
	3	D4: direct solution method for 1-D, 2-D and moderate sized 3-D models.
	4	ORTHOMIN: iterative, preconditioned conjugate gradient algorithm for large 2-D and 3-D models.
NERR	0	Material balance error control technique is off.
	1	Material balance error control technique is on.

7. **Heading** Up to 80 characters.

8. **WEIGHT**

WEIGHT Fluid property weighting factor.

Code Value	Meaning
0.5	Average properties are used.
1.0	Upstream properties are used.

NOTE: The weighting factor applies to formation volume factor and viscosity of oil, water, natural gas and solvents; the solubility of natural gas and solvents in oil; and the solubility of natural gas and base solvent in water.

21.10 Analytic Aquifer Models

1. **Heading** Up to 80 characters.

2. **IAQOPT**
   IAQOPT Analytic aquifer model code.

Code	Value	Meaning
IAQOPT	0	No analytic aquifer model
	1	Steady-state aquifer model (constant aquifer pressure)

NOTE: Different aquifer influx strengths may be specified for a given aquifer.

3. **NAQEN**
   Omit this record if IAQOPT ≠ 1.
   NAQEN Number of regions containing a steady-state aquifer.

4. **I1, I2, J1, J2, K1, K2, SSAQ**

Omit this record if IAQOPT ≠1.

I1	Coordinate of first region gridblock in I-direction.
I2	Coordinate of last region gridblock in I-direction.
J1	Coordinate of first region gridblock in J-direction.
J2	Coordinate of last region gridblock in J-direction.
K1	Coordinate of first region gridblock in K-direction.
K2	Coordinate of last region gridblock in K-direction.
SSAQ	Steady-state aquifer strength (SCF/day/psia).

NOTE: NAQEN records must be read.

21.11 Coal Gas Model

1. **Heading** Up to 80 characters.

2. **ICGOPT**

ICGOPT Coal gas model code.

Code	Value	Meaning
ICGOPT	0	No coal gas model
	1	Coal gas model with diffusive desorption

3. **NCGREG**

Omit this record if ICQOPT ≠ 1.

NCGREG Number of regions containing a coalbed.

4. **ITMPCG, ITMPMOD, NCGSUB**

Omit this record if ICGOPT ≠ 1.

ITMPCG Coal gas region number.

ITMPMOD Coal gas model number.

NCGSUB Number of subregions within coal gas region.

Code	Value	Meaning
ITMPMOD	1	Saturated coal gas model with diffusive desorption
ITMPMOD	2	Undersaturated coal gas model with diffusive desorption and critical desorption pressure

NOTE: ITMPCG and NCGSUB must be greater than zero.

5. **CGDIFF, CGRAD, CGDEN, CGVL, CGPL, CGASH, CGWC, CGPCD**

Omit this record if ICGOPT = 0.

CGDIFF Coal diffusion (ft^2/day)

CGRAD Spherical radius of coal (ft)

CGDEN Coal density (g/cc)

CGVL Langmuir isotherm volume (SCF gas/ton coal)

CGPL Langmuir isotherm pressure (psia)

CGASH Ash content of coal (wt fraction)

CGWC Moisture content of coal (wt fraction)

CGPCD Critical desorption pressure (psia)

NOTE: Set CGPCD = 0 psia if ITMPMOD = 1.

6. **I1, I2, J1, J2, K1, K2**

Omit this record if ICGOPT = 0.

I1 Coordinate of first region gridblock in I-direction.

I2 Coordinate of last region gridblock in I-direction.

J1	Coordinate of first region gridblock in J-direction.
J2	Coordinate of last region gridblock in J-direction.
K1	Coordinate of first region gridblock in K-direction.
K2	Coordinate of last region gridblock in K-direction.

NOTE: NCGSUB records must be read.

NOTE: Records 4 and 5 should be repeated NCGREG times.

Chapter 22

Recurrent Data

Recurrent data records are read periodically during the course of the simulation run. These data include the location and specification of wells in the model, changes in well completions and field operations over time, a schedule of well rate or pressure performance over time (or both), timestep control information for advancing the simulation through time, and controls on the type and frequency of printout information provided by the simulator.

1. **Major Heading** Up to 80 characters.

   NOTE: This record signifies the start of the recurrent data section.

22.1 Timestep and Output Control

1. **Heading** Up to 80 characters.

2. **IWREAD, IOMETH, IWLREP, ISUMRY**

IWREAD	Controls input of well information.
IOMETH	Controls scheduling of well input and array print controls.
IWLREP	Controls output of well report.

ISUMRY Controls output of summary report.

Code	Value	Meaning
IWREAD	0	Do not read well information
	1	Read well information
IOMETH	≥ 1	Number of elapsed time values to be read on record 3. The program will print results to output files at these elapsed times and allow you to change well characteristics after the last elapsed time entered during this recurrent data period.
IWLREP	0	Do not print well report
	1	Print well report
ISUMRY	0	Do not print summary report
	1	Print summary report
	2	Write ITEMP.ARR file

3. **FTIO**

FTIO Array containing total elapsed times at which output will occur (days). Up to 50 monotonically increasing values may be entered. The first entry must be greater than 0 and each succeeding entry must be greater than any previous entry.

NOTE: When the elapsed time of a run equals an FTIO value, the well and basic summary reports will be printed. Maps will also be printed according to the instructions given below. When the elapsed time of a run equals the last FTIO value, the program will allow the user to enter a new set of recurrent data records (repeat Sections 22.1 and 22.2).

4. **IPMAP, ISOMAP, ISWMAP, ISGMAP, IPBMAP, IRSMAP**

IPMAP Control code for printing pressure array.

ISOMAP Control code for printing oil saturation array.
ISWMAP Control code for printing water saturation array.
ISGMAP Control code for printing gas saturation array.
IPBMAP Control code for printing bubble point pressure array.
IRSMAP Control code for printing natural gas solubility array.

Code Value	Meaning
0	Do not print the array
1	Print the array

5. **IS1MAP, IS2MAP, IS3MAP, IS4MAP, IAQMAP**

ISIMAP Control code for printing base solvent volume fraction array.
IS2MAP Control code for printing solvent 2 volume fraction array.
IS3MAP Control code for printing solvent 3 volume fraction array.
IS4MAP Control code for printing solvent 4 volume fraction array.
IAQMAP Control code for printing aquifer influx array.

Code Value	Meaning
0	Do not print the array
1	Print the array

6. **IVPMAP, IZMAP, IRCMAP, IVSMAP, IVRMAP**

IVPMAP Control code for printing seismic compressional velocity (Vp) array.
IZMAP Control code for printing seismic acoustic impedance array.

IRCMAP Control code for printing seismic reflection coefficient array.

IVSMAP Control code for printing seismic shear velocity (Vs) array.

IVRMAP Control code for printing seismic velocity ratio Vp/Vs array.

Code Value	Meaning
0	Do not print the array
1	Print the array

7. **INUMAP, IYMMAP, IUNMAP, ISVMAP, ISHMAP**

INUMAP Control code for printing Poisson's ratio array.

IYMMAP Control code for printing Young's modulus array.

IUNMAP Control code for printing uniaxial compaction array.

ISVMAP Control code for printing vertical stress (confining pressure) array.

ISHMAP Control code for printing horizontal stress array.

Code Value	Meaning
0	Do not print the array
1	Print the array

8. **DT, DTMIN, DTMAX**

DT Starting timestep size (days).

DTMIN Minimum timestep size (days). A typical value is 1 day.

DTMAX Maximum timestep size (days). A typical value is 3 - 5 days.

22.2 Well Information

Omit this section if IWREAD = 0.

1. **Heading** Up to 80 characters

2. **NWELLN, NWELLO, KSIS**
   - NWELLN — Number of new wells for which complete well information is entered
   - NWELLO — Number of previously defined wells for which new rates and/or rate controls are entered
   - KSIS — Control code for surfactant-water injection

Code	Value	Meaning
NWELLN	0	Do not read new well information
	≥1	Read new well information
NWELLO	0	Do not change data for previously defined wells
	≥1	Change data for previously defined wells
KSIS	0	Do not inject surfactant
	2, -2, or -12	Inject surfactant in the water phase as a gas phase mobility control agent

3. **Heading** Up to 80 characters.
   Include this record if NWELLN > 0.

4. **WELLID**
   Include this record if NWELLN > 0.
   - WELLID — Well name with up to five characters

5. **IDWELL, KONECT, KWCNTL, KWPID**
   Include this record if NWELLN > 0.

IDWELL Well identification number. Each well should have a unique IDWELL number. If two or more wells have the same IDWELL number, the characteristics of the last well entered will be used.

KONECT Total number of gridblocks connected to well IDWELL

KWCNTL Control code for well limits applied to well IDWELL

KWPID Control code for calculating well PID

Code	Value	Meaning
KWCNTL	0	Do not read well rate constraints and workovers
	1	Read well rate constraints and workovers
KWPID	0	User enters PID
	1	Model calculates PID

6. **I, J, K, PID, PWF**

Include this record if NWELLN > 0 and KWPID = 0.

I *x*-coordinate of gridblock containing well

J *y*-coordinate of gridblock containing well

K *z*-coordinate of gridblock containing well

PID Layer flow index for gridblock

PWF Flowing bottom-hole pressure for gridblock (psia)

NOTE: KONECT records must be read.

Deviated (slanted) and horizontal wells may be represented by calculating an appropriate PID and specifying gridblock locations that model the expected well trajectory. For example, a horizontal well that is aligned in the *x-direction* will have constant J and K indices, and index I will vary if there is more than one connection.

To shut in a connection, set that connection PID to 0. To shut in a well, set all of its connection PID values to zero.

7A. **I, J, K, IWDIR, KHMOD, PIDRW, PIDS, PWF**

Include this record if NWELLN > 0 and KWPID = 1.

I	*x*-coordinate of gridblock containing well
J	*y*-coordinate of gridblock containing well
K	*z*-coordinate of gridblock containing well
IWDIR	Well orientation
KHMOD	Flow capacity model for PID calculation
PIDRW	Wellbore radius (ft.)
PIDS	Well skin (fr.)
PWF	Flowing bottom-hole pressure for gridblock (psia)

Code	Value	Meaning
IWDIR	1	Well aligned in *x*-direction
	2	Well aligned in *y*-direction
	3	Well aligned in *z*-direction
KHMOD	0	PID calculated with constant KH
	1	PID calculated with pressure dependent KH

NOTE: The *x*-direction ϕ-K model is

$$K_x = K_{x0}\left\{a_1\left(\frac{\phi}{\phi_0}\right)^{b_1} + a_2 e^{\left[b_2(\phi-\phi_0)\right]}\right\}$$

where K_{x0} is the initial permeability and ϕ_0 is initial porosity. Similar models apply to *y*-direction and *z*-direction permeabilities. Coefficients for the directional ϕ-*K* models are specified below. Values of net thickness and permeability in well PID are calculated as functions of pressure and saturation when KPHIMOD > 0.

7B. **XKA1, XKB1, XKA2, XKB2**

Include this record if NWELLN > 0, KWPID = 1 and KHMOD = 1.

XKA1	Coefficient a_1 for ϕ-K model in x-direction
XKB1	Coefficient b_1 for ϕ-K model in x-direction
XKA2	Coefficient a_2 for ϕ-K model in x-direction
XKB2	Coefficient b_2 for ϕ-K model in x-direction

7C. **YKA1, YKB1, YKA2, YKB2**

Include this record if NWELLN > 0, KWPID = 1 and KHMOD = 1.

YKA1	Coefficient a_1 for ϕ-K model in y-direction
YKB1	Coefficient b_1 for ϕ-K model in y-direction
YKA2	Coefficient a_2 for ϕ-K model in y-direction
YKB2	Coefficient b_2 for ϕ-K model in y-direction

7D. **ZKA1, ZKB1, ZKA2, ZKB2**

Include this record if NWELLN > 0, KWPID = 1 and KHMOD = 1.

ZKA1	Coefficient a_1 for ϕ-K model in z-direction
ZKB1	Coefficient b_1 for ϕ-K model in z-direction
ZKA2	Coefficient a_2 for ϕ-K model in z-direction
ZKB2	Coefficient b_2 for ϕ-K model in z-direction

NOTE: Repeat records 7A through 7D a total of KONECT times (one set of records for each connection).

8. **KIP, QO, QW, QG, QT, QS**

Include this record if NWELLN > 0.

KIP	Code for specifying well operating characteristics
QO	Oil rate (STB/D)
QW	Water rate (STB/D)
QG	Natural gas rate (MSCF/D)

QT	Total fluid voidage rate (RB/D). QT includes oil, water, natural gas, and solvent.
QS	Solvent rate (MSCF/D)

NOTE: Sign conventions for rates: negative rates indicate fluid injection and positive rates indicate fluid production. To impose a maximum target rate on an explicit pressure controlled well, set KWCNTL = 1 and set the primary phase rate (QO, QW, QG, or QT) to the maximum target rate.

9. **ALIT, BLIT**

Include this record if NWELLN > 0 and KIP = 10.

ALIT	"a" coefficient of LIT gas well analysis
BLIT	"b" coefficient of LIT gas well analysis

NOTE: Gas rate QG > 0 in Record 8 will be used as a target rate if KWCNTL = 1; if KWCNTL = 0, the value of QG will be ignored.

10. **WQMAX, WQMIN, WWOR, WGOR**

Include this record if NWELLN > 0 and KWCNTL = 1.

WQMAX	Maximum allowed rate for primary phase (QO, QW, QG, or QT)
WQMIN	Minimum allowed rate for primary phase (QO, QW, QG, or QT)
WWOR	Maximum allowed WOR (STB/STB); shut worst offending connection. Set WWOR = 0 to ignore.
WGOR	Maximum allowed GOR (SCF/STB); shut worst offending connection. Set WGOR = 0 to ignore.

NOTE: Rates are expressed in the same units as the rates in Record 8. WOR and GOR constraints apply to production wells only. If a maximum target rate is set in Record 8 for an explicit

pressure controlled well, the value of WQMAX will take precedence.

Records 4 through 10 should be repeated NWELLN times.

11. **Heading** Up to 80 characters.
Include this record if NWELLO > 0.

12. **WELLID**
Include this record if NWELLO > 0.
WELLID Well name with up to five characters.

13. **IDWELL, KONECT, KWCNTL**
Include this record if NWELLO > 0.
IDWELL Well identification number
KONECT Total number of gridblocks connected to well IDWELL
KWCNTL Control code for well limits applied to well IDWELL

14. **I, J, K, PID, PWF**
Include this record if NWELLO > 0 and KWPID = 0.
I *x*-coordinate of gridblock containing well
J *y*-coordinate of gridblock containing well
K *z*-coordinate of gridblock containing well
PID Layer flow index for gridblock.
PWF Flowing bottom-hole pressure for gridblock (psia).

NOTE: KONECT records must be read.

15A. **I, J, K, IWDIR, KHMOD, PIDRW, PIDS, PWF**
Include this record if NWELLO > 0 and KWPID = 1.
I *x*-coordinate of gridblock containing well
J *y*-coordinate of gridblock containing well

K	*z*-coordinate of gridblock containing well
IWDIR	Well orientation
KHMOD	Flow capacity model for PID calculation
PIDRW	Wellbore radius (ft.)
PIDS	Well skin (fr.)
PWF	Flowing bottom-hole pressure for gridblock (psia)

Code	Value	Meaning
IWDIR	1	Well aligned in *x*-direction
	2	Well aligned in *y*-direction
	3	Well aligned in *z*-direction
KHMOD	0	PID calculated with constant KH
	1	PID calculated with pressure dependent KH

NOTE: The x-direction ϕ-K model is

$$K_x = K_{x0}\left\{a_1\left(\frac{\phi}{\phi_0}\right)^{b_1} + a_2 e^{\left[b_2(\phi-\phi_0)\right]}\right\}$$

where K_{x0} is the initial permeability and ϕ_0 is initial porosity. Similar models apply to *y*-direction and *z*-direction permeabilities. Coefficients for the directional ϕ-*K* models are specified below. Values of net thickness and permeability in well PID are calculated as functions of pressure and saturation when KPHIMOD > 0.

15B. **XKA1, XKB1, XKA2, XKB2**

Include this record if NWELLO > 0, KWPID = 1 and KHMOD = 1.

XKA1	Coefficient a_1 for ϕ-*K* model in *x*-direction
XKB1	Coefficient b_1 for ϕ-*K* model in *x*-direction
XKA2	Coefficient a_2 for ϕ-*K* model in *x*-direction
XKB2	Coefficient b_2 for ϕ-*K* model in *x*-direction

15C. **YKA1, YKB1, YKA2, YKB2**

Include this record if NWELLO > 0, KWPID = 1 and KHMOD = 1.

YKA1	Coefficient a_1 for ϕ-K model in y-direction
YKB1	Coefficient b_1 for ϕ-K model in y-direction
YKA2	Coefficient a_2 for ϕ-K model in y-direction
YKB2	Coefficient b_2 for ϕ-K model in y-direction

15D. **ZKA1, ZKB1, ZKA2, ZKB2**

Include this record if NWELLO > 0, KWPID = 1 and KHMOD = 1.

ZKA1	Coefficient a_1 for ϕ-K model in z-direction
ZKB1	Coefficient b_1 for ϕ-K model in z-direction
ZKA2	Coefficient a_2 for ϕ-K model in z-direction
ZKB2	Coefficient b_2 for ϕ-K model in z-direction

NOTE: Repeat records 15A through 15D a total of KONECT times (one set of records for each connection).

16. **KIP, QO, QW, QG, QT, QS**

Include this record if NWELLO > 0.

KIP	Code for specifying well operating characteristics
QO	Oil rate (STB/D)
QW	Water rate (STB/D)
QG	Natural gas rate (MSCF/D)
QT	Total fluid voidage rate (RB/D)
QS	Solvent rate (MSCF/D)

NOTE: Sign conventions for rates: negative rates indicate fluid injection and positive rates indicate fluid production. To impose a maximum target rate on an explicit pressure controlled well, set KWCNTL = 1 and set the primary phase rate (QO, QW, QG, or QT) to the maximum target rate.

17. **ALIT, BLIT**

Include this record if NWELLO > 0 and KIP = 10.

ALIT	"a" coefficient of LIT gas well analysis
BLIT	"b" coefficient of LIT gas well analysis

NOTE: Gas rate QG > 0 in Record 16 will be used as a target rate if KWCNTL = 1; if KWCNTL = 0, the value of QG will be ignored.

18. **WQMAX, WQMIN, WWOR, WGOR**

Include this record if NWELLO > 0 and KWCNTL = 1.

WQMAX	Maximum allowed rate for primary phase (QO, QW, QG, or QT)
WQMIN	Minimum allowed rate for primary phase (QO, QW, QG, or QT)
WWOR	Maximum allowed WOR (STB/STB); shut worst offending connection. Set WWOR = 0 to ignore.
WGOR	Maximum allowed GOR (SCF/STB); shut worst offending connection. Set WGOR = 0 to ignore.

NOTE: Rates are expressed in the same units as the rates in Record 16. WOR and GOR constraints apply to production wells only. If a maximum target rate is set in Record 16 for an explicit pressure controlled well, the value of WQMAX will take precedence.

Records 12 through 18 should be repeated NWELLO times.

Table 22-1. Options for Controlling Production Wells

Primary Phase	Well Control	KIP	Non-Zero Rates	Well Controls?
Oil	Rate	1	QO > 0	Yes
	Explicit P	-1	QO > 0	Yes
	Implicit P	-11		No
Gas	Rate	1	QG > 0	Yes
	Explicit P	-1	QG > 0	Yes
	Implicit P			No
	LIT	10	QG > 0	Yes
Water	Rate	1	QW > 0	Yes
	Explicit P	-1	QW > 0	Yes
	Implicit P			No
Total OWG	Rate	1	QT > 0	Yes
	Explicit P	-1	QT > 0	Yes
	Implicit P			No

Table 22-2. Options for Controlling Injection Wells

Primary Phase	Well Control	KIP	Non-Zero Rates	Well Controls?
Water	Rate	2	QW < 0	Yes
	Explicit P	-2	QW < 0	Yes
	Implicit P	-12		No
Gas	Rate	3	QG < 0	Yes
	Explicit P	-3	QG < 0	Yes
	Implicit P	-13		No
Base Solvent (Solvent 1)	Rate	100	QS < 0	No
	Explicit P	-4		No
	Implicit P	-14		No
Solvent 2	Rate	200	QS < 0	No
	Explicit P	-5		No
	Implicit P	-15		No
Solvent 3	Rate	300	QS < 0	No
	Explicit P	-6		No
	Implicit P	-16		No
Solvent 4	Rate	400	QS < 0	No
	Explicit P	-7		No
	Implicit P	-17		No

Appendix A:
Unit Conversion Factors

TIME

1 hour = 1 hr = 3600 s

1 day = 8.64×10^4 s

1 year = 1 yr = 3.1536×10^7 s

LENGTH

1 foot = 1 ft = 0.3048 m

1 kilometer = 1 km = 1000 m

1 mile = 1 mi = 1.609 km

VELOCITY

1 foot per second = 0.3048 m/s

1 kilometer per hour = 1 kph = 1000 m/hr = 0.278 m/s

1 mile per hour = 1 mph = 1.609 km/hr = 1609 m/hr = 0.447 m/s

AREA

1 square foot = 1 ft^2 = 0.0929 m^2

1 square mile = 1 mi^2 = 2.589 km^2 = 2.589×10^6 m^2

1 square mile = 1 mi^2 = 640 acres

1 acre = 1 ac = 4047 m^2

1 hectare = 1 ha = 1.0×10^4 m^2

1 millidarcy = 1 md = 0.986923×10^{-15} m^2
1 Darcy = 1000 md = 0.986923×10^{-12} m^2

VOLUME
1 liter = 1 L = 0.001 m^3
1 cubic foot = 1 ft^3 = 2.83×10^{-2} m^3
1 standard cubic foot = 1 SCF = 1 ft^3 at standard conditions
1 acre-foot = 1 ac-ft = 1233.5 m^3
1 barrel = 1 bbl = 0.1589 m^3
1 gallon (U.S. liquid) = 1 gal = 3.785×10^{-3} m^3
1 barrel = 42 gallons = 0.1589 m^3

MASS
1 gram = 1 g = 0.001 kg
1 pound (avoirdupois) = 1 lb (avdp) = 1 lbm = 0.453592 kg
1 tonne = 1000 kg

MASS DENSITY
1 g/cm^3 = 1000 kg/m^3

FORCE
1 pound-force = 1 lbf = 4.4482 N

PRESSURE
1 Pascal = 1 Pa = 1 N/m^2 = 1 $kg/m \cdot s^2$
1 Megapascal = 1 MPa = 10^6 Pa
1 Gigapascal = 1 GPa = 10^9 Pa
1 pound-force per square inch = 1 psi = 6894.8 Pa
1 atmosphere = 1 atm = 1.01325×10^5 Pa
1 atmosphere = 1 atm =14.7 psi

ENERGY
1 BTU = 1055 J
1 calorie (thermochemical) = 1 cal = 4.184 J

1 kilocalorie = 1 kcal = 1000 calories = 4.184×10^3 J

1 Calorie = 1000 calories = 4.184×10^3 J

1 kilowatt-hour = 1 kWh = 1 kW · 1 hr = 3.6×10^6 J

1 quad = 1 quadrillion BTU = 1.0×10^{15} BTU = 1.055×10^{18} J

ENERGY DENSITY

1 BTU/lbm = 2326 J/kg

1 BTU/SCF = 3.73×10^4 J/m^3

POWER

1 Watt = 1 W = 1 J/s

1 Megawatt = 10^6 W = 10^6 J/s

1 kilowatt-hour per year = 1 kWh/yr = 0.114 W = 0.114 J/s

1 horsepower = 1 hp = 745.7 W

VISCOSITY

1 centipoise = 1 cp = 0.001 Pa ·s

1 mPa·s = 0.001 Pa ·s =1 cp = 10^3 Pa·s

1 poise = 100 cp = 0.1 Pa ·s

Appendix B:
Example IFLO Input Data Set

```
    CASE STUDY - PRIMARY DEPLETION PREDICTION
MODEL DIMENSIONS
  10, 7, 4, 1, 4
GRID BLOCK LENGTHS
 -1  -1   0   0
  200.0
  200.0
   80.0  20.0  80.0  40.0
   72.0   0.1  64.0  32.0
GRID BLOCK LENGTH MODIFICATIONS
   0,   0,   0,  5,   0
   8  8  1  7  1  1  18
   9 10  1  7  1  1   0
   9  9  1  7  3  3  16
  10 10  1  7  3  3   0
  10 10  1  7  4  4   8
DEPTH TO TOP OF UPPER SAND
  1
  9575  9490  9405  9320  9235  9150  9065  8980  8895  8810
  9575  9490  9405  9320  9235  9150  9065  8980  8895  8810
  9575  9490  9405  9320  9235  9150  9065  8980  8895  8810
  9575  9490  9405  9320  9235  9150  9065  8980  8895  8810
  9575  9490  9405  9320  9235  9150  9065  8980  8895  8810
  9575  9490  9405  9320  9235  9150  9065  8980  8895  8810
  9575  9490  9405  9320  9235  9150  9065  8980  8895  8810
```

```
POROSITY AND PERMEABILITY DISTRIBUTIONS
   0    0    0    0
   0.20  0.05  0.25  0.25
   75  0  250  250
   75  0  250  250
   7.5  0  25  25
POROSITY AND PERMEABILITY MODIFICATION CARDS
   0,   0,   0,   0,   0
RELATIVE PERMEABILITY-CAPILLARY PRESSURE DATA
   2    1    0
  SWT   KROW    KRW  PCOW
0.000  1.000  0.000   0.0
0.300  1.000  0.000   0.0
0.350  0.590  0.005   0.0
0.400  0.320  0.010   0.0
0.450  0.180  0.017   0.0
0.500  0.080  0.023   0.0
0.550  0.030  0.034   0.0
0.600  0.010  0.045   0.0
0.650  0.001  0.064   0.0
0.700  .0001  0.083   0.0
0.750  0.000  0.100   0.0
0.800  0.000  0.120   0.0
1.000  0.000  0.120   0.0
  SGT   KROG    KRG  PCGO
0.000  1.000  0.000   0.0
0.030  0.750  0.000   0.0
0.050  0.590  0.020   0.0
0.100  0.320  0.090   0.0
0.150  0.180  0.160   0.0
0.200  0.080  0.240   0.0
0.250  0.030  0.330   0.0
0.300  0.010  0.430   0.0
0.350  0.001  0.550   0.0
0.400  0.000  0.670   0.0
0.450  0.000  0.810   0.0
0.500  0.000  1.000   0.0
1.000  0.000  1.000   0.0
```

```
PORE VOLUME AND TRANSMISSIBILITY MODIFICATIONS
  11,   0,   0,   2,  0
 1  2  1  1  1  4  0.9
 3  4  1  1  1  4  0.7
 5  6  1  1  1  4  0.5
 7  8  1  1  1  4  0.3
 9 10  1  1  1  4  0.1
 1  1  2  3  1  4  0.8
 1  1  4  6  1  4  0.7
 1  1  7  7  1  4  0.3
 2  4  7  7  1  4  0.6
 5  7  7  7  1  4  0.8
 8 10  7  7  1  4  0.9
 1 10  1  7  2  3  0.0
 1 10  1  7  4  4  0.1
PETROPHYSICAL MODEL
 0 0
MODULI AND ROCK DENSITY
  -1 -1 -1 -1
  3E6
  3E6
  3E6
  168
CONFINING P AND CLAY CONTENT MODIFICATIONS
  3*0
PBO    VOSLP    BOSLP    BWSLP    PMAX
2514.7 .000046, -.000023, -3E-6,   6014.7
OIL:    P       MUO       BO       RSO
     14.7,   1.0400,   1.0620,     1.0
    514.7,   0.9100,   1.1110,    89.0
   1014.7,   0.8300,   1.1920,   208.0
   1514.7,   0.7650,   1.2560,   309.0
   2014.7,   0.6950,   1.3200,   392.0
   2514.7,   0.6410,   1.3800,   457.0
   3014.7,   0.5940,   1.4260,   521.0
   4014.7,   0.5100,   1.4720,   586.0
   5014.7,   0.4500,   1.4900,   622.0
   6014.7,   0.4100,   1.5000,   650.0
```

```
WATER:  P       MUW       BW       RSW
     14.7,   0.5000,   1.0190,      0.0
    514.7,   0.5005,   1.0175       0.0
   1014.7,   0.5010,   1.0160,      0.0
   1514.7,   0.5015,   1.0145,      0.0
   2014.7,   0.5020,   1.0130,      0.0
   2514.7,   0.5025,   1.0115,      0.0
   3014.7,   0.5030,   1.0100,      0.0
   4014.7,   0.5040,   1.0070,      0.0
   5014.7,   0.5050,   1.0040,      0.0
   6014.7,   0.5060,   1.0010,      0.0
GAS AND ROCK PROPERTIES
0
GAS:    P       MUG       BG    PSI        CR
     14.7, 0.008000, 0.935800,   0.0   0.000003
    514.7, 0.011200, 0.035200,   0.0   0.000003
   1014.7, 0.014000, 0.018000,   0.0   0.000003
   1514.7, 0.016500, 0.012000,   0.0   0.000003
   2014.7, 0.018900, 0.009100,   0.0   0.000003
   2514.7, 0.020800, 0.007400,   0.0   0.000003
   3014.7, 0.022800, 0.006300,   0.0   0.000003
   4014.7, 0.026000, 0.004900,   0.0   0.000003
   5014.7, 0.028500, 0.004000,   0.0   0.000003
   6014.7, 0.030000, 0.003400,   0.0   0.000003
   RHOSCO    RHOSCW    RHOSCG
   46.244,   62.238,   0.0647
SOLVENT MODEL
    0,     0
EQUIL PRESSURE INIT / CONSTANT SATN INIT
    0,     3
 9600,  4000,   0,   0
 0.70,  0,   0.25
 KSW1 KSW2 KSW3 KSW4
   0    0    0    0
 NMX  FACT1  FACT2  TMX  WORMX  GORMX  PAMIN  PAMX
 1000   1.50   0.50  2920     5.0  500000   1500   6000
 KSOL  MITR  OM TOL NCYC DSMX  DPMX  ITMX   RTOL  NERR
   3   100   1.20  0.001      0    0.05  100.0      5  0.001     1
 WEIGHT
   1.0
```

```
AQUIFER MODEL
 1
 2
 1  1  1  7  1  1  2.0
 1  1  1  7  3  4  2.0
COAL GAS MODEL
 0
RECURRENT DATA
  *** DATA SET 1 - HISTORY ***
   1,   1,   1,   1
   365.0
   1,   1,   1,    0,    0,    0
   0,   0,   0,    0,    0
   0,   0,   0,    0,    1
   0,   0,   0,    0,    0
   1.0,   1.0,   15.0
  WELL INFORMATION
   1    0    0
  WELL P-1
  P-1
   1,   4,   0,    0
   4,   4,   1,  8.4  2600
   4,   4,   2,  0.0  2600
   4,   4,   3, 24.8  2600
   4,   4,   4, 12.4  2600
   1,    500.0,      0.0,      0.0,      0.0,    0.0
  *** DATA SET 2 - PRIMARY DEPLETION PREDICTION ***
   1,   7,   1,   1
   730  1095  1460  1825  2190  2555  2920
   1,   1,   1,    0,    0,    0
   0,   0,   0,    0,    0
   0,   0,   0,    0,    1
   0,   0,   0,    0,    0
   1.0,   1.0,   15.0
```

```
WELL INFORMATION
  0    1    0
WELL P-1
P-1
  1,   4,   0,    0
  4,   4,   1,  8.4  2600
  4,   4,   2,  0.0  2600
  4,   4,   3, 24.8  2600
  4,   4,   4, 12.4  2600
  1,    500.0,      0.0,      0.0,      0.0,    0.0
```

References

Abramowitz, M.A. and I.A. Stegun (1972): **Handbook of Mathematical Functions**, ninth printing, New York: Dover.

Aguilera, R. (1980): **Naturally Fractured Reservoirs**, Tulsa, Oklahoma: PennWell Publishing.

Aguilera, R. (July 1999): "Recovery Factors and Reserves in Naturally Fractured Reservoirs," *Journal of Canadian Petroleum Technology*, pages 15-18.

Ahmed, T. (2000): **Reservoir Engineering Handbook**, Houston, Texas: Gulf Publishing.

Akin, S. (2001): "Estimation of Fracture Relative Permeabilities from Unsteady State Corefloods," *Journal of Petroleum Science and Engineering*, Volume 30, pages 1-14.

Al-Hussainy, R. and N. Humphreys (1996): "Reservoir Management: Principles and Practices," *Journal of Petroleum Technology*, pages 1129-1135.

Al-Marhoun, M.A. (June 2003): "Adjustment of Differential Liberation Data to Separator Conditions," *SPE Reservoir Evaluation & Engineering*, pages 142-146.

Allan, J. and S.Q. Sun (2003): "Controls on Recovery Factor in Fractured Reservoirs: Lessons Learned from 100 Fractured Fields," Paper SPE 84590, presented at the 2003 SPE Annual Technical Conference and Exhibition, Richardson, Texas: Society of Petroleum Engineers.

Ammer, J.R., A.C. Brummert and W.N. Sams (1991): "Miscible Applied Simulation Techniques for Energy Recovery – Version 2.0," U.S. Department of Energy Report DOE/BC-91/2/SP, Morgantown Energy Technology Center, West Virginia.

Amyx, J.W., D.H. Bass, and R.L. Whiting (1960): **Petroleum Reservoir Engineering**, New York: McGraw-Hill.

Ancell, K.L., S. Lambert, and F.S. Johnson (1980): "Analysis of the Coalbed Degasification Process at a Seventeen Well Pattern in the Warrior Basin of Alabama," Paper SPE/DOE 8971, presented at the 1980 SPE/DOE Symposium on Unconventional Gas Recovery, Pittsburgh, Pennsylvania (18-21 May); Richardson, Texas: Society of Petroleum Engineers.

Anderson, R.N. (1995): "Method Described for using 4D Seismic to Track Reservoir Fluid Movement," *Oil & Gas Journal*, pages 70-74, April 3.

Arps, J.J. (1945): "Analysis of Decline Curves," Transaction of AIME, Volume 160, pages 228-247.

Asquith, G. And D. Krygowski (2004): **Basic Well Log Analysis for Geologists**, Tulsa, Oklahoma: American Association of Petroleum Geologists.

Ates, H., A. Bahar, S. El-Abd, M. Charfeddine, M. Kelkar, ad A. Datta-Gupta (February 2005): "Ranking and Upscaling of Geostatistical Reservoir Models by Use of Streamline Simulation: A Field Case Study," *SPE Reservoir Evaluation & Engineering*, pages 22-32.

Ausburn, B.E., A.K. Nath and T.R. Wittick (November 1978): "Modern Seismic Methods – An Aid for the Petroleum Engineer," *Journal of Petroleum Technology*, pages 1519-1530.

Aziz, K. (1993): "Reservoir Simulation Grids: Opportunities and Problems," *Journal of Petroleum Technology*, pages 658-663.

Aziz, K., Z.E. Heinemann, C. Wolfsteiner, and M.J. Mlacnik (February 2002): "The Changing World of Reservoir Simulation," *Journal of Petroleum Technology*, pages 26-28.

Aziz, K. and A. Settari (1979): **Petroleum Reservoir Simulation**, New York: Elsevier.

Babu, D.K. and A. S. Odeh (1989): "Productivity of a Horizontal Well," *Society of Petroleum Engineers Journal*, pages 417-421.

Barree, R.D. and M.W. Conway (March 2005): "Beyond Beta Factors: A Model for Darcy, Forchheimer, and Trans-Forchheimer Flow in Porous Media," *Journal of Petroleum Technology*, pages 43-45.

Bashore, W.M. (2000): "Data Integration Realizes the Promise of Multidisciplinary Efforts," Paper OTC 11956, presented at the *Offshore Technology Conference*, Houston, 1 – 4 May.

Bassiouni, Z. (1994): **Theory, Measurement, and Interpretation of Well Logs**, Richardson, Texas: Society of Petroleum Engineers.

Bear, J. (1972): **Dynamics of Fluids in Porous Media**, New York: Elsevier.

Beasley, C.J. (1996): "Seismic Advances Aid Reservoir Description," *Journal of Petroleum Technology*, pages 29-30.

Beggs, H.D. (1991): **Production Optimization Using Nodal Analysis**, Tulsa, Oklahoma: OGCI Publications.

Beggs, H.D., and J.P. Brill (May 1973): "A Study of Two-Phase Flow in Inclined Pipes," *Journal of Petroleum Technology*, page 607.

Benedict, M., G.B. Webb, and L.C. Rubin (1940): *Journal of Chemical Physics*, Volume 8, page 334.

Blackwelder, B., L. Canales, and J. Dubose (1996): "New Technologies in Reservoir Characterization," *Journal of Petroleum Technology*, pages 26-27.

Blunt, M.J. (1999): "An Empirical Model for Three-Phase Relative Permeability," Paper SPE 56474, presented at the 1999 Annual Technical Conference and Exhibition of the Society of Petroleum Engineers, Richardson, Texas: Society of Petroleum Engineers.

Bradley, M.E. and A.R.O. Wood (November 1994): "Forecasting Oil Field Economic Performances," *Journal of Petroleum Technology*, pages 965-971 and references therein.

Brill, J.P. (January 1987): "Multiphase Flow in Wells," *Journal of Petroleum Technology*, pages 15-21.

Brill, J.P., and S.J. Arirachakaran (May 1992): "State of the Art in Multiphase Flow," *Journal of Petroleum Technology*, pages 538-541.

Brill, J.P., and H. Mukherjee (1999): **Multiphase Flow in Wells**, SPE Monograph Volume 17, Richardson, Texas: Society of Petroleum Engineers.

Brown, K.E. and J.F. Lea (October 1985): "Nodal Systems Analysis of Oil and Gas Wells," *Journal of Petroleum Technology*, pages 1751-1763.

Brown, L.P. and R.V. Hawkes (May 2005): "Rules of Thumb in Well Testing: What Works and Doesn't Work – and Why," *Journal of Canadian Petroleum Technology*, pages 51-55.

Brownlee, M.H. and L.A. Sugg (1987): "East Vacuum Grayburg-San Andres Unit CO_2 Injection Project: Development and Results to Date," Paper SPE 16721, presented at the 62nd Annual Technical Conference and Exhibition of the Society of Petroleum Engineers, Richardson, Texas: Society of Petroleum Engineers.

Brock, J. (1986): **Applied Open-Hole Log Analysis**, Houston: Gulf Publishing.

Brundtland, G. (1987): **Our Common Future**, Oxford University Press, Oxford, United Kingdom.

de Buyl, M., T. Guidish, and F. Bell (1988): "Reservoir Description from Seismic Lithologic Parameter Estimation," *Journal of Petroleum Technology*, pages 475-482.

Carlson, M.R. (2003): **Practical Reservoir Simulation**, Tulsa, Oklahoma: PennWell.

Carr, N.L., R. Kobayashi, and D.B. Burrows (1954): "Viscosity of Hydrocarbon Gases under Pressure," *Transactions of AIME*, Volume 201, pages 264-272.

Carter, R.D. and G.W. Tracy (1960) "An Improved Method for Calculating Water Influx," *Transactions of AIME*, Volume 219, pages 415-417.

Chambers, R.L., J.M. Yarus, and K.B. Hird (2000): "Petroleum geostatistics for nongeostatisticians," *The Leading Edge*, Part 1, pages 474- 479, May; and Part 2, pages 592-599, June.

Chase, C. A., Jr. and M. R. Todd (1984): "Numerical Simulation of CO_2 Flood Performance," *Society of Petroleum Engineers Journal*, pages 597-604.

Chaudhry, A.U. (2003a): **Gas Well Testing Handbook**, Boston: Elsevier.

Chaudhry, A.U. (2003b): **Oil Well Testing Handbook**, Boston: Elsevier.

Chawathé, A. and I. Taggart (August 2004): "Insights into Upscaling using 3D Streamlines," SPE Reservoir Evaluation & Engineering, pages 285-296.

Chin, W.C. (1993): **Modern Reservoir Flow and Well Transient Analysis**, Houston: Gulf Publishing.

Christie, M.A. (November 1996): "Upscaling for Reservoir Simulation," *Journal of Petroleum Technology*, pages 1004-1010.

Christie, M.A. and M.J. Blunt (2001): "Tenth SPE Comparative Solution Project: A Comparison of Upscaling Techniques," Paper SPE 66599, presented at the 2001 SPE Reservoir Simulation Symposium, Richardson, Texas: Society of Petroleum Engineers.

Chorn, L.G. and M. Croft (August 2000): "Resolving Reservoir Uncertainty to Create Value," *Journal of Petroleum Technology*, pages 52-59.

Chu, W.C. (September, 2000): "Pressure-transient Testing Ideal for Reservoir Management," *Hart's E&P*, pages 47-50.

Clark, I. and W. Harper (2000): **Practical Geostatistics 2000 Book and CD**, Columbus, Ohio: Ecosse North America, LLC.

Clark, N.J. (1969): **Elements of Petroleum Reservoirs**, Richardson, Texas: Society of Petroleum Engineers.

Coats, K.H. (1969): "Use and Misuse of Reservoir Simulation Models," *Journal of Petroleum Technology*, pages 183-190.

Cope, G. (2001): "Improving Efficiency through Reservoir Modeling and Production Simulation," *Journal of Canadian Petroleum Technology*, pages 7-11.

Collins, R.E. (1961): **Flow of Fluids through Porous Materials**, Tulsa, Oklahoma: Petroleum Publishing-Reinhold.

Craft, B.C., M.F. Hawkins, and R.E. Terry (1991): **Applied Petroleum Reservoir Engineering, Second Edition**, Englewood Cliffs, New Jersey: Prentice-Hall.

Craig, F.F. (1971): **The Reservoir Engineering Aspects of Waterflooding**, SPE Monograph Series, Richardson, Texas: Society of Petroleum Engineers.

Craig, F.F., P.J. Wilcox, J.R. Ballard and W.R. Nation (July 1977): "Optimized Recovery through Continuing Interdisciplinary Cooperation," *Journal of Petroleum Technology*, pages 755-760.

Crichlow, H.B. (1977): **Modern Reservoir Engineering – A Simulation Approach**, Englewood Cliffs, New Jersey: Prentice Hall.

Daccord, G., J. Nittmann and H.E. Stanley (1986): "Radial Viscous Fingers and Diffusion-Limited Aggregation: Fractal Dimension and Growth Sites," *Physical Review Letters*, Volume 56, 336-339.

Dahlberg, E.C. (1975): "Relative Effectiveness of Geologists and Computers in Mapping Potential Hydrocarbon Exploration Targets," *Mathematical Geology*, Volume 7, pages 373-394.

Dake, L.P. (1978): **Fundamentals of Reservoir Engineering**, Amsterdam: Elsevier.

Dake, L.P. (2001): **The Practice of Reservoir Engineering**, Revised Edition, Amsterdam: Elsevier.

Dean, R.H., X. Gai, C.M. Stone and E. Minkoff (2003), "A Comparison of Techniques for Coupling Porous Flow and Geomechanics," Paper SPE 79709, presented at the SPE Reservoir Simulation Symposium, Richardson, Texas: Society of Petroleum Engineers.

Deghmoum, A.H., D. Tiab, and A. Mazouzi (December 2001): "Relative Permeability in Dual Porosity Porous Media," *Journal of Canadian Petroleum Technology*, pages 32-42.

Deutsch, C.V. and A.G. Journel (1998): **GSLIB: Geostatistical Software Library and User's Guide**, New York, New York: Oxford University Press.

Dietrich, J.K. and P.L. Bondor (1976): "Three-Phase Oil Relative Permeability Models," Paper SPE 6044, presented at the 51st Fall Technical Conference and Exhibition of Society of Petroleum Engineers, Richardson, Texas: Society of Petroleum Engineers.

Dietrich, F.L., F.G. Brown, Z.H. Zhou, M.A. Maure (1996): "Microbial EOR Technology Advancement: Case Studies of Successful Projects," paper SPE 36746 presented at the 1996 SPE Annual Technical Conference and Exhibition of the Society of Petroleum Engineers, Richardson, Texas: Society of Petroleum Engineers.

Dogru, A.H. (May, 2000): "Megacell Reservoir Simulation," *Journal of Petroleum Technology*, pages 54-60.

Dogru, A.H., H.A. Sunaidi, L.S. Fung, W.A. Habiballah, N. Al-Zamel, and K.G. Li (February 2002): "A Parallel Reservoir Simulator for Large-Scale Reservoir Simulation," *SPE Reservoir Evaluation & Engineering*, pages 11-23.

Dorn, G.A. (September, 1998): "Modern 3-D Seismic Interpretation," *The Leading Edge*, pages 1262-1283.

Dranchuk, P.M., R.A. Purvis, and D.B. Robinson (1974): "Computer Calculation of Natural Gas Compressibility Factors Using the Standing and Katz Correlations," *Institute of Petroleum Technology*, IP-74-008.

Dubrule, O. (2003): **Geostatistics for Seismic Data Integration in Earth Models**, 2003 Distinguished Instructor Short Course, Tulsa: Society of Exploration Geophysicists.

van Dyke, K. (1997): **Fundamentals of Petroleum**, 4th Edition, The University of Texas at Austin: Petroleum Extension Service.

Earlougher, R.C., Jr. (1977): **Advances in Well Test Analysis**, SPE Monograph Series, Richardson, Texas: Society of Petroleum Engineers.

Ebanks, W.J., Jr. (1987): "Flow Unit Concept – Integrated Approach to Reservoir Description for Engineering Projects," paper presented at the AAPG Annual Meeting, Los Angeles.

Englund, E. and A. Sparks (1991): "Geo-EAS 1.2.1 User's Guide," *EPA Report #600/8-91/008 Environmental Protection Agency-EMSL*, Las Vegas, NV.

Ertekin, T., J.H. Abou-Kassem and G.R. King (2001): **Basic Applied Reservoir Simulation**, Richardson, Texas: Society of Petroleum Engineers.

Evans, S. (May 17, 2004): "Reservoir Modeling and Simulation in Today's High-Performance Computing Environments," *Oil & Gas Journal*, pages 33-37.

Evans, W.S. (1996): "Technologies for Multidisciplinary Reservoir Characterization," *Journal of Petroleum Technology*, pages 24-25.

van Everdingen, A.F. and W. Hurst (1949): "The Application of the Laplace Transformation to Flow Problems in Reservoirs," *Transactions of AIME*, Volume 186, pages 305-324.

Fanchi, J.R., K.J. Harpole, and H.B. Carroll (13 September 1982): "Black-Oil Reservoir Simulator is now Available," *Oil & Gas Journal*, pages 66-68.

Fanchi, J.R. (1983): "Multidimensional Numerical Dispersion," *Society of Petroleum Engineering Journal*, pages 143-151.

Fanchi, J.R. (June 1985): "Analytical Representation of the van Everdingen-Hurst Aquifer Influence Functions for Reservoir Simulation," *Society of Petroleum Engineering Journal*, pages 405-406.

Fanchi, J.R. (1986): "BOAST-DRC: Black Oil and Condensate Reservoir Simulation on an IBM-PC," Paper SPE 15297, presented at the Symposium on Petroleum Industry Applications of Microcomputers of the Society of Petroleum Engineers, Richardson, Texas: Society of Petroleum Engineers.

Fanchi, J.R. (1990): "Calculation of Parachors for Compositional Simulation: An Update," *Society of Petroleum Engineers Reservoir Engineering*, pages 433-436.

Fanchi, J.R. (1999): "Flow Models Time 4-D Seismic Surveys," *Oil & Gas Journal*, pages 46-51.

Fanchi, J.R. (2000): **Integrated Flow Modeling**, Amsterdam: Elsevier.

Fanchi, J.R. (2002a): **Shared Earth Modeling**, Boston: Butterworth-Heinemann-Elsevier.

Fanchi, J.R. (2002b): "Estimating Subsidence during Coalbed Methane Production," Paper SPE 75511, presented at the SPE Gas Technology Symposium, Richardson, Texas: Society of Petroleum Engineers.

Fanchi, J.R. (2003a): "The Han-Eberhart-Phillips model and integrated flow modeling," *Geophysics*, Volume 68, pages 574-576.

Fanchi, J.R. (2003b): "Feasibility of Monitoring CO_2 Sequestration in a Mature Oil Field using Time-Lapse Seismic Analysis," Paper SPE 66569, presented at SPE/EPA/DOE Exploration and Production Environmental Conference, Richardson, Texas: Society of Petroleum Engineers.

Fanchi, J.R. (2003c): "Estimating Geomechanical Properties Using an Integrated Flow Model," *SPE Reservoir Evaluation and Engineering*, pages 108-116.

Fanchi, J.R. (2004): **Energy: Technology and Directions for the Future**, Boston: Elsevier-Academic Press.

Fanchi, J.R. (2006): **Math Refresher for Scientists and Engineers, Third Edition**, New York: J. Wiley and Sons.

Fanchi, J.R. and R.L. Christiansen (1989): "Applicability of Fractals to the Description of Viscous Fingering," Paper SPE 19782, presented at the 64th Annual Technical Conference and Exhibition of Society of Petroleum Engineers, Richardson, Texas: Society of Petroleum Engineers.

Fanchi, J.R., K.J. Harpole, and S.W. Bujnowski (1982): "BOAST: A Three- Dimensional, Three-Phase Black Oil Applied Simulation Tool," 2 Volumes, U.S. Department of Energy, Bartlesville Energy Technology Center, Oklahoma.

Fanchi, J.R., J.E. Kennedy, and D.L. Dauben (1987): "BOAST II: A Three-Dimensional, Three-Phase Black Oil Applied Simulation Tool," U.S. Department of Energy, Bartlesville Energy Technology Center, Oklahoma.

Fanchi, J.R., H.Z. Meng, R.P. Stoltz, and M.W. Owen (1996): "Nash Reservoir Management Study with Stochastic Images: A Case Study," *Society of Petroleum Engineers Formation Evaluation*, pages 155-161.

Fanchi, J.R., T.A. Pagano and T.L. Davis (1999): "State of the Art of 4D Seismic Monitoring: The Technique, The Record, and The Future," *Oil & Gas Journal*, pages 38-43.

Fayers, F.J. and T.A. Hewett (1992): "A Review of Current Trends in Petroleum Reservoir Description and Assessing the Impacts on Oil Recovery," *Proceedings of Ninth International Conference On Computational Methods in Water Resources*, June 9-11.

Felder, R.D. (1994): "Advances in Openhole Well Logging," *Journal of Petroleum Technology*, pages 693-701.

Fetkovich, M.J. (July 1971): "A Simplified Approach to Water Influx Calculations – Finite Aquifer Systems," *Journal of Petroleum Technology*, pages 814-828.

Fetkovich, M.J. (1973): "The Isochronal Testing of Oil Wells," Paper SPE 4529 presented at the 1973 SPE Fall Technical Conference and Exhibition, Richardson, Texas: Society of Petroleum Engineers.

Firoozabadi, A. (November 2000): "Recovery Mechanisms in Fractured Reservoirs and Field Performance," *Journal of Canadian Petroleum Technology*, pages 13-17.

Firoozabadi, A. and J. Hauge (1989): "Capillary Pressure in Fractured Porous Media," Paper SPE 18747, presented at SPE California Regional Meeting, Richardson, Texas: Society of Petroleum Engineers.

Fredrich, J.T., G.L. Deitrick, J.G. Arguello and E.P. DeRouffignac (1998): "Reservoir Compaction, Surface Subsidence, and Casing Damage: A Geomechanics Approach to Mitigation and Reservoir Management," *Journal of Petroleum Technology*, pages 68-70.

Gaddy, D.E. (April 26, 1999): "Coalbed Methane Production Shows Wide Range of Variability," *Oil & Gas Journal*, pages 41-42.

Ganzer, L.J. (2002): "Simulating Fractured Reservoirs using Adaptive Dual Continuum," Paper SPE 75233, presented at the SPE/DOE Improved Oil Recovery Symposium, Richardson, Texas: Society of Petroleum Engineers.

Gardner, H.F., L.W. Gardner, and A.H. Gregory (1974): "Formation Velocity and Density – the Diagnostic Basis for Stratigraphic Traps," *Geophysics* Volume 39, pages 770-780.

Gassmann, F. (1951): "Elastic Waves through a Packing of Spheres," *Geophysics*, Volume 16, pages 673-685.

Gilbert, W.E. (1954): "Flowing and Gas-Lift Well Performance," *Drilling and Production Practices*, page 126 ff.

Gilman, J.R., H-Z. Meng, M.J. Uland, P.J. Dzurman, and S. Cosic (2002): "Statistical Ranking of Stochastic Geomodels using Streamline Simulation: A Field Application," Paper SP 77374, presented at the 2002 Annual Technical Conference and Exhibition of Society of Petroleum Engineers, Richardson, Texas: Society of Petroleum Engineers.

Golan, M. (2000): Keynote address to the Productivity Enhancement Session, Improved Recovery Symposium (IRS) 2000, sponsored by ONGC (Oil and Natural Gas Corporation), Ahmedabad, India, July.

Golf-Racht, T.D. van (1982): **Fundamentals of Fractured Reservoir Engineering**, New York: Elsevier.

Govier, G.W., Editor (1978): **Theory and Practice of the Testing of Gas Wells**, Calgary: Energy Resources Conservation Board.

Grace, J.D., R.H. Caldwell, and D.I. Heather (Sept. 1993): "Comparative Reserves Definitions: USA, Europe, and the Former Soviet Union," *Journal of Petroleum Technology*, pages 866-872.

Green, D.W. and G.P. Wilhite (1998): **Enhanced Oil Recovery**, Richardson, Texas: Society of Petroleum Engineers.

Griffith, P. (March 1984), "Multiphase Flow in Pipes," *Journal of Petroleum Technology*, pages 361-367.

Grigg, R.B. and D.S. Schechter (1998): "Improved Efficiency of Miscible CO_2 Floods and Enhanced Prospects for CO_2 Flooding Heterogeneous Reservoirs," Report PRRC 98-29, and Annual

Report to the U.S. Department of Energy for the Period June 1, 1997 through May 31, 1998; National Petroleum Technology Office, Tulsa.

Guan, L., Y. Du, S.G. Johnson, and M.K. Choudhary (May 2005): "Advances of Interwell Tracer Analysis in the Petroleum Industry," *Journal of Canadian Petroleum Technology*, pages 12-15.

Guéguen, Y. and V. Palciauskas (1994): **Introduction to the Physics of Rocks**, Princeton, New Jersey: Princeton University Press.

Guerrero, E.T. (1966): "Material Balance Principles," Reservoir Engineering Refresher Course, Tulsa: Mid-Continent Section of AIME.

Gunter, G.W., J.M. Finneran, D.J. Hartmann, and J.D. Miller (1997): "Early Determination of Reservoir Flow Units Using an Integrated Petrophysical Method," Paper SPE 38679, presented at the 1997 SPE Annual Technical Conference and Exhibition of the Society of Petroleum Engineers, Richardson, Texas: Society of Petroleum Engineers.

Haldorsen, H.H. and E. Damsleth (1993): "Challenges in Reservoir Characterization," *American Association of Petroleum Geologists Bulletin*, Volume 77, No. 4, pages 541-551.

Haldorsen, H.H. and E. Damsleth (April 1990): "Stochastic Modeling," *Journal of Petroleum Technology*, pages 404-412.

Haldorsen, H.H. and L.W. Lake (1989): "A New Approach to Shale Management in Field-Scale Models," **Reservoir Characterization 2**, SPE Reprint Series #27, Richardson, Texas: Society of Petroleum Engineers.

Harpole, K.J. (1985): **Reservoir Environments and Their Characterization**, Boston: International Human Resources Development Corporation.

Harris, D.G. (May 1975): "The Role of Geology in Reservoir Simulation Studies," *Journal of Petroleum Technology*, pages 625-632.

Harris, D.G. and C.H. Hewitt (July 1977): "Synergism in Reservoir Management – The Geologic Perspective," *Journal of Petroleum Technology*, pages 761-770.

He, W., R.N. Anderson, L. Xu, A. Boulanger, B. Meadow, and R. Neal (May 20, 1996): "4D Seismic Monitoring Grows as Production Tool," *Oil & Gas Journal*, pages 41-46.

Hebert, H., A.T. Bourgoyne, Jr., and J. Tyler (May 1993): "BOAST II for the IBM 3090 and RISC 6000", U.S. Department of Energy Report DOE/ID/12842-2, Bartlesville Energy Technology Center, Oklahoma.

Hegre, T.M., V. Dalen, and A. Henriquez (1986): "Generalized Transmissibilities for Distorted Grids in Reservoir Simulation," Paper SPE 15622, presented at the 61st Annual Technical Conference and Exhibition of the Society of Petroleum Engineers, Richardson, Texas: Society of Petroleum Engineers.

Heinemann, R.F., S.L. Lyons, S. Vasantharajan, and W.-P. Tai (January 1998): "Next Generation Reservoir Optimization," *World Oil*, pages 47-54.

Heinemann, Z.E. (1994): "Interactive Generation of Irregular Simulation Grids and its Practical Applications," Paper SPE 27998, Richardson, Texas: Society of Petroleum Engineers.

Heinemann, Z.E. and G.F. Heinemann (1998): "Modeling Heavily Faulted Reservoirs," Paper SPE 48998, presented at the 1998 Society of Petroleum Engineers Annual Technical Conference and Exhibition of the Society of Petroleum Engineers, Richardson, Texas: Society of Petroleum Engineers.

Hirsche, K., J. Porter-Hirsche, L. Mewhort, and R. Davis (March 1997): "The use and abuse of geostatistics," *The Leading Edge*, pages 253-260.

Hite, J.R., S.M. Avasthi, and P.L. Bondor (March 2005): "Planning Successful EOR Projects," *Journal of Petroleum Technology*, pages 28-29.

Holmes, J.A. (November 2001): "Modeling Advanced Wells in Reservoir Simulation," *Journal of Petroleum Technology*, pages 54-66.

Honarpour, M., L.F. Koederitz, and A.H. Harvey (1982): "Empirical Equations for Estimating Two-Phase Relative Permeability in Consolidated Rock," *Journal of Petroleum Technology*, pages 2905-2908.

Horne, R.N. (1995): **Modern Well Test Analysis**, Palo Alto, California: Petroway.

Hui, M-H., D. Zhou, X-H. Wen, and L.J. Durlofsky (June 2005): "Development and Application of a New Technique for Upscaling Miscible Processes," *SPE Reservoir Evaluation & Engineering*, pages 189-195.

Isaaks, E.H. and R.M. Srivastava (1989): **Applied Geostatistics**, New York: Oxford University Press.

Jack, I. (1998): **Time-Lapse Seismic in Reservoir Management**, 1998 Distinguished Instructor Short Course, Tulsa: Society of Exploration Geophysicists.

Jefferys, W.H. and J.O. Berger (1992): "Ockham's Razor and Bayesian Analysis," *American Scientist*, Volume 80, pages 64-72.

Jennings, J.W., Jr., and F.J. Lucia (August 2003): "Predicting Permeability from Well Logs in Carbonates with a Link to Geology for Interwell Permeability Mapping," *SPE Reservoir Evaluation & Engineering*, pages 215-225.

Johnston, D.H. (1997): "A Tutorial on Time-Lapse Seismic Reservoir Monitoring," *Journal of Petroleum Technology*, pages 473-475.

Jones, A.H., G.J. Bell, and R.A. Schraufnagel (1988): "A Review of the Physical and Mechanical Properties of Coal with Implications for Coal-Bed Methane Well Completion and Production," **Geology and Coal-Bed Methane Resources of the Northern San Juan Basin, New Mexico and Colorado**, edited by J.E. Fasset, Rocky Mountain Assoc. of Geologists, 169-81; reprinted in SPE Reprint Series #35 **Coalbed Methane**, Society of Petroleum Engineers, Richardson, Texas (1992).

Joshi, S.D. (June 1988): "Augmentation of Well Productivity with Slant and Horizontal Wells," *Journal of Petroleum Technology*, page 729 ff.

Joshi, S.D. (1991): **Horizontal Well Technology**, Tulsa, Oklahoma: PennWell Publishing Company.

Kabir, C.S. and N.J. Young (April 2004): "Handling Production Data Uncertainty in History Matching: The Meren Reservoir Case Study," *SPE Reservoir Evaluation & Engineering*, pages 123-131.

Kamal, M.M., D.G. Freyder, and M.A. Murray (1995): "Use of Transient Testing in Reservoir Management," *Journal of Petroleum Technology*, pages 992-999.

Kanter, R.M. (1988): "When a Thousand Flowers Bloom: Structural, Collective and Social Conditions for Innovation in Organization," *Research in Organizational Behavior*, Volume 10, pages 169-211.

Kasap, E. and L.W. Lake (June 1990): "Calculating the Effective Permeability Tensor of a Gridblock," *Society of Petroleum Engineers Formation Evaluation*, pages 192-200.

Katz, D.L. and R.L. Lee (1990): **Natural Gas Engineering**, New York: McGraw-Hill.

Kazemi, H. (October 1996): "Future of Reservoir Simulation", *Society of Petroleum Engineers Computer Applications*, pages 120-121.

Kelkar, M. (2000): "Application of Geostatistics for Reservoir Characterization – Accomplishments and Challenges," *Journal of Canadian Petroleum Technology*, Volume 59, pages 25-29.

Killough, J.E. (1976): "Reservoir Simulation with History-Dependent Saturation Functions," *Society of Petroleum Engineers Journal*, pages 37-48.

King, G.R. and T. Ertekin (1995): "State-of-the-art Modeling for Unconventional Gas Recovery, Part II: Recent Developments (1989-1994)," Paper SPE 29575, presented at the SPE Rocky Mountain Regional/Low-Permeability Reservoirs Symposium, Richardson, Texas: Society of Petroleum Engineers.

King, M.J. and M. Mansfield (August 1999): "Flow Simulation of Geologic Models," *SPE Reservoir Evaluation & Engineering*, pages 351-367.

Koederitz, L.F., A.H. Harvey, and M. Honarpour (1989): **Introduction to Petroleum Reservoir Analysis**, Houston: Gulf Publishing.

Kreyszig, E. (1999): **Advanced Engineering Mathematics, Eighth Edition**, New York: J. Wiley and Sons.

Kuuskraa, V.A. and C.F. Brandenburg (October 9, 1989): "Coalbed Methane Sparks a New Energy Industry," *Oil & Gas Journal*, pages 49.

Kuuskraa, V.A. and G.C. Bank (December 8, 2003): "Gas from Tight Sands, Shales a Growing Share of U.S. Supply," *Oil & Gas Journal*, pages 34-43.

Lake, L.W. (April 1988): "The Origins of Anisotropy," *Journal of Petroleum Technology*, pages 395-396.

Lake, L.W. (1989): **Enhanced Oil Recovery**, Englewood Cliffs, New Jersey: Prentice Hall.

Lantz, R.B. (1971): "Quantitative Evaluation of Numerical Diffusion," *Society of Petroleum Engineering Journal*, pages 315-320.

Lasseter, T.J. and S.A. Jackson (November 2004): "Improving Integrated Interpretation Accuracy and Efficiency using a Single Consistent Reservoir Model from Seismic to Simulation," *The Leading Edge*, pages 1118-1121.

Lea, J., H.V. Nickens, and M. Wells, (2003): **Gas Well Deliquification**, Burlington, Massachusetts: Elsevier-Gulf Professional Publishing.

Lea, J.F., and H.V. Nickens (April 2004): "Solving Gas-Well Liquid-Loading Problems," *Journal of Petroleum Technology*, pages 30-31 and 69-74.

Lee, S.H., L.J. Durlofsky, M.F. Lough, and W.H. Chen (1997): "Finite Difference Simulation of Geologically Complex Reservoirs with Tensor Permeabilities," Paper SPE 38002, presented at the 1997 SPE Reservoir Simulation Symposium, Richardson, Texas: Society of Petroleum Engineers.

Levitan, L.L. and M. Murtha (1999): "New Correlations estimate P_b, FVF," *Oil & Gas Journal*, pages 70-76.

Lide, D.R., 2002, **CRC Handbook of Chemistry and Physics**, 83rd Edition, Boca Raton, Florida: CRC Press.

Lieber, Bob (Mar/Apr 1996): "Geostatistics: The Next Step in Reservoir Modeling," *Petro Systems World*, pages 28-29.

Liner, C. (2004): **Elements of 3-D Seismology**, Tulsa: PennWell Books

Litvak, M.L., and B.L. Darlow, (1995): "Surface Network and Well Tubing-head Pressure Constraints in Compositional Simulation," Paper SPE 29125 presented at the 1995 SPE Symposium on Reservoir Simulation, Richardson, Texas: Society of Petroleum Engineers.

Lough, M.F., S.H. Lee, and J. Kamath (November 1996): "Gridblock Effective-Permeability Calculation for Simulation of Naturally Fractured Reservoirs," *Journal of Petroleum Technology*, pages 1033-1034.

Louisiana State University (1997): " 'BOAST 3' A Modified Version of BOAST II with Post Processors B3PLOT2 and COLORGRID," Version 1.50, U.S. Department of Energy Report DOE/BC/14831-18, Bartlesville Energy Technology Center, Oklahoma.

Lumley, D. and R. Behrens (1997): "Practical Issues for 4D Reservoir Modeling," *Journal of Petroleum Technology*, pages 998-999.

Lumley, D. (2004): "Business and Technology Challenges for 4D Seismic Reservoir Monitoring," *The Leading Edge*, pages 1166-1168.

Lynch, M.C. (1996): "The Mirage of Higher Petroleum Prices," *Journal of Petroleum Technology*, pages 169-170.

Maddox, R.B. (1988): **Team Building: An Exercise in Leadership**, Crisp Publications, Inc.

Makogon, Y.F., W.A. Dunlap and S.A. Holditch (1997): "Recent Research on Properties of Gas Hydrates," Paper OTC 8299, presented at the 1997 Offshore Technology Conference, Richardson, Texas: Society of Petroleum Engineers.

Martin, F.D. (1992): "Enhanced Oil Recovery for Independent Producers," Paper SPE/DOE 24142, presented at the SPE/DOE Eighth Symposium, Richardson, Texas: Society of Petroleum Engineers.

Martin, F.D., J.E. Stevens, and K.J. Harpole (1995): "CO_2-Foam Field Test at the East Vacuum Grayburg/San Andres Unit," *SPE Reservoir Engineering* (November), pages 266-272.

Mattax, C.C. and R.L. Dalton (1990): **Reservoir Simulation**, SPE Monograph #13, Richardson, Texas: Society of Petroleum Engineers.

Matthews, C.S. and D.G. Russell (1967): **Pressure Buildup and Flow Tests in Wells**, SPE Monograph Series, Richardson, Texas: Society of Petroleum Engineers.

Mavko, G., T. Mukerji, J. Dvorkin (1998): **The Rock Physics Handbook**, Cambridge, United Kingdom: Cambridge University Press.

Mavor, M., T. Pratt and R. DeBruyn (April 26, 1999): "Study Quantifies Powder River Coal Seam Properties," *Oil & Gas Journal*, pages 35-40.

McCain, W.D., Jr. (1990): **The Properties of Petroleum Fluids, Second Edition**, Tulsa, Oklahoma: PennWell Publishing.

McCain, W.D., Jr. (1991): "Reservoir-Fluid Property Correlations – State of the Art," *Society of Petroleum Engineers Reservoir Engineering*, pages 266-272.

McCain, W.D., Jr. (2002): "Analysis of Black Oil PVT Reports Revisited," Paper SPE 77386, presented at the 2002 SPE Annual Technical Conference and Exhibition, Richardson, Texas: Society of Petroleum Engineers.

McDonald, A.E., B.L. Becknew, H.M. Chan, T.A. Jones and S.O. Wooten (1991): "Some Important Considerations in the Simulation of Naturally Fractured Reservoirs," Paper SPE 21814, presented at the Rocky Mountain Regional Meeting, Richardson, Texas: Society of Petroleum Engineers.

McIntosh, I., H. Salzew, and C. Christensen (1991): "The Challenge of Teamwork," Paper CIM/AOSTRA 91-19, presented at the CIM/AOSTRA 1991 Technical Conference, Banff, Canada.

McKee, C.R., A.C. Bumb, and R.A. Koenig (March, 1988): "Stress-Dependent Permeability and Porosity of Coal and Other Geologic Formations," *SPE Formation Evaluation*, pages 81-91.

McQuillin, R., M. Bacon, and W. Barclay (1984): **An Introduction to Seismic Interpretation,** Houston: Gulf Publishing.

Medvin, E. and J. Rennie (July 1996): "Time to Depth: Where Geologists and Geophysicists Meet," *of Petroleum Technology*, pages 595-599.

Mian, M.A. (1992): **Petroleum Engineering Handbook for the Practicing Engineer**, Volumes I and II, Tulsa, Oklahoma: PennWell Publishing.

Millheim, K.M. (1997): "Fields of Vision," *Journal of Petroleum Technology*, page 684.

Mlacnik, M.J., and Z.E. Heinemann, (August 2003), "Using Well Windows in Full-Field Reservoir Simulation," *SPE Reservoir Evaluation and Engineering*, pages 275-285.

Mlacnik, M.J., A.W. Harrer, G.F. Heinemann, and Z.E. Heinemann (March 2004): "State-of-the-Art of the Windowing Technique," *Journal of Canadian Petroleum Technology*, pages 25-30.

Moses, P.L. (July 1986): "Engineering Applications of Phase Behavior of Crude Oil and Condensate Systems," *Journal of Petroleum Technology*, pages 715-723.

Munka, M. and J. Pápay (2001): **4D Numerical Modeling of Petroleum Reservoir Recovery**, Budapest, Hungary: Akadémiai Kiadó.

Murphy, W., A. Reisher, and K. Hsu (1993): "Modulus Decomposition of Compressional and Shear Velocities in Sand Bodies," *Geophysics*, Volume 58, pages 227-239.

Murtha, J.A. (1997): "Monte Carlo Simulation: Its Status and Future," *Journal of Petroleum Technology*, pages 361-373.

Nelson, P.H. (November 2004): "Permeability-Porosity Data Sets for Sandstones," *The Leading Edge*, pages 1143-1144.

Nemchenko, N.N., M. Ya. Zykin, A.A. Arbatov, V.I. Poroskun, and I.S. Gutman (1995): "Distinctions in the Oil and Gas Reserves and Resources Classifications Assumed in Russia and USA – Source of Distinctions," *Energy Exploration and Exploitation*, Volume 13, #6, Essex, United Kingdom: Multi-Science Publishing Company.

Newendorp, P. and J. Schuyler (2000): **Decision Analysis for Petroleum Exploration**, Second Edition, Aurora, Colorado: Planning Press.

Nolen, J.S. and D.W. Berry (1973): "Test of the Stability and Time-Step Sensitivity of Semi-Implicit Reservoir Simulation Techniques," **Numerical Simulation**, SPE Reprint Series #11, Richardson, Texas: Society of Petroleum Engineers.

Norton, R. (November 1994): "Economics for Managers," *Fortune*, p. 3.

Novakovic, D. (1999): "Gravity Assisted Tertiary Gas Injection in Water-flooded Reservoirs – Mathematical Modeling of Drive Parameters," Louisiana State University preprint, presented at the June 1999 Reservoir Management Summer School, Dubrovnik, Croatia.

Odeh, A.S. (1981): "Comparison of Solutions to a Three-Dimensional Black-Oil Reservoir Simulation Problem," *Journal of Petroleum Technology*, pages 13-25.

Odeh, A.S. (February 1985): "The Proper Interpretation of Field-Determined Buildup Pressure and Skin Values for Simulator Use," *Society of Petroleum Engineering Journal*, pages 125-131.

Offshore staff (September 1998): 'Refurbishment/Abandonment," *Offshore Magazine*, pages 148 and 186.

Oreskes, N., K. Shrader-Frechette, and K. Belitz (1994): "Verification, Validation, and Confirmation of Numerical Models in the Earth Sciences", *Science*, pages 641-646, February 4.

Ouenes, A., A.M. Zellou, G.C. Robinson, D.R. Balogh, and U.G. Araktingi (2004): "Improved Reservoir Simulation with Seismically Derived Fracture Models," Paper SPE 90822, presented at the 2004 SPE Annual Technical Conference and Exhibition, Richardson, Texas: Society of Petroleum Engineers.

Pannatier, Y. (1996): **VARIOWIN: Software for Spatial Data Analysis in 2D**, New York: Springer-Verlag.

Paterson, L. (January 1985): "Fingering with Miscible Fluids in a Hele-Shaw Cell," *Physics of Fluids*, Volume 28 (1), 26-30.

Paul, G.W., W.K. Sawyer and R.H. Dean (1990): "Validation of 3D Coalbed Simulators," Paper SPE 20733, presented at the 65th Annual Technical Conference and Exhibition (23-25 September); Richardson, Texas: Society of Petroleum Engineers.

Peaceman, D.W. (1977): **Fundamentals of Numerical Reservoir Simulation**, New York: Elsevier.

Peaceman, D.W. (June 1978): "Interpretation of Well-Block Pressures in Numerical Reservoir Simulation," *Society of Petroleum Engineering Journal*, pages 183-194.

Peaceman, D.W. (June 1983): "Interpretation of Well-Block Pressures in Numerical Reservoir Simulation with Non-square Grid Blocks and Anisotropic Permeability," *Society of Petroleum Engineering Journal*, pages 531-543.

Pedersen, K.S., A. Fredenslund, and P. Thomassen (1989): **Properties of Oil and Natural Gases**, Houston: Gulf Publishing.

Persoff, P., K. Preuss and L. Myer (1991): "Two-Phase Flow Visualization and Relative Permeability Measurements in Transparent Replicas of Rough-Walled Rock Fractures," Report LBL-30161, Earth Sciences Division, Lawrence Berkeley Lab., presented at 16th Workshop on Geothermal Res. Eng., Stanford, Jan. 23-25.

Petalas, N., and K. Aziz (June 2000): "A Mechanistic Model for Multiphase Flow in Pipes," *Journal of Canadian Petroleum Technology*, pages 43-55.

Pletcher, J.L. (February 2002): “Improvements to Reservoir Material Balance Methods,” *SPE Reservoir Evaluation & Engineering*, pages 49-59.

Poettmann, F.H. and R.S. Thompson (1986): “Discussion of Engineering Applications of Phase Behavior of Crude Oil and Condensate Systems,” *Journal of Petroleum Technology*, pages 1263-1264.

Prats, M. (1982): **Thermal Recovery**, SPE Monograph Series, Richardson Texas: Society of Petroleum Engineers.

Preuss, K. and Y.W. Tsang (1990): "On Two-Phase Relative Permeability and Capillary Pressure of Rough-Walled Rock Fractures," *Water Resources Research*, Volume 26, pages 1915-1926.

Raghavan, R. and L.Y. Chin (August 2004): “Productivity Changes in Reservoirs with Stress-Dependent Permeability,” *SPE Reservoir Evaluation & Engineering*, pages 308-315.

Raleigh, M. (Sept. 1991): *ECLIPSE Newsletter*, Houston: Schlumberger GeoQuest.

Rao, N.D. and M.G. Girard (January 1997): “A New Technique for Reservoir Wettability Characterization,” *Journal of Canadian Petroleum Technology*, Volume 35, pages 31-39.

Raza, S.H. (1992): “Data Acquisition and Analysis for Efficient Reservoir Management,” *Journal of Petroleum Technology*, pages 466-468.

Reiss, L.H. (1980): **The Reservoir Engineering Aspects of Fractured Reservoirs**, Houston: Gulf Publishing.

Reyes, L. and S.O. Osisanya (December 2002): “Empirical Correlation of Effective Stress Dependent Shale Rock Properties,” *Journal of Canadian Petroleum Technology*, pages 47-53.

Richardson, J.G., J.B. Sangree, and R.M. Sneider (1987a): “Applications of Geophysics to Geologic Models and to Reservoir Descriptions,” *Journal of Petroleum Technology*, pages 753-755.

Richardson, J.G., J.B. Sangree and R.M. Sneider (1987b): “Introduction to Geologic Models,” *Journal of Petroleum Technology* (first of series), pages 401-403.

Richardson, J.G. (February 1989): "Appraisal and Development of Reservoirs," *Geophysics: The Leading Edge of Exploration*, pages 42 ff.

Rogers, R.E. (1994): **Coalbed Methane: Principles and Practice**, Englewood Cliffs, New Jersey: Prentice-Hall.

Rosenberg, D. U. von (1977): **Methods for the Numerical Solution of Partial Differential Equations**, Tulsa, Oklahoma: Farrar and Associates.

Rossini, C., F. Brega, L. Piro, M. Rovellini, and G. Spotti (November 1994): "Combined Geostatistical and Dynamic Simulations for Developing a Reservoir Management Strategy: A Case History," *Journal of Petroleum Technology*, pages 979-985.

Ruijtenberg, P.A., R. Buchanan, and P. Marke (1990): "Three-Dimensional Data Improve Reservoir Mapping," *Journal of Petroleum Technology*, pages 22-25, 59-61.

Sabet, M.A. (1991): **Well Test Analysis**, Houston: Gulf Publishing.

Saleri, N.G. (1993): "Reservoir Performance Forecasting: Acceleration by Parallel Planning," *Journal of Petroleum Technology*, pages 652-657.

Saleri, N.G. (2002): "'Learning' Reservoirs: Adapting to Disruptive Technologies," *Journal of Petroleum Technology*, pages 57-60.

Saleri, N.G. (2005): "Reservoir Management Tenets: Why They Matter to Sustainable Supplies," *Journal of Petroleum Technology*, pages 28-30.

Saleri, N.G., R.M. Toronyi, and D.E. Snyder (1992): "Data and Data Hierarchy," *Journal of Petroleum Technology*, pages 1286-1293.

Satter, A. and G. Thakur (1994): **Integrated Petroleum Reservoir Management**, Tulsa: PennWell Publishing.

Satter, A., J.E. Varnon, and M.T. Hoang (1994): "Integrated Reservoir Management," *Journal of Petroleum Technology*, pages 1057-1064.

Sawyer, W.K. and J.C. Mercer (August 1978): "Applied Simulation Techniques for Energy Recovery," Department of Energy Report METC/RI-78/9, Morgantown, West Virginia.

Schneider, F.N. (May 1987): "Three Procedures Enhance Relative Permeability Data," *Oil & Gas Journal*, pages 45-51.

Schilthuis, R.D. (1936): "Active Oil and Reservoir Energy," *Transactions of the AIME*, Volume 118, page 33 ff.

Schön, J.H. (1996): **Physical Properties of Rocks: Fundamentals and Principles of Petrophysics**, Volume 18, New York: Elsevier.

Schraufnagel, R. (1991): "Improved Evaluation of Coal Reservoirs through Specialized Core Analysis," 1990 Annual Report from Core Laboratories to Gas Research Institute (1 March).

Schutjens, P.M.T.M., T.H. Hanssen, M.H.H. Hettema, J. Merour, P. de Bree, J.W.A. Coremans, and G. Helliesen (June 2004): "Compaction-Induced Porosity-Permeability Reduction in Sandstone Reservoirs: Data and Model for Elasticity-Dominated Deformation," *SPE Reservoir Evaluation & Engineering*, pages 202-216.

Sears, M. (June 1994): organizational development specialist at Bell Atlantic, quoted in *Journal of Petroleum Technology*, page 505.

Seba, R.D. (1998): **Economics of Worldwide Petroleum Production**, Tulsa, Oklahoma: Oil & Gas Consultants International.

Selley, R.C. (1998): **Elements of Petroleum Geology**, 2nd Edition, San Diego: Academic Press.

Settari, A. (August 2002): "Reservoir Compaction," *Journal of Petroleum Technology*, pages 62-69.

Settari, A., and K. Aziz, (June 1974): "A Computer Model for Two-Phase Coning Simulation," *Society of Petroleum Engineers Journal*, pages 221-236.

Settari, A. and D.A. Walters (1999): "Advances in Coupled Geomechanical and Reservoir Modeling with Applications to Reservoir Compaction," Paper SPE 51927, presented at the 1999 SPE Reservoir Simulation Symposium, Richardson, Texas: Society of Petroleum Engineers.

Settari, A., D.A. Walters, and G.A. Behie (December 2001): "Use of Coupled Reservoir and Geomechanical Modeling for Integrated Reservoir Analysis and Management," *Journal of Canadian Petroleum Technology*, pages 55-61.

Shaw, B.S. and T.G. Morris (2005): "Managing the Tradeoffs: Similarities Between Managing Product Development and a Well Drilling-Completion Project," *Journal of Petroleum Technology*, pages 36-44.

Sheriff, R.E. (1989): **Geophysical Methods**, Englewood Cliffs, New Jersey: Prentice-Hall.

Shi, H., J.A. Holmes, L.J. Durlofsky, K. Aziz, L.R. Diaz, B. Alkaya, and G. Oddie (2003): "Drift-flux Modeling of Multiphase Flow in Wellbores," Paper SPE 84228, presented at the 2003 SPE Annual Technical Conference and Exhibition, Richardson, Texas: Society of Petroleum Engineers.

Shi, J-Q. and S. Durucan (August 2005): "A Model for Changes in Coalbed Permeability During Primary and Enhanced Methane Recovery," *SPE Reservoir Evaluation & Engineering*, pages 291-299.

Slatt, R.M. and G.L. Hopkins (1990): "Scaling Geologic Reservoir Description to Engineering Needs," *Journal of Petroleum Technology*, pages 202-210.

Smith, R.V. (1990): **Practical Natural Gas Engineering**, Tulsa: PennWell Publishing.

Soares, A.C., F.H. Ferreira, and E.A. Vargas, Jr. (December 2002): "An Experimental Study for Mechanical Formation Damage," *SPE Reservoir Evaluation & Engineering*, pages 480-487.

Spillette, A.G, J.G. Hillestad, and H.L. Stone (1986): "A High-Stability Sequential Solution Approach to Reservoir Simulation," **Numerical Simulation II**, SPE Reprint Series #20, Richardson, Texas: Society of Petroleum Engineers.

Staff-JPT (August 1994): "New Management Structures: Flat and Lean, Not Mean," *Journal of Petroleum Technology*, pages 647-648.

Staff-JPT (May 1997): "SPE/WPC Reserves Definitions Approved," *Journal of Petroleum Technology*, pages 527-528.

Standing, M.B. and D.L. Katz (1942): "Density of Natural Gases," *Transactions of AIME*, Volume 146, 140.

Stern, D. (September 2005): "Practical Aspects of Scaleup of Simulation Models," *Journal of Petroleum Technology*, pages 74-82.

Stolz, A-K. and R.M. Graves (2003): "Sensitivity Study of Flow Unit Definition by Use of Reservoir Simulation," Paper SPE 84277, presented at the 2003 SPE Annual Technical Conference and Exhibition, Richardson, Texas: Society of Petroleum Engineers.

Stone, H.L. (October-December 1973): "Estimation of Three-Phase Relative Permeability and Residual Oil Data," *Journal of Canadian Petroleum Technology*, pages 53 ff.

Taber, J.J. and F.D. Martin (1983): "Technical Screening Guides for the Enhanced Recovery of Oil," Paper SPE 12069, presented at the 58th Annual Technical Conference and Exhibition, Richardson, Texas: Society of Petroleum Engineers.

Taber, J.J., F.D. Martin and R.S. Seright (1997a): "EOR Screening Criteria Revisited: Part 1 – Introduction to Screening Criteria and Enhanced Recovery Field Projects," *SPE Reservoir Evaluation and Engineering*, pages 189-198.

Taber, J.J., F.D. Martin and R.S. Seright (1997b): "EOR Screening Criteria Revisited: Part 2 – Applications and Implications of Oil Prices," *SPE Reservoir Evaluation and Engineering*, pages 199-205.

Taggart, I.J., E. Soedarmo, and L. Paterson (1995): "Limitations in the Use of Pseudofunctions for Up-Scaling Reservoir Simulation Models," Paper SPE 29126, presented at the 13th Society of Petroleum Engineers Symposium on Reservoir Simulation, Richardson, Texas: Society of Petroleum Engineers.

Tearpock, D.J., R.E. Bischke and L.G. Walker (2002): **Applied Subsurface Geological Mapping with Structural Methods**, Englewood Cliffs, New Jersey: Prentice Hall.

Tearpock, D.J. and J.C. Brenneke (2001): "Multidisciplinary teams, integrated software for shared-earth modeling key E&P success," *Oil & Gas Journal*, pages 84-88 (10 December).

Teeuw, D. (Sept. 1971): "Prediction of Formation Compaction from Laboratory Compressibility Data," *Society of Petroleum Engineering Journal*, pages 263-271.

Tek, M.R. (1996): **Natural Gas Storage Underground: Inventory and Deliverability**, Tulsa: PennWell Publishing.

Telford, W.M., L.P. Geldart, R.E. Sheriff, and D.A. Keys (1976): **Applied Geophysics**, Cambridge: Cambridge University Press.

Thakur, G.C. (1996): "What Is Reservoir Management?" *Journal of Petroleum Technology*, pages 520-525.

Thomas, F.B., E. Shtepani, D. Imer, and D.B. Bennion (January 2002): "How Many Pseudo-Components are Needed to Model Phase Behaviour?" *Journal of Canadian Petroleum Technology*, pages 48-54.

Thomas, G.W. (1982): **Principles of Hydrocarbon Reservoir Simulation**, Boston: International Human Resources Development Corporation.

Thomas, L. K., W. B. Lumkin and G. M. Reheis (1976): "Reservoir Simulation of Variable Bubble Point Problems," *Society of Petroleum Engineers Journal*, pages 10-16.

Thompson, R.S. and J.D. Wright (1985): **Oil Property Evaluation**, Second Edition, Golden, Colorado: Thompson-Wright Associates.

Tiab, D. and E.C. Donaldson (2003): **Petrophysics**, Second Edition, Boston: Elsevier.

Tippee, Bob (1998): "Collaborative Effort Seeks Computing Platform for Shared Earth Modeling," *Oil & Gas Journal*, pages 58-62 (30 November).

Tobias, S. (1998): "From G&G to S&S: Watershed Changes in Exploration-Development Work Flow," *Oil and Gas Journal*, pages 38-47 (30 November).

Todd, M.R. and W.J. Longstaff (1972): "The Development, Testing and Application of a Numerical Simulator for Predicting Miscible Flood Performance," *Journal of Petroleum Technology*, pages 874-882.

Todd, M.R., P.M. Odell, and G.J. Hiraski (December 1972): "Methods for Increased Accuracy in Numerical Reservoir Simulators," *Society of Petroleum Engineering Journal*, pages 515-530.

Toronyi, R.M. and N.G. Saleri (1988): "Engineering Control in Reservoir Simulation," Paper SPE 17937, presented at the 1988

Society of Petroleum Engineers Annual Technical Conference and Exhibition, Richardson, Texas: Society of Petroleum Engineers.

Towler, B.F. (2002): **Fundamental Principles of Reservoir Engineering**, Richardson, Texas: Society of Petroleum Engineers.

Tran, D., A. Settari, and L. Nghiem (2002): "New Iterative Coupling Between a Reservoir Simulator and a Geomechanics Module," SPE/ISRM 78192, presented at the 2002 SPE/ISRM Rock Mechanics Conference, Irving, Texas (23-25 October).

Turner, R.G., M.G. Hubbard, and A.E. Dukler (November 1969): "Analysis and Prediction of Minimum Flow Rate for the Continuous Removal of Liquids from Gas Wells," *Journal of Petroleum Technology*, pages 1475-1482.

Uland, M.J., S.W. Tinker, and D.H. Caldwell (1997): "3-D Reservoir Characterization for Improved Reservoir Management," paper presented at the 1997 Society of Petroleum Engineers' 10th Middle East Oil Show and Conference, Bahrain (March 15-18).

Verma, S. and K. Aziz (1997): "A Control Volume Scheme for Flexible Grids in Reservoir Simulation," Paper SPE 37999, presented at the 1997 Society of Petroleum Engineers Reservoir Simulation Symposium, Richardson, Texas: Society of Petroleum Engineers.

Vogel, J.V. (January 1968): "Inflow Performance Relationships for Solution-Gas Drive Wells," *Journal of Petroleum Technology*, page 83 ff.

Waal, H. de, and R. Calvert (2003): "Overview of Global 4D Seismic Implementation Strategy," *Petroleum Geosciences*, Volume 9, pages 1-6.

Wade, J.M. and V.I. Fryer (1997): "A Case Study of a Multi-Disciplinary Asset Management Team, with Special Emphasis on the Impact on Performance and Business Growth," Paper SPE 38823, presented at the 1997 Society of Petroleum Engineers Annual Technical Conference and Exhibition, Richardson, Texas: Society of Petroleum Engineers.

Walsh, M.P. and L.W. Lake (2003): **A Generalized Approach to Primary Hydrocarbon Recovery**, Amsterdam: Elsevier.

Wang, F.P., J. Dai, and C. Kerans (1998): "Modeling Dolomitized Carbonate-Ramp Reservoirs: A Case Study of the Seminole San Andres Unit – Part II, Seismic Modeling, Reservoir Geostatistics, and Reservoir Simulation," *Geophysics*, Volume 63, pages 1876-1884.

Wang, P. and G.A. Pope (July 2001): "Proper use of Equations of State for Compositional Reservoir Simulation," *Journal of Petroleum Technology*, pages 74-81.

Wang, Z. (2000): "Dynamic versus Static Elastic Properties of Reservoir Rocks," in **Seismic and Acoustic Velocities in Reservoir Rocks,** Volume 3, Recent Developments, edited by Z. Wang and A. Nur, Tulsa, Oklahoma: Society of Exploration Geophysicists.

Watkins, R. W. (1982): "The Development and Testing of a Sequential, Semi-Implicit Four Component Reservoir Simulator," Paper SPE 10513, Richardson, Texas: Society of Petroleum Engineers.

Wattenbarger, R.A. (July 2002): "Trends in Tight Gas Sand Production," *Journal of Canadian Petroleum Technology*, pages 17-20.

Weinstein, H.G., J.E. Chappelear, and J.S. Nolen (1986): "Second Comparative Solution Project: A Three-Phase Coning Study," *Journal of Petroleum Technology*, pages 345-353.

Westlake, D.W.S. (1999): "Bioremediation, Regulatory Agencies, and Public Acceptance of this Technology," *Journal of Canadian Petroleum Technology*, Volume 38, pages 48-50.

Whitson, C.H. and M.R. Brulé (2000): **Phase Behavior**, SPE Monograph Series, Richardson, Texas: Society of Petroleum Engineers.

Whittaker, M. (1999): "Emerging 'triple bottom line' model for industry weighs environmental, economic, and social considerations," *Oil & Gas Journal*, pages 23-28 (20 December).

Wiggins, M.L. and R.A. Startzman (1990): "An Approach to Reservoir Management," Paper SPE 20747, presented at the 65th Annual Technical Conference And Exhibition of the Society of Petroleum Engineers, Richardson, Texas: Society of Petroleum Engineers.

Wigley, T.M.L., R. Richels, and J.A. Edmonds (1996): "Economic and environmental choices in the stabilization of atmospheric CO_2 concentrations," *Nature* (18 January), pages 240-243.

Wilhite, G.P. (1986): **Waterflooding**, SPE Textbook Series Volume 3, Richardson, Texas: Society of Petroleum Engineers.

Wilkinson, A.J. (September 1997): "Improving Risk-Based Communications and Decision Making," *Journal of Petroleum Technology*, pages 936-943.

Williamson, A.E. and J.E. Chappelear (June 1981): "Representing Wells in Numerical Reservoir Simulation: Part I – Theory," *Society of Petroleum Engineers Journal*, pages 323-338; and "Part II – Implementation," *Society of Petroleum Engineers Journal*, pages 339-344.

Winterfeld, P.H. (June 1989): "Simulation of Pressure Buildup in a Multiphase Wellbore-Reservoir System," *SPE Formation Evaluation*, pages 247-252.

Worthington, P.F. and L. Cosentino (August 2005): "The Role of Cutoffs in Integrated Reservoir Studies," *SPE Reservoir Evaluation & Engineering*, pages 276-290.

Yale, D.P. (2002): "Coupled Geomechanics-Fluid Flow Modeling: Effects of Plasticity and Permeability Alteration," SPE/ISRM 78202, presented at the 2002 SPE/ISRM Rock Mechanics Conference, Richardson, Texas: Society of Petroleum Engineers.

Young, L.C. (1984): "A Study of Spatial Approximations for Simulating Fluid Displacements in Petroleum Reservoirs," **Computer Methods in Applied Mechanics and Engineering**, New York: Elsevier, pages 3-46.

Zuber, N., and J.A. Findlay, (1965): "Average Volumetric Concentration in Two-Phase Flow Systems," *Journal of Heat Transfer, Transactions ASME*, Volume 87, pages 453-468.

INDEX

C

D

E

F

G

H

M

N

O

P

Q

R

S

T

U

V

W

Y

Z